UNIVERSITÀ
DEGLI STUDI
FIRENZE

DOTTORATO DI RICERCA IN
Architettura

CICLO XXXIII

COORDINATORE Prof. Giuseppe De Luca

Seismic vulnerability assessment of the residential URM buildings built during the XX century in Florence

Settore Scientifico Disciplinare ICAR/09

Dottorando
Dott. Cardinali Vieri

(firma)

Tutore
Prof. Tanganelli Marco

(firma)

Coordinatore
Prof. De Luca Giuseppe
(firma)

Anni 2017/2020

ACKNOWLEDGMENTS

The presented thesis would have not been possible without the support of many people and institutions that helped me during my three years of research.

I would like to thank my supervisor, Prof. Marco Tanganelli, for the continuous help, the encouragement and support that he constantly demonstrated throughout these years. His experience and intellectual curiosity guided me in the development of the research and the achievement of its conclusions.

I would like to acknowledge Prof. Stefania Viti for her support and tremendous assistance, for her priceless advices concerning my research and how to present it.

I express gratitude to Prof. Mario De Stefano for involving me in several university research-projects, providing scholarships that allowed me to pursuit my objectives.

I would like to thank Prof. Rita Bento for hosting me six months at the Instituto Superior Técnico in Lisbon. She was a precious guidance in the development of the analytical part of this work and she inspired me towards the advancements of my research.

I would like to thank Casa S.P.A. for the disposition and the interested towards the topics treated in this work. Especially I am grateful to engineers Lorenzo Panerai, Angela Bevilacqua and Leonardo Boschi from the Project and Sites Office.

I want to thank the archivists Elisabetta Bettio and Rita Romanelli for their support during the archive research, for their practical advices and the knowledge they shared with me.

I would like to thank all the members of the PhD body, especially from the curriculum "Structures and conservation of Architecture and Cultural Heritage", for their classes and their direct or indirect support. I thank Grazia Poli for her precious work in the maintenance of the PhD.

I express my gratitude to everyone that, directly or not, helped me in the achievement of this work. I thank my colleagues from Prof. De Stefano's research group: Barbara Paoletti, Maria Teresa Cristofaro, Marta Castellini, Anna Caranti. Moreover, I want to thank Prof. Tommaso Rotunno, Prof. Raffaele Nudo and arch. Maurizio Ferrini for everything they shared with me. I thank prof. Massimo Coli and his group from Earth's Science and Riccardo Mario Azzara from INGV for the continuous exchange of interests. I also would like to acknowledge the technicians of the ex-construction departments of DIDA for the didactic and stimulating moments we shared.

I would like to thank my PhD colleagues Maria Teresa Miele, Margherita Vicario for the path we experienced together, and the "Mexican" colleagues Matteo Bigongiari, Jacopo Giuseppe Vitale, Nuria Chiara Palazzi and Giacomo Talozzi for all the beautiful moments and the stimulating discussions.

I would like to acknowledge my colleagues and friends met in Lisbon, Maria Victoria Requena Garcìa de la Cruz, Madalena Ponte, Claudia Caruso, Rita Couto, Jelena Milosevic, for the moments together and the challenging conversations we had in Técnico.

Finally, I want to thank the people close to me. I want to express my deepest gratitude to my parents, because my achievements are also theirs. I'm thankful they offered me the possibility to study and I seized this opportunity until this last achievement. I love them more than I can express.

I thank my girlfriend Lea for her personal support and for believing in me. She gave me the right peace of mind that helped me in the accomplishment of this work.

Finally, I express my gratitude to my friends and everyone that, gone or still present in my life, directly or not, supported my research and encouraged me in the development and the writing of this thesis.

ABSTRACT

This work deals with the urban scale vulnerability assessment of the unreinforced masonry buildings with RC slabs built during the XX century in Florence. The public housing interventions, for their numerosity and the archive documentation of the design projects, have been chosen as representative of the coeval urban stock. A meaningful database with a large number of selected buildings was realized. Every construction has been firstly investigated adopting an empirical approach based on geometrical and mechanical parameters; houses have been divided into typological classes in function of geometrical and architectonical features. Then, a typology with a specific related case study has been selected and assessed by an analytical procedure. An equivalent frame modeling discretization has been adopted and the seismic performance has been evaluated by means of nonlinear static analyses. Both aleatory and epistemic uncertainties have been considered; then, their sensitivity has been studied. The aleatory uncertainties have been investigated adopting the star design with the central star approach, while the epistemic uncertainties have been modeled through a logic tree approach. Analytical fragility curves have been finally derived, considering both the dispersions in terms of capacity and seismic demand. The fragility curves pointed out the vulnerability of the case study and the related damage scenarios for different expected return periods. Specifically, they showed a high vulnerability of these buildings for the 475 and 975 years return period; for the Life Safety limit state (SLV), around 40% of probability to have DL4 and 40% to reach DL5 is expected. The results have been finally extended to the building class population through a simplified procedure calibrated on the analytical results. The results point out homogeneous outcomes, exhibiting a high vulnerability and a relevant brittle behavior in the plastic phase.

Keywords: urban scale approach, hybrid approach, URM buildings, nonlinear static analysis, EF discretization, residential buildings.

[this page intentionally left blank]

INDEX

LIST OF FIGURES

LIST OF TABLES

[this page intentionally left blank]

LIST OF SYMBOLS

Symbol	*Definition*	*Unit*
$\Delta_{PLi,Xk}$	Variable that expresses the sensitivity to the aleatory uncertainties	
$\Delta_{PLi,Yj}$	Variable that expresses the sensitivity to the epistemic uncertainties	
T_1	Fundamental period	*s*
Δ_{LS4}	Interstory drift limit of the pan	
$\Lambda_{P,DLk}$	internal drift limit for the attainment of strength degradation	
τ_x	Masonry shear strength of the wall	
$A_{u,X}$	Spectral accelerations at the ultimate displacement	m/s^2
$D_{u,SPWS}$	Ultimate displacement for SPWS configurations	*m*
$D_{u,WPSS}$	Ultimate displacement for WPSS configurations	*m*
D_y	Displacement at the yielding point	*m*
$F_{el,max}$	Idealized maximum base shear	*kN*
F_y	Base shear at the yielding point	*kN*
H_f	Heaviside function	
$K_{i,x}$	Correction factors of the DVM	
M_u	Ultimate bending moment	
V_u	Ultimate shear	
$\bar{X}$	Mean value of performed tests	
k_r	Vertical regularity factor	
$p_{DSk}(im)$	Discrete probability considering the k-th LS considered.	
γ_i	Masonry specific weight at i-th level	kN/m^3
μ_D	Expected level of damage	
$a_{x,y,i}$	The ratio between the resistant masonry area in the considered direction over the gross area, for each *i*-th, level	
d^*	Displacement of the equivalent SDOF system	*m*
E	Elastic Young's Modulus	*MPa*
E_d	Energy dissipated during the hysteretic cycle	
E_{s0}	Elastic energy produced towards the two senses of the cyclic analysis	
f_m	Compressive strength	*MPa*

f_t	Tensile strenght	*MPa*
f_{v0}	Shear strength according to the Mann and Muller criterion	*MPa*
$f_{x,y}$	Base shear at the ground floor	*kN*
f_{ym}	Characteristic yielding stress	*MPa*
g	Gravity acceleration	*9.81 m/s²*
G	Shear Modulus	*MPa*
H	Total height of the building	*m*
h_i	Interstory height of the i-th level	
H_p	Minimum value between the tensile resistance of the interposed element and $0.4\, f_h ht$	
k	Ratio between variance of performed tests prior distribution variance	
$k_{x,y,i}$	Spandrels contribution factor defined as the ratio between the total volume of the wall over the volume of the piers	
m^*	Mass of the equivalent SDOF system	
m_i	Mass of the i-th node of the model	
n	Number of tests of the Bayesian approach	
Nf	Number of floors of the building	
N_p	Number of piers	
q	Q factor behavior	
Q	Macroseismic ductility factor	
q_i	Seismic floor load considering the deal loads and a fraction of the live loads	*daN/m²*
Rc	Cubic compressive strength	*MPa*
S_a	Spectral acceleation	*m/s²*
S_d	Spectral displacement	*m*
T^*	Equivalent period	*s*
$u_{i,j}$	Displacements of the nodes	
V^*	Base shear of the MDOF system	*kN*
Y	Vector that collects the values $log(IM_{LS,i})$, i = 1,…,M	
Z	Matrix of the normalized values	
$\boldsymbol{\alpha}_i$	Angular coefficient of the hyperplane of the normalized variables	
β_C	Dispersion in the seismic capacity	
β_D	Dispersion in the seismic demand	
Γ	Participation factor	
δ_{Ei}	Drift values	

ε_x	Coefficient ranging between 0 and 1 expressing the behavior of the structure	
$\zeta_{x,i}$	Fraction component in the considered direction	%
η	Damping correction factor	
μ'	Prior mean value	
ξ_{el}	Elastic viscous damping	%
ξ_{eq}	Equivalent viscous damping	%
ξ_{visc}	Hysteretic damping	%
σ_x	Average vertical compressive stress at the middle height of the first level	
τ_0	Shear strength according the Turnskek and Cacovic criterion	*MPa*
ϕ_i	Referred normalized displacement	
$\varphi_{i,j}$	Rotation of the nodes	
Φ	Standard cumulative distribution function	
N	Axial force	
b	Ratio of height and length of the panel	
l	Length of the element	*m*
t	Thickness of the element	*m*
θ	Drift at the building scale	
μ"	Updated mean value	
μ'	Prior mean value	
σ"	Updated standard deviation	
σ'	Prior standard deviation	

[this page intentionally left blank]

LIST OF ACRONYMS

Acronym	*Definition*
AMB	Ancient masonry buildings
Ater	Azienda Territoriale per l'Edilizia Residenziale
BC	Before Christ
BBM	block-based model
CAD	Computer Aided Design
CB	Clay brick masonry
CD	Compressive diagonal test
CF	Confidence Factor
CM	Continuum model
CSM	Capacity Spectrum Method
DBM	Displacement-based Vulnerability method
DJF	Double falt-jack test
DL	Damage level
DPM	Damage probability matrix
DS	Damage state
EFM	Equivalent frame model
EMS-98	European macroscale
ENCEP	Ente Nazionale Combattenti Edilizia Popolare (
FEM	Finite element model
GBM	Geometry-based model
GIS	Geographic Information System
GNDT	Gruppo Nazionale Difesa Terremoti
HB	Clay blocks with vacuum range 45-65%
IACP	Istituto Autonomo per le Case Popolari
IM	Intensity measure
IMB	Improved-ancient masonry buildings
KL	Knowledge Level
LS	Limit state
MDOF	Multi-degrees-of-freedom
MM	Macroelement model
MMB	Modern masonry buildings
MSC	Mercalli-Cancani-Sieberg
MSK	Medvedev-Sponheuer-Karnik

NLDA	Nonlinear dynamic analysis
NLSA	Nonlinear static analysis
OSR	Overstrength ratio
PBA	Performance-based assessment
PDF	Probability density function
PMF	Probability mass function
PGA	Peak ground acceleration
PGD	Peak ground displacement
PGV	Peak ground velocity
QB	Quasi full bricks with cement mortar
PL	Performance level
RC	Reinforce concrete
RFI	Rete Ferroviaria Italiana
RS	Rubble Stone Masonry
RTM	Regional Technical Map
SAE	Società Anonima Edificatrice di Firenze
SC	Sensitivity class
SCH	High Sensitivity Class
SCL	Low Sensitivity Class
SCM	Medium Sensitivity Class
SDOF	Single-degree-of-freedom
SPWS	Strong-piers-weak-spandrels
TMDB	Tuscan Masonry Database
URM	Unreinforced masonry buildings
WPSS	Weak-piers-strong-spandrels
WWII	The second World War

1. INTRODUCTION

1.1 ASSESSMENT OF THE SEISMIC RISK IN URBAN AREAS

The assessment of the seismic risk of urban areas is an important task in many parts of the world. Seismicity affects several areas of the Earth with relevant ground motions. The combination of the intrinsic hazard of our planet, the vulnerability and the exposure of our cities increases the seismic risk which human being are subjected to (Martínez-Cuevas *et al.* 2017). The vulnerability of the urban stock is strictly correlated with the time of construction of buildings, based on economic and knowledge features. Nowadays, National and International (FEMA-356, EC 8-3) codes provide the necessary tools in order to verify the capacity of new constructions; however, the vulnerability of existing buildings is more difficult to be defined. In the existing stock, the safety of the places where people live, the houses, is primarily important (Dolce *et al.* 2020). For these reasons, the seismic assessment of existing buildings plays a crucial role in the evaluation - and mitigation - of the seismic risk. As regards Italy, the high seismic hazard is combined with rich and complex monumental goods and constructive traditions. The seismic codes, suitable to verify the structures to the seismic actions, became effective only recently; from a culturally point of view, for centuries, the probability of occurrence of a seismic action has not been considered. A huge number of existing buildings, in Italy, needs to be preserved, retrofitted and improved in order to assure the required safety standards, and to preserve the National and local history and traditions.

The earthquakes that occurred in Italy in the last decades (San Giuliano di Puglia, L'Aquila, Medolla, Accumoli) marked the vulnerability of stocks where people live (Augenti and Parisi, 2010, Parisi *et al.* 2012, Gl-INGV 2016); the majority of existing buildings was realized before the introduction of seismic codes and without a-seismic criteria. This vulnerability affects all types of buildings; however, masonry buildings, due to their number and age, deserve a particular attention. Nowadays, masonry structures still represent a large percentage of the urban fabrics. The most studied masonry structures consist of monumental historical buildings; they have a special value for their cultural and architectural importance and collected a significant part of research efforts and contributions. However, most part of masonry buildings is represented by residential ones; the assessment of these buildings is usually left to the will of the single owners, since they are too many to be faced by the Government. Nevertheless, in the last years, the Institutions promoted some renovation interventions, in order to improve the seismic performance of existing buildings, defining contributions and tax relieves (MIT2017, Cosenza *et al.* 2018). The post-earthquake damage scenarios of urban clusters like the city center of Amatrice, completely destroyed by the 2016 Central Italy Earthquake, pointed out that the vulnerability of

the single houses (and their relative urban aggregates) is not a private issue, related to the owners of each specific construction. In fact, it deals with the preservation and conservation of authentic historical centers, the conservation of the minor centers and the safeguard of the historical heritage of the human development in urban areas. For these reasons, the researchers are facing their assessment at the urban scale, in order to provide general and useful benchmarks for the assessment of single cases. Certainly, the heterogeneity of conditions, structural technologies and mechanical properties leads to a difficult comprehension of the collected building classifications and the related single representative case studies (Polese *et al.* 2020).

ISTAT database updated in 2001 shows that 61,5% of residential buildings has been realized in bearing walls; furthermore, although the great expansion of the last century, 19,2% of residential buildings have been erected before 1919. Since the constructions made before 1945 can be considered as "historical", historical masonry buildings represent 31,5% of all the existing residential ones (Metelli *et al.* 2017).

Looking at the database about the urban fabric, 80% of Italian districts are realized from more than 50% in masonry, while 44% of districts have a range of 75-100% of masonry buildings (Cartis 2014, Zuccaro *et al.* 2015). In the city of Florence, which represents the target of this Thesis, 24308 residential buildings of the total residential stock (31070 buildings) are composed by masonry structures (78,2 %), while just 4840 are composed by RC (15,5%) and 1'110 with different technologies (6,3%). Such information is shown in Figure 1.1.

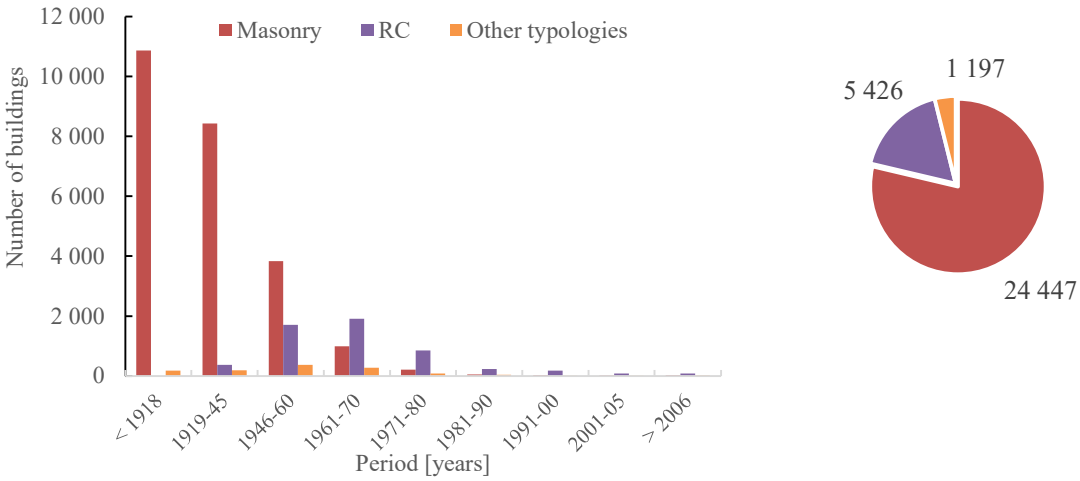

Fig. 1.1. Advancement of the number of buildings related to technological features in Florence.

In the last century, different studies (empirical, analytical and hybrid methods) have been carried out for a vulnerability assessment of urban stocks at urban scale. Empirical methods are the most basic ones; they reduce the computational costs analyzing the vulnerability based on statistic damage examinations of past earthquakes and achieving a consequent typological classification.

Analytical methods assess the damage with numerical analysis performing mechanical computational models; they demand an adequate knowledge of the structure and usually refer to individual structural units or specific building classes. Finally, hybrid methods start from the definition of buildings-types which are representative of different constructions, combining empirical and analytical techniques for an implementation of the empirical typological classifications with specific mechanical analyses. Computational costs of the assessment at urban scale are then limited to the evaluation of selected case-studies.

The research project deals with the vulnerability assessment of masonry residential interventions in Florence. This proposal is aimed at developing the urban seismic vulnerability by adopting a hybrid methodological approach. The latter joins the development of a database of buildings investigated by empirical approaches with the assessment of representative buildings with analytical techniques. The outcomes of the analytical methodology are finally extended to an homogeneous building class proposing simplified parameters able to represent the building capacity (and the relative vulnerability) of the stock.

1.2 Aims and Objectives

The main contents of this Thesis regard the seismic vulnerability assessment of the residential building stock of Florence, with a specific focus on masonry structures with RC slabs. In fact, despite the city of Florence is famous all over the world for its historical and artistic heritage, it is mostly constituted by external districts developed during the last two centuries. They have been realized by RC and masonry constructions developed through several interventions. Masonry structures are the majority of these buildings, characterized by regular configurations with modern masonry walls, rigid slabs and perimetral ring beams. Florence has been classified seismic zone only in 1982; therefore, most part of the considered population of buildings has been built without seismic criteria. It is worth noting that Florence is characterized by a medium seismicity (expected Peak Ground Acceleration, PGA, equal to 0.131 g for Return Period of 475 years and a soil type A); nevertheless, the last significant earthquake occurred only in 1895, therefore, the residential stock made in the XX century has never been hit by relevant ground motions. The masonry buildings realized in the last 100 years present common characteristics; in fact, in the XX century the constructive methodologies became more standardized than before. The masonry walls are generally constructed with artificial resistant elements such as clay bricks, but the most relevant issue concerning the global behavior consists of floors made of reinforced concrete slabs with perimetral ring beams. They cannot be considered as mixed masonry-RC buildings, as the reinforced concrete is only used for the perimetral horizontal elements; nevertheless, they present common features, especially referring to the in-plane seismic response of the structures (Correia Lopes *et al.* 2019). The typical residential building has an unreinforced masonry (URM) structure,

even if its behavior is affected by the RC slabs, so that it cannot be considered like the ancient masonry buildings. The presence of rigid diaphragms allows a box-behavior to the residential structures realized in this period. Due to the diaphragms, the local mechanisms are not common, and the entire structure participates to the structural performance of the building. Sandoli and Calderoni (2018) divide the unreinforced masonry structures in three classes, coming consecutively in the time. Ancient masonry buildings (AMB), Improved-ancient masonry buildings (IMB) and Modern masonry buildings (MMB). They consider the buildings from their capacity to resist to horizontal actions. While the first two types are referred to traditional masonry structures realized by empirical concepts (masonry buildings and wooden no-rigid slabs), in the first class the failure mechanisms are mainly activated by local phenomena. Considering the second class, the buildings, improved by punctual and light interventions (steel tie-rods connections) overcome the failures provided by out-of-plane actions involving the in-plane resistance of the structures. The general in-plane capacity of these structures is usually referred to a strong-piers-weak-spandrels behavior (SPWS). The behavior of such type of buildings can be compared to free cantilevers embedded at the ground level where the coupling effects are given by the spandrels. Finally, the third class is referred to modern buildings realized after the 1937. The latter are characterized by rigid diaphragms and ring beams that allows a real global behavior. In this third class, the out-of-plane mechanisms are avoided, and the in-plane capacities of the walls are involved. Considering the distinction made by Calderoni in the masonry structures, the buildings studied in this work lead to the latest class. These buildings, despite the box-like configurations, present an in-plane capacity mostly driven by the shear capacity of the walls. The ring beams divide the piers, promoting a weak-piers-strong-spandrels behavior (WPSS).

In this thesis, the targeted XX century residential masonry buildings have been selected within the public houses. The public housing interventions have been chosen as representative of the residential stock of the period because of the elevated number of realized constructions in the several external districts contextually developed. Indeed, a high number of public houses has been realized in Florence from the second half of the XIX century to nowadays, by different institutions. This assumption allowed the collection of the geometrical and structural features of several structures avoiding the economic costs and the time consuming of direct surveys.

The presented thesis starts from some of the last studies made over the Florentine urban stock, in particular, the SISMED Project, promoted by the University of Florence involving the Department of Architecture, the Department of Earth's Science and the Department of Statistics (Lacanna *et al.* 2016, Ripepe *et al.* 2018). It aimed to define the seismic risk of the city of Florence, considering the vulnerability of the urban stock, as well as the site-specific hazard of the area. The project was conducted in a GIS framework, and the first results defined empirical and simplified fragility curves for masonry and reinforced concrete (RC) structures. Nevertheless, throughout the project, the lack of knowledge resources in terms of urban stock have been

highlighted. Therefore, the presented thesis aims both to improve the knowledge about the structural characteristics of a buildings type, the URM XX century buildings, as to enhance the vulnerability assessment by means of mechanical analysis. As the first step of this thesis, a relevant investigation campaign has been conducted regarding the public masonry buildings made in Florence during the last century. Hence, selected a specific building class and a benchmark building, nonlinear static procedures have been selected to evaluate their seismic performance.

A seismic vulnerability assessment of the residential URM buildings in Florence is needed in order to point out the fragility of this heritage at the current state. During the INA-Casa period, the institution supported different didactic papers that explained how to build public interventions. They recommended architectonical typologies, residential aggregations and spatial distributions (Piano incremento occupazione operaia, 1949). The technical standardization of the XX century about elements and materials suggests to select single representative case-studies and to use them as starting point for of vulnerability studies at urban scale.

The project aims to analyze the seismic vulnerability of residential masonry buildings at urban scale using hybrid methodologies to represent a relevant part of buildings population through a limited number of case-studies. The development of a careful analysis of the masonry building stock represents a crucial issue still present, especially looking at the Italian context.

In Switzerland, a series of studies were conducted over the URM buildings with RC slabs proposing experimental tests and mechanical validation of elements and half-scale buildings. (Beyer *et al.* 2014, Beyer *et al.* 2015). Their contributions provide indications for the behavior of such type of structures, for the modeling approaches, for the code limits and retrofitting solutions, pointing out the needs of evaluation of such type of structures in the Swiss context.

Recently, Italy has developed the RINTC (-E) PROJECT 2015-2018 a joint ReLUIS-EUCENTRE research project to assess the (implicit) seismic risk of code conforming structures in Italy starting from building-types representative of the main building stock population (RINTC Workgroup 2018, Iervolino *et al.* 2018, Manzini *et al.* 2018). Concerning the public housing assets, some effort at the National scale dealing with the seismic vulnerability of public residential stock was already done (ISI, 2015). Recently, Calderoni *et al.* (2020) presented an overview about the damage assessment of modern masonry buildings after the L'Aquila earthquake, both including public housing interventions. The results point out a global behavior of these structures under seismic load, nonetheless, they also express a severe damage related to their reduced in-plane shear capacity. The research project of this PhD thesis aims to develop a study in this context, starting from a real site-specific database and pre-normative buildings.

The thesis is divided into two parts, adopting two different perspectives both enclosed into a hybrid approach. At the urban scale, the research mostly regards a cognitive study of the investigated area. A series of information has been collected, aiming to define the building

taxonomy of the XX century masonry stock, focusing on structural and mechanical features. At the building level, the adopted procedure follows the indications provided by the CNR-DT documentation regarding the probabilistic assessment of the seismic safety of existing buildings (CNR-DT212, 2013). The analytical part adopts theoretical assumptions presented in literature, and it aims to develop a probabilistic methodology, overcoming the limits of the National and International codes as regards the measurement of the probability of exceedance of each limit state. The performance-based assessment is herein based on equivalent frame models and the execution of nonlinear static procedure (pushover analysis). Both epistemic and aleatory uncertainties involved in the analysis have been considered. The epistemic uncertainties have been modeled through a logic tree approach; the aleatory uncertainties have been treated by a star design approach. Finally, the different assumptions have been assessed by means of sensitivity analysis, defining the influence of the different parameters on the seismic response. Sensitive studies are targeted to understand the main parameters influencing the seismic response, as well to set up further investigation protocols aimed to deepen the more sensitive features. Robust modeling assumptions have been used for the seismic analysis of the selected buildings. Finally, the thesis was targeted at selecting and calibrating simplified parameters to express the seismic performance of the investigated class of buildings. Such part of the work has been made through a displacement-based method following the mechanical approach available in literature and it allowed the seismic vulnerability assessment of a specific building class in the Florentine area.

1.3 Contents of the Thesis

The project deals with the definition of fragility curves referred to specific types of buildings, able to represent a significant percentage of the current historical masonry buildings population. The construction of fragility curves allows the evaluation of the expected level of damage for each considered seismic intensity. For each intensity level, in fact, the fragility curve represents the probability that the building exceeds an assigned threshold value. This methodology allows an increase of information regarding the seismic performance of the investigated building-classes. The significance of the obtained results is related to the effectiveness of the buildings classification, which should be detailed enough to account for the specificities of the considered buildings but general enough to cover a significant number of cases. In this work, the fragility curves were computed according two different approaches. At the building scale, on the selected case study, they have been analytically derived from the results of the mechanical analyses, which have been performed through nonlinear static analysis. At the urban level, the outcomes of the latter have been considered in order to extend the analytical results to a wider sample of buildings. Proper dispersion values have been defined for each direction of the analysis, for the different considered limit states. The dispersion took into account the capacity of the structure and the

seismic demand. The seismic input considered in the analysis has been assumed with reference to the National hazard classification for the site of the area, in the hypothesis of soil-classes compatible to the considered area, by selecting 30 accelerogram spectrum-compatible to the Code spectrum.

The contents of the thesis are developed as it follows. The first Chapter introduces to an overview regarding the seismic vulnerability assessment, the aims and the objective of the thesis. *Chapter 2* presents the Florentine case studies and the cognitive approach adopted to characterize the investigated stock. A significant number of information has been collected on the public housing interventions, including the age of construction, the adopted material and technology, and their historical contribution to the development of the city. In *Chapter 3* the methodology for the seismic vulnerability assessment is described. It deals with different scale of interest, unbalanced towards the analytical phase. *Chapter 4* is focused on the application of the cognitive phases to the investigated urban stock. This part regarded the data acquisition for the seismic vulnerability and the definition of the building class chosen for in-depth studies. *Chapter 5* is targeted on the analytical phase, which it concerns the application of the nonlinear static procedure and the derivation of fragility curves. In the last sections, evidences from the analysis are discussed; furthermore, some contribution is offered in terms of linear elastic procedure, through the discussion of the ductility *q-factor*. *Chapter 6* presents the hybrid implementation of the analytical results to a larger number of buildings. In this section the adopted parameters are introduced and discussed, expressing the variability of their response after a coherent application. Finally, *Chapter 7* presents the conclusive remarks of this thesis' work and further future perspectives to continue the research improving the outcomes for the seismic vulnerability assessment of the XX century URM in Florence.

[this page intentionally left blank]

2. URM BUILDINGS MADE IN THE XX CENTURY IN FLORENCE

In this chapter an overview about the outskirts of Florence is presented. Despite the City is known all over the world for its artistic and architectural heritage and as the *Capital of Renaissance*, most part of its urban stock consists of residential, and not relevant, buildings. Considering the urban growth of the city, the biggest part of the Municipality has been made during the XX century. Since the demolition of the urban town walls in the XIX century (when Florence became the capital of Italy) several districts have been erected in the external areas. These buildings, secondary of importance but primary for number, are still in use, and they require an assessment of their seismic performances.

The development of the Florence's outskirts has been affected by the new contents introduced by the Modern Movement. It concerned different urban configurations, with different interactions between the units. Specifically, comparing to the historic stocks, the new districts are characterized by regular structures. Each of them can be isolated or aggregated. In some case, the plan design of the outskirts in various areas of the town was done all together, realizing the different structural units at the same time.

In this chapter, the public housing interventions have been selected as representative of this residential stock. The public housing institutions promoted several interventions, for about 20000 apartments (Pierini, 2001). Nowadays, most part of these buildings have been sold and they are anymore included in the public provisions; nevertheless, the archive documentation of the projects is well-conserved and documented, able to provide the information needed for an *as-built* modeling.

2.1 URBAN DEVELOPMENT OF THE CITY

Florence was founded by the Roman Civilization in the I century BC, in a plain area close to the Arno river. The first core of the city was built over a geometrical grid with a square shape. During the centuries, different Town Walls hosted the growth of the city in the Medieval period, when Florence earned an important position in commerce and financial loans. The city grew in prestige and fame in the Renaissance period with the Medici court and its intellectual circle. During the centuries, important Monumental buildings, both religious and private, were built, establishing the exceptionality of its historical center. Nevertheless, from an urbanistic point of view, the city didn't grow and remained in the Medieval wall ring until the XIX century (Lopes Pegna, 1974).

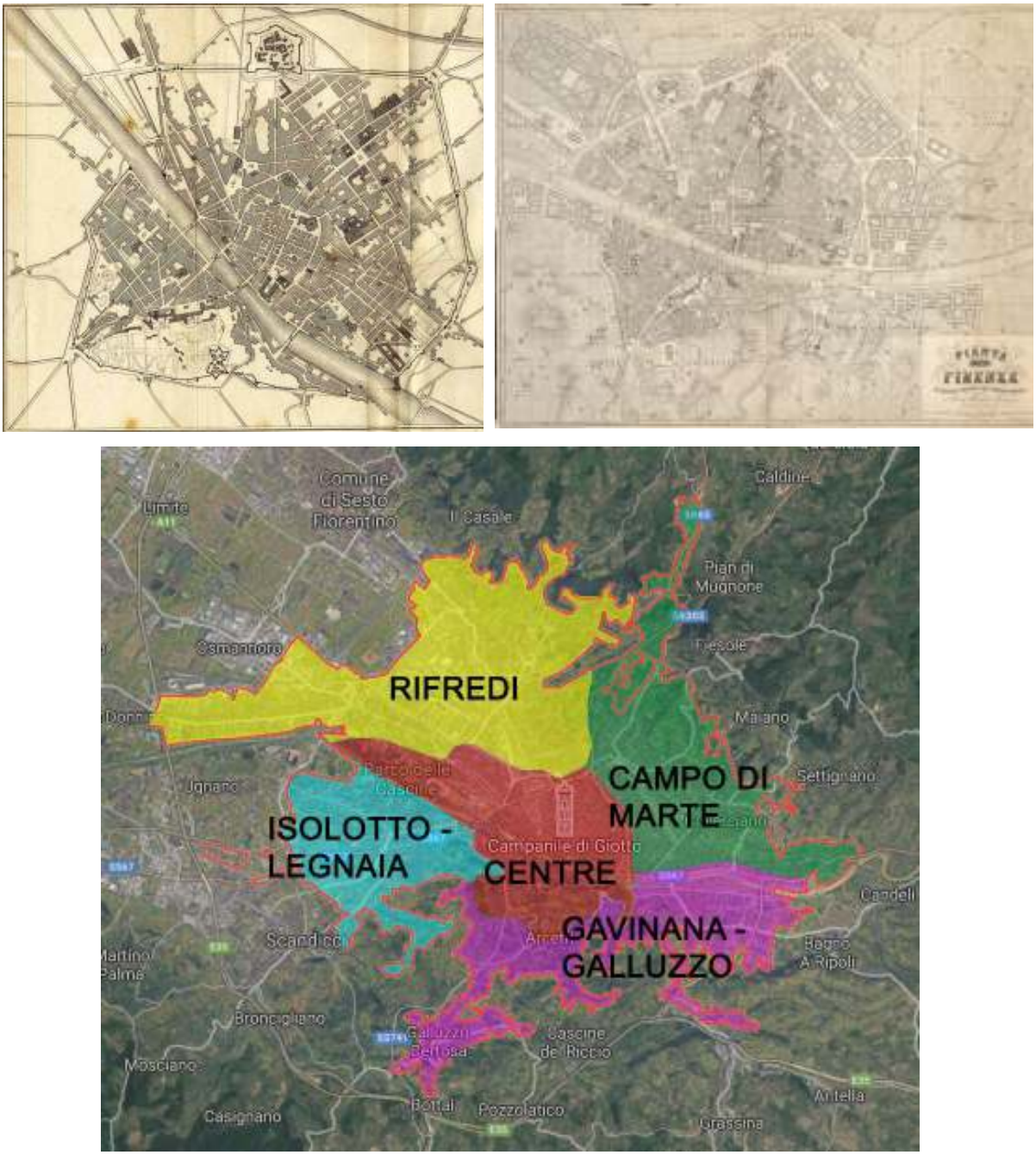

Figure 2.1 The Florence city maps. On the left: a1853 city map. The town was all enclosure into the town walls. On the right: the city in 1872; the town walls were demolished and new districts were born. (source: Repertorio delle Architetture civili, Palazzo Spinelli). Below: the Contemporary city with its main districts.

In 1865 Florence became the Capital of Italy; due to this event, new districts were designed, and the Town walls were demolished. Inspired by the Vienna's Ringstrasse and the Hausmann's Boulevards in Paris, an external ring of representative buildings was realized and the development of the city in the plan areas around started. This phase is represented in (Figure 2.1), where it is possible to compare the dimension of the city before/after the XX century. In that period, Florence grew in the East direction along the *Campo di Marte* area and in the West direction to the *Rifredi* area. The development of the city continued in the gap between the two WWs, with a saturation process of the existing outskirts. The post-war reconstruction marked a crucial point for the

development of the contemporary city (Marcetti et al. 2006). After the IIWW other new residential districts were planned, like the *Isolotto* and the expansion of *Novoli*. The urban plans of the 60's developed new areas of the city in order to host and manage industries and work activities with the residential districts (Fantozzi Micali et al. 2007). The last growths mostly regarded RC areas such as the suburbs of *Le Piagge* or *Torri a Cintoia*. Nowadays the city hosts over 380 000 citizens and it is the chief town of a metropolitan area with over 1 million inhabitants. In 1982 two important documents signed the future of its development. In this date, the city center was recognized by Unesco World Heritage; in the same times, the Government declared the municipality as a seismic zone (http://www.firenzepatrimoniomondiale.it , D.M. 19/03/1982).

2.2 The Public Housing Interventions

The public housing interventions were carried out to solve the housing problem which represented a large number of cases in the city. Since the XIX century many public housing interventions have been made. Due to their dimensions, they contributed to the transformation of the city in the external areas. According to Pierini (2001), more than 20000 apartments have been realized by Public Housing Institutions. Nowadays, they represent a not negligible percentage of the residential buildings made in Florence in the last century. These buildings precede the introduction of seismic codes; while they have been studied for social purposes and urban planning, their vulnerability have never been examined (Cardinali and Tanganelli, 2018). Furthermore, their projects are, customarily, more detailed and reachable than others, aside from being more "homogenized" than the private ones, as they have settled a standard in morphology and mechanical properties. Masonry buildings represent the most significant part of public housing population, characterized by constructions realized until the early '60s. In this work the archive research played a crucial role in the data acquisition for the following analytical phases. In fact, due to the urban scale aim of the project, a specific survey of each structure would be unsustainable. Hence, the project considers the acquisition of geometrical and structural information provided by the archives of the Public Housing Institutions. The realized buildings are modern, and the produced documentation is still available. The comprehension of the available documentation and the common features of the buildings passed through the study of the historical evolution of the public housing interventions in the city of Florence, which is presented in Section 2.2. For the mechanical properties, a site-specific implementation of the mechanical properties provided by the code was made through a Bayesian approach. This has used the data obtained by the Tuscany Masonry Database (Boschi *et al.* 2015) for the same typologies of masonry. The specific methodology is presented in Section 2.4.

Concerning the historical evolution of the public residential constructions in Florence, the first public housing interventions in Florence are dated back to 1848 when the *Società Anonima Edificatrice di Firenze* (SAE) was created. It aimed to realize houses for the working classes. They contributed to the realization of several buildings characterized by the adoption of regular block types with internal courtyards, such as the buildings in *S. Gallo*, *Borgo Pinti*, *via del Campuccio*, *via della Mattonaia*, *S. Niccolò* and *S. Jacopino* (Gobbi Sica, 2006). In 1885 the *Comitato per la Case ad uso degli indigenti* was promoted. Starting from 1911 they realized 14 interventions of residential buildings, hosting 342 houses (Pierini, 2001). The standard building of the period consisted of a big regular block. In 1912 the Railways started to promote housing interventions for their workers, realizing several aggregates.

In 1909 the *Istituto Autonomo per le Case Popolari* (IACP) was created. It has been the main promoter of public residential interventions in Florence and the one that, switching into *Ater* (*Azienda Territoriale per l'Edilizia Residenziale*) in 1986, today is still managing the public properties. Nowadays it is called *Casa S.P.A*. IACP, since the first realizations proposed different buildings types, alternating the block types, also called *barrack buildings* (via Rubieri, via Zanella, via Bronzino) with linear typologies proposing different spatial configurations (via Erbosa, via Annibal Caro, via Circondaria). From the 20s, IACP led different projects over the architectonical types (Metelli, 2016). In this period, the ampliation of the via Erbosa stock was made, and the village of minimum houses in via Carlo del Prete was realized. In the 30s, the *Ente Nazionale Combattenti Edilizia Popolare* (ENCEP) planned several interventions in the peripheric areas of the city. The interventions suffered an interruption after the Fascist period and caused the failure of an important residential project located in *via Antonio del Pollaiolo*. The public housing activities restarted only after WWII, thanks to the INCIS interventions and the INA-Casa plan. Particularly, the INA-Casa (and, later, Gescal, the association which replaced it) promoted an exceptional number of public housing interventions in the 50s. The Isolotto district, aimed by La Pira major, is the most emblematic intervention, for the dimensions, the theoretical contributions and the architects that followed the design of the buildings. After INA-Casa, the building activity slowed down (Bettio and Romanelli 2003). In the 60s, the public housing continued in the new areas localized by the new city urban plan dated 1962. After that, the public interventions will be constituted only by RC buildings. The expansions regarded *Torri a Cintoia*, *Le Piagge* and other areas like *Mantignano* or *Rocca Tedalda*.

Nowadays, most part of this heritage has become private, given to the tenants through hire-purchase procedures. Nevertheless, a public housing institution, *Casa SPA*, still exists and it manages over 12000 residential units scattered over 33 municipalities of the Florentine hinterland. The project and constructions office of the company has been partially involved in the present

project; they allowed the access some existing structures where some visual inspections of the interior parts and some experimental tests have been performed (Palermo *et al.* 2019).

In this section, an overview about the performed archive research is shown. The research concerned different catalogues in Florence (Archivio Ater/Casa SPA, Archivio Storico del Comune di Firenze, Archivio delle Ferrovie dello Stato) and has identified a relevant number of projects of residential buildings. For each project, the definitive design related by technical specifications and quantity surveying of materials has been researched. The level of information is quite heterogeneous and not always the same, depending by catalogue, the contractor society, the years of constructions and the researched intervention. The *Ferrovie dello Stato* records are exceptional documents for the quantity and the quality of specifications and details. In Figure 2.2 some representations of the documentation found in the archives are presented. A rapid overview of the archive collections is finally presented in Table 2.1. Herein, the documentation is listed within the different archives, describing the information found in terms of textual contents and drawing ones. The latter are divided between the main structural elements composing a building: foundations (F), walls (W) and slabs/roofs (S).

Fig. 2.2 From top left: public housing in via Manni, D'Orso, Gelli (1930), Carlo del Prete (1930) and in via Erbosa (1934). Below interventions in piazza Terzolle ('30s), Isolotto ('50s), via Baracca ('50s) (Source IACP/Ater archive, Fantozzi Micali *et al.* 2007).

Table 2.1. Overview of the archive collections investigated for this work

Archive source	Period	Technical documentation		Drawings	Drawing details
IACP / Ater	XIXth century	Literature documentation; aerial views, photos of the interventions	F	/	/
			W	/	/
			S	/	/
	IACP 30s	Literature documentation; aerial views, photos of the interventions	F	/	/
			W	●	/
			S	/	/
	INA-Casa/ Gescal (‘50s-‘60s)	General relations; tender specifications; metric computations	F	/	●
			W	●	●
			S	●	/
Ferrovie dello Stato	RFI – between the two WWs (20s-50s)	General relations; tender specifications; metric computations, site quantifications	F	/	●
			W	●	●
			S	●	●
Archivio storico	30s	/	F	/	/
			W	●	/
			S	●	/
	INA-Casa/ Gescal (50s-60s)	/	F	●	/
			W	●	/
			S	●	/

2.2.1 IACP / ATER di Firenze Archive

This Archive is the main reference of this research. Despite the loss of part of the documentation due to the flood of Florence in 1966 and to a fire, it hosts the documentation obtained by several institutions ended in the IACP (Ratti 2001, Bettio and Romanelli 2003). It includes the documentation of over 100 years of public housing in Florence. The archive is well documented, especially for the *INA-Casa* period. The oldest projects have been lost but some design can be obtained through the IACP publications and the private documentation of the head engineer of the Institution, Carlo Burci (IACP Firenze 1932, Istituto per le Case Popolari in Firenze, 1932) (Figure 2.3).

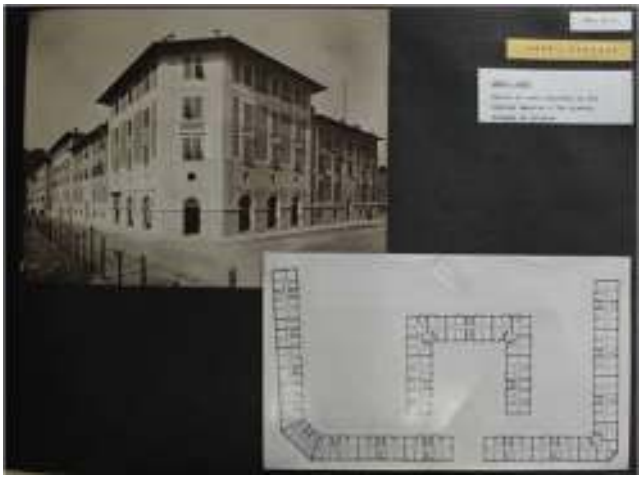

Figure 2.3. Public housing in via Zanella/ via Aleardi. Published project by the head engineer of IACP, Carlo Burci. (source IACP/Ater archive).

Regarding the interventions, the documentation here located may provide a good level of information. For the INA-Casa buildings, the rows of the different projects provide a general report, including the tender specifications and the metric computations. The drawings are generally represented in 1:50 scale. Regarding the slabs, the direction of the beams is generally not specified and information regarding the steel bars in the concrete ring beam are missing. In Figure 2.4 some drawings of the archive are presented. Specifically, for the INA-Casa buildings, it is not common to find executive documentation or reports from the construction site. That documentation is presented in the section Drawing rolls. They host only the drawing of some project in which most part of the documentation has been lost. Nevertheless, there are also "measurement plans" which are executive drawings referred to the masonry typologies and the concrete elements. For this reason, the checkmark in Table 2.1 has been done.

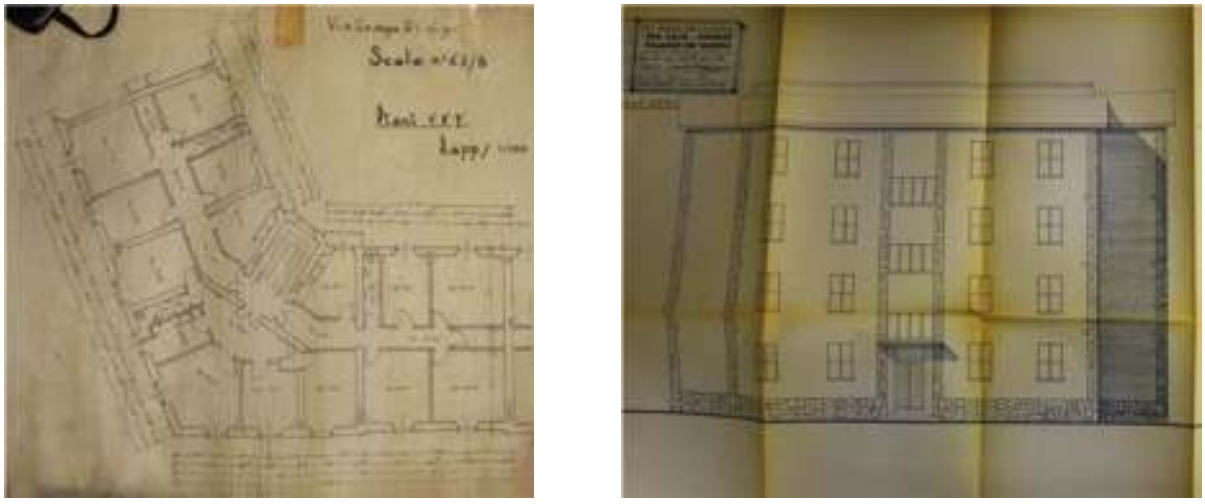

Figure 2.4. Left, bilding plan for a project in via Campo d'Arrigo. On the right, façade of a building in the Isolotto Area (source IACP/Ater archive).

2.2.2 Archivio Ferrovie dello Stato – ex Direzione compartimentale di Firenze

The archive of the Italian Railways hosts the documentation produced by *Ferrovie dello Stato* from the end of the XIX century. It is divided between the two main companies constituting the group, *Ferservizi Spa* and *Rete Ferroviaria Italiana* (RFI). Since the documentation provided by *Ferservizi* contains only bureaucratic parts concerning the acquisitions of the areas and the permissions, the real archive part is hosted by RFI. Here the technical part may be found. The Railways had the Government permissions to construct over their areas without licenses from to the municipalities. For this reason, the technical part is very accurate and

characterized by an executive documentation instead of a definitive one. The drawings are orientated towards the realization of the houses and they are rich of details concerning each part of the work. Specific information for the lintels over the openings are shown, as well as the number of steel bars in the RC elements and their shape. The technical typologies are similar to the ones found in the *Ater* archives but richer of information that could be extended to the entire residential stock of the period. Nowadays *Ferrovie dello Stato* company sold all the houses that they realized in Florence during the years, therefor they became private properties. In Figure 2.5 the executive drawings found in the archive are presented. For further information please see Cardinali and Tanganelli (2018).

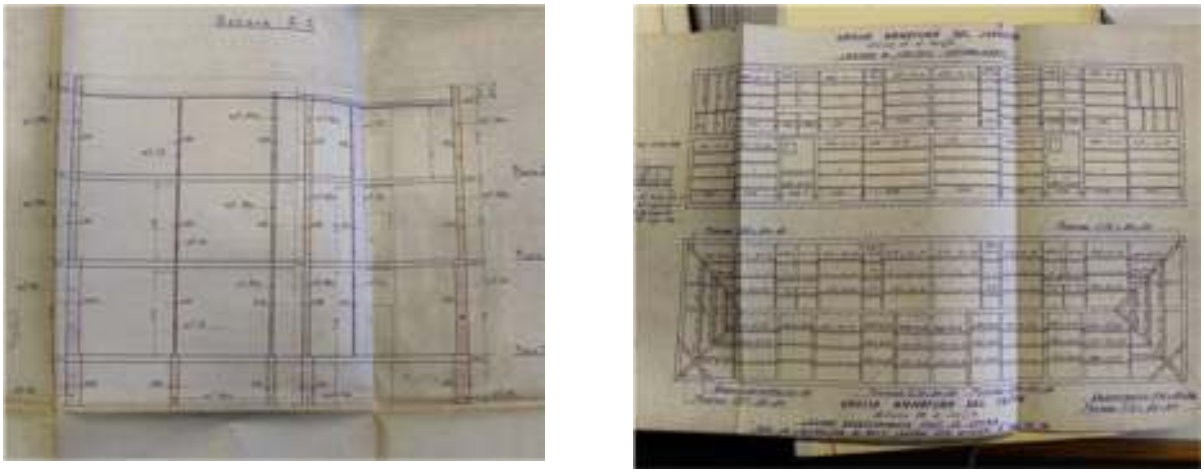

Figure 2.5 Executive section for an intervention in via Centostelle (1949); the different colours indicate the different masonry typologies in the building. On the right; executive drawings for a wooden roof in via Paesiello (1946) (source RFI archive).

2.2.3 Archivio Storico del Comune di Firenze

This archive was instituted in 1781; it hosts the material presented by different companies and owners to the municipality. Namely, the projects realized by privates or institutions were deposited to the City Hall, which it allowed (or not) the permission to realize the interventions. Then, a private copy of the projects remained to the owners of the areas; in case of the public housing interventions, these copies historically fed the archives described in the previous sections. However, a particular correspondence between the project found in the Archivio Storico and the private archive does not exist. One of the most documented interventions is the realization of the *Isolotto* suburb. Within the stored documentation, a digital archive with the only drawing was created (Bertocci 1998). Here it was possible to find the projects of some interventions not found anyplace else, like the residential stock realized in *via Forlanini*. In the Archive it is possible to find information concerning residential complexes realized by construction cooperative societies. Their birth aimed to

provide for specific social categories (Aquilani *et al.* 1979). In 1908 in Florence, there were 25 different societies and they had already built 192 houses.

2.3 BUILDING TAXONOMY: EVIDENCES FROM THE RESEARCH

The conducted archive research allowed a technical characterisation of the masonry Public Housing interventions, and more in general, of the modern masonry residential stock settled in Florence. Considering the obtained full database of public housing intervention, the most part of the buildings have the ground floor detached from the soil level. The 90.67% of the database has a detached ground level. They can be divided into the 42.16% of the stock, just presenting a ventilation floor under the soil level (A-type), and a 48.50% characterized by an underground floor (B-Type). Only the 9.33% of the database doesn't have the ground floor, with the structure directly located over the ground (C-Type) (Figure 2.6). An overview about the structural components of the building is proposed in the following sections.

Figure 2.6. On the left: classification of the database from the relationship of the building levels with the soil. On the right: an example of public house with underground cellars.

Foundations. These building types usually present linear continuous foundations. Their role is the stress transmission from the bearing walls to the soil. The Foundation of masonry structures are usually continuous because of the linearity of the structural elements constituting the structure itself. Materially, they used to be realized through masonry foundations, concrete / inert-materials foundations. In minor cases, they can be realized by RC structures. The first two techniques represent the oldest ones and the most adopted too, where the deeper layers are characterized by compact material stressed by normal actions. The introduction of the RC elements at the basis of the walls allows the definition or wider foundations, able to transmit the vertical action to the wings of the basement thanks to the shear capacity of the steel bars. In the investigated buildings several foundations realized with constipated concrete have been found. Basically, a larger rectangular (or constipated masonry or concrete with inert material) is at the base of the foundation wall, characterized by a larger thickness than the upper structures. The clarification about the materials adopted in the

foundation system is provided by the technical documentation attached to the design. The excavation was usually punctual for the basement of the foundation, then the following layer grew in height. The excavation dimension was about 50-60 cm under the ground for the larger bearing structures. Following the classic scheme, they are usually 20-30 cm larger than the superior walls. In case of RC foundation some rectangular basement around 150 cm has been found. In Figure 2.7 some example of foundations found in the archive documentation is presented.

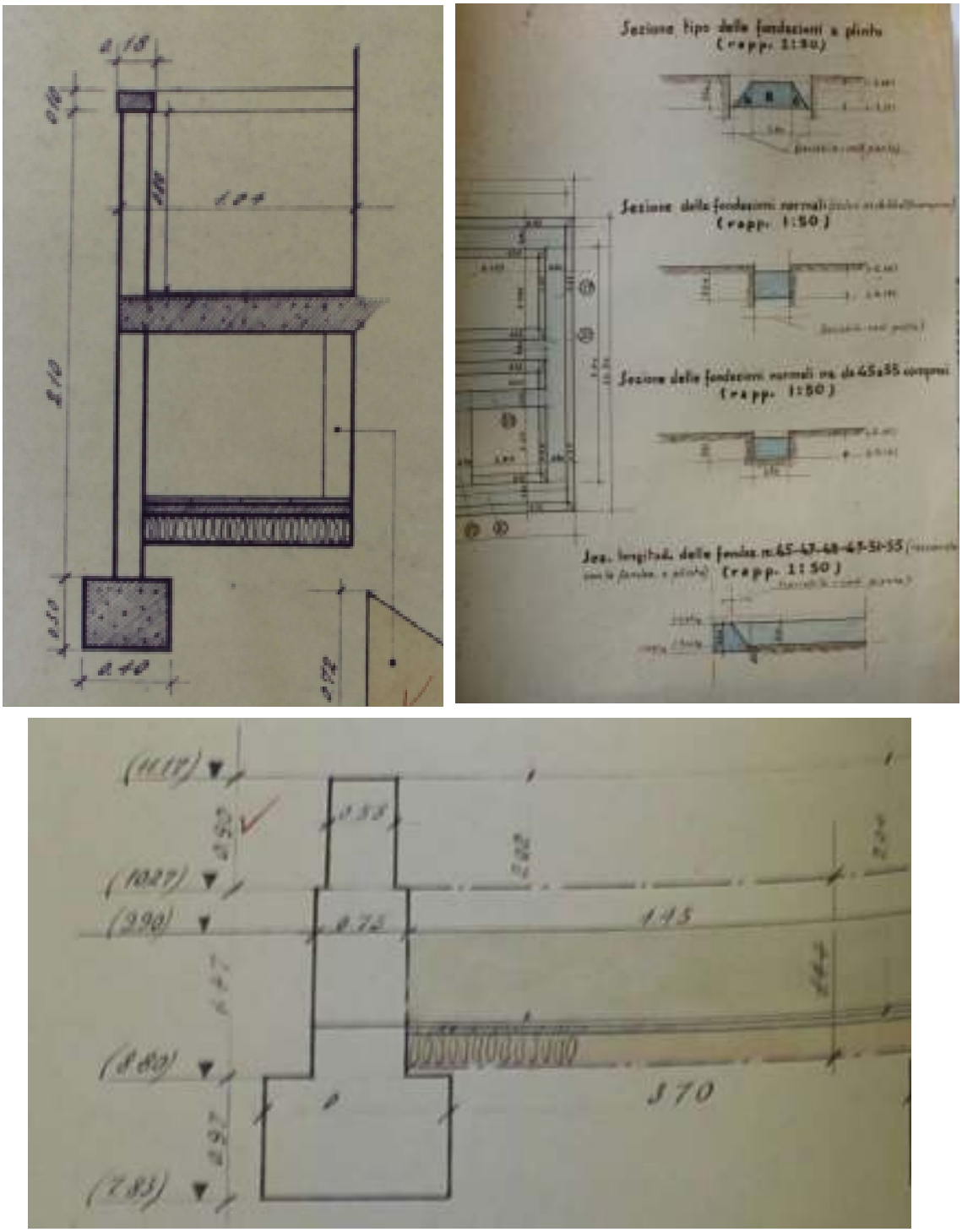

Figure 2.7 Details for the foundations of the investigated masonry buildings (source RFI archive).

Bearing walls. The bearing walls present common rules. Since these buildings are assimilated as URM structures, their technical system follows ancient and proven schemes. In the XX century the masonry structures were realized adopting common features for the good art of construction. Specifically, the investigated buildings present good empirical treatments. The bearing walls have structural continuity from the foundation of the building to the last level.

The masses are coherently distributed along the height. The perimetral walls of the lower levels are realized by rubble stone masonries; at the upper floor the thickness of the walls decreases and they are generally realized by artificial materials. The latter can usually change from solid clay bricks to hollow masonry types. The rubble stone masonry of the lowest floor can be enriched by courses of clay bricks; they are targeted to align horizontally the masonry and distribute homogeneously the loads. The rubble stone panels are composed by irregular stone elements joint with hydraulic mortar. The horizontal courses are usually 1 meter spaced. Specific attention to the corner connection may be found, but this is an evidence obtainable with visual inspections rather than from the archive documents. At the upper floors, in some case, when the bearing walls were constituted by hollow clay bricks, a bad disposition of the resistant elements was found. Namely, the internal partitions in the artificial elements have been found disposed along the horizontal direction instead than the vertical one. Nevertheless, some shrewdness for the connection slabs-walls was found, by the disposition of an horizontal layer of solid clay bricks under the concrete ring beam. In Figure 2.8, some examples are shown.

Fig. 2.8. On the left: drawings from RFI Archive, details of masonry structures. On the right: removal of the plaster layer to check the material constituting the walls; a non-optimal disposition of the hollow clay elements was found.

For what concern the variability of the walls, the 52.7% of the buildings has the perimetral walls with a variable thickness, while the 47.3% have a constant thickness. Basically, these data are related with the total height of the structures. Low buildings, ranging between one

and two floors more likely present a constant thickness of the bearing walls. On the other hand, buildings with three, four or more floors tend to have recesses in the thickness of the walls. It is worth pointing out that the obtained data suffer of some uncertainty tending for the variable thickness of the bearing walls; in some case the plans found in the archives are not the deposited projects but just cadastral references to the contracts, with no quotes in the drawings. Since the plans, except for the thickness of the walls, were the same at each level, it is reasonable assume that they could have used the same plan for each contract, without having the accuracy of putting the real plan for each document. So, for a minority of buildings that present the constant thickness of the walls, this aspect could be in-depth investigated. Moreover, the obtained archive research database contains also terraced houses with a maximum height of 2 storeys. Removing this latter class from the database, it counts 36.73% of the buildings as A-Type, 53.06% for B-Type and 10.21% for C-Type. Concerning the thickness of the walls, the 57.89% has a variable thickness with the bearing structures characterized by recesses, only the 42.11% is made of constant buildings. In Table 2.2, a brief resume of the characteristics of the investigated buildings is shown.

Table 2.2. Building features; ventilation floor and thickness of the bearing walls.

	A-type	B-type	C-type	Variable	Constant
Total	42.16%	48.50%	9.33%	52.7%	47.3%
No terraced houses	36.73%	53.06%	10.21%	57.89%	42.11%
3 storeys	54.76%	26.19%	19.04%	50.00%	50.00%
4 storeys	23.07%	75.82%	1.09%	78.82%	21.17%

Slabs. The floors are realized through RC joists alternated with hollow clay elements, topped by a 4-cm concrete slab. The hollow bricks can have different shapes that can lead at different distances between the joists. This represents a common technology for slabs in Italy. They are called *solai in latero-cemento* which corresponds to mixed slabs; the thickness of the structural part is around 16/20 cm. In the first configurations the beams were reinforced only by the presence of a steel bar in the inferior part in order to get the tensile stress. In the further configurations, three bars per beam were designed, two below and one in the upper part. The superior slab of 4 cm was usually reinforced with a crossed steel fence, otherwise characterized by only concrete. Over time, the presence of steel fences became the practice trend, due to its capacity of distribute the stress and reduce the planar deformations.

The terraces of the buildings, when they are realized inside the building shape through the definition of loggias, they follow the same rules; in case of ledge terraces, they are mostly obtained by unique RC slabs. The connection between the slabs and the vertical elements (the bearing walls) is guaranteed by the presence of RC ring beams all over the main structures.

Unfortunately, for both slabs and ring beams a lot of information about the steel bars of the RC elements were not available. A detailed quantification of the steel bars was present for the Railways buildings (*RFI archive*). In that buildings, the documentation showed the presence of 4 bars ϕ14 in the perimetral ring beam; moreover, ϕ14 and ϕ10 were used for the reinforce of the slabs. The brackets had a dimension of ϕ6/20-30 cm. Concerning the ceilings, they are used for crawl spaces where there are not live loads. Sometimes they are realized with the same technology but lower (12/16 cm) depth, otherwise they are composed by steel beams alternated to hollow tiles generally without concrete slab. In Figure 2.9 some example both concerning drilling tests performed over the buildings, both technical details about the slabs realization are shown.

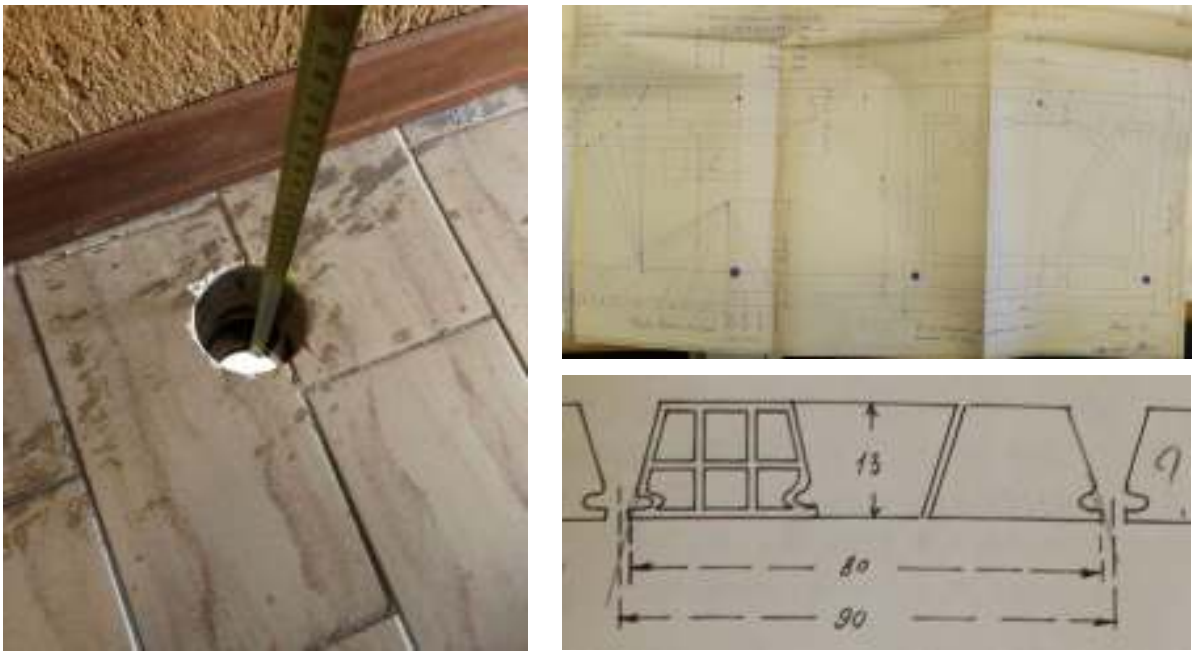

Fig. 2.9. On the left: drilling test for the check of the slabs of the terraces of the public houses. On the right; two technical drawings referred to the realization of the mixed-RC slabs (source RFI archive).

Roofs. Roofs are generally made through wooden beams covered by wooden planks and roof tiles; sometimes, they are composed by prefabricated RC joists (Varese joists or similar), hollow tiles and finally hollow roof tiles. Normally, the crawl space has the concrete kerb over the perimeter of the building and it is joined with the level floor, while the roof structure is not linked with the concrete ring. In Figure 2.10 some technical drawing about the structural details of masonry walls and slab elements is shown.

Stairs. Stairs are usually located in the central position of the building, in order to distribute mutually to several apartments. They are realized mostly by cantilever structures jointed to the masonry walls. They can be done by pre-fabricated steps or by RC elements cast in-situ or made of grit (Figure 2.11).

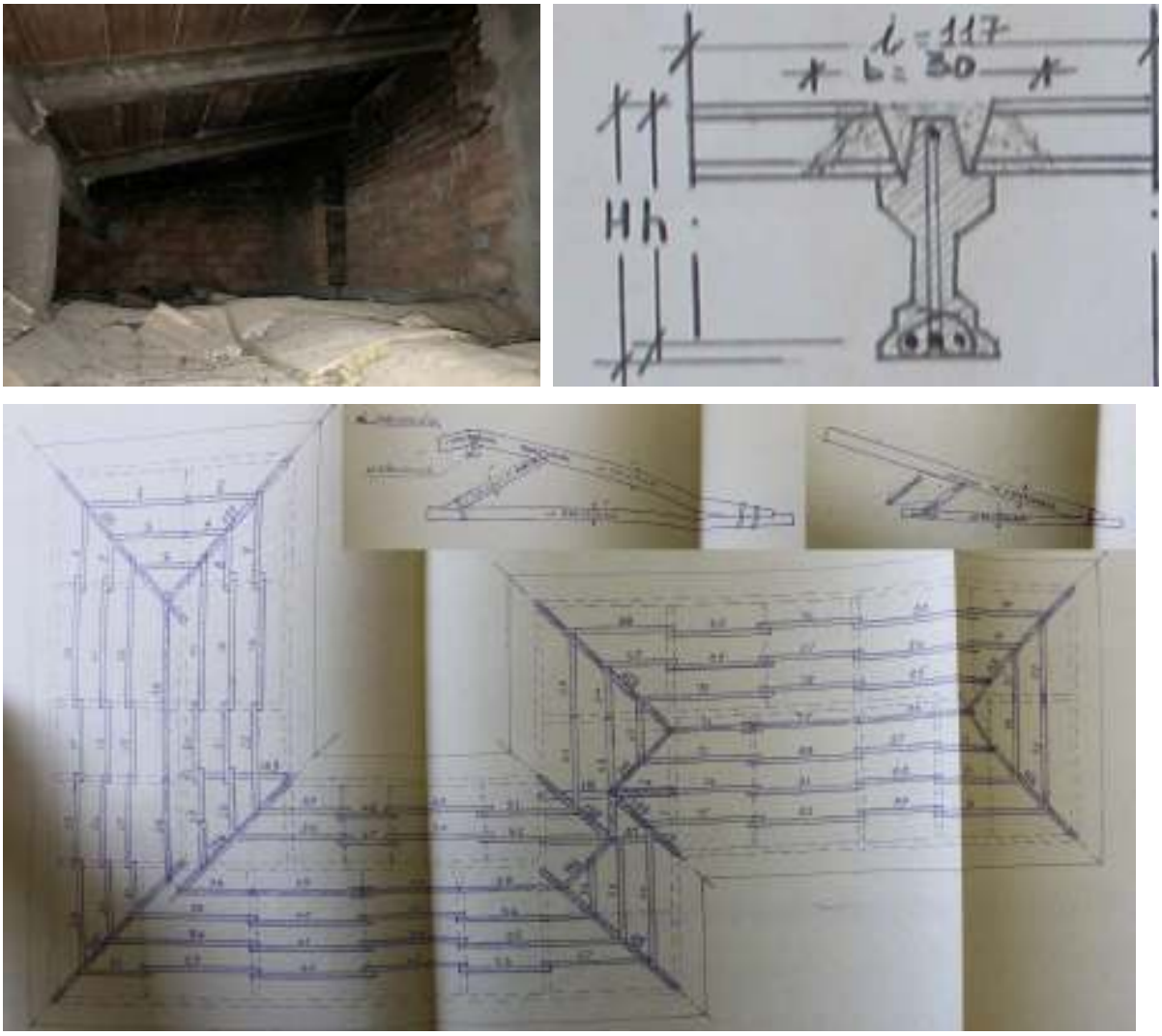

Fig. 2.10. Top on the left: the attic floor with the RC beams sustaining the roof. On the right: detail drawing of the Varese joist for the roof. Below: timber roof structures. (Source RFI archive).

Fig. 2.11. On the left: an internal stair distributing to two apartments for floor. On the right, up: detail of the connection of the steps into the masonry wall; below: drawing of the steps of a stair.

2.4 MECHANICAL PROPERTIES OF THE MATERIALS

In this section the mechanical properties of the materials adopted in the investigated buildings are presented and discussed.

Masonry. Concerning the mechanical properties of the materials, this work started from the mechanical values proposed by the Italian codes in case of existing buildings. The characterization of the mechanical values of materials is a complicated task, especially referred to masonry structures. The latter depends not only on the quality of the material in itself but it involves the disposition of the elements and the personnel qualifications during the executive phase. Nowadays the Italian codes (MIT 2009, MIT 2019) provide mechanical parameters for different existing masonry typologies of the peninsula. The codes present range of values for different properties and they recommend, based on the Knowledge Level (KL) achieved, which value is statistically the most reliable to adopt. It is worth noting that the values presented in the codes are the worst values for the considered typologies. As reported in MIT2019 (C.8.5.3.1) they are referred to masonry walls in specific conditions: lime mortar with moderate mechanical characteristics (0.7-1.5 MPa), no horizontal bricks planes, drawn closed sides or bad-jointed faces, element disposition in a workmanlike manner (just for regular masonries), non-consolidate masonry. Based on the existing condition, a Table, referred to ameliorative coefficient is presented too.

As known, in the seismic vulnerability assessment of the existing structures, the Knowledge path plays a crucial role, both for the definition (and the comprehension) of the structural system, both for the characterization of the mechanical properties of the adopted materials. For the case of masonry buildings, an expert judgment, based on the survey and the inspection of the investigated building, can be able to detect the structural organism and propose the most reliable analyses for the examined conditions. A qualitative judgment can be also done concerning the quality of the masonry structures and their seismic behavior, nevertheless, without invasive tests, nothing can be said about the values of the mechanical properties involved. For this reason, the KLs and their relative Confidence Factors (CF) entered in the codes. Therefore, despite the performance of invasive tests in order to define the mechanical properties of the masonry walls is the most recommended method to characterize the masonry walls, their use in engineer practice is limited, because of their high costs of execution, their invasive issues and the needed of at least one test for each masonry typology involved in a construction. Several non-destructive and minor destructive techniques (NDT and MDT respectively), calibrated on the results of the destructive ones have been defined. Nonetheless, their application is still not recognized by the code, confining their usability to academic researches and cultural heritage contexts. Aiming to study a class of building at urban scale through an hybrid procedure, the mechanical properties involved

in the analysis have to be enough detailed to be reliable, but also sufficient general to be shared with the different structures.

In this work, the initial mechanical values have been updated through a Bayesian approach. The starting mechanical values are obtained by the Italian code, which has been considered for the initial values for each masonry typology. Hence, they have been updated through the use of *in-situ* values experimentally defined in Tuscany. First of all, the most recurring masonry typologies presented in the investigated buildings have been selected. For these typologies, the mechanical values and their probability distribution coming from MIT2019 have been assumed. Then, the mechanical data have been implemented taking into account the experimental tests executed in the Tuscan Region for the same typologies of masonry.

Bayesian approaches have been introduced by the Scientific Community, due to the fact that they allow the update of the starting values, based on the implementation of new samples over a prior distribution (Bracchi et al. 2016.; Milosevic et al. 2018). The last MIT2019 has recently implemented these concepts in the updating of mechanical values. In Table 3 the ranges of values for the mechanical properties of the masonry typologies identified for the XX century URM building stock are shown. As presented in Section 2.2.2, the *rubble stone masonry* and *clay brick masonry* are identified for the external bearing walls of the structures. Hollow clay bricks can be also be found at the upper levels, as presented in Figure 3.8. Referring to the quasi-full bricks with cement mortar, this class has been considered for some partition wall. Moreover, the concrete clock typology has been taken into account, since it came out in some in-situ investigation made during this research.

Table 2.3. Prior values: minimum and maximum ranges defined by the Italian codes for the mechanical parameters of different masonry typologies.

	f_m (Mpa)	τ_0 (Mpa)	f_{v0} (Mpa)	E (Mpa)	G (Mpa)
Chaotic rubble stone masonry	1	0.018	-	690	230
	2	0.032	-	1050	350
Clay bricks and lime mortar	2.6	0.05	0.13	1200	400
	4.3	0.13	0.27	1800	600
Quasi-full bricks with cement mortar	5	0.08	0.2	3500	875
	8	0.17	0.36	5600	1400
Concrete or clay blocks (vacuum range 45-65%)	1.5	0.095		1200	300
	2	0.125		1600	400
Semi-hollow concrete blocks	3	0.18		2400	600
	4.4	0.24		3250	880

In Table 2.3, the elastic moduli of the masonries (Elastic Young's Modulus E and Shear Modulus G, respectively) are shown; finally, f_m expresses the compressive strength of the material, while f_{v0} and τ_0 are referred to the shear capacity. The MIT2019 consider alternatively two types of shear

failure, the Mohr-Coulomb criterion (Mann and Müller 1980) and the Turnsek and Cacovic one (Turnšek, and Cacovic 1970, Turnšek and Sheppard, 1980). Until the last seismic code of 2018 (NTC2018 and MIT2019), only the Turnsek and Cacovic criterion was considered. The introduction of both mechanisms has been recently done, after the evidences in masonry buildings provided during the Emilia Romagna seismic sequence. The first one, expressed by the coefficient f_{v0} is generally activated by the disposition of the resistant elements along the short face, which generates a slight vertical misalignment and ladder ruptures. It is based on the cohesion of the resistant elements and their friction coefficients. The Turnsek and Cacovic criterion instead, expressed by τ_0, is more reliable in case of irregular structures and where the textures of the masonry lead to a proper engagement of the elements. In this work, the second criterion has been considered and estimated as the most reliable for the studied masonry types. In fact, in the clay brick masonries of the Tuscany area the resistant elements are usually disposed along the long face, which it hardly leads to damage patterns through the mortar layers.

Starting from the values presented Table 2.3, the Bayes' inference based on the Bayes' theorem is used to update the initial probability distribution by introducing a sample of experimental values. Given the prior normal distribution of values (set on a mean value and the standard deviation of the sample), the update of values follows the proposed equation:

$$\mu'' = \frac{(n\bar{X}+k\mu\prime)}{(n+k)}; \qquad \sigma'' = \sigma' \sqrt{\frac{nk}{n+k}} \tag{2.1-2.2}$$

Where n is the number of tests, $\bar{X}$ the mean value of performed tests and μ' represents the mean value obtained by the code range; k represents a coefficient provided by the MIT2019 that considers the ratio between variance of performed tests prior distribution variance. (Simoes 2019). Different k values are proposed for several experimental tests.

For the experimental tests, the data contained into the Tuscan Masonry Database (TMDB) published by Boschi *et al.* (2018) have been used. The latter contains a wide number of experimental tests performed in the Tuscany Region during the last decades by different research institutions. The mechanical values for the implementation have been selected between the tests performed over wall panels made during the XX century for the same masonry typologies. Data of experimental campaigns have been found for all the masonry types considered except the semi-hollow clay blocks, for which the code values have been used. In Table 2.4 the experimental tests adopted for the mechanical value upgrade for the chaotic rubble stone masonry are shown (*DFJ* is double flat-jack test, *CD* diagonal compression test, *C* compression test; f_m for compressive strength, τ_0 shear strength, *E* Young Modulus, *G* Shear Modulus). The number of the different tests (MP062, CD005) are referred to the names coded in the TMDB. For sake of brevity, the other parameters are presented in the final Appendix (Appendix 2).

Complexly, 27 CD tests, 11 DJF tests and 2 C tests have been used. The Compression Diagonal tests provide information about the Shear Modulus G, and for the shear strength τ_0. The Double flat-jack tests and the Compressive tests provide results for the Elastic Modulus *E* and for the compressive strength f_m. The results of the updated values are shown below. (Table 2.4).

Table 2.4. Rubble stone masonry, Bayesian approach.

			f_m (MPa)	cov	τ_0 (MPa)	cov	E (MPa)	cov	G (MPa)	cov
Chaotic rubble stone masonry	*prior*	MIT2019	1.5	0.33	0.025	0.28	870	0.21	290	0.21
	DJF	MP062					2174			
	CD	CD005			0.025				284	
		CD006			0.038				232	
		CD007			0.032				338	
		CD008			0.036				106	
		CD009			0.022				43	
		CD014			0.03				566	
		CD015			0.039				360	
		CD016			0.031					
		CD017			0.044				629	
		CD018			0.024					
		CD019			0.023					
		CD020			0.023					
		CD021			0.069				407	
		CD028			0.042					
		CD029			0.058				1236	
		CD030			0.023				933	
		CD031			0.041				267	
		CD037			0.025				272	
		CD050			0.023					
	C	C109	1.04				322			
		C110					456			
	mean		1.04		0.03411		984		436.385	
	updated		1.270	0.278	0.034	0.203	970.47	0.158	421.24	0.165
			1.270	0.278	0.034	0.203	1263.72	0.165	421.24	0.165

The final updated values for the different identified masonry typologies are shown in Table 2.5. Figure 2.12 shows a comparison for the four investigated parameters, between the prior and the updated values. In some case, the final values have been taken considering both the updates each parameter independently, and the relationships between the parameters in themselves. For instance, in case of chaotic rubble stone masonry, an extensive number of experimental tests for the definition of the *G* Modulus has been used, while a lower number characterized the *E* modulus. Therefore, despite the upgrade of both parameters, as final results the Bayesian approach has been

adopted to define *G*, while *E* were obtained by their relationship, where *G* is usually adopted as *G= E/3*. The results present some differences between them. In some case, the updated values are lower than the mean values provided by the code. Nevertheless, the adopted mean values usually remain in the range of the prior distribution. It is worth noting that the experimental values have been found concerning masonry buildings built in the same Region during the same referred century. Therefore, the obtained upgrade is specifically referred for the Tuscan context, switching from general data valid for the entire Italian territory, to site-specific results. Despite the results in some case provide lower values than the MIT2019 ones, the site-specificity of the samples can be assumed as more accurate than the standard prior values provided by the Italian standard. As well, a set of experimental campaigns focused on the investigated buildings and involving the Public housing institutions ruling the properties would be a further step for a more accurate mechanical definition.

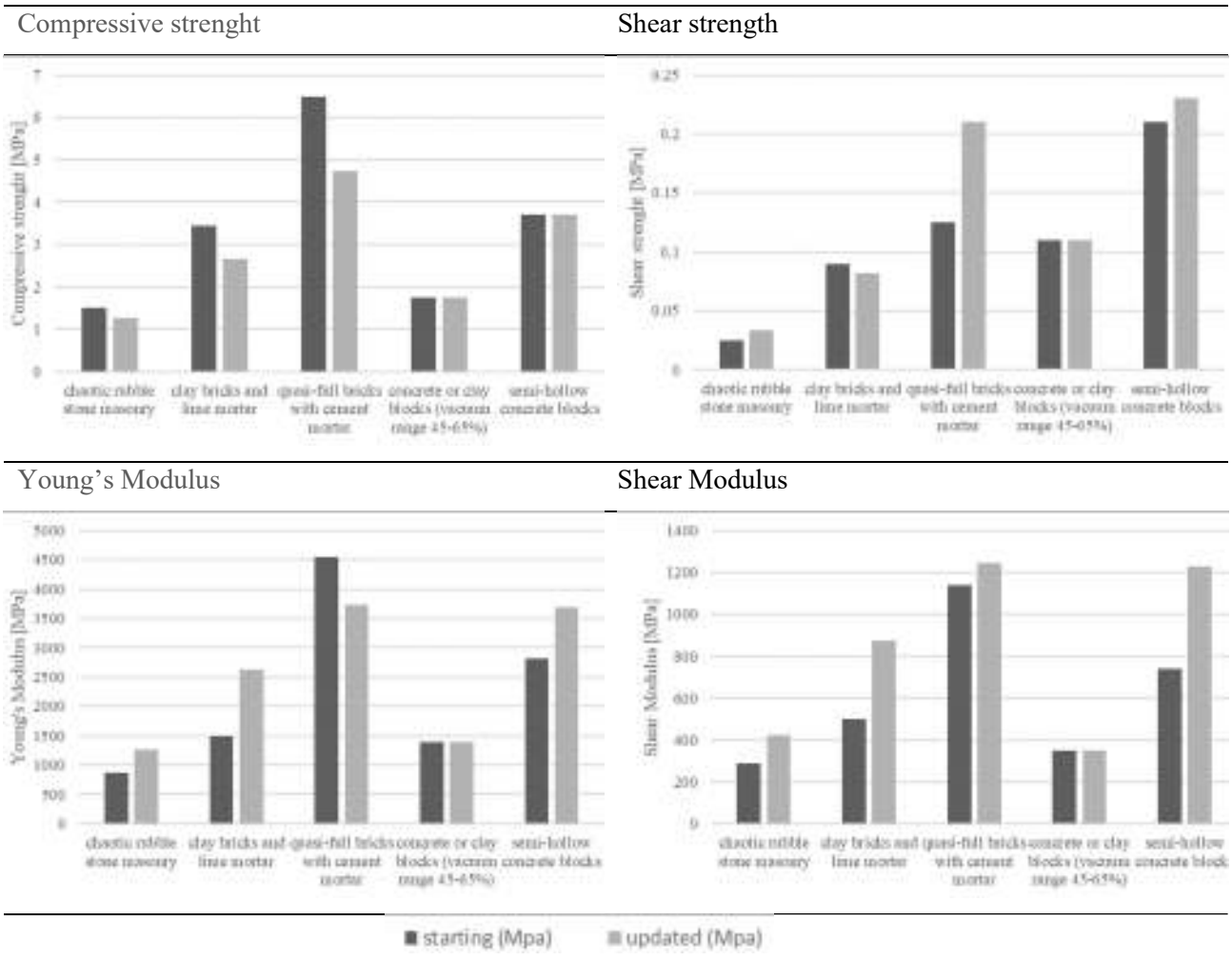

Fig. 2.12. Prior and updated distribution for the different mechanical parameters investigated.

Table 2.5. Updated mechanical values: minimum and maximum ranges defined by the Italian codes for the mechanical parameters of different masonry typologies.

	f_m (Mpa)	τ_0 (Mpa)	f_{v0} (Mpa)	E (Mpa)	G (Mpa)
Chaotic rubble stone masonry	0.916	0.027	-	1054	351
	1.624	0.040	-	1472	490
Clay bricks and lime mortar	1.972	0.049	0.13	2284	761
	3.360	0.115	0.27	2965	988
Quasi-full bricks with cement mortar	3.237	0.170	0.20	2916	972
	6.237	0.250	0.36	4543	1514
Concrete or clay blocks (vacuum range 45-65%)	1.500	0.095		1200	300
	2.000	0.125		1600	400
Semi-hollow concrete blocks	3.000	0.206		3301	1100
	4.400	0.254		4078	1359

Concrete. For the concrete material, several studies have been conducted for the Tuscany Region. In particular, a relevant quantity of samples has been extracted from public civil buildings. In Cristofaro *et al.* (2009) the *mean* values and the relative *standard deviation* for concrete classes depending on the decade have been presented. Starting from these parameters, a minimum, mean and maximum value for the cubic compressive strength $R_{c,\ mean}$ have been considered. Hence, three different values equal to 13.25, 21.18 and 30.92 MPa have been adopted.

Steel. In this work, the steel elements are only referred to the bars into the reinforced concrete. At the time the steel bars were smooth reinforcing bars, characterized by the absence of shaped ridge structures. For the mechanical characteristics of this materials, particular site-specific researches were not been found. Therefore, the mechanical properties were assumed based on the publications from the Campania Region (Verderame *et al.* 2011). Herein, a common steel material characterized by an Elastic Young's Modulus of 206000 MPa and a characteristic yielding stress f_{ym} of 350 MPa was assumed.

3. THE PROPOSED PROCEDURE FOR THE SEISMIC VULNERABILITY ASSESSMENT OF FLORENCE'S URM BUILDINGS

The seismic vulnerability assessment of masonry buildings - and civil structures in general – is an important topic for contemporary societies in seismic prone areas. Between them, residential constructions constitute bigger percentage of the urban stocks. Different constructive systems are involved, dealing with different intrinsic vulnerability propensions. Masonry constructions are part of the oldest structures on Earth (Roca *et al.* 2019, Lourenço *et al.* 2015, Varum *et al*. 2015). This technique, able to build big and important buildings through the use of small elements aggregated between them has remained the main technique since the introduction of the modern materials. Masonry buildings, as a result of the disposition of the resistant elements, combined through the use of mortar, is extremely good in order to resist to vertical actions (Como, 2013). Nevertheless, the capacity of masonry structures towards the earthquakes is different. In fact, the resistance of masonry buildings towards horizontal action mostly depends on the quality of the connections between walls. (Lourenço, 2015) Essentially, the masonry buildings may respond to the seismic actions following two types of mechanisms: the out-of-plane mechanisms and the in-plane ones. The out-of-plane phenomena depend on the connection between orthogonal walls and the resistant capacity of the horizontal diaphragms (slabs, vaults). They can be considered as kinematic actions around cylindrical hinges that may be generated at different heights of the masonry walls because of constructive discontinuities or different reasons. This type of mechanism is not specifically referred to the mechanical characteristics of the masonry in itself. In fact, the masonry wall may be considered as a rigid block. For this reason, since the out-of-plane actions are the first which are usually activated, the in-plane behaviour is researched. The in-plane capacity of the masonry panels depends on the mechanical characteristic of the masonry. Moreover, the diaphragms allow the transmission and the distributions of the seismic loads to all the masonry structures. Further, the so-called *box behaviour* is required. As presented in the introduction, the masonry buildings may be divided into three classes, depending on their response to the seismic actions. Between these typologies of unreinforced masonry (URM) buildings, the constructions studied in this thesis, URM buildings with RC slabs, are part of the third group. They are able to distribute the seismic actions over the different masonry walls and their capacity mostly depend on in-plan actions.

The study of the seismic performances of the buildings started through the evidences of the damages produced by past earthquakes. At urban scale, several procedures have been obtained by the study of these samples. The EMS-98 vulnerability classes have been developed in this way, as several empirical procedures (Vicente *et al.* 2011, Kassem et al. 2020). These empirical

methodologies have the pro that they have been calibrated on the basis of direct data. Nevertheless, their applicability is strictly extensible for similar contexts where the conditions don't change. Referring to the building stock, considering different conditions as the materials adopted (with their mechanical characteristics) or the seismic hazard of the area, their use can be unreliable. For these reasons, analytical procedures have been developed.

Different approaches have been developed for the structural assessment of the masonry buildings (Asteris *et al.* 2019). D'Altri *et al.* (2019) consider four different types of modeling: continuum models (CM), macroelement models (MM) block-based models (BBM) and geometry-based models (GBM). BBMs consider the masonry as a texture discretized in rigid (or deformable) elements mutually connected mostly through mortar. The damage and failure responses are given by the interaction elements, which lead the nonlinearity in the response. Discrete elements approaches are largely used. These types of approaches have the cons to require huge computational efforts more adequate for the scale of single walls or elements than for the building scale. Moreover, referring to historical buildings, the core of the masonry structures is often unknown; therefore, the building modeling can present various sources of uncertainties. CMs consider the masonry as a deformable continuum material without distinction between the resistant elements and the mortar. Several constitutive laws can be assumed, and the mesh possibilities allow these approaches to be advantageous at every scale of element. MMs are modeling approaches for walls or entire buildings. They are based on the observation of seismic data in order to discretize the walls in few elements connected through rigid nodes. The elements hold the constitutive laws of the materials, which are modelled as a continuum. The easy mesh of MMs conducts to law computation efforts, suitable for the engineer practice in the analysis of masonry buildings. Furthermore, their use is not attainable for a lower scale. The presented approaches, despite their differences in terms of definition, accuracy or computational efforts, are acknowledged strategies for the global assessment of buildings. Perhaps, in certain cases, global modeling is completely unreliable. Historical buildings with deformable floors and lack of connection between orthogonal walls don't participate to the global seismic response, so that local mechanisms occur. GBMs consider the structures as rigid bodies and study the failure mechanisms and their activations. This type of approach can be considered as a smart procedure, often required by the codes for masonry buildings where the lack of connection between walls leads to local mechanisms without involving the full system. In these cases, this method can bring to a good assessment of the structural safety of the structure.

The assessment of the seismic performance of buildings requires the assumption of a seismic demand and the definition of the structural capacity of the building under horizonal actions. In the engineer practice, linear constitutive law adopting the *q-factor* are very used; however, they are based on significant simplification not always able to catch the correct behavior of the

structures (Magenes 2006). Modeling the nonlinear response of materials and elements accounting for their energy dissipation is a relevant source of uncertainties. In literature, several robust models can be found. Performance-based approaches (PBA) require the use of the nonlinearity of the masonry (Lagomarsino and Cattari 2015). Nonlinear static analyses (NLSA) are valid tools for the structural evaluation of buildings and their use is wide recommended by National and International codes (NTC2018, Eurocode8, FEMA 2005). They consist of the application of a horizontal monotonic force to the structure. The seismic capacity is computed as a "capacity curve", i.e. a curve described through the base shear and the displacement of a selected control node, generally located at the upper level of the building. Two different distributions of the load pattern are normally requested. Then, on the capacity curves, the identification of attained Performance Levels (PLs) to define the Limit States (LS) is demanded (Lagomarsino *et al.* 2018). NLS procedures require the conversion of the capacity curve from a multi-degrees-of-freedom (MDOF) system into a single-degree-of-freedom (SDOF). This is targeted at comparing the defined capacity with the seismic demand. N2 Method by Fajfar (2000) and the Capacity Spectrum Method (Freeman, 1998) are between the most acknowledged conversion procedures. The selection of the target point in order to define the displacement of the structure is the main source of uncertainty for the capacity, especially in case of irregular buildings with deformable floors able to affect the results (Marino *et al.* 2018). Nonlinear dynamic analyses (NLSA) with scaled real ground motions and cyclic pushover analyses proved the worth of nonlinear static procedures. Nevertheless, their use in the engineer practice is still limited because of the high computational efforts, convergence problems, the availability of effective constitutive laws and expert judgment expertise for the interpretation of results and the choice of time-histories (Lagomarsino *et al.* 2018).

As described, the use of such types of discretization depends on the target of the analysis, the dimension of the studied element and the type of analysis in itself. Moreover, the structural characteristics of the target building address the type of analysis to choose. Accurate studies can be defined at small scales, whilst these types of the structural assessments are not suitable for entire and complex buildings, due of their time-consuming and computational efforts. In the engineer practice, finite element (FE) models and equivalent frame (EF) models are within the most used approaches in order to study the structural performance of masonry buildings at global scale. FE models probably represent the most acknowledged and validated methods for structural analysis. They belong to the CMs approach and determine the analytical solutions of equilibrium through partial differential equations subdividing large-scale problems into several smaller ones, the so-called finite elements. Equivalent frame methods represent a MM discretization adopted for masonry buildings. They convert the bearing walls into macroelements subdividing the masonry in piers, spandrels and rigid joints limiting the number of degrees of freedoms considering equilibrium of internal and external forces.

With regards to the urban scale, the definition of the vulnerability of the urban stocks where people live is primary important. To this aim, the definition of fragility curves allows the definition of the probability of occurrence of a certain damage level as a function of the intensity measure of the ground motion (Maio and Tsionis, 2015). For each considered seismic intensity, indeed, the fragility curve represents the probability that the building exceeds an assigned threshold value. Different fragility curves have been developed in the last years through several different contributions (Calvi *et al.* 2006; Pitilakis *et al.* 2014). Fragility functions may be derived adopting different approaches:

- Empirical; based on the observation of the direct damage of past earthquakes (Rossetto *et al.* 2003; Colombi *et al.* 2008; Rosti *et al.* 2020)
- Expert judgments; estimated by the opinions of experts on the basis of vulnerability index models (Lagomarsino and Giovinazzi 2006; Jaiswal *et al.* 2012)
- Analytical; obtained from the results of static or dynamic analyses over structural models (Calvi 1999, Rota *et al.* 2010; Remki and Kehila, 2018)
- Hybrid; on the basis of the combination of the aforementioned methodologies (Kappos *et al.* 2006; Cavaleri *et al.* 2017; Kappos 2016).

At the basis of the derivation of fragility functions, two parameters are necessary, the Intensity Measyre IM_{LS} and the Dispersion β_{LS}. The Intensity Measure producing the attainment of a specific limit state (LS), depends on the type of fragility curve and can be determined through the damage observation of past earthquakes or through the assumption of performance points evaluated by mechanical models. The involved dispersions depend on different sources of uncertainty. Lagomarsino and Cattari, (2014) presented four different sources that can be involved in the derivation of fragility curves, such as the spectral shape of the seismic demand, the epistemic uncertainty on the hazard curve, the uncertainty on the capacity curve and the uncertainty on the limit state thresholds. Basically, the first two sources are referred to the seismic demand, while the other two to the performance of the structural models. The uncertainties are considered as statistically independent and the final value of the dispersion of the system is computed as the square root of the sum of squares of each of them.

3.1 LAYOUT OF THE PROCEDURE

In this section the theorical framework of the thesis is presented. A macro framework of the adopted methodology is shown in Figure 3.1. The three different moments of the work are exhibited by different colour patterns. The flow-chart presents the phases in a chronological order; each phase can be considered propaedeutic to the following one. The procedure is developed separately for what concern the urban scale approach to the analytical one. Then, an hybrid approach that implements the results to a larger urban scale is finally obtained. The urban approach can be associated to a cognitive approach, based on the acquisition of the main

geometrical and structural features influencing the seismic response of the investigated buildings. This part does not only consist of the application of a methodology but is strictly connected to the Knowledge path developed at urban scale. In fact, it allowed the acknowledgement of the principal information about the investigated stock, collecting information useful for the following analytical phase. The gathered data were used to subdivide the building database into typological classes and to choose the benchmark case study adopted in the analytical part. Moreover, other outcomes of the cognitive phase are given by the definition of the main structural and mechanical characteristics; some results have been already presented in Section 2.4.

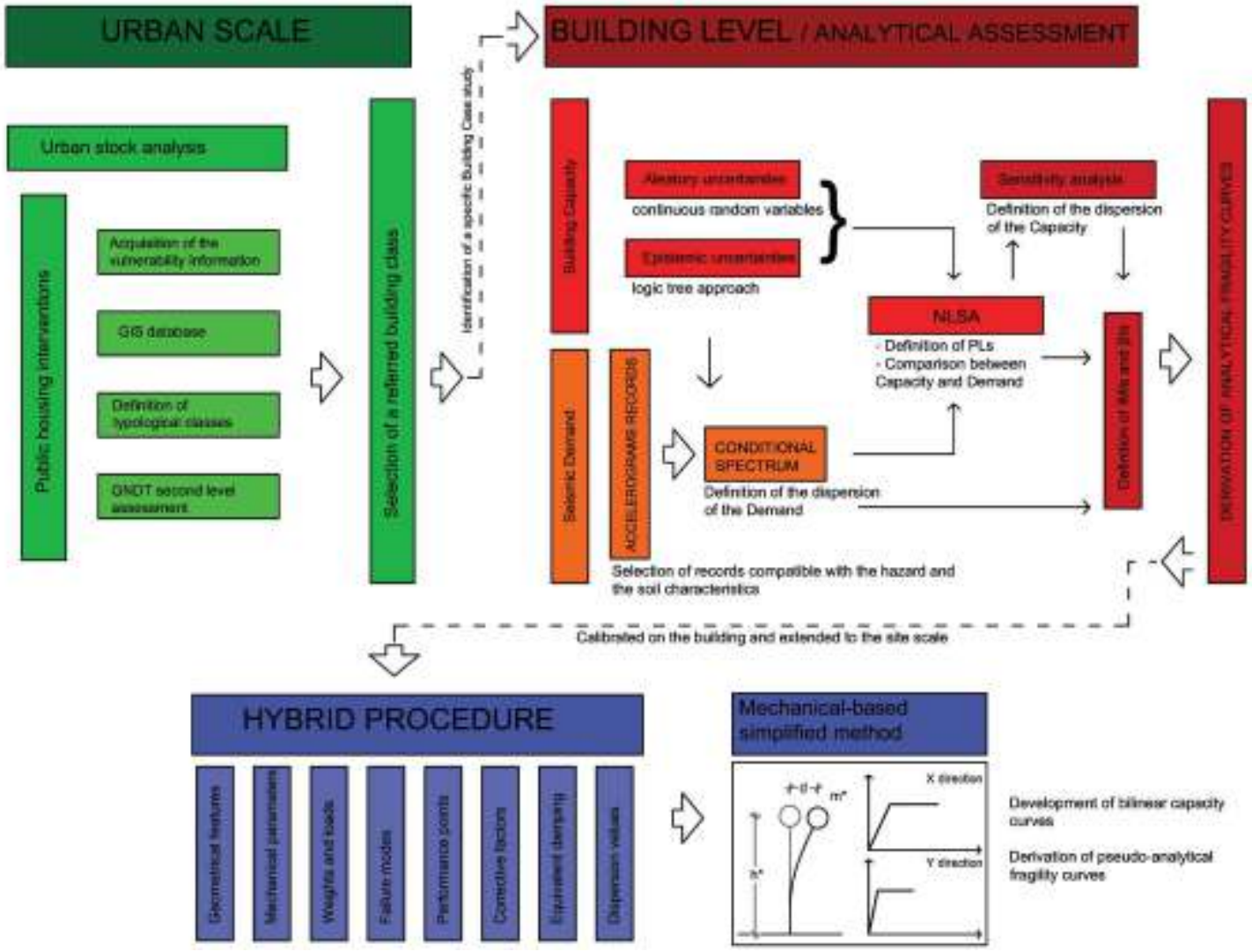

Figure 3.1. Thesis flow-chart divided between the three different moments of the work. The urban scale cognitive approach (green colour), the analytical probabilistic procedure based on nonlinear static analysis (red colour), the definition of general outcomes and the implementation of the results through an hybrid approach (blue colour).

The second part of the work represents the core of the thesis; it concerns the analytical assessment of the selected case studies through the use of nonlinear static analysis. A probabilistic framework is defined, aimed to assess the seismic performance of the building by comparing the capacity of

the structural model with the demand of the area. The results are expressed in terms of probabilistic fragility curves. Analytical methods present positive aspects that promote their use for the definition and calibration of fragility curves. Indeed, comparing the analytical methodologies to the empirical ones, the parameters describing the ground motion do not depend on the damage itself as in the macroscale. They allow the assessment of urban stock independently from the availability of data; so, their use can be extended to different typological classes. The specificity of the structural model can exhibit different failure mechanisms not pointed out from empirical data (Faravelli *et al.* 2019).

Concerning the thesis procedure, general outcomes in terms of behaviour insights and prevalent characteristics are obtained. The latter allow the implementation to a larger building classification, defining the seismic vulnerability assessment of an homogenous class through a simplified procedure.

The thesis aims at defining the fragility curves for selected masonry buildings. Namely, given a value *im* of the Intensity Measure (*IM*), the fragility function expresses the probability that a Limit State (LS) is reached.

$$p_{ls}(im): P\,(\,d > D_{LS}\,|im\,) = P\,(im_{LS} < im\,) = \Phi\left(\frac{\log\frac{im}{IM_{LS}}}{\beta_{LS}}\right) \qquad (3.1)$$

where *d* is the displacement considered for the assessment of seismic behaviour, *DLs* is the Limit State Treshold, IM_{LS} is the median value of the lognormal distribution of the intensity measure im_{LS} that reaches the *LS* threshold and β is the total standard dispersion.

Uncertainties are taken into account in the procedure; both aleatory and epistemic uncertainties have been considered. The aleatory uncertainties are characterized by a probability density function *f(x)* or the cumulative distribution function *F(x)*. They describe continuous random variables, and they are used to characterize the inherent variability of the properties of the structures (such as mechanical properties, capacity of the models). Their description passes through the use of the *mean* and the *standard deviation* of the specimens. Concerning the mechanical properties of the materials, the update of the prior values is made following the CNR DT-212 recommendations through the updating of the a-priori values. The Bayes theorem has been used for the implementation of the starting values. Sensitivity analysis has been performed over the aleatory uncertainties in order to weight their influence in the Performance-based assessment (PBA) (Croce *et al.* 2019). The sensitivity analysis model has been applied adopting the star design with the central star approach, based on the performance of *2N+1* numerical analyses (where *N* is the number of uncertain variables involved). The referred partial dispersion has been calculated using the Response Surface Technique (Pinto *et al.* 2004). The epistemic uncertainties are referred to features characterized by an imperfect knowledge of the structure.

They are modelled as discrete random variables related to their mass probability functions $p(x_i)$ (Bartoli *et al.* 2019). The epistemic uncertainties are herein modelled through a logic-tree approach, in which each different branch represents the combination of the values of the variables. The branches are assumed characterized by a statistical independence, so the final probability associated to the model is obtained as the product of the probabilities of the variable values in the branches.

3.2 THE ANALYSIS OF THE URBAN STOCK

At urban scale, the seismic vulnerability of structures can be evaluated using qualitative descriptors of specific macro-seismic scales, vulnerability indexes and capacity curves. The expected physical damage can be expressed by damage probability matrices, vulnerability functions and fragility curves (Lantada *et al.* 2010, Maio *et al.* 2015, Bento 2019). Damage probability matrices (DPMs) and fragility curves are within the most used methodologies. The DPMs are matrices where, given a seismic intensity, each number expresses the probability that a building attains a specific damage level (Whitman *et al.* 1973). Vulnerability curves show the relationship between the *mean* level of damage attained by a building and the value of the seismic intensity (Peduto *et al.* 2017). Finally, the fragility curves express the probability of reaching or exceeding a specific Performance Level (PL) for a selected intensity of the ground motion.

Initially, empirical methods were developed through the information gathered during the post-earthquake inspections. Braga, Dolce and Liberatore developed the first DMPs for the Italian territories on the basis of the damage patterns produced by the Irpinia earthquake in 1980 (Braga *et al.* 1982). Various Intensity measures may be used; the seismic intensity has been descripted in terms of Medvedev-Sponheuer-Karnik scale (MSK), Mercalli-Cancani-Sieberg)scale (MSC): more recently, the macroseismic scale introduced by Grunthal has been extensively used. (Grünthal, 1998). The EMS-98, both for masonry structures and for RC structures, defines 5 damage levels DLs based on the evidence of post-earthquake data. Its use, based on the definitions of typological classes, has been later extended to buildings non-subjected by ground motions, in order to forecast damage scenarios (Lagomarsino and Giovinazzi 2006). Finally, the intensity measure to describe the ground motion events can be express in terms of Peak ground acceleration (PGA) and their relative peak ground velocity and displacement (PGV and PGD, respectively). Within the different im_s, several conversion formula are presented in literature; a summary is presented in Kassem et al. (2020).

In this work, an empirical methodology has been extensive adopted all over the investigated building stock. Within the various rapid approaches, the GNDT second level methodology has been adopted. Its use allowed the collection of the building information needed for the in-depth studies, and the obtainment of the vulnerability scores (GNDT 1994). Two different GNDT sheets can be found in literature, respectively for RC and masonry buildings. For the masonry buildings,

the sheet is composed by 11 parameters (Table 3.1); it concerns different information, including the foundations, the materials adopted in the masonry walls, the roof structures, the geometrical shape of the buildings etc. Each parameter, depending on its importance, is weighted through proper coefficients, ranging from 0.2 to 1.5. The final value of the vulnerability is expressed between 0 and 100, where 0 represents a building without any vulnerability and 100 an extreme high level of vulnerability.

Table 3.1. GNDT second level parameters and their relative scores.

Parameter	P_i				w_i
	A	B	C	D	
P1 Type of resisting system	0	5	20	45	1.5
P2 Quality of resisting system	0	5	25	45	0.25
P3 Conventional strength	0	5	25	45	1.5
P4 Location and soil condition	0	5	25	45	0.75
P5 Horizontal diaphragms	0	5	15	45	variable
P6 Planimetric configuration	0	5	25	45	0.5
P7 Regularity in height	0	5	25	45	variable
P8 Maximum distance between masonries	0	5	25	45	0.25
P9 Roofing system	0	15	25	45	variable
P10 Non-structural elements	0	0	25	45	0.25
P11 Conservation state	0	5	25	45	1

The GNDT second level assessment has been widely used over time in Italy. The "weight" to assume for each parameter is empirically calibrated on the basis of the Italian earthquakes occurred in the last century. The vulnerability of the urban stock may then be then expressed through the macroseismic scale. Different conversions between GNDT approaches and the EMS-98 descriptors can be found in literature. Vicente *et al.* (2011) and Formisano *et al.* (2011) implemented the GNDT second levels sheets introducing new parameters and calibrating their conversation into a macroseismic scale. Finally, the vulnerability can be expressed through the adoption of vulnerability curves. The curve is plotted through:

$$\mu_D = 2.5\left[1 + tanh\left(\frac{I+6.25V-13.1}{Q}\right)\right]; 0 \leq \mu_D \leq 5 \quad (3.2)$$

where μ_D is the expected level of damage ranging between 0 (*No Damage*) to 5 (*Collapse*). The hyperbolic tangent accounts a ratio combining the Intensity level of the expected earthquake (ranging between 0 and 12), the Vulnerability Index already defined and a Ductility Factor Q. Different values of Q can be assumed; in this work, a Q value equal to 2.3, following the Lagomarsino suggestions has been adopted (2006).

Finally, the probability that a certain damage occurs for a given level of seismic intensity *I* has been expressed according to the probability mass function of the binomial distribution:

$$PMF: pb = \frac{a!}{b!(a-b)!} \cdot d_b \cdot (1-d)^{a-b} \quad a \geq 0 \tag{3.3}$$

In this work, the determination of fragility curves based on empirical data is not a main target. The urban scale approach has been used in order to gather the main information of the residential urban stock realized in the XX century by masonry structures, to understand the common characteristics of the buildings and to define some building type able to represent a large number of cases. The achievement of this part has been possible thank to the archive research made for the building and the collection of the data. The in-depth collected knowledge has been used to limit the epistemic analysis and to convey the efforts to supported data.

3.3 The analysis at the building Level

At the building level, the assumptions regard selected case studies indicated after the knowledge achieved through the research phases. A specific description of the case study within the investigated database is described in the next chapter. Herein, the theoretical frameworks beside the seismic vulnerability assessment at the building level is proposed.

3.3.1 Modeling assumptions

The seismic vulnerability assumption at the building level has been investigated by means of mechanical analysis. To this aim, a structural model of the buildings to perform the seismic analysis is needed. In this work an equivalent frame model has been adopted. Stimulated by the National code indications, the use of EFMs for the seismic assessment of masonry buildings is strongly recommended (CNR-DT212, 2013). EF methods are based on the assumptions that the behavior of masonry panels under seismic loads follow general principles. Their upside is related to the low computational demand given by an *ad-hoc* structural discretization. Other modeling assumptions, such as FEMs, present bigger difficulties in the definition of the several parameters that rule the nonlinear response. Furthermore, the definition of the structural macroelements and their stress assessment in terms of generic forces lead to additional problems that make the choice of FEM in the engineer practice unpreferable. Concerning the EFM, this strategy considers only the in-plane action, while for the out-of-plane action other types of analysis are demanded. Starting from a masonry wall, the mesh is defined subdividing the structure between piers, spandrels and rigid nodes. This assumption is based on the evidences of the post-earthquake damages in masonry structures. Hence, the piers and the spandrels rule the nonlinear response of the materials. In literature, different works prove the reliability of such type of discretization (Marques and Lourenço 1998, Cattari *et al.* 2017, Siano *et al.* 2018; Aşıkoğlu *et al.* 2020)

In this work, for the definition of the EFM the software Tremuri, developed by the University of Genova has been adopted (Lagomarsino *et al.* 2013; Penna *et al.* 2014). The Scientific version implemented in the commercial software 3Muri (Stadata) has been used to model the structures. The mesh discretization (piers, spandrel and rigid nodes) was obtained through the procedure described in Lagomarsino *et al.* (2013). Piers and spandrels are modeled as nonlinear beam characterized by 6 degrees-of-freedom (Figure 3.2).

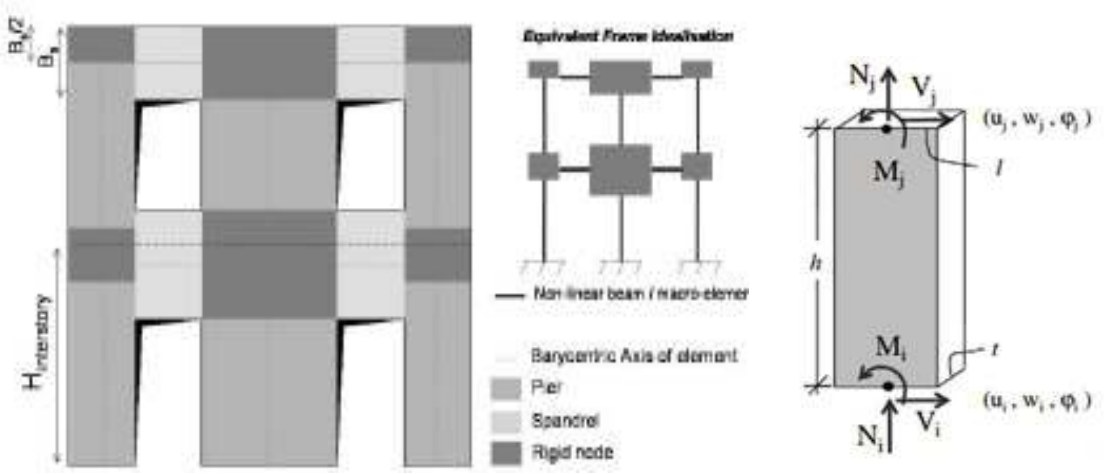

Figure 3.2. On the left: idealization of the equivalent frame model and its division into piers, spandrels and rigid nodes. On the right, the nonlinear beam describing the behavior of the masonry structures (From Lagomarsino *et al.* 2013).

The masonry is modelled as a nonlinear beam element with six degrees of freedom and a constitutive model with a resistance limit. A multilinear constitutive law based on a phenomenological approach and characterized by both, a monotonic and a cyclic response is assumed (Cattari and Lagomarsino 2013b). It considers a bilinear relation with a cut-off in strength and stiffness decay in the nonlinear phase (Figure 3.3). According to the Beam theory, the elastic branch is given by the initial stiffness, which is computed starting from a cracked configuration as recommended in the Italian codes; then, a secant stiffness representing the progressive degradation of the material is assumed. The constitutive law allows to describe the nonlinear response defining damage levels DLs that correspond to the strength degradations (β_{Ei}) (Lagomarsino et al. 2018).

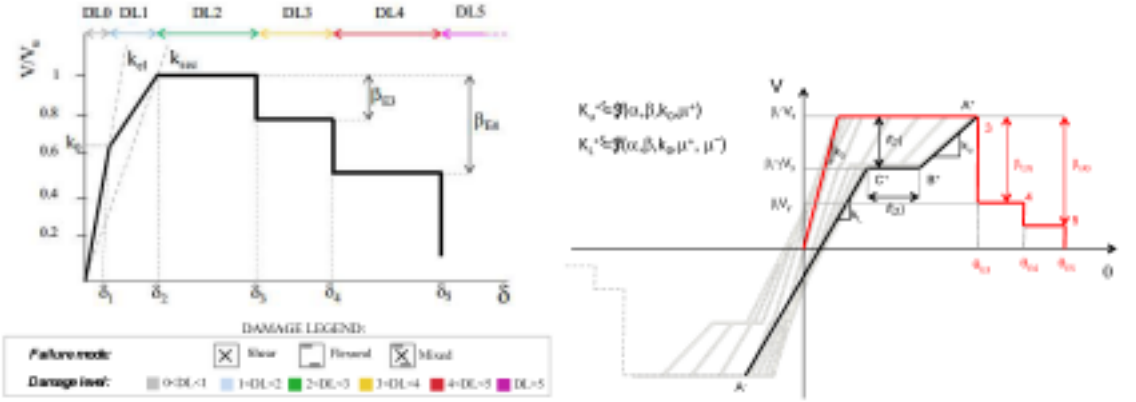

Fig. 3.3. Multi-piecewise constitutive law for the masonry structures; on the left, the monotonic response, on the right the cyclic one (From Lagomarsino and Cattari, 2015b).

These last ones are associated with the attainment of achieved values of drift (δ_{Ei}), from DL1 – *slight damage* to DL5 – *collapse* (Grunthal, 1998). The values of the drift levels and the strength decays have been taken from other works and experimental campaigns presented in literature (Beyer *et al.* 2012, Morandi *et al.* 2018, Petri *et al.* 2014, Milosevic *et al.* 2019) (Table 3.2); their sensitivity is further discussed in the following chapter of the work.

Table 3.2. Values of the drift levels θ and strength decays β adopted in the work for piers (P) and spandrels (S), respectively, accounting for the combined axial/bending moment and the shear failure.

drift piers	$\theta_{P,PF3}$	0.006
	$\theta_{P,PF4}$	0.01
	$\theta_{P,PF5}$	0.015
	$\beta_{PF,E3}$	1.00
	$\beta_{PF,E4}$	0.85
	$\theta_{P,S3}$	0.003
	$\theta_{P,S4}$	0.005
	$\theta_{P,S5}$	0.015
	$\beta_{S,E3}$	0.7
	$\beta_{S,E4}$	0.4
drift spandrels	$\theta_{S,3}$	0.002
	$\theta_{S,4}$	0.006
	$\theta_{S,5}$	0.02
	$\beta_{PF,E3}$	0.5
	$\beta_{PF,E4}$	0.5

Three different failure criteria are implemented in the software. The nonlinear behavior is activated when the first criterium achieves his maximum value. The drift is taken into account in order to control the ductility of the elements. Two different values of drift limit, for shear and flexural respectively are defined. The internal stresses are redistributed in order to maintain the

equilibrium, while the software deletes automatically from the calculation the elements that reach their ultimate drift. Flexural rocking, shear sliding and diagonal-cracking represent the mentioned in-plane failures (Figure 3.4).

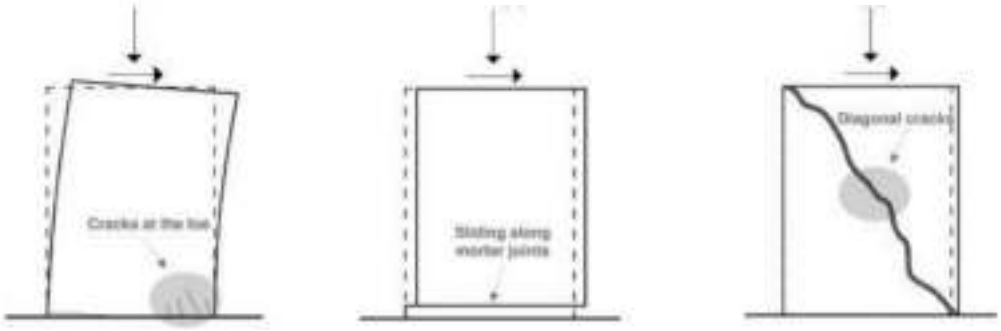

Figure 3.4. In-plane failure criteria implemented in the software. From left to right: flexural rocking, shear sliding and diagonal-cracking (From Oliveira *et al.* 2016).

Because of their boundary conditions, different criteria are implemented for piers and spandrels. Namely, while the piers are the elements that keeps the load from the structure to the ground, the spandrels may be considered as coupling beams between two wall elements if they are regularly bonded to the adjoining walls and connected both to the floor tie beam and to the lintel below. Depending on their condition, the system can be described as weak, intermediate and strong spandrel systems (Graziotti *et al.* 2012). In piers, the ultimate bending moment is based on a no-traction material where a nonlinear reallocation of the stress is performed (rectangular stress-block). It follows the presented formula:

$$M_u = \frac{l^2 t \sigma_0}{2}\left(1 - \frac{\sigma_0}{0.85\ m}\right) = \frac{Nl}{2}\left(1 - \frac{N}{N_u}\right) \tag{3.4}$$

Where l is the width of the masonry element, t the thickness, σ_0 is the normal compressive stress, N the axial compressive action and f_m is the compressive strength of the masonry. Since the global equilibrium has to be satisfied, when the moment is reduced to the ultimate bending moment, the shear is calculated as:

$$V_i = -V_j = \frac{M_i + M_j}{h} \tag{3.5}$$

For the shear, the Turnsek and Cacovic criterion is assumed. The ultimate shear is defined as:

$$V_u = lt\ \frac{1.5\tau_0}{b}\sqrt{1 + \frac{\sigma_0}{1.5\tau_0}} = lt\ \frac{f_t}{b}\sqrt{1 + \frac{\sigma_0}{f_t}} = lt\ \frac{1.5\tau_0}{b}\sqrt{1 + \frac{N}{1.5\tau_0 lt}} \tag{3.6}$$

Where τ_0 is the is the equivalent shear strength of the masonry and f_t is the tensile strength; their relationship is defined as $f_t = 1.5\ \tau_0$. Finally, b is a corrective coefficient defined by the ratio of height and length of the masonry panel ($b = h/l$ with $1 \leq b \leq 1.5$).

In the spandrels, since the axial compression is ineffective, the shear resistance is assumed as:

$$V_{u,\,lintel} = htf_{v0} \tag{3.7}$$

Where h is the height of the masonry wall, t the thickness and fv_0 is the shear resistance in absence of compression. The corresponding maximum bending moment is given by:

$$M_{u,lintel} = \frac{hH_p}{2}\left[1 - \frac{H_p}{0.85\,f_h ht}\right] \tag{3.8}$$

Where H_p is the minimum value between the tensile resistance of the interposed element in the lintel and $0.4\,f_h ht$, with f_h represents the in-plane horizontal compression resistance.

In this work, since the studied masonry buildings are characterized by the presence of RC slabs with ring beams, the coupling between the spandrels and the RC elements generates a strut-and-tie mechanism, where the maximum compression value in the spandrels is assumed equal to the tension strength in the coupled elements. (Milosevic 2019.)

Concerning the RC elements, they are modeled assuming elasto-perfectly plastic hinges concentrated at the end of the elements. Different failure mechanisms are considered, such as shear and compressive/tensile failures, brittle failures and combined axial/bending moment. Initially, the elastic branch is given by the stiffness contribution obtained only in terms of shear and flexural behavior, neglecting the reinforcements. The cracking reduction during the analysis is assumed as constant and determined by simplified factors (Cattari and Lagomarsino 2013b).

The diaphragms are modeled as rigid membranes able to distribute the seismic actions in the perimetral nodes. Tremuri models the slabs as orthotropic membrane elements characterized by different Elastic Moduli $E_{1,2}$ and the equivalent shear modulus G. The assumption of the RC membranes realized through RC joists topped by a reinforced slab allows to consider the diaphragms as rigid. The execution of an ambient vibration test performed over two case studies confirmed the reliability of the rigid slabs, as well as other publications presented in literature (Palermo *et al.* 2019, Michel *et al.* 2018b, Sivori *et al.* 2020).

3.3.2 LIMIT STATES

In this work, nonlinear static analyses (NLSA) have been chosen as assessment method. Conforming to the national and international codes (NTC2018, Eurocode8, FEMA 2005), the seismic forces are applied to the mass barycenter and incremented step by step monotonically. Two different load patterns, one proportional to the masses of the building and one to the inverse triangular pattern have been used, separately, according the two different examined directions.

For each specific analysis, by plotting the node displacement of the upper level with the base shear of the masonry walls of the considered direction, the pushover curve is obtained. It defines a base-shear/displacement relationship able to describe the capacity of the structures. Depending on the mechanical properties of the materials involved and on the morphological shape of the

structure, the pushover curve is usually characterized by a first linear branch with a positive slope, followed by a nonlinear phase. The plastic range of the curve can assume different shapes depending on the adopted constitutive materials in the nonlinear phase. Finally, on the pushover curve, the performance points highlighting the attainment of the different Damage Limit State DLs need to be found.

The definition of the performance levels (PLs) is at the basis of the quantification of the average annual frequency of exceeding a specific threshold. The PLs start with a direct correlation between the observational Damage States. Namely, they are defined, starting from *DL1*, slight damage, *DL2* moderate, *DL3* heavy, *DL4* very heavy, *DL5* collapse. For each PL codes provide a related hazard level, which is expressed as the annual rate of exceedance $\lambda r = 1/Tr$, where *Tr* if the Return Period of the earthquake for a specific site. Referring to the PBA, different approaches may be used. Some between them, presented in codes (ASCE/SEI 41–13, 2014) consider the attainment of the PL for the model achieved when the first structural element reaches the PL; nevertheless, this methodology may be too conservative, especially considering URM buildings, where the structure are able to dissipate the seismic energy through the plasticization of the elements. Lagomarsino and Cattari (2015a) contextually at the CNR-DT recommendations defined a heuristic approach based on a multiscale criterium. It considers three different scale of interest for the building, the global level (*G*), the macroelement level (*M*) and the element one (*E*). The attainment of each PL is achieved when for the minimum performance point on the pushover curve according to the three aforementioned criteria; the evolution of the nonlinear phase is verified in each scale (Lagomarsino *et al.* 2018). Finally, the PLs are defined over the pushover curve and expressed in terms of displacement of the control node. For each scale of interest, the definition of the PLs is defined (Table 3.3).

Global scale. At the global scale the PLs are defined over the pushover curve. *DL1* and *DL2* are considered in the linear phase of the shear-displacement plotted curve, while the attainment of *DL3* and *DL4* are located in the descending branch. Referring to the maximum shear of the curve $V_{b,\,max}$, the definition of the thresholds k_{DLk} has been calculated as ($k_G = V_b/V_{b,\,max}$). The DLs has been selected as percentage of the maximum shear. The adopted values correspond to 0.65 and 0.95 of the elastic branch for *DL1* and *DL2*, and 0.85, 0.65 in the nonlinear phase for *DL3* and *DL4* respectively.

Macroelement scale. Considering the macroelement scale, the inter-story drift of the masonry walls and the angular strain of the slabs are considered; in this work, since the slabs of the building are considered as rigid membranes, only the inter-story drift has been taken into account. The drift is estimated assessing both rotations and rotations of the nodes according to the CNR guidelines:

$$\theta = \frac{\varphi_j+\varphi_i}{2} + \frac{u_j-u_i}{h} \tag{3.9}$$

Where $\varphi_{i,j}$ are the rotation of the nodes located at the two levels (i and j), u the displacements of the same node and h is the height of the wall. Different values of the drift may be found in literature (Calvi, 1999); the values adopted in this research for the inter-story drift for each DL have been taken from Lagomarsino *et al.* (2018) and corresponding to 0.00075 for *DL1*, 0.00225 for *DL2*, 0.00425 for *DL3* and 0.00625 for *DL4*.

Element Scale. For the element scale, the cumulative rate of panels that reach a certain DL_i is considered. The original formulation both considers damage quantification in piers and spandrels; perhaps, the hierarchic role between them is taken into account, allowing a higher level of damage into the piers. As presented in Milosevic (2019) the presence of RC beams generates a coupling between them and the spandrels, so that a higher strength is presented in this type of elements. For this reason, the check at the element scale is adopted only for the piers. The cumulative rate of damage ($\Lambda_{P,\,DLk}$) represents the percentage of panels that reach a certain DL_i, weighted on the resisting cross section Ap

$$\Lambda_{P,DLk} = \frac{\sum_P A_P H_f \left(\frac{\delta_P}{\delta_{DLi}}-1\right)}{\sum_P A_P H} \qquad i = k+1 \tag{3.10}$$

Λ_p is defined as the internal drift limit for the attainment of strength degradation given by the assumed constitutive laws. H_f is the Heaviside function (equal to 0 until the demand δ_p in the piers does not reach the capacity Λ_{DLi}, then it switches to 1). The value of Λ_p is defined as $\Lambda_p = 0.04 + \Lambda_{P(S),DLk,0} + \frac{2}{N_{P(x)}}$; which has been calibrated by an extensive use of the multiscale approach to several buildings (Cattari and Lagomarsino, 2013a). The formulation considers the threshold the damage given by the gravity loads (Λ_p, D_{lk}) and the number of piers in the building N_p.

Table 3.3. Threshold values for the different scale of interest.

Local	$0.04 + \Lambda_{P(S),DLk,0} + \frac{2}{N_{P(x)}}$
Macroelement	0.00075 – 0.00225 – 0.00425 – 0.00625
Global	0.65 – 0.95 / 0.85 – 0.65

The attainment is finally given for:

$$u_{DLk} = \min(u_{E,DLk}; u_{M,DLk};\, u_{G,DLk}) \qquad k = 1, \ldots\ldots, 4 \tag{3.11}$$

Where E, M and G express the element, macroscale and global level of the assessment. In Figure 3.5 the relationships between the different scales of the approach are shown.

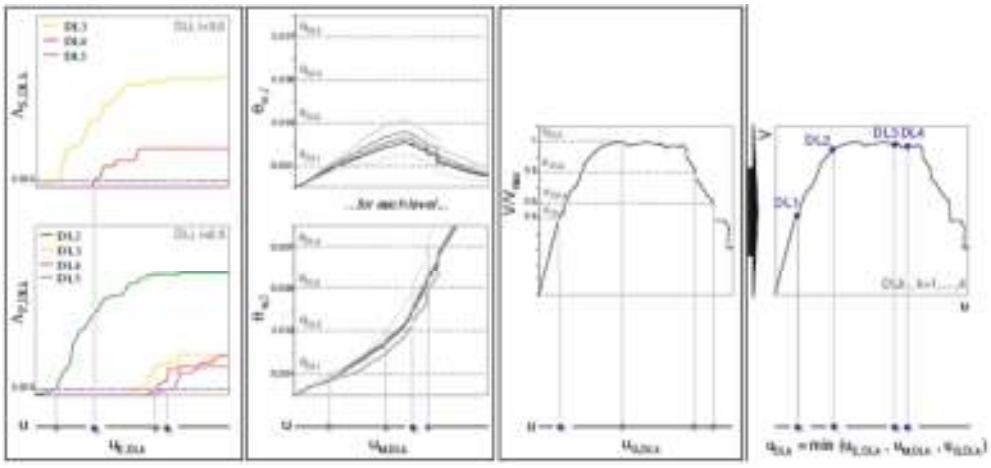

Fig. 3.5. The multiscale approach for the definition of PLs. (from Lagomarsino and Cattari, 2015a).

3.3.3 Intensity Measure

In order to define the Performance Levels able to attain a certain Damage Level, the Intensity Measure IM to express the PL is needed. Numerous IMs exist in literature (Douglas, 2014); namely, the choice of the optimal IM is not unique and varies with the target of the analysis (e.g. bridges, long-period structures, RC buildings). In this thesis, referring to the URM buildings, the peak ground acceleration PGA has been adopted. This assumption equals the choose of spectral acceleration for an infinitely-stiff structure (T=0s). Its reliability towards the investigated structures is justified since masonry buildings are characterized by short fundamental periods (Lagomarsino and Cattari, 2014). PGA is the most IM used to characterize the seismic hazard of a site; as IM, it certainly has the pros to be one of the most available parameters. However, this choice needs to be justified on the basis of the structural features related to the targeted structures, since several studies showed how the PGA could lead to poor correlations with the structural damage for other building typologies (Matsumura, 1992, Yakut and Yilmaz, 2008). Therefore, nowadays the IMs can be divided into two main categories, non-structure-specific IMs and structure-specific ones. This classification depends on whether they concern the natural hazard only or refer to the structural features of the buildings too (Kostinakis *et al.* 2018). In this field, the PGA proved its reliability for URM structures in different contexts (Erberik 2008, Lourenço *et al.* 2013, Cescatti *et al.* 2020).

In this work the Capacity Spectrum Method CSM (Freeman, 1998) with over-damped spectrum has been adopted. The analysis is based on the comparison between the displacement capacity, defined by the pushover analysis, and the displacement demand, obtained by reduced acceleration-displacement response spectrum. Its adoption has been preferred to the N2 method (Fajfar, 1999) following the PERPETUATE guidelines and other contributions pointing out the reliability of the CSM procedure towards the N2 method (Marino *et al.* 2019).

In order to express the PL of the pushover (PO) curve into PGA values comparable with the seismic demand, the conversion of the PO curve representative of the MDOF into the Capacity curve of the equivalent SDOF is expected. To this aim, as recommended by the codes, the participation factor Γ is adopted:

$$\Gamma = \frac{\sum m_i \phi_i}{\sum m_i \phi_i^2} = \frac{m^*}{\sum m_i \phi_i^2} \tag{3.12}$$

Where m^* is the mass of the equivalent SDOF system, mi the mass of the i-th node of the model and ϕ_i is the referred normalized displacement. The capacity curve is given defining the base shear V^* and the displacement d^* of the equivalent SDOF system adopting $V^*=V/\Gamma$ and $d^*=d/\Gamma$ where V and d are the base shear and the displacement of the MDOF system, respectively. The capacity curve is finally plotted in terms of spectral coordinates through:

$$S_a = V^* / m^* \tag{3.13}$$

$$S_d = d^* \tag{3.14}$$

The CSM method consider the overdamped spectra, defined according to the damping correction factor η. This factor is expressed as the function of the equivalent viscous damping ξ_{eq}, which represents the sum of the elastic viscous and hysteretic contributions $\xi_{eq} = \xi_{el} + \xi_{visc}$. The elastic viscous damping has been considered equal to 5%. For the hysteretic damping, literature values may be used (Blandon and Priestley 2005, Sullivan and Calvi 2013); in this work, the hysteretic damping has been analytically calculated performing cyclic pushover analysis. The cyclic pushover analyses have been performed over the mean models considered in the probabilistic assessment. Two different distributions, according to the load patterns adopted in the NLSA have been accounted. The cyclic analyses have been made applying as maximum displacement of the load the one corresponding to the attainment of the DL considered. The hysteretic contribution has been assessed performing two full loading cycles:

$$\xi_{hist} = \frac{E_d}{2\pi\,(E_{So+}+E_{So-})} \tag{3.15}$$

Where E_d is the energy dissipated during the cycle and E_{s0} is the elastic energy produced for the two verses.

Finally, the PLs can be defined in terms of PGA adopting the following formula:

$$PGA_{DL} = \frac{d^*_{DL}}{S_{d1}(T^*)\eta(\xi_{DLi})} \tag{3.16}$$

Where d^*_{DL} is the spectral displacement for each Damage State, S_{d1} is the spectral displacement calculated at the period T^* and η is the hysteretic contribution function of the equivalent damping. T^* and η are computed following:

$$T^*_{DLi} = 2\pi \sqrt{\frac{S_d}{S_a}} \tag{3.17}$$

$$\eta = \sqrt{\frac{10}{5+\xi_{PLk}}} \tag{3.18}$$

3.3.4 DISPERSION

The quantification of the sample's dispersion is at the basis of the derivation of fragility curves. In this work, two sources of uncertainties have been assumed and considered as statistically independent: the uncertainties in the seismic demand β_D and the seismic capacity β_C. The final computation of the uncertainty of the model is given by:

$$\beta_{tot,DL} = \sqrt{\beta^2_{D,DL} + \beta^2_{C,DL}} \tag{3.19}$$

Essentially, the contributions of the dispersion are related to the LSs previously defined over the capacity of the building. It is worth noting that the contribution of the seismic demand presents the same dispersion for the different limit states, since it is correlated to the characteristics of the area. For the seismic hazard, the seismic demand has been considered for a referred Return Period considering the soil spectrum defined by the Italian code. In this work, a set of 30 accelerograms soil-compatible with the Florentine hazard has been assumed; the median spectrum has been then conditioned by the fundamental mode of the building models, computed by linear dynamic analysis. A more specific description has been presented in Chapter 5. The uncertainty in the spectral shape is given by calculating the median spectra of a sample of selected ground motions soil compatible with the referred area. The median spectrum represents the 50% fractile of the sample. The uncertainty is finally given considering the 16th and 84th fractile response spectra of the selected time histories.

$$\beta_D = \frac{\log PGA_{D,84} - \log PGA_{D,16}}{2} \tag{3.20}$$

Concerning the Seismic Capacity, the uncertainty propagation has been assessed through the Response Surface Method (Pinto *et al.* 2004). The aleatory uncertainties have been considered through a simplified procedure defined as the star design with central star approach. Its adoption, useful in practice-oriented assessment, is characterized by the performance of *2N+1* analyses, where N represents the number of variables. The sensitivity of this approach has been recently studied and compared to a fully probabilistic one, showing off its reliability (Haddad *et al.* 2019). The RSM approximates the surface of $log(im_{LS})$ in the hyperspace of the significant random variables. They are expressed by a hyper-plane whose coefficients are determined by a least square regression of a set of numerical experiments (Lagomarsino and Cattari, 2014). In a fully

probabilistic approach, given N the number of random variables, a factorial combination where $M=2^N$ models are defined. Given the Matrix **Z** (M rows x N columns) the partial dispersion of the capacity is defined as the angular coefficient of the hyperplane of the normalized variables, expressed by:

$$\boldsymbol{\alpha}_i = (\mathbf{Z}^T\mathbf{Z})^{-1}\mathbf{Z}^T\mathbf{Y} \tag{3.21}$$

where **Y** is the vector that collects the values $log(IM_{LS,i})$, i = 1,…,M. **Z** represents the matrix of the normalized values (M rows x N columns) composed by (-1 and +1 values for the two fractile levels 16% and 84 %). Assuming the parameters as statistically independent, the dispersion is obtained by:

$$\boldsymbol{\beta}_c = \sqrt{\alpha^T \alpha} \tag{3.22}$$

Describing the aleatory variables by their distribution through X_{low} and X_{up} values through a star design approach, the regression is made in a two-dimensional plane. The extreme values are represented by -1 and +1 values and the **Z** matrix that collects the row vectors may be generalized to the case of *2xN* sensitivity parametric design (Milosevic *et al.* 2019).

3.3.5 Determination of the damage scenarios

After the definition of the described methodologies, the fragility curves can be derived according to (3.1). Fragility curves are obtained for both directions, considering two seismic load patterns, and the four *LS* previously defined. This is given for all the modeled logic tree branches, assumed as statistically independent. Then, the worst conditions are selected to express the fragility of the selected case.

Once the fragility curves are derived, the damage state *DS* probability distribution can be obtained. These discrete probabilities have different formulations considering the k-th LS considered. For $LS_{k\,1,2,3}$ they are expressed by:

$$p_{DSk}(im) = p_{LS\,k}(im) - p_{LS\,k+}(im) = \Phi\left(\frac{\log\frac{im}{IM_{LS\,k}}}{\beta_{LS\,k}}\right) - \Phi\left(\frac{\log\frac{im}{IM_{LS\,k+1}}}{\beta_{LS\,k+1}}\right) \tag{3.23}$$

Where the expression is fully described by (3.1) and the references made. Referring to the DS4, the definition of LS5 for its definition is a tough problem, related with the intrinsic assumptions of *near-collapse* for LS4 in the analytical formulations (Lagomarsino and Cattari 2014). In order to represent the *DS* by binomial probability distribution, they can be described according the following expressions:

$$p_{DS5}(im) = 0.8\left[1-\left(1-0.14\ \mu_{DS}^{1.4}\right)^{0.35}\right]p_{LS\,4}(im) \tag{3.24}$$

$$p_{DS\,4}(im) = p_{LS\,4}(im) - p_{DS5}(im) \tag{3.25}$$

$$\text{With}\ \ \mu_{DS} = \sum_1^4 p_{LS\,k} \tag{3.26}$$

Finally, in order to complete the DS distribution, the probability of having a DS0 is described by:

$$p_{DS0}(im) = 1 - p_{LS\,1}(im) = 1 - \Phi\left(\frac{\log\frac{im}{IM_{LS\,1}}}{\beta_{LS\,1}}\right) \tag{3.27}$$

So, given a certain fragility curve, the discrete probability distributions can now be obtained. It is aimed to forecast damage scenarios and expected damage levels for different levels of the intensity measure.

3.4 HYBRID SEISMIC VULNERABILITY ANALYSIS AT THE URBAN SCALE

The results obtained by the analytical model aims to obtain simplified parameters able to describe the seismic behavior and the seismic performances of the building type. The development of rapid procedures in PBA is a target of several contributions aimed to be used in the engineer practice (Lagomarsino and Cattari 2013, Michel *et al.* 2018a, Hannewald *et al.* 2020). To this aim, the mechanical model, initially proposed by Cattari *et al.* (2004) and developed by different authors (Lagomarsino and Giovinazzi 2006, Lagomarsino and Cattari 2014) has been adopted. The procedure is based on a Displacement-based Vulnerability method (DVM) and it aims to represent the capacity of the structures through the adoption of few mechanical and geometrical parameters. The method was conceived to combine the results obtained through the empirical methodologies with the performance-based analysis and it targets a wide urban scale assessment through the definition of proper selected case-studies within the building classes. Selected a masonry building, the procedure aims to define, for each direction, a bilinear capacity curve representing the vulnerability of the structure. Fundamentally, the parameters needed in each direction are the equivalent period T^*, the spectral acceleration A_u and the ultimate displacement d_u. The methodology is based on the obtainment of a spectral displacement / spectral acceleration curve, accounting for the masses and the base shear involved in the performance. The capacity curve is expressed through a bi-linear idealization defined by a constant value of the spectral acceleration, a yielding and a ultimate point for the displacement.

The first branch of the curve has a growing linear behavior, then, reached the yielding point at the maximum spectral acceleration, the curve continues through a horizontal *plateau* until the attainment of the ultimate displacement. The bi-linear idealization is proposed in the Italian seismic code and it is used together with the N2 method. Different idealizations of the capacity

curve can be found, proposing softening branches able to simulate the decreasing capacity of the pushover curves (Vamvatsikos and Cornell 2006, FEMA 2009, De Luca *et al.* 2012). Despite the softening behavior of the constitutive model presented in section 3.3.1, in this thesis the bi-linear backbone has been considered for the implementation of the mechanical model. The performance points had to be reviewed on the basis of the threshold limit states defined in section 3.3.2. In fact, the bilinearization methods usually define the initial stiffness of the linear branch by imposing the passage from the 60% of the maximum base-shear; hence, they define the yielding point by an equivalence of the area under the capacity curve, considering the displacement until a strength decay of the 20%. In this work, the decay has been considered until the 35%, in order to follow the limit states defined in the previous section. Further studies could implement this aspect trying to define fitter idealizations.

To describe the capacity curve, the spectral accelerations $A_{u,x,}$ and $A_{u,y}$ respectively, at the yielding and ultimate displacement are needed. Referring to the *X* direction:

$$A_{u,X} = \frac{f_x}{m^*{}_x \Gamma_x} g \tag{3.28}$$

Where f_x represents the base shear at the ground floor, g is the gravity acceleration (equal to 9.81 m/s^2), Γ_x and m^*x are the participation factor and the equivalent mass of the equivalent SDOF system computed in (3.10). Referring to this last one, the m_i represents the mass of the i-th level given by:

$$m_i = q_i + 0.5 \sum_i^{i+1} h_i \gamma_i \left(a_{x,i} k_{x,i} + a_{y,i} k_{y,i}\right) \tag{3.29}$$

where q_i represents the seismic floor load considering the deal loads and a fraction of the live loads, γ_i is the masonry specific weight at i-th level; h_i is the inter-story height of the *i*-th level, $a_{x,y,i}$ represents the ratio between the resistant masonry area in the considered direction over the gross area, for each *i*-th, level, $k_{x,y,i}$ is the spandrels contribution factor defined as the ratio between the total volume of the wall over the volume of the piers.
Referring to the *X* direction, the base shear at the ground floor is computed as:

$$f_x = a_{x,1} \tau_x \prod_1^4 K_{i,x} \tag{3.30}$$

In this equation, the generalized formula considers the introduction of four coefficient *k*, depending on the structural characteristics of the building. Specifically, k_1 deals with the masonry strength at the piers level, varying from 0.8 for the prevailing of a flexural behavior, to 1.5; k_2 considers the non-homogenous size of the masonry piers, k_3 takes into account the irregularities involved in the shape of the building and the plan distribution; finally, k_4 accounts for the effectiveness of the spandrels in global failure mechanisms of the building. Different values are

proposed in Lagomarsino and Cattari (2014), accounting to weak-spandrels-strong-piers configurations (WSSP), strong-piers-weak-spandrels-distributions (SPWS) and equivalent frame intermediate ones (EF). τ_x is the masonry shear strength of the wall, computed according to the Turnsek and Cacovic criterion:

$$\tau_x = \tau_{i,x}\sqrt{1+\frac{\sigma_x}{1.5\,\tau_{i,x}}} \tag{3.31}$$

where σ_x represent the average vertical compressive stress at the middle height of the first level:

$$\sigma_x = \frac{\sum \zeta_{x,i} q_i + \sum \gamma_i h_i\, a_{x,i} k_{x,i} - 0.5\,\gamma_1 h_1\, a_{x,1} k_{x,1}}{a_{x,1}} \tag{3.32}$$

and $\zeta_{x,i}$ represents the fraction component in the considered direction.

The equivalent period of the structure is expressed by:

$$T^* = 2\,\pi\sqrt{\frac{m^*}{g\,k^*}} = 2\,\pi\,H\sqrt{\frac{\sum m_i \phi_i}{g\,\prod_5^6 k_i \sum G_i h_i a_i}} \tag{3.33}$$

where H is the total height of the building. The formulation accounts to the shear stiffness through the correlation with the Elastic Shear Modulus G and two correction factors, k_5 and k_6 respectively. k_5 has been introduced to consider the flexural contribution in the piers, while k_6 assesses the coupling effectiveness of the spandrels (Lagomarsino and Cattari 2013). The value of k^* is given by:

$$k^* = \frac{\prod_5^5 k_i \sum G_i h_i a_i}{H^2} \tag{3.34}$$

Finally, the ultimate displacement can be defined. Two different formulation are proposed, accounting for both WPSS-SPWS formulations. In the first case, a linear deformed collapse shape is assumed, so the $Du_{,WSSP}$ is given by:

$$D_{u,WPSS} = \Delta_{LS4}\frac{H}{\Gamma_x} \tag{3.35}$$

where Δ_{LS4} is the inter-story drift limit of the panel; its value it is assumed alternatively considering the shear ($\Delta_{S,LS4}$) and the flexural mode ($\Delta_{F,LS4}$), accounting on the characteristics of the building.

In case of SPWS the ultimate displacement is expressed as:

$$D_{u,SPWS} = \Delta_{LS4} h_i + D_y\left(1-\frac{\Gamma_x}{N}\right) \tag{3.36}$$

N represents the number of floors of the structure, while the displacement at the yielding point is expressed as:

$$D_y = A_u\left(\frac{T}{2\pi}\right)^2 \tag{3.37}$$

Finally, a linear relation allows to consider different intermediate failure mode between the two extreme configurations:

$$D_{u,EF} = \varepsilon_x D_{u,WPSS} + (1 - \varepsilon_x) D_{u,SPWP} \quad (3.38)$$

In this case, ε_x represents a coefficient ranging between 0 and 1 expressing the behavior of the structure.

Adopting the mechanical method, the capacity curves of the investigated building can be defined through simplified parameters. Its use is suitable with the documentation provided by the archive research and the CAD reconstructions made. It is worth noting that the main difference between the DVM and the empirical methodologies is given by defining proper mechanical characteristics. To do this, not only the properties of the materials are involved but also a survey concerning the resistant walls their features in plan and in height.

[this page intentionally left blank]

4. ANALYSIS AT THE URBAN LEVEL

The procedure developed in the previous chapter has been applied to the city of Florence, namely to the URM buildings of the external areas. The first step of the work consisted in the collection of the data obtained from the archive research. To this aim, a GIS environment has been adopted. GIS software are useful tools for the wide collection of data and the superimposition of different *layers* of interest; in the last decades they have been adopted for the management of complex environment (Ferreira *et al.* 2014, Cavaleri *et al.* 2017, Catulo *et al.* 2018, Cardinali *et al.* 2020a). The GNDT second level methodology has been used to empirically define a preliminary vulnerability of the stock. Then, the building database has been divided into typological classes gathered for geometrical and architectonical features.

4.1 BUILDING DATABASE AND TYPOLOGICAL CLASSES

The identified buildings coming from the archive research were localized on the map of the City, hence, several information have been collected. To this aim, the open source software QGIS has been used. The urban database was taken from the Regional Technical Map (RTM), which provides the building shapes of all the constructions of the municipality. Within the geometry, also general information are given by RTMs. The building stock was divided between RC and masonry structures, however, this classification was not always corrected, so it had to be uploaded for the investigated structures. Furthermore, the total height of the structures, from the ground level to the roof, was listed. A new layer for the public houses has been made in order to collect the public housing intervention in Florence. Every building has been amply recorded, being identified with an *ID* number and spatially geo-referred. Passing from the archive research to the GIS environment, an assessment of the spatial distribution of the interventions has been possible. The buildings are spread in the different districts of Florence, showing the reliability of their assumption as representative of the URM buildings of the XX century (Figure 4.1).

Quantitatively, the public housing interventions follow the development trends of the last century, when the city grew mainly along the north-west direction (Marcelli *et al.* 2006). From an urban point of view, several interventions are clustered in big planning allotments defining vast zones of several outskirts; this is the case of the Isolotto Area, the Rifredi area, the block intervention in via Baracca and many others (Figure 4.2). It is worth noting that these residential clusters followed the prevailing zoning ideas of the time, promoting an urban differentiation between the areas of a city, encouraging the realization of only-residential districts connected with different ones (Jacobs, 1961). In some other cases, the urban planning was approached through a more organic approach: this is the case of the Isolotto area, where

the buildings were related between them through green spaces and pedestrian connection, with the realization of main commercial axis and hierarchical distributions (Astengo, 1951).

Figure 4.1. In red, the spatial distribution of the public housing interventions collected. The blue line indicates the perimeter of the historical center of the city.

Contextually to the collection of data in the GIS environment, the CAD planimetries of each project have been reproduced. Hence, the building planimetries have been linked to the GIS identification number. The database is characterized by more than 300 URM buildings, realized through 143 planimetries, i.e., several structures have been realized through the same building plan (Cardinali *et al.* 2019).

The CAD reconstruction represented a time-consuming phase of the work; nevertheless, it brought to obtain the geometrical survey of a relevant number of structures without executing direct surveys and so limiting the operational cost at site scale. This assumption has been mostly possible dealing with modern architectures characterized by uniformed technologies, clear separation of duties and involvement of professionals (architects, engineers). The building typologies have been divided as a function of their structural shape. Looking at the apartment's disposition, the localization of the stairs usually represents the distributive core of the houses. Namely, they serve two apartments per floor, one for each side in a symmetric way. The simplest case is represented by the simple-block case study. Herein, the structure presents a symmetric axis along the *Y* direction, passing from the stairs. From the single-block different configurations can be obtained, combining linear and scattered aggregations. In Figure 4.3 a building classification of the database has been done. Considering the block-type as the elementary cell, the addition of more elements leads to different classes, depending on the number of staircases. The elementary cell is called Block-building-typology (*BT*), then their aggregation takes the Roman number before the acronym, i.e. *IIBT*, *IIIBT*, *IVBT*.

Moreover, other configurations have been found, named accounting for their planar shape. Specifically, they have called "*LBT*, *CBT* and *TCB*", where the first Capital letter indicates the planimetry shape. Moreover, the terraced-house typology, *THT*, characterized by a linear aggregation of the same singular cell is shown. Finally, the *XBT* collects the buildings not included in the previous structures where an irregular structure is shown.

Figure 4.2. On top: distribution of three interventions along via Baracca occurred after WWII. (from Tanganelli *et al.* 2018). Below: GIS screening in the Isolotto district. In green, the shapefiles of buildings taken from the Regional Technical Map; in red, the identified masonry buildings.

BT	IIBT
	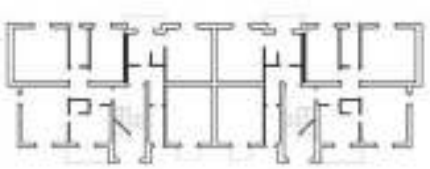

IIIBT
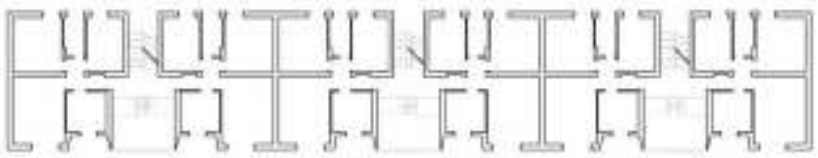

IVBT


LBT	TBT
	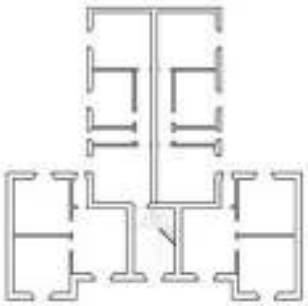

CBT	XBT
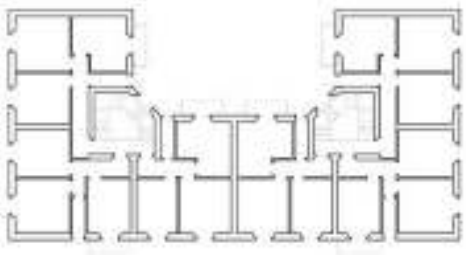	

THT
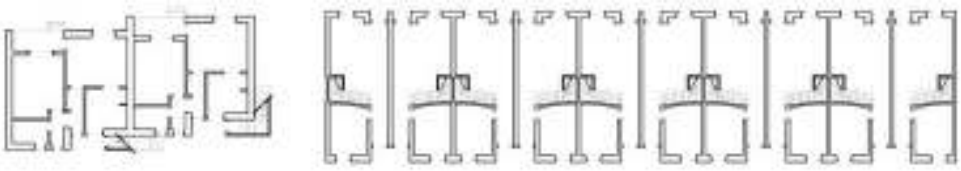

Figure 4.3. Definition of the building classes of the database.

After the typological classification, each building of the database has been investigated through the GNDT second level methodology. Of the over 300 buildings, not the total amount presented all the features to fill the method; complexly, 286 buildings have been investigated through this approach. For each building, a vulnerability index *Iv* has been obtained. At the database scale, the *Iv* ranges between 13% and 39%; it presents a *mean* value equal to 29% with a *c.o.v.* of 0.14. As described in Section 2.3, the database is quite homogeneous in its constructive features; this homogeneity has been pointed out by the GNDT sheets too. As shown in Figure 4.4, the buildings have most of the parameters in the same class. It is worth noting that the GNDT second level was conceived to evaluate the seismic vulnerability of entire urban stocks constituted by different building classes realized during several centuries. For this reason, the parameter classes have wide definitions complying with the empirical vocation of the sheet.

Specifically, about the 11 parameters, the most sensitive to the database features are parameters #3, #6, #7, #8 and #9. Such parameters are described here below, while the results of the assessment are shown in Figure 4.4.

Parameter #3, *Conventional strength*, is based on geometrical and mechanical data. It involves the resistant area of the masonry walls along the two direction, the gross area of the building, the number of storeys and mechanical properties of the materials combined with the effective loads. Since the mechanical properties have been chosen following normative guidelines and assuming their values constant between the different buildings, the variability of the parameter mostly depends by the geometrical features, such as the resistant area of the ground level, the height of the construction, the number of floors. Resistant area varies in a range from 8 to 22 % of the total area of buildings. It is usually not equi-distributed between *X* and *Y* directions depending on typological and architectonical features.

Parameter #6, the *Planimetric configuration*, depends on the regularity of the building plan; the main characteristics of the index are resumed in the examination of the building classes done before. The irregular building branches are assessed through simplified formulation defining the scatter between the regular configuration and the additions.

Parameter #7, *Regularity in height*, is one of the most variable parameters. It deals with the percentage decrease of resistant area along the height of the fabric. In the URM structures with RC slabs, the masonry thickness is usually constant along the inter-story height of the walls. Hence, the ring beams leads to a clear-cut interruption of the vertical continuity of the structures, given by the execution of a new wall over the slab level. In such category of buildings, the masonry setbacks are mostly given by the change of masonry typology along the vertical axis. In the database of buildings, there is some variability of results; as shown in Section 2.3, this is dependent from the height of bearing and the relationship into the bearing

walls. Moreover, some differences between the side walls and the façades of the residential structures have been pointed out.

Parameter #8, *Maximum distance between the bearing walls*, highlights the lack of homogenous distributions of the resistant walls along the gross area. The masonry structures characterized by the wall structures along both directions provide better scores; generally, the buildings with the prevailing of an unidirectional main direction are penalized. As widely described, the building of the database can be considered characterized by a box-behavior obtained through concrete ring beams and rigid slabs. However, when the distance between two consecutive bearing walls is excessive, undesirable torsional effects can occur.

Finally, parameter #9 concerns the roof system of buildings through a quality assessment; most part of the considered buildings resulted to have the same classification.

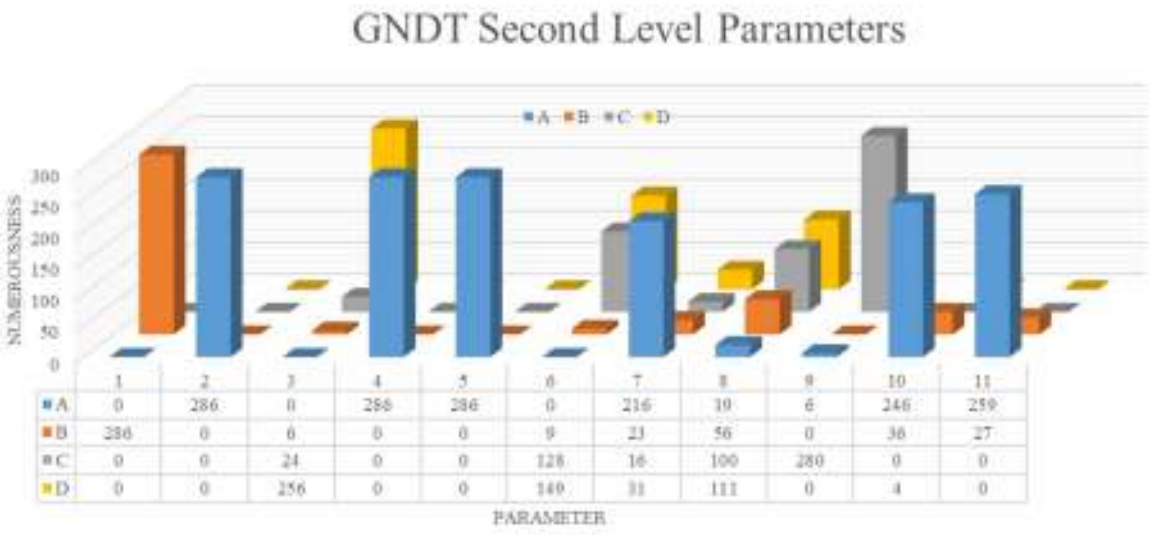

Figure 4.4. Parameters distributions inside the investigated buildings.

Empirical vulnerability curves and damage scenarios have been then described according to (3.2) and (3.3). The main results of this empirical procedure may be found in Cardinali *et al.* (2019). The results obtained are quite optimistic. For an intensity level VIII the most expected damage is damage level 2 (*DL2*) with a 34% of probability and a 26% of probability for *DL3*. Nevertheless, the paper showed the limits of the procedure developed. First of all, as already specified, the GNDT method is probably not adequate to assess such an homogeneous category of buildings; secondly, the evaluation assumes empirical calibrations obtained for contexts different from the Florentine one. Moreover, the damage scenarios are obtained adopting the macroseismic intensity as Intensity Measure (IM). In the following chapters, the *IM* adopted for the Demand will be the Peak Ground Acceleration (PGA), which is directly obtained from the geological studies and can be compared with the Capacity obtained by the analytical models.

4.2 THE SIMPLE-BLOCK MODEL

Inside the gathered database, the simple block model has been selected as building typology for the in-depth studies. Several building plans have been found, as shown in Figure 4.5.

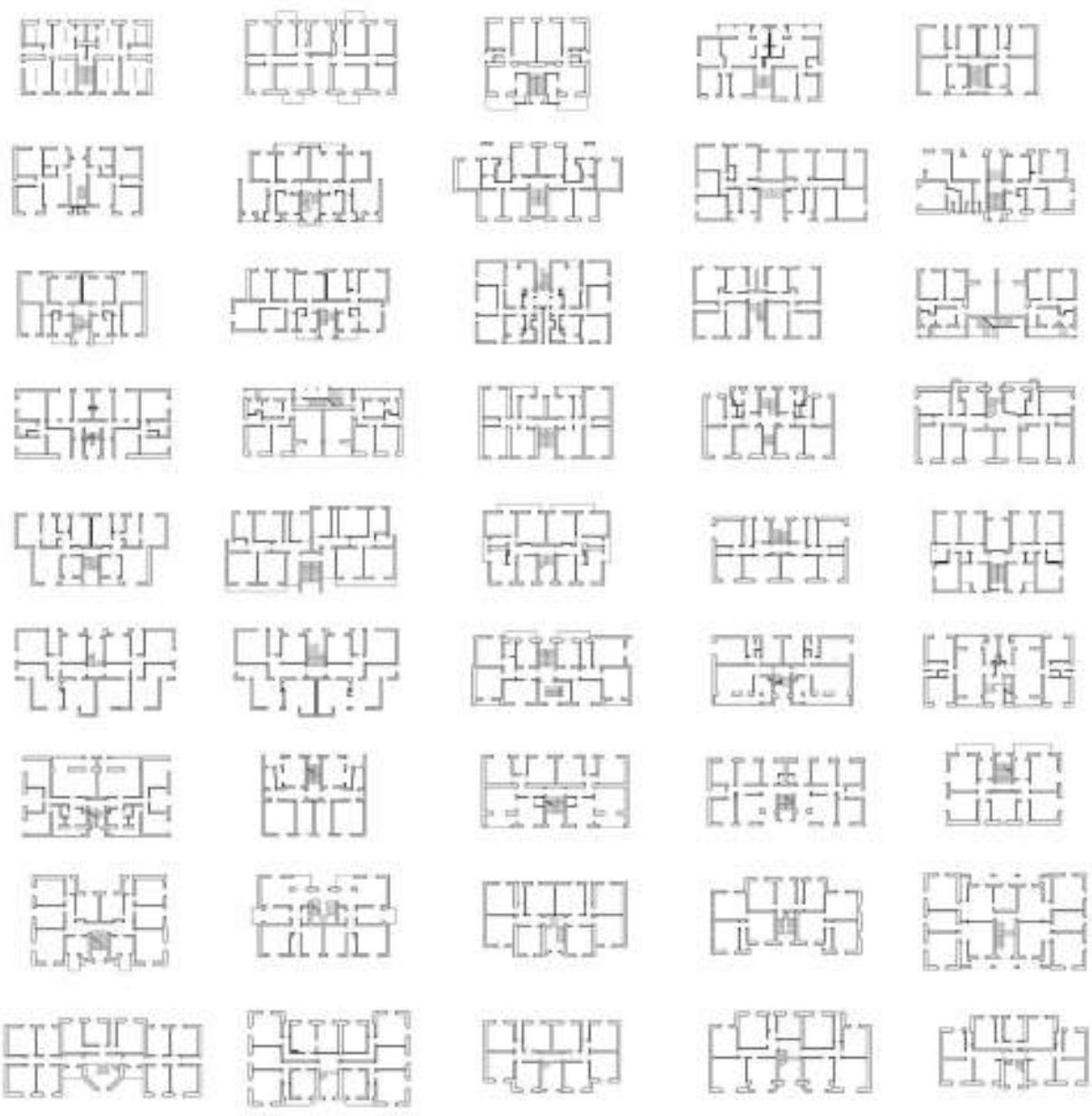

Figure 4.5. Building planimetries for the block-case

They can differ for several parameters; the most part of the building plans presents a stairwell disposed in a central position, nevertheless, the block-type collects also irregular configurations where the two served apartments may have different floor areas. Concerning the shape of this structures, they start from the simple rectangular configuration, then, some scattered volumes can be found, both in the central position, both along the wings of the structure. This leads to some irregularity along the Y direction, where the symmetry is not

presented. For the extensions of the structures, the block-type collects from very compact buildings, with rectangular shapes closed to the squared ones, to structures where the ratio between the two main directions is over 1 to 2. This building typology is recurrent in many cities of the Italian and European context. In fact, it has been used both in linear aggregation along the streets, both in isolated shapes, depending on the main urbanistic ideas during the time of constructions.

Concerning the structural disposition of the masonry walls, the buildings may have different configurations. In fact, besides the external structural bearing walls along the two directions, the internal walls may be disposed differently, depending on the design of the apartments. It is worth mentioning that in the middle part of the last century, the progresses in the conceptualization of structures, enriched by the creative uses of reinforced concrete, led to measure out the bearing walls in the buildings, supported by the analytical assumptions slowly tearing down the empirical fears. The URM structures of the time have been influenced by the frame idealizations of the RC structures in the disposition and the treatment of the bearing walls.

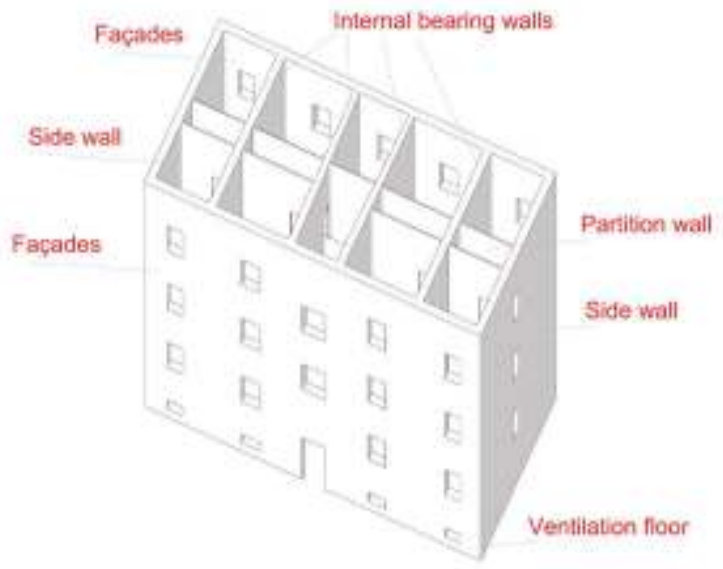

Figure 4.6. Axonometric view of a typical URM XX century intervention in Florence.

The most recurring configurations are with the internal resistant walls along the two main directions; then, irregular dispositions may be found. Concerning the structural elements of these buildings, despite the different possible situations, a main differentiation can be done between the façades and the side walls. It is given by the possibility of aggregation of this type of structure along the *X* direction. This leads to different characteristics of the bearing walls; the side walls are characterized by massive bearing walls with few openings. The façades are

instead more divided between piers and spandrels. In Figure 4.6 an axonometric view of a typical URM XX century intervention is shown.

In the shown building, the structural walls are mainly distributed along the *Y* direction, where a series of internal bearing wall follows the side wall orientation. The partitions occupy the remaining direction subdividing the internal space for the residential purposes. In this case study, the openings are regularly distributed and they follow the vertical alignment. Looking at the façades, the openings invest a low percentage of the total area of the masonry walls, generating piers larger than the spandrels and still following the empirical rules of regularity. The presence of the side walls with just a small opening per floor shows how the buildings were close to be aggregated with other adjacent structures. In the following Chapter, a case study between the different block-case buildings have been chosen for in-depth analyses.
The analytical dissertation invests a full Chapter of this work.

[this page intentionally left blank]

5. ANALYTICAL ASSESSMENT OF THE CASE-STUDY

Inside the building database, selected the block-case type for further analyses, a specific building should be finally selected as case study. Two different strategies could be used for such selection. The first one concerns the definition of a metamodel obtained combining the several information about the building class in order to achieve a representative benchmark that, despite it doesn't exist inside the database, perfectly describes the building family. The second approach regards the assumption of a real case-study inside the database on the basis of the most recurrent features of the investigated buildings. In this thesis, the second approach has been adopted. The selected case-study (Fig. 5.1) is a real case-study building located in the Novoli district, in the western part of the city.

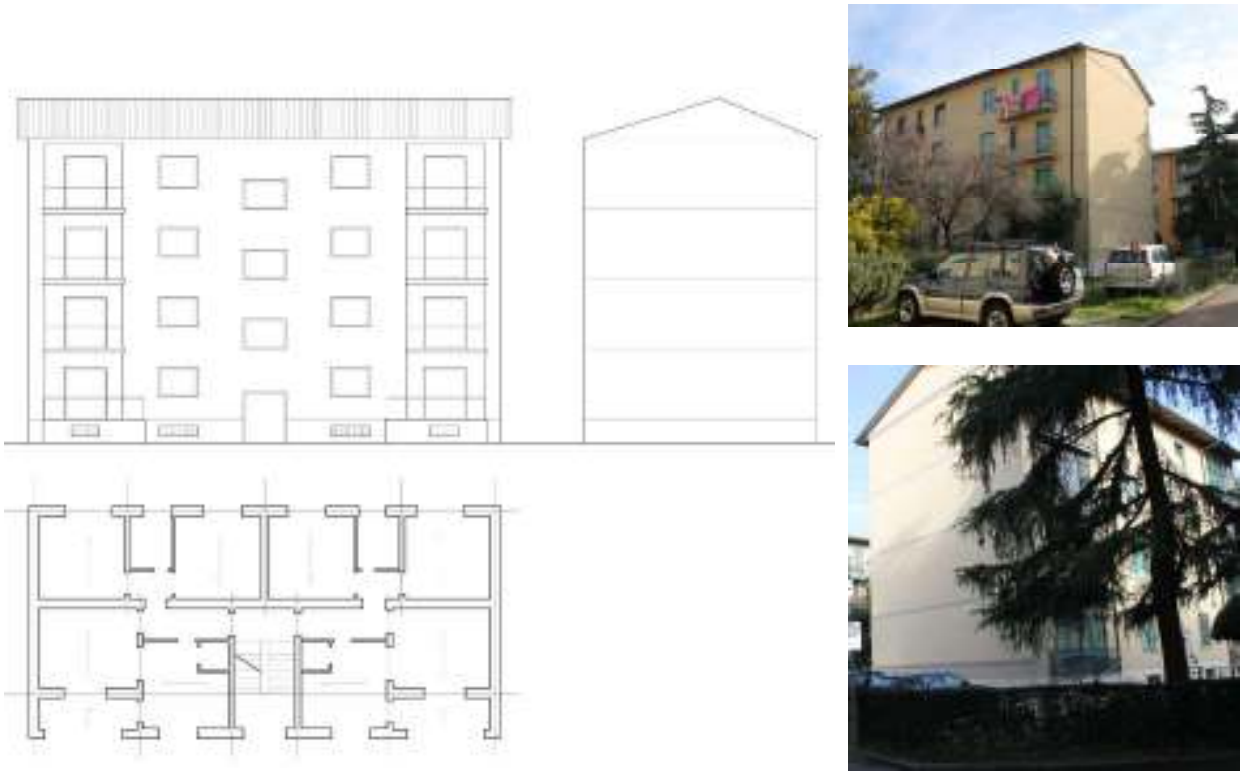

Figure 5.1. The selected case-study; building drawings and photos from the exterior.

The building is part of a parceling plan realized during the 50's. In the area where the building is settled, 18 different constructions were realized adopting 11 different planimetries (Tanganelli *et al.* 2018). Referring to the building plan shown in Figure 5.1, it led the realization of two distinct constructions. The house is a block-case building, constituted by four levels plus the basement level generating the ventilation floor. The construction has been selected on the basis of several features. First of all, its geometrical planar shape is perfectly inscribed into a rectangular, without external appendices excluding the terraces. Secondly, its ratio between the two geometrical sides, *X* and *Y*, is really close to the mean value of the ratio between the two geometrical sides of the total building database. The Vulnerability Index coming from the GNDT second level approach

was of 0.278, close to the mean value of the entire database of 0.29. Coherently with the majority of the investigated structures, the bearing walls present a decreasing of their thickness along the building height. Looking at the plan, the resistant wall disposition tends to highlight the characteristics pointed out in the previous section, showing a clear distinction between the façades and the side walls. In the internal part, the walls oriented in the *Y* direction are mostly solid walls with few openings. Since the walls and the slabs are orientated along both directions, the internal bearing wall's disposition can be also partially considered as a mixed one. Due to this, the case study represents a reliable benchmark characterized by the proper requested features without exasperated properties that bring to particular results. As a last reason of this choice, the building is characterized by four levels, which is still one of the most recurrent characteristics of the stock. In Figure 5.2 the numerousness of the buildings for their number of floors is presented. Despite the buildings presenting only 3 floors are a little bit more than the ones characterized by 4 storeys, the latter are considered more vulnerable and so they have been selected for the analytical analysis.

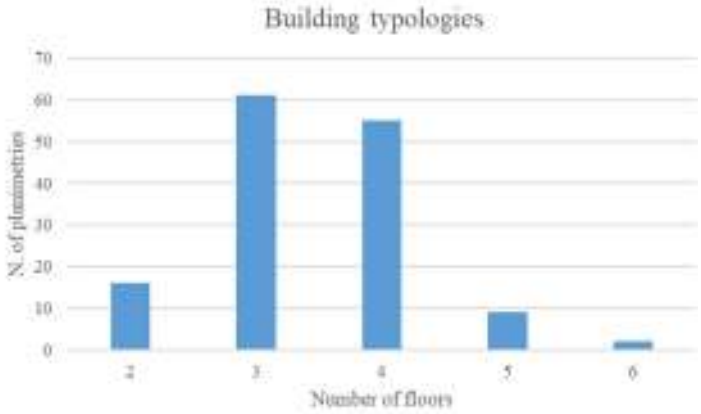

Figure 5.2. The numerousness of the buildings for each number of floors category.

Looking at the building plan, two symmetric apartments are served from the stairwell. The houses are mainly divided between the living area and the bedrooms space. The first one is faced to the entrance of the building and the main façade, while the bedroom area insists over the backfront of the structure. The entrance leads to a corridor, core of the house. From there, it is possible to access to the dining room (equipped with a kitchenette) and the living room. Both rooms are faced to a private loggia, given by the withdraw of a bearing wall from the external perimeter. The bedroom area is separated by the horizontal bearing wall that subdivide the internal space; here, two bedrooms and a restroom are located. Considering the plan, the building masses are symmetrical distributed. They present a symmetric axis along the *Y* direction, while a few differences occur in the *X* direction. Specifically, the stiffness barycenter of the structure is aligned along the *X* direction with the geometric one; in *Y* direction, a deviation of its position is given by a value of 4.9 %.

5.1 STRUCTURAL MODELING

Before the development of the probabilistic description at the building level, some preliminary and general considerations have been made. A first tridimensional structural model was realized in order to assess the main characteristics of the building in terms of gravity loads. During the procedure presented in the following sections, different structural models have been realized in order to take into account the lack of knowledges presented. In this section, a first EF discretization has been made. The structural model was obtained through the 3Muri (STA DATA, 2015). Namely, the software approach concerns the definition of the structural axis of the walls given by the mean alignments of the panels. Then, the elevation of each level is treated one by one, defining the wall thicknesses and the masonry characteristics. Coherently with the description of the real building, the connection between bearing walls and horizontal membranes is guaranteed by RC ring beams. The effectiveness of the RC beams over the masonry walls was considered assuming a full length of the coupling elements. The slabs structures have been modelled as rigid membranes; hence, the different live and dead loads were accounted. In this work, roof structures have been considered as masses over the bearing walls coherently with different other EF modeling. The stairs of the building too have been computed as linear distributed loads over the competence walls. During the nonlinear static analyses (not presented in this section), the elastic moduli of the masonry typologies have been computed the 50% reduced according to the MIT2019 indications.

The results of the vertical static analysis conducted with the gravity load over this first model are presented. In terms of slenderness, the bearing walls of the structures does not have critical issues. Nevertheless, the results of the gravity load according to the Italian codes (NTC2018) show static problems at the lowest levels of the structure. This is a common trend in all the bearing walls, and it is related with the high demands on the contemporary codes applied to building that were not conceived with the same formulations. In Figure 5.3 the results of the normal stress over the area of the bearing wall at the ground level are plotted.

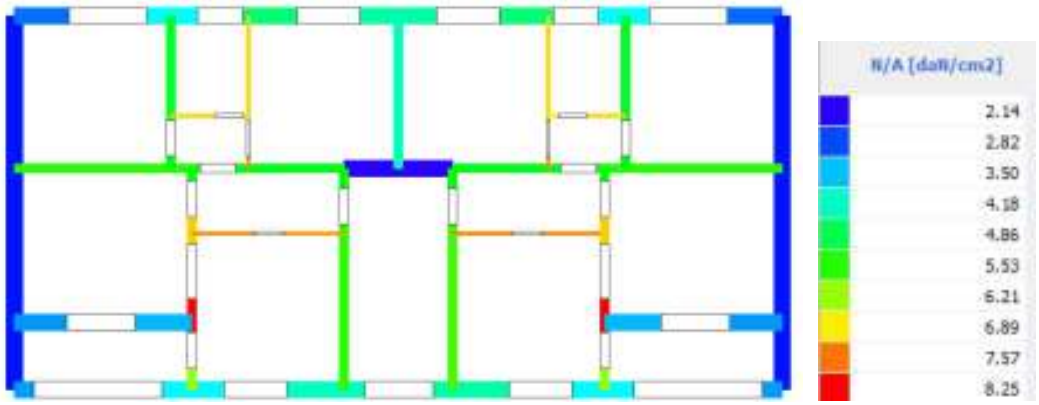

Figure 5.3. N/A stress at the ground level of the building for the static analysis.

The stress variation in the different piers is mainly given by their dimensions and their different thickness values. The slab orientations, despite the perimetral ring beam, affects the stress distribution. The most critical point is found in proximity of the loggias, where the bearing walls of the latter weigh on small piers in the orthogonal direction. The normal stress in the piers ranges between the 2 daN/cm^2 up to the 8.25 daN/cm^2.

This preliminary study was conducted adopting the commercial 3Muri version developed by Sta Data (STA DATA 2015). Successively, the following phases of the thesis were performed adopting Tremuri (Lagomarsino *et al.* 2013; Penna *et al.* 2014), which represents the research version of the software developed by the University of Genova. The geometrical and mechanical characteristics of the case studies were uploaded to the research software by an exporting procedure. Before the performance of the nonlinear static analyses through Tremuri, the multi-piecewise constitutive laws presented in Section 3.2.2.1 were implemented in the *.txt* scripts.

The selected building has been investigated by means of nonlinear static analysis performed over different EF models. The seismic demand has been defined coherently with the Florentine soil conditions. Hence, the seismic capacity of the structure has been investigated both considering aleatory and epistemic uncertainties.

5.2 EPISTEMIC UNCERTAINTIES AND LOGIC TREE APPROACH

The case-study has been finally investigated through the nonlinear static procedure described in Section 3.3. The building was chosen on the basis of its geometrical and structural features, which they represent the most recurrent ones of the database. Despite the defined geometric issues of the case-study, some uncertainty was still involved, especially regarding the material characteristics of the bearing walls at the different levels. These lacks of knowledge were modelled through a logic tree approach. In order to assess the sensitivity of the different logic branches, different EF models have been obtained. The preliminary pushover analyses have been conducted through Tremuri considering the pushover curves in terms of linear stiffness, base shear and displacement comparisons. The models were set accounting to the mechanical materials presented in Section 2.4 and assuming the mean values of the several properties.

Considering the evidences of the investigation phase of this thesis, different alternatives could be found. The first evident differentiation is obtained distinguishing the models according to the eventual presence of lintels over the openings. The latter deals with the structural behavior of the structures. The presence of RC elements over the openings defines a clearer shear-type model, where the spandrels couple the piers between them. Looking at the building plan, the presence (or

not) of lintels is expected to be more sensitive in the *X* direction, where more openings are presented. The distinction between the models with lintels and the models without lintels is described by the first letter of the acronym given to each model, *Y* for yes lintels, *N* for no lintels, respectively. Above this first categorization of the logic tree, two other different classes have been gathered.

Concerning the resistant wall typologies, different hypothetical configurations have been examined. They are based on the information given by the archive research dealing with structures characterized by a thickness decreasing along the height and their hierarchical masonry dispositions. Namely, some specific order between the masonry typologies was conceived; four different thicknesses of the masonry walls, based on the drawing of the structure, have been assigned. Specifically, the bearing walls are characterized by 45 cm thickness at the ground level, 38 cm at the first level and 25 cm at the upper floors. Considering the possible typologies that could be realized such structures, the materials presented in Section 2.4 have been adopted. Specifically, Rubble stone masonry (RS), Clay brick masonry (CB) and Clay blocks with vacuum range 45-65% (HB), have been considered for the bearing structures. Quasi full bricks with cement mortar has been adopted for the partition walls (QB). Hence, different combinations have been studied; six different models for each logic tree have been then considered (Figure 5.4). The order of the three masonry typologies over the four different levels of the models was given considering the thickness and the specific weights of each type. The RS masonry was accounted at the ground level and at the first floor. The CB masonry was proposed both at the first, the second and the third floor. Finally, the HB masonry was considered at the last two levels. Assuming that the HB masonry was always utilized over the CB masonry and never under it, six different models have been obtained. The procedure of the logic tree is shown in Figure 5.5.

In the following parts, the acronym of the building cases will be represented adopting the masonry typology abbreviations starting from the ground up to the last floor (Ground Level/First Floor/Second Floors/Third Floor). The models have been firstly grouped considering the differentiation proposed at the first level, where RS or CB masonry was proposed (RS/RS/../.. and RS/CB/../..). In fact, the results of the PO curves showed that the variability of the second floor represented the core of the response variations. Then, considering the variability of the other floors, the three different models analyzed for the upper levels (../../CB/CB; ../../CB/HB; ../../HB/HB;). The pushover responses showed a low sensitivity of these different assumptions to the seismic performance of the structural models, so the logic tree has been simplified considering just one model representative of the three different configurations. RS/RS/CB/HB and RS/CB/CB/HB, for both configurations, Y and N, respectively, have been adopted.

A final uncertainty was given by the ceiling characteristics. As described in Section 2.3, the ceilings are fitted out with an external ring beam avoiding the out-of-plane failure mechanisms of

the last floor. Furthermore, they have been collected considering only one representative model of the different configurations. As mentioned, the slabs at each level are characterized by rigid membranes given by RC joists topped by a reinforced slab. Only the ceiling of the last floor may be done through different techniques. In this context, two different configurations for the last floor have been considered; one adopting a rigid and heavy slab (RH) and the other assuming a light and deformable membrane (LD). The PO analyses have been performed along the two directions, assuming two different load patterns. For the selection of the control node, a central node was assumed, then, the PO curve was plotted considering a mean displacement of the most up level of the structure. The results in terms of global response showed the low sensitivity of the PO for the considered aspect. Of course, in-depth studies concerning the ceiling failure in case of the light and deformable cases and the specific role of the vertical/horizontal connection should be carried out. In this work, based on the aforementioned reasons, only one model was adopted.

Finally, four different branches have been selected and four structural models have been assumed as representative of the possible obtainable structural configurations of the case-study. Then, each model has been studied independently from the other configurations, performing nonlinear static analyses and studying the aleatory uncertainties presented.

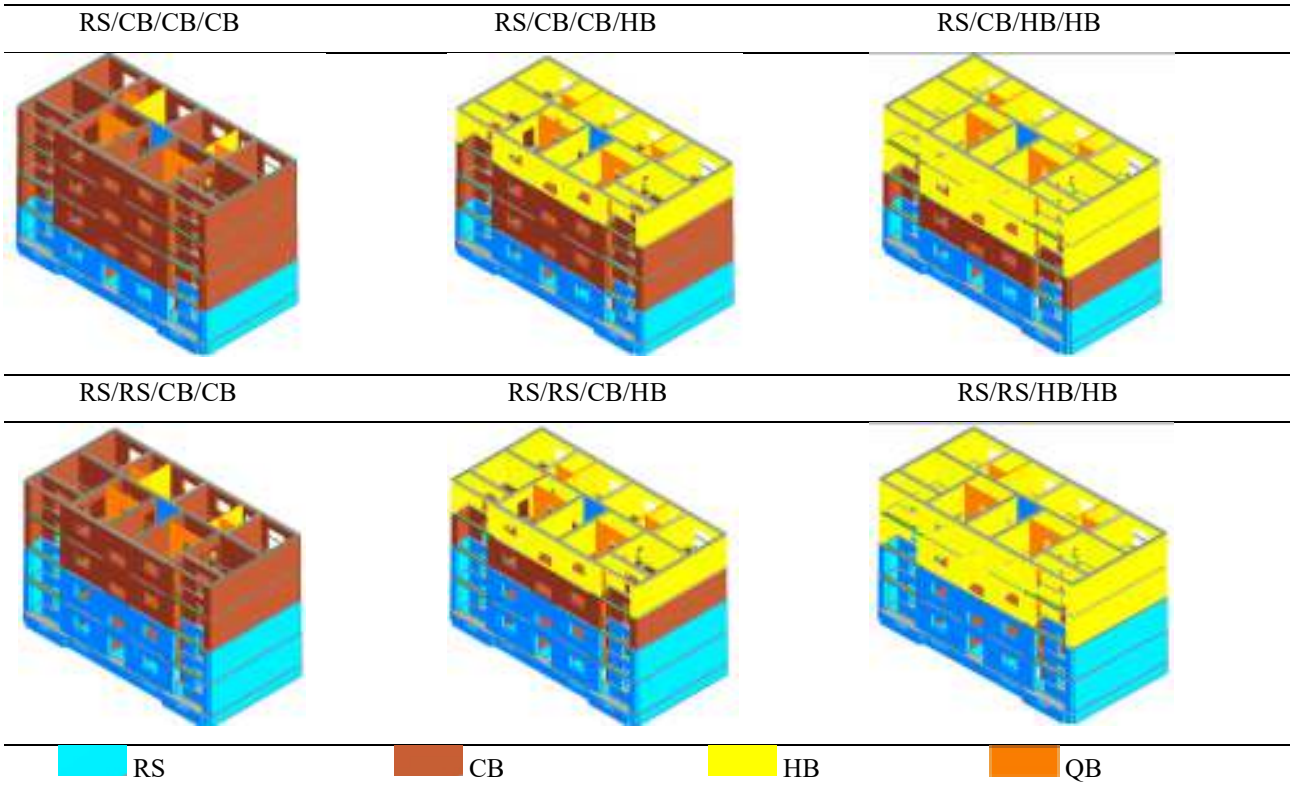

Figure 5.4. The structural models considered in the logic tree approach, for both the main divisions, yes lintels (Y) and no lintels (N) over the openings.

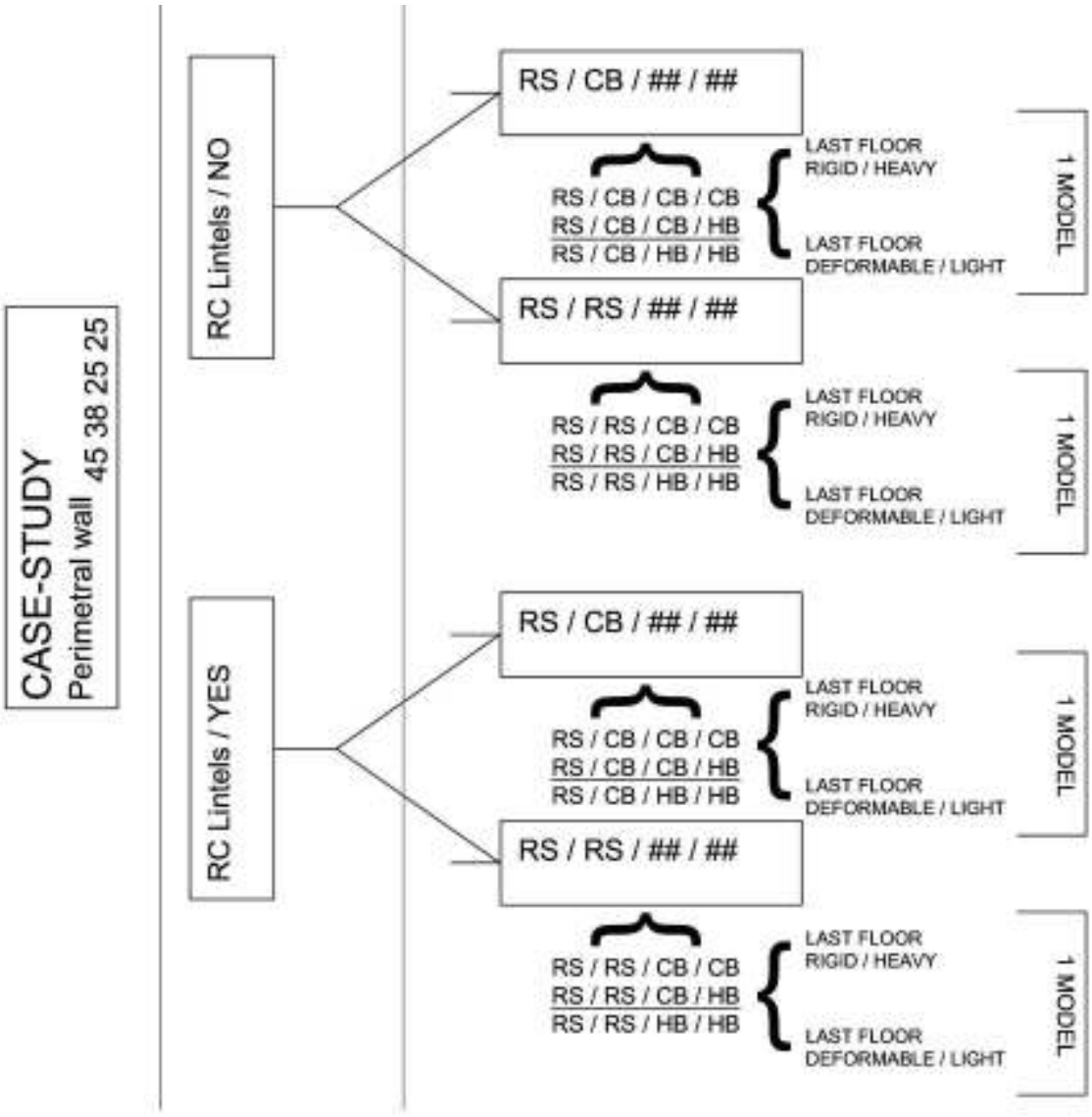

Figure 5.5. The logic tree approach used in this thesis.

Evidences from the pushover analysis. In order to assess the influence of the different logic tree branches, nonlinear static analyses have been performed. In this section, the main results of the procedure are pointed out. Successively, the same assessment has been done for all the aleatory variables considered, over the four different structural models. The results in terms of pushover curves are shown in Figure 5.6. The different colors indicate the performance of the different models. The PO plotted curves assume the displacement *d* normalized to the total height *h* of the model in abscissa (d/h), while in ordinate it plots the base shear *V* normalized over the total weight of the building, *W* (V/W).

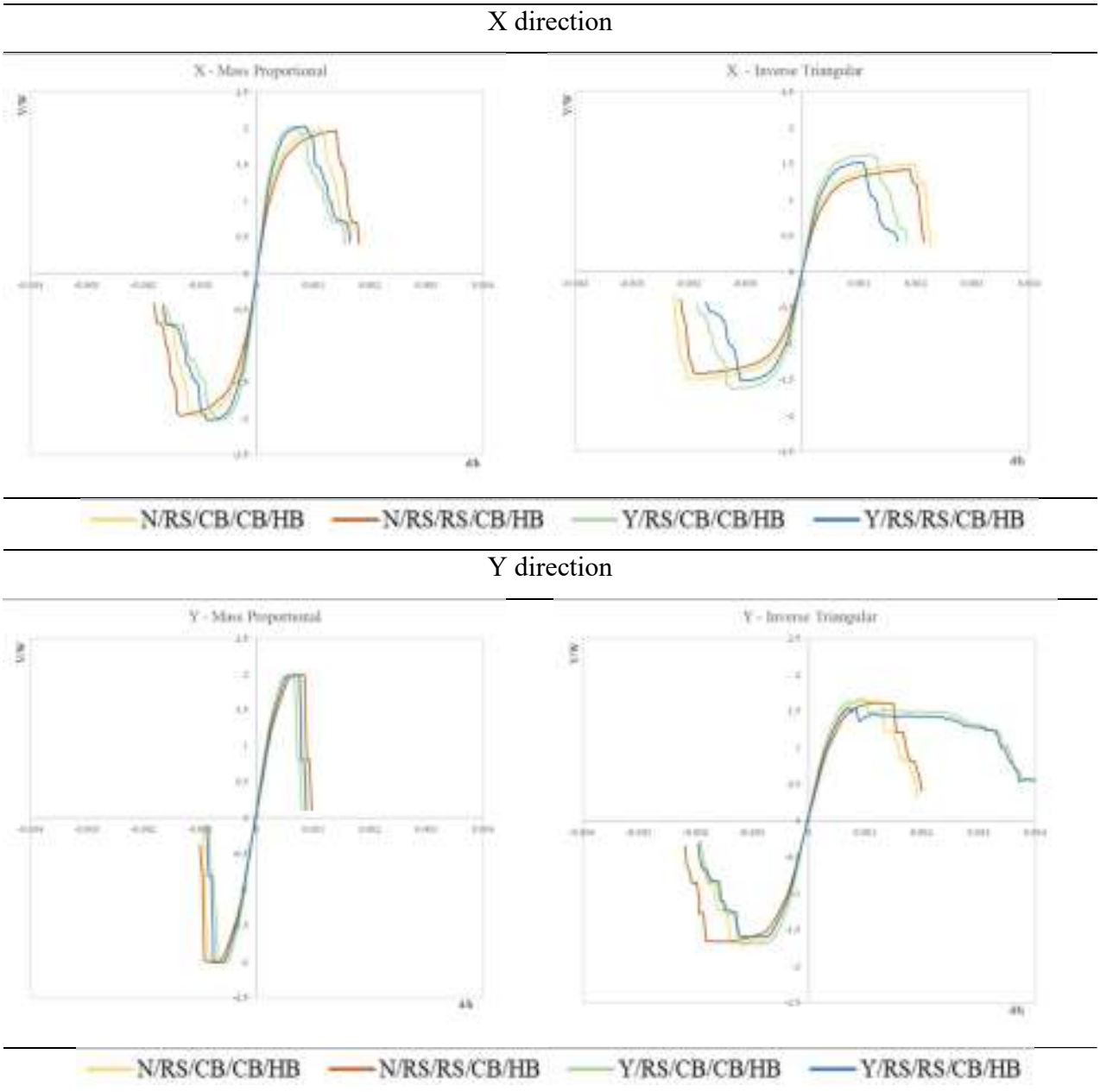

Figure 5.6. PO curves of the No-lintels and Yes-lintels models according to the two directions and the two load patterns.

For each direction, the PO curves separately show the capacity of the models according to the two considered load patterns, the mass proportional and the inverse triangular, respectively. The sense of the analysis is distinct by positive and negative contributions.

Comparing the four models, the lintels contribution in the coupling role between the different piers can be noted, mostly in *X* direction, where several openings characterize the bearing walls. In fact, in this direction, the models without lintels present a lower elastic stiffness and a more pronounced ductility. Despite the differences in the PO curves between the N and Y models, some common features can be observed. In all the four models, the two load patterns highlight the same different structural behaviors. The mass proportional ones always present a higher stiffness slope and generally, a higher maximum value of the base shear too. On the contrary, the inverse

triangular pattern shows a lower stiffness and lower maximum base shear values, but it allows a major contribution in the plastic phase, leading to wider plasticization of the elements before the collapse. This can be mostly asserted by looking at the damage patterns and the failure mechanisms of the structural models.

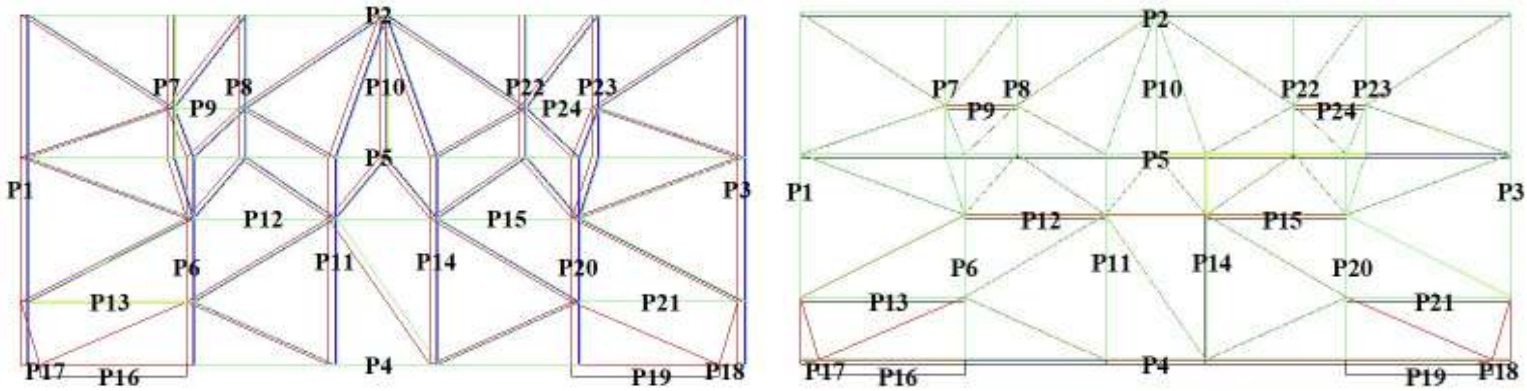

Figure 5.7. Planar deformed shape of the structural model with a mass proportional pattern for the two considered directions. On the left, X direction, on the right, X direction.

In the *X* direction, the model tends to exhibit a more plasticity rather than in *Y* direction. During the first phases of the analyses, in the *X* direction, the façades present a diffuse shear cracking in the spandrels, passing from *DL1* to *DL2*. This phase involves the different levels of the structure, but generally avoid the spandrels located at the last floor. The piers generally reach a lower DL, highlighting a shear failure at the ground floor and a flexural one at the upper levels. Hence, the spandrels continue their damage progressing, reaching the *DL3* for several panels disposed at the ground and the first floor. The quantity of them is related to the accounted model between the four logic tree branches considered, but also to the load pattern distribution. In fact, the shear failure of the masonry piers of the ground floor represents, for each seismic distribution, the failure mode of the structural models; the inverse triangular pattern allows a more distribute damage along the façades, stressing differently the lower and the upper part. For this reason, when the piers crisis is exhibited, almost the total of the spandrels reached the *DL3*. For the structural configuration of the case study, the inverse proportional pattern leads to lower base shear values, nonetheless it points out a bigger nonlinear ductility. On the other side, the mass proportional pattern seems to be more demanding in the plastic phase, quickly increasing a damage degradation in the piers of the ground floor. The piers at the other levels they usually point out flexural failures and doesn't exceed the *DL2*. Complexly, all the models exhibit the same failure patterns, *i.e.* the shear failure of piers at the ground level, with both seismic distributions. Only the model Y_RS_RS_CB_HB, with an inverse triangular pattern points out the shear crisis at the first level. This is due to the combination of the seismic pattern, the coupling effect of the spandrels and the mechanical properties of the RS masonry for the considered level. The deformation of the plan of the models generally shows a rigid translational behavior of the structure along the direction,

without highlighting torsional phenomena (Figure 5.7). The presence of spandrels over the openings define a more evident coupling between the piers, which anticipate their crisis because of the shear actions.

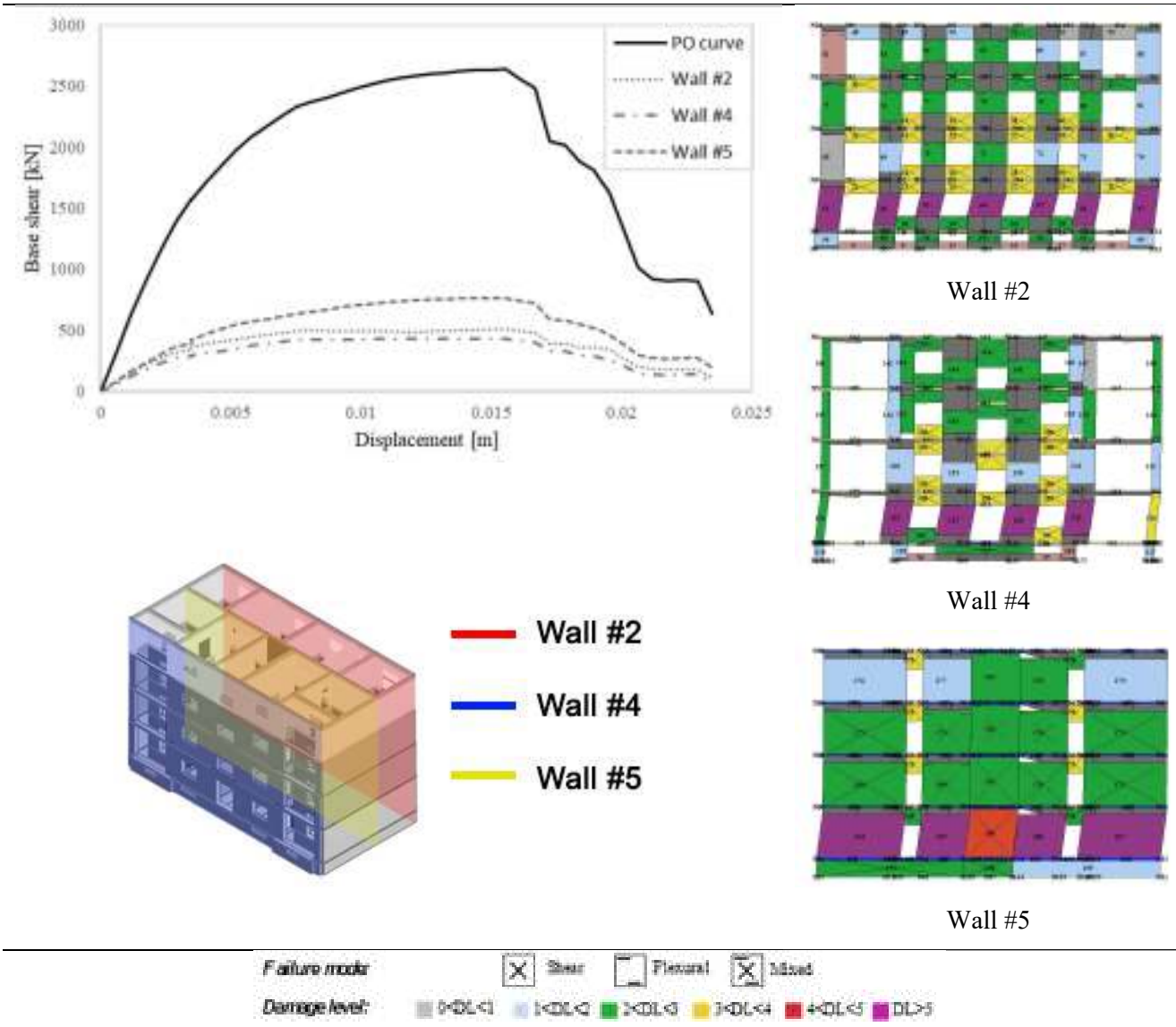

Figure 5.8. On the right; Capacity comparison between the total PO curve and the resistant walls in X direction, for the mass proportional pattern. On the left, damage patterns of the walls.

In Figure 5.8 the results in terms of capacity of the single masonry walls is shown. The PO curve and the damage patterns are referred to the N_RS_CB_CB_HB model. The geometry of the elevation walls combined with the relationship between the openings and the resistant masses rule the performance of the macroelement under seismic excitations. It is worth noting that Wall #5, since it is characterized by full massive walls, exhibit a higher capacity, carrying a higher base shear. For the same reason, Wall #4, which represents the main façades of the building, contribute in a minor way to the capacity of the building. As shown in the damage pattern of the masonry walls, the spandrels receive most part of the damage, then, the failure of the ground level occurs.

In *Y* direction, the PO curves denounce an evident brittle behavior, exhibiting a low nonlinear capacity. In Figure 5.9, the capacity of the global model is compared with the one of the singles walls along the *X* direction. For sake of brevity, only a PO curve for the N_RS_CB_CB_HB according to the mass proportional load pattern is presented. As expected, Wall #1 highlights a base shear over twice the maximum values obtained in the other macroelements. Other interest aspects are related are the capacities of Wall #6, 10 and 11.

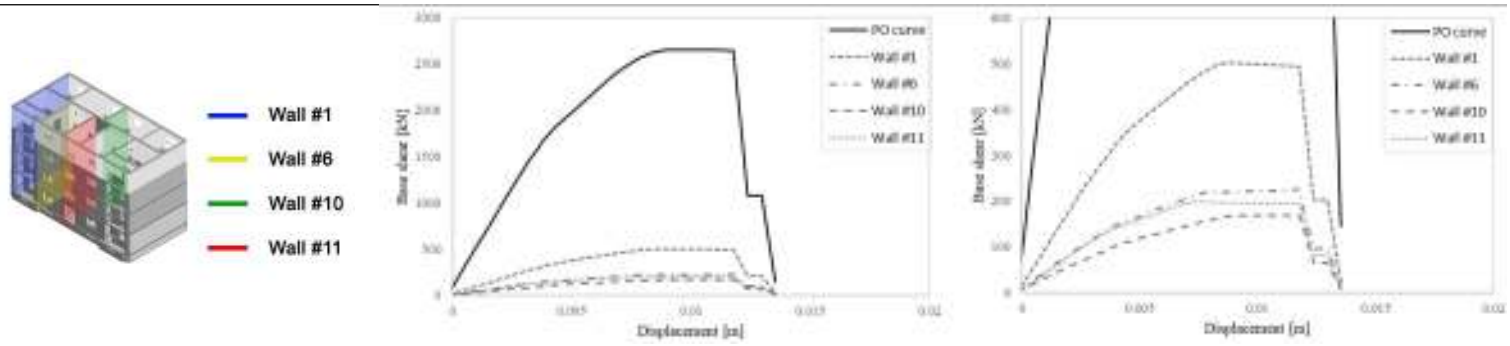

Figure 5.9. Capacity comparison between the total PO curve and the resistant walls in *Y* direction, for the mass proportional pattern.

The two last bearing walls, despite their massive proportions are not able to exhibit some higher capacity, since all the resistance is only demanded at the ventilation level. This is clear from the damage patterns of the model, presented in Figure 5.10. Herein, some difference involving the four models is presented. Nevertheless, the crack pattern shows that in case of a mass proportional pattern, the collapse of the models is given for a shear failure at the ventilation floor level. The damage is fairly limited to the upper structures and concentrated at the lowest level. Concerning the inverse triangular pattern, it leads to two different crises. For the two models without lintels over the opening, as already described for the *X* direction, the inverse triangular pattern, thanks to its distribution stresses differently the resistant walls, delaying the shear failure. This time, the collapse is given by a shear failure of the ground level; the masonry panels present a higher damage diffused along the height. On the other hand, in both models with lintels, the PO curves with the inverse triangular load are characterized by a flexural failure of the last level.

The different behavior of the models towards the load patterns along the two main directions can be justified by the different distribution – firstly – of the resistant walls -and secondly – by their masonry discretization. In *Y* direction, the predominant behavior of the structure can be associated with a frame-behavior, while in *X* direction the façades tend the structure to the perfect idealization of the frame structure. In the case of inverse triangular pattern, the lintels at the lower levels, exploit their plastic capacity during their coupling action, limiting the action transmitted to the piers. This last phenomenon, combined with the frame behavior of the walls in this direction, prevent the failure of the lower levels, so that the collapse of the structure deals with

the flexural failure of the last floor. The presence of lintels does not point out the same behavior in *X* direction, because of the different configuration of the masonry walls.

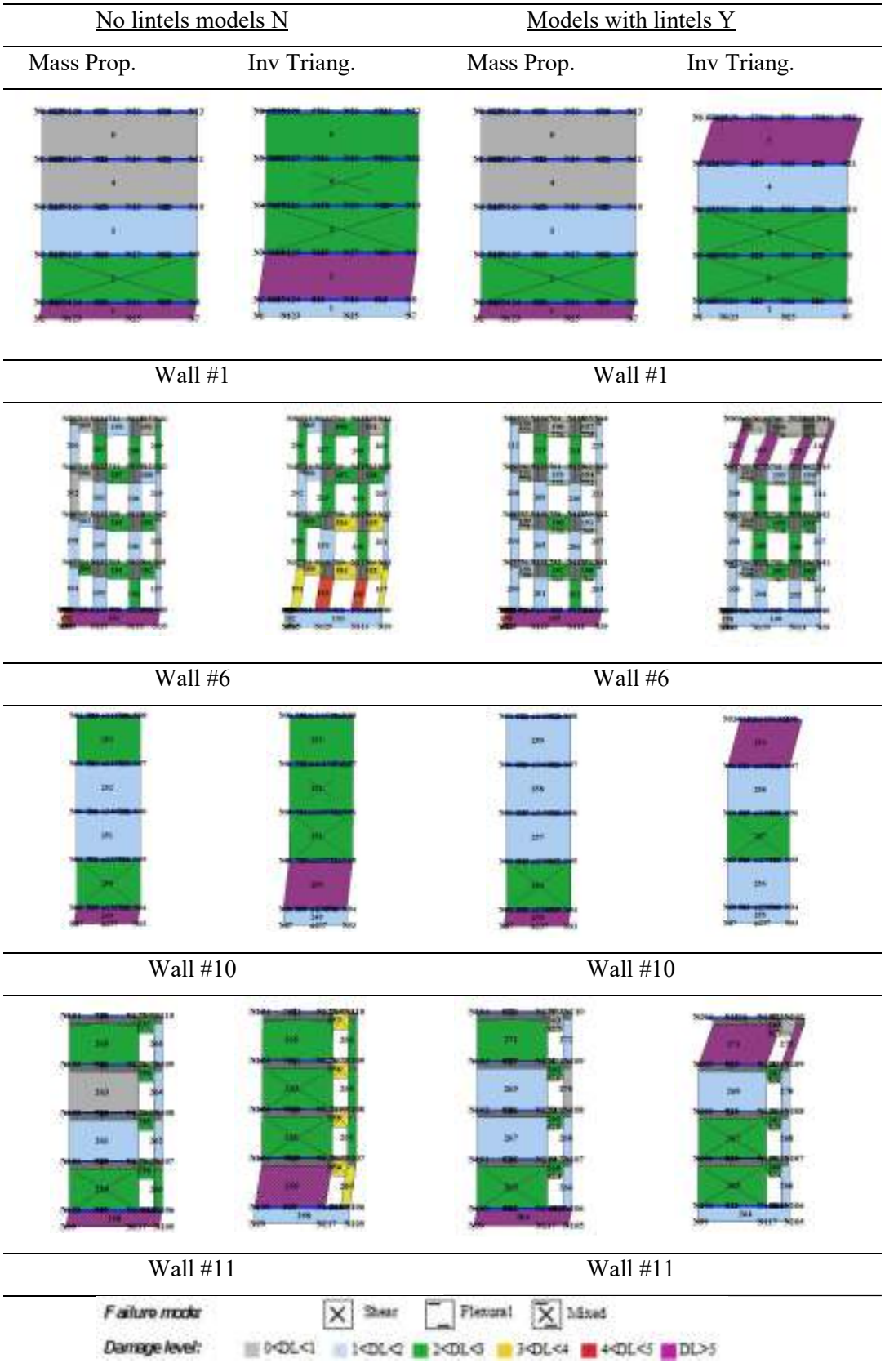

Figure 5.10. Damage patterns of the resistant walls in Y direction for the four considered models, for the two different seismic load patterns.

5.3 DEFINITION OF SEISMIC DEMAND

In this section, the seismic demand adopted for the risk analysis, was defined. The identification of the seismic hazard was essential for the adoption of the CSM and the comparison of the PLs (capacity) with the occurrence of a certain seismic intensity (demand).

The Florence basin has been developing since late Pliocene. The geological evolution led to the filling of the basin by plio-pleistocene palustrine and alluvial deposits, followed by two sedimentary cycles related to the paleo-Arno river and the holocene geomorphic evolution, respectively (Coli *et al.* 2015, Coli and Rubellini 2013). In Figure 5.11 the geological section of the Florence is shown.

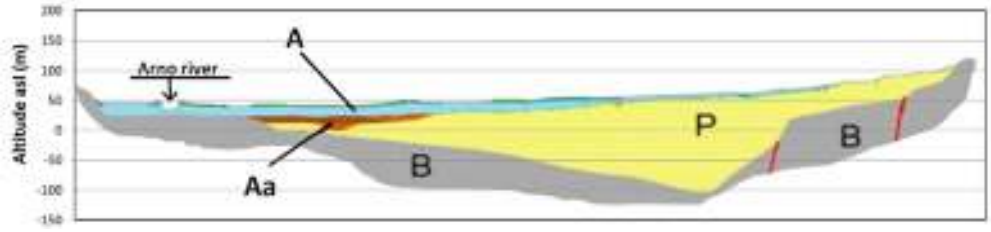

Figure 5.11. Geological section of the Florentine area (From Coli & Rubellini, 2015). B bedrock, P Plio-Pleistocene palustrine and alluvial deposits, A recent alluvial deposits of the Arno River and its tributaries, Aa ancient channel deposits of the palaeo-Arno River. Red line, faults.

The area is characterized by a moderate telluric activity; historical earthquakes estimated at 5 ML and their epicenters were located around Florence (Mugello 1542 and 1919, Impruneta 1456 and 1895, Valdarno 1770). Historical seismology is the main information to define the hazard of a place. Historical records show that the most severe earthquakes occurred in 09/28/1453 and 05/18/1895, both estimated at VII-VIII MCS level (Molin & Paciello, 1999, Rovida *et al.* 2016). In the past years, the soil of Florence has been checked through an extensive experimental investigation, which was based on the results of almost 2000 drillings, enhanced by 52 downhole proofs. For each test the maximum peak of the transfer function has been found, which has been combined with information provided by the downhole proofs about the stratigraphy of the area. More recently, these detailed studies underpin the seismic micro-zonation developed from the 2019. In the presented thesis these last works of micro-zoning developed by the Earth's Science Department had not been considered, since they were not finished in time to support the analytical part of this work.

The seismic demand has been defined accounting on the soil conditions and the hazard of the referred area. According to the CNR recommendations, a sample of 30 accelerograms compatible with the selected spectrum has been considered. In this work the data obtained by the Italian databases of INGV have been used. The selection of the compatible records was conducted using the software Rexel (Iervolino *et al.* 2009) through the *Rexel light* version. The database adopted for the ground motion research has been the European strong motion database

(http://esm.mi.ingv.it) promoted by the Working Group ESM (ESM working group, 2015). Complexly, a set of 30 accelerograms compatible with the area of interest have been selected. The spectra have been considered by the geometrical mean between the two planar directions. Following, they have been scaled over the fundamental period of the structures computed through linear modal analysis of the structural models. In this work, as presented in the previous section, four different structural models have been considered, which they provide four different fundamental models, one for each direction. In Table 5.1 the main fundamental modes of each structural model for each seismic direction are shown.

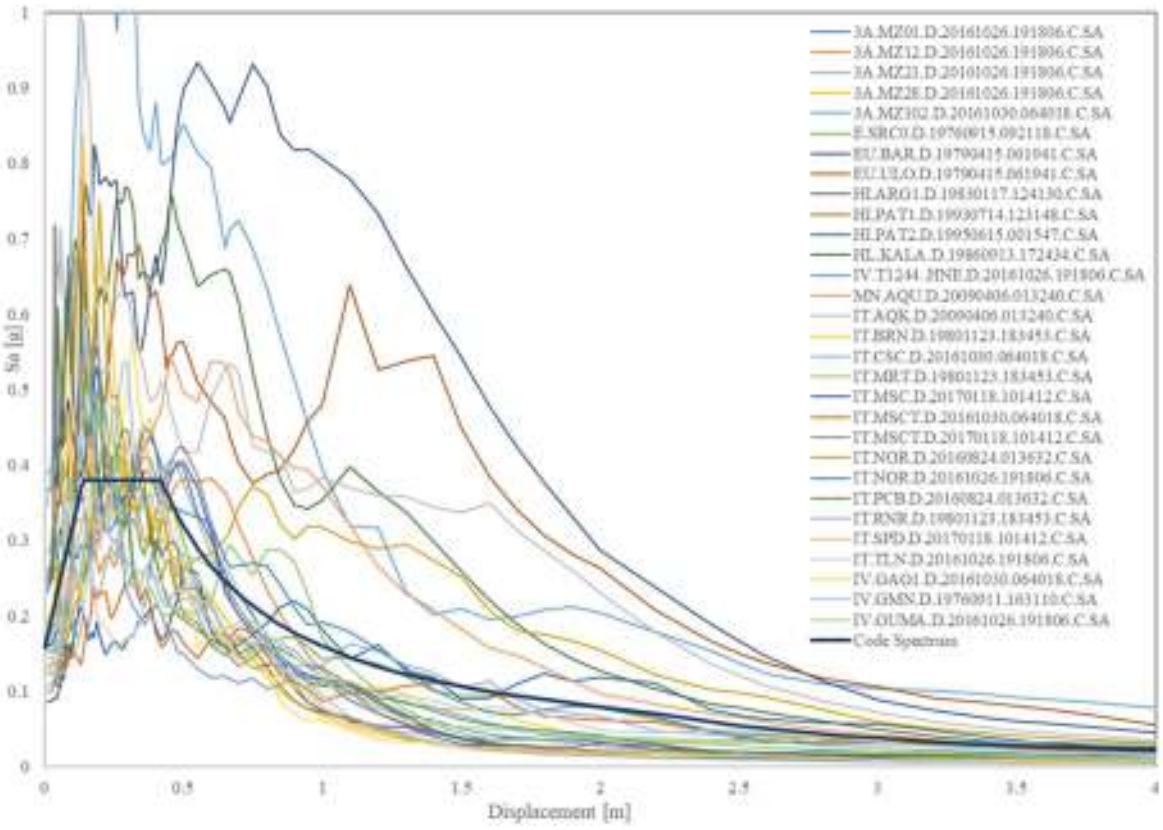

Figure 5.12. Set of accelerograms compatible with the soil of Florence for the definition of the Seismic Demand conditioned for the 0.335 s.

Table 5.1. Fundamental period of the different structural models assessed in this work.

	Fundamental period T_1 [s]	
	x	y
N/RS/CB/CB/HB	0.312	0.322
N/RS/RS/CB/HB	0.327	0.335
Y/RS/CB/CB/HB	0.297	0.313
Y/RS/RS/CB/HB	0.312	0.327

In the presented work, the seismic action has been considered as the demand of the performance-based methodology adopted. Considering the seismic spectra of Florence, in this thesis a return period of 475 years and a soil class B are taken into account. This specific soil class has been

assumed as the most reliable of Florence considering the last hazard maps and the soil stratigraphy's maps before the new micro-zoning studies. Of course, these assumptions could be improved in further studies, accounting for the new insights about the Florentine subsoils. The selected records extracted by Rexel have been scaled over the fundamental period of the structures shown in Table 5.1. In Figure 5.12 the sample of 30 accelerogram spectrum compatible with the Florence area are presented.

5.4 ALEATORY UNCERTAINTIES AND SENSITIVITY ANALYSIS

The aleatory uncertainties have been considered on the basis of the procedure descripted in Chapter 3. They have been assessed for each branch of the logic tree separately. The epistemic uncertainties were assessed on the *mean* models, characterized by the mean characteristics of mechanical properties and constitutive models. Hence, for each of the four models previously described, 7 aleatory uncertainties have been considered. To this aim, the star design with a central point approach has been adopted. Assuming the $2N+1$ analyses, with N is the number of aleatory uncertainties, 15 different models have been studied for each logic tree branch. Complexly, 60 different models have been assessed by means of nonlinear static analysis. The aleatory variables considered in this thesis are presented in Table 5.2. The first three variables, $X_{1,2,3}$ concern the mechanical properties of the resistant walls. Each parameter is referred to one of the three masonry typologies explained in the logic tree model. The different mechanical properties of each material are considered as dependent parameters, so they varied together. The fourth variable, X_4, is represented by the uncertainties in the concrete. For its value, as presented in Section 2.4, the mechanical property of the cubic compressive strength R_c has been deterministically assumed by the evidences of experimental researches made in Tuscany. It has been used in order to model the ring beams and the lintels over the openings. For the steel bars, a deterministic value has been adopted, without performing any sensitivity. In fact, in the presented thesis, the RC elements have been considered by their mechanical properties; in different works (Haddad *et al.* 2019, Milosevic *et al.* 2019a), the sensitivity of these latter was assumed considering the stiffness of the membranes. In this work, the assumptions made were firstly supported by the knowledge of the building case studies. Despite the mechanical property variations, the rigid contribution of the slabs was not questioned.

As described in the CNR-212 DT, the aleatory variables of the mechanical properties of the materials are described through lognormal distributions. Concerning the concrete, the have been instead defined deterministically. Regarding the last three parameters, $X_{5,6,7}$ they are related to the properties of the nonlinear constitutive law adopted in the modeling. X_5 rules the degradation of the initial stiffness assumed for the masonry panels. Finally, X_6 and X_7 collect parameters that affect the plastic phase and the nonlinear degradation. The values of θ_p indicate the drift values associated to the progressing damage, for different failures, for combined compressive and

bending stress or for shear, respectively; the β values indicate the associated residual strength. Their mean values are shown in Table 5.2. Different values are considered for the piers and for the spandrels respectively. For these parameters, since the distribution ranges in a finite interval, the Beta distribution has been adopted (CNR-DT212, 2013).

Table 5.2. Aleatory variables introduced in this work.

	Aleatory uncertainties		*min*	*mean*	*max*	
X_1	RS	*E (MPa)*	1054.9	1263.7	1472.4	Lognormal distrib
		G (MPa)	351.6	421.2	490.8	
		f_m *(MPa)*	0.916	1.27	1.623	
		τ_0 *(MPa)*	0.026	0.033	0.040	
X_2	CB	*E (MPa)*	2284.9	2625.1	2965.3	Lognormal distrib
		G (MPa)	761.6	875.0	988.4	
		f_m *(MPa)*	1.97	2.66	3.36	
		τ_0 *(MPa)*	0.049	0.082	0.114	
X_3	HB	*E (MPa)*	1200	1400	1600	Lognormal distrib
		G (MPa)	300	350	400	
		f_m *(MPa)*	1.50	1.75	2.00	
		τ_0 *(MPa)*	0.095	0.11	0.125	
X_4	concrete	*Rcmean (MPa)*	13.25	21.18	30.92	Deterministic
X_5	*kr*		0.5	0.65	0.8	Beta distrib
	kel		1.25	1.50	1.75	
X_6	*drift piers*	$\theta_{P,PF3}$	0.0046	0.006	0.0074	Beta distrib
		$\theta_{P,PF4}$	0.0078	0.01	0.0122	
		$\theta_{P,PF5}$	0.012	0.015	0.01796	
		$\beta_{PF,E3}$		1.00		
		$\beta_{PF,E4}$	0.8	0.85	0.9	
		$\theta_{P,S3}$	0.0023	0.003	0.0037	
		$\theta_{P,S4}$	0.0039	0.005	0.0061	
		$\theta_{P,S5}$	0.012	0.015	0.01796	
		$\beta_{S,E3}$	0.6	0.7	0.8	
		$\beta_{S,E4}$	0.25	0.4	0.55	
X_7	*drift spandrels*	$\theta_{S,3}$	0.0015	0.002	0.0025	Beta distrib
		$\theta_{S,4}$	0.0045	0.006	0.0075	
		$\theta_{S,5}$	0.015	0.020	0.025	
		$\beta_{PF,E3}$	0.3	0.500	0.7	
		$\beta_{PF,E4}$	0.3	0.500	0.7	

The different PO results have been firstly discussed in terms of capacity curves, then in terms of intensity measure values for the limit state attainments. To this aim, the definition of the LSs was needed. In the procedure the multi-scale criterium presented in Section 3.3.2 has been used. The different LSs were plotted on the PO curves accounting for the first attainment of the threshold value according to checks done at the element scale (*E*), the macroelement scale (*M*) and the global building level (*G*). The results provided different results, nevertheless, in general it is possible to point out a main prevalence of the *G* criterium for the attainment of the LSs. Especially for the last performance points, the *E* criterium has been rarely the first one. This can be mostly justified by the story failure of the buildings which characterize a limited number of elements. On the other side, especially for the yes-lintel models, the drift computations have been the ones

attaining before the LS thresholds, especially in *Y* direction. In Figure 5.13 some example of the progression of the different criteria during the performance of the PO analyses are shown.

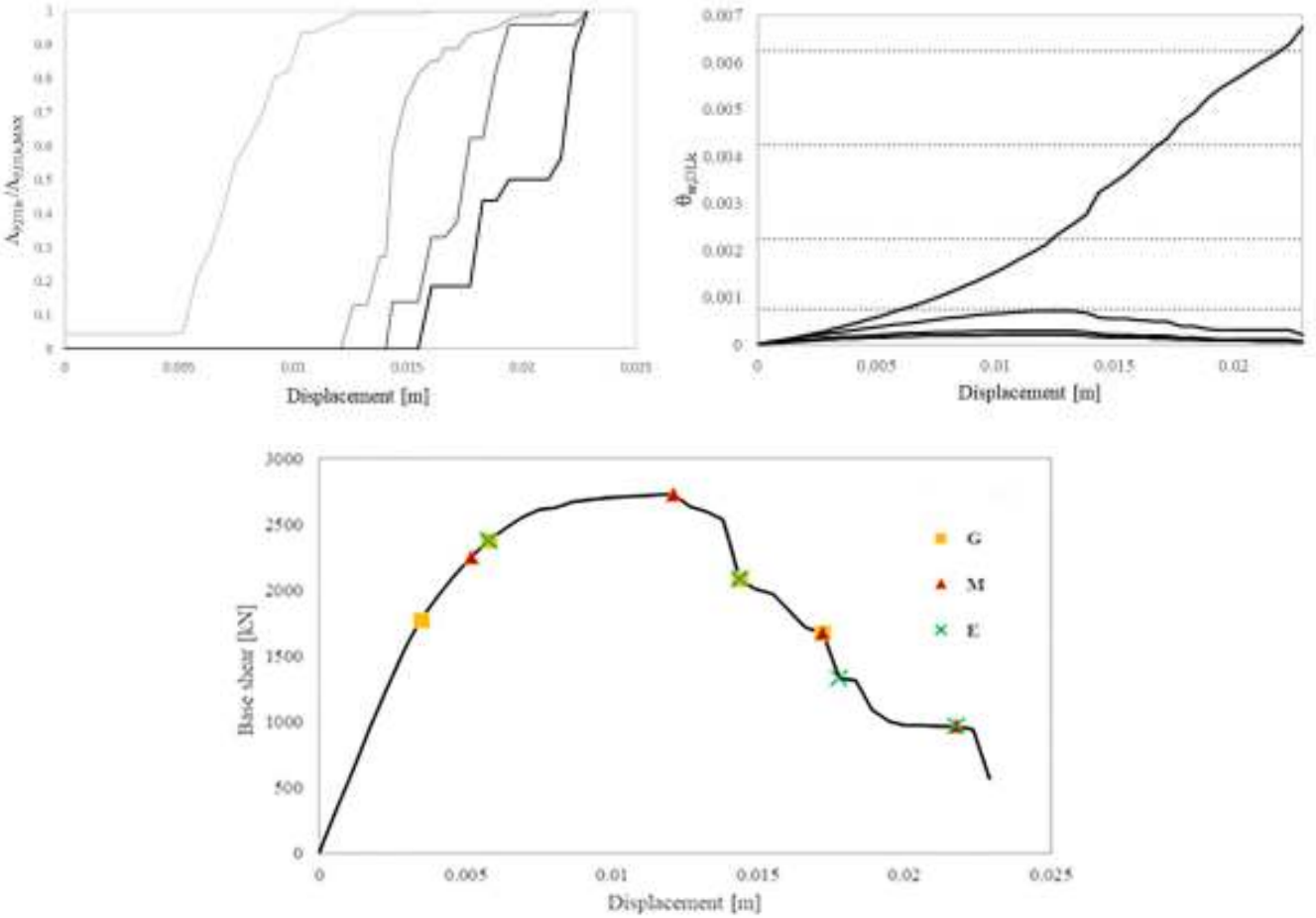

Figure 5.13. On top: normalized cumulative damage and drift distribution. Below: the multi-scale approach.

5.4.1 Definition of the Equivalent viscous damping

The cyclic pushover analyses have been performed for the PLs previously defined. Their target was the definition of proper hysteretic damping values ξ_{visc} for the computation of the equivalent viscous damping ξ_{eq}. Namely, it deals with the hysteretic capacity of the models during the seismic excitation. In this work, cyclic pushover analyses have been performed along the two directions accounting for both senses of the analysis (positive and negative contributions), for each different LS. The analyses were performed in displacement-control, where the displacement of the n-th LS defined by means of nonlinear static analysis has been assigned as the maximum displacement of the cyclic pushover one. In Figure 5.14 the cyclic PO analysis graphs for the N/RS/CB/CB/HB model, inverse triangular load pattern and *Y* direction are plotted; all the graphical results for the cyclic pushover curves are shown in the Appendix. The results are finally provided in terms of elastic viscous damping for the different LS (Table 5.3).

Table 5.3. Viscous damping for the different considered models.

DL1		X Direction				Y Direction			
		MP +	MP -	IT +	IT -	MP +	MP -	IT +	IT -
	RS CB	0.071	0.067	0.072	0.069	0.061	0.058	0.062	0.059
N	RS RS	0.079	0.075	0.078	0.076	0.057	0.059	0.060	0.062
	RS CB	0.071	0.072	0.085	0.085	0.059	0.061	0.064	0.066
Y	RS RS	0.060	0.060	0.062	0.052	0.055	0.059	0.062	0.063
DL2		X Direction				Y Direction			
		MP +	MP -	IT +	IT -	MP +	MP -	IT +	IT -
	RS CB	0.120	0.100	0.114	0.099	0.066	0.069	0.074	0.109
N	RS RS	0.121	0.122	0.134	0.129	0.068	0.073	0.082	0.104
	RS CB	0.110	0.110	0.132	0.132	0.072	0.076	0.084	0.086
Y	RS RS	0.082	0.103	0.113	0.091	0.072	0.077	0.076	0.082
DL3		X Direction				Y Direction			
		MP +	MP -	IT +	IT -	MP +	MP -	IT +	IT -
	RS CB	0.178	0.145	0.153	0.148	0.100	0.122	0.163	0.164
N	RS RS	0.176	0.175	0.244	0.161	0.116	0.126	0.139	0.152
	RS CB	0.200	0.199	0.200	0.193	0.128	0.129	0.180	0.145
Y	RS RS	0.223	0.221	0.204	0.142	0.112	0.122	0.144	0.172
DL4		X Direction				Y Direction			
		MP +	MP -	IT +	IT -	MP +	MP -	IT +	IT -
	RS CB	0.354	0.310	0.297	0.284	0.124	0.130	0.233	0.205
N	RS RS	0.221	0.352	0.348	0.176	0.320	0.141	0.195	0.362
	RS CB	0.267	0.265	0.356	0.357	0.173	0.232	0.363	0.257
Y	RS RS	0.324	0.267	0.313	0.219	0.231	0.125	0.240	0.232

Concerning the execution of the cyclic pushover, a different behavior towards the *X* and the *Y* direction is shown. This is still ascribable to the different distribution and the different features of the resistant walls along the two axes. In *X* direction, a higher hysteretic capacity is expressed, already related to the lowest LSs. This is barely notable for *DL1*, then, for *DL2* it increases its evidence. In *X* direction, a mean value of 0.113 is given for *DL2*, against a 0.079 in *Y* direction. The difference becomes more relevant for the higher DLs, with a mean value of 0.185 against 0.138 for *DL3* and 0.294 compared to 0.222 for *DL4*, for *X* and *Y*, respectively. Looking at the two load patterns, the inverse triangular pattern generally highlights a higher dispersion in the damping values. Comparing the coefficient of variations along the two direction, the *Y* one denounces lower coefficient of variations; only for the *DL4* the dispersion is the higher one, bigger than the one in *X* direction. The hysteretic damping values points out, coherently with the PO curves analyses, the different performances of the structures along the two directions. The brittle behavior of the models in *Y* direction is shown by lower damping values; on the other hand, the

ductility capacity of the structures in *X* direction highlights higher values of its hysteretic behavior.

Y Direction – Inverse Triangular Pattern

DL1

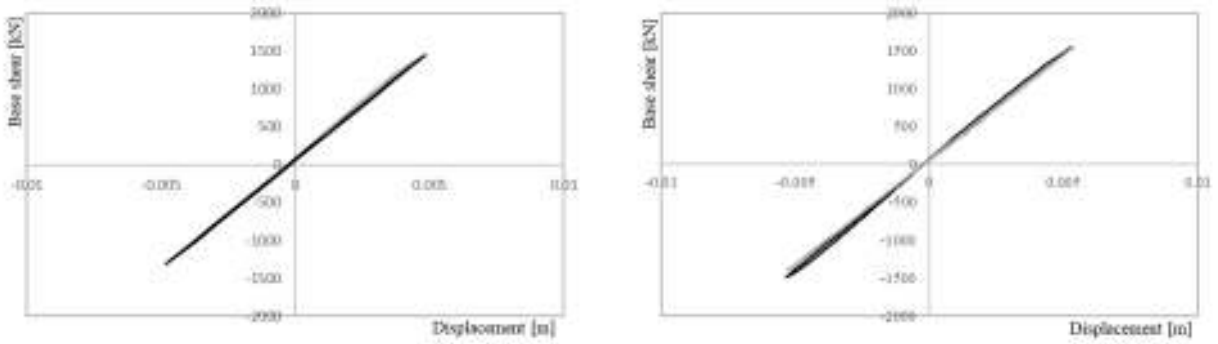

DL2

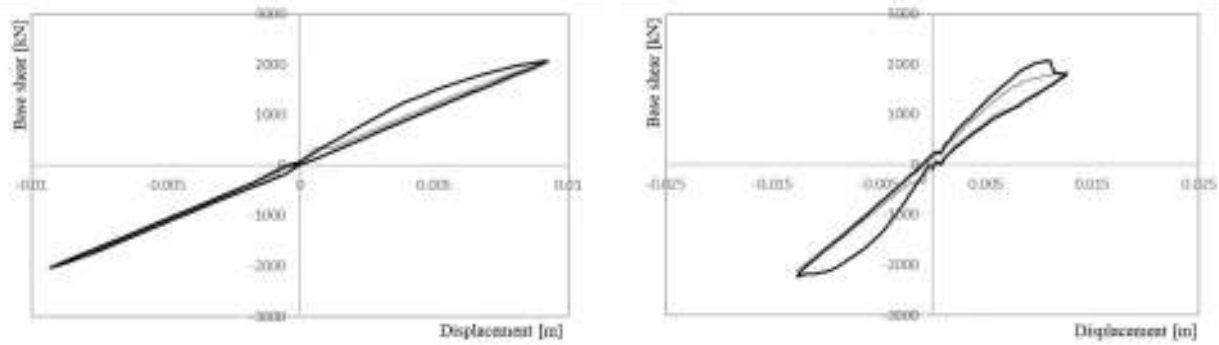

DL3

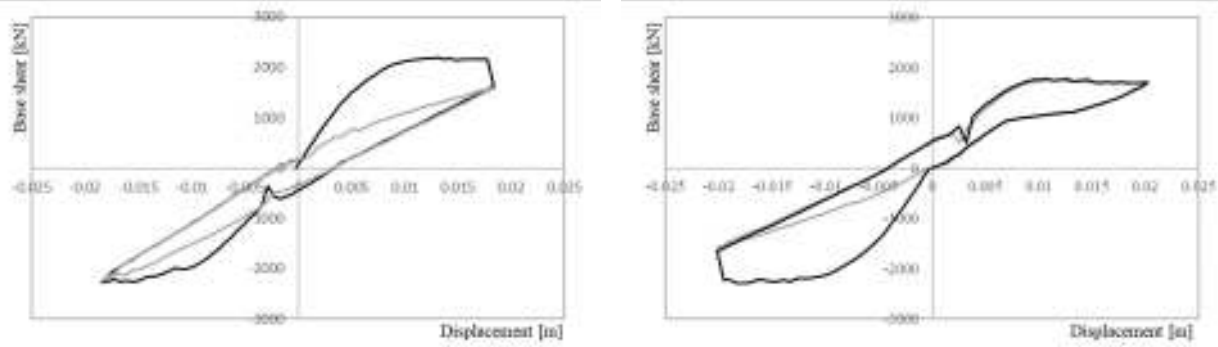

DL4

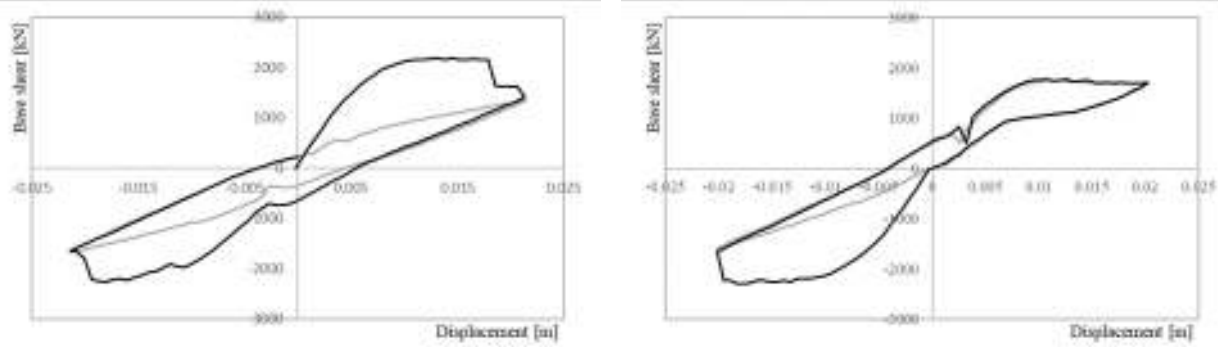

Figure 5.14. Cyclic pushover curves for the N/RS/CB/CB/HB model along the *Y* direction according the inverse triangular seismic pattern.

5.4.2 Definition of the Intensity Measure and Sensitivity Analysis

The procedure developed in 5.4.1 was necessary in order to express the different PLs in terms of the selected IM. In this work, the sensitivity of the different parameters previously descripted has been finally assessed. For each model, according to the central star approach, NLSAs have been performed. The graphs presented in Figure 5.15 and 5.16 shows the variability of the response towards the aleatory uncertainties.

N_RS_CB_CB_HB

X direction	Y direction
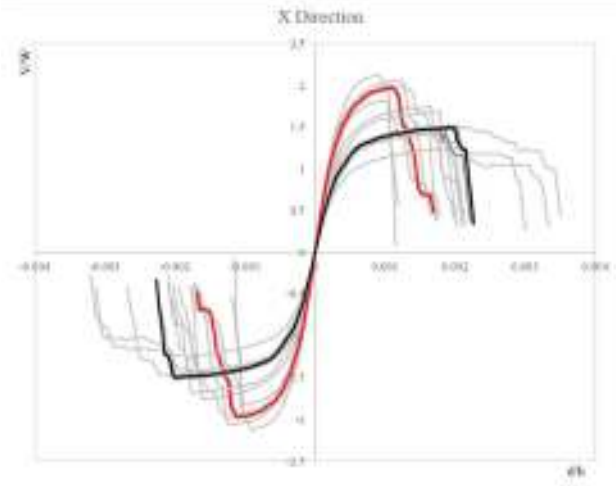	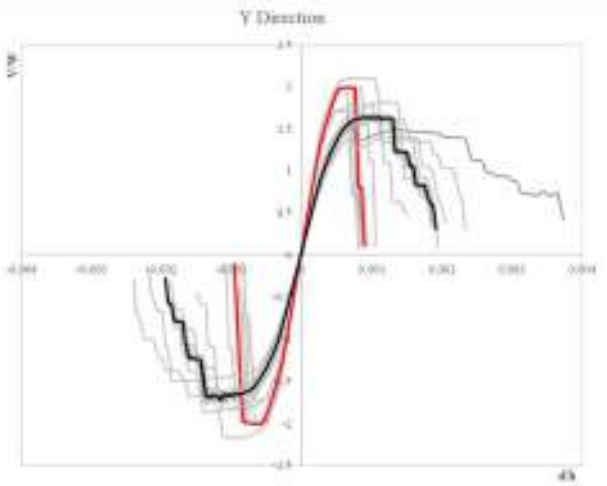

N_RS_RS_CB_HB

X direction	Y direction
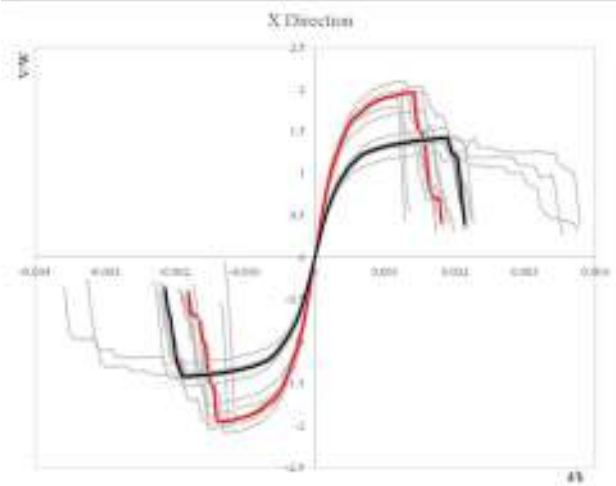	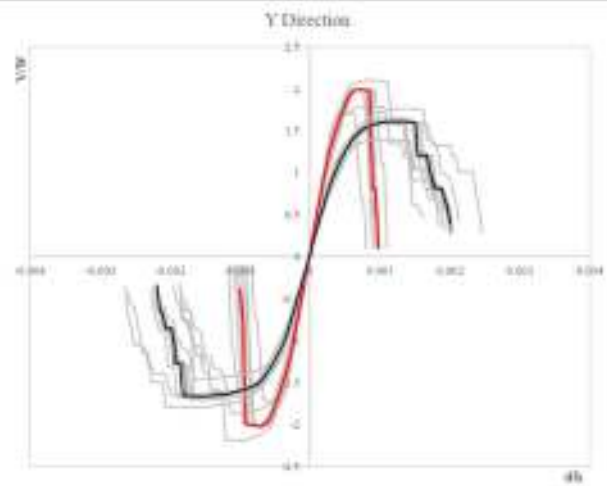

Figure 5.15. PO curves of the No-lintel models according to the two directions and the two load patterns.

The colored lines represent the PO curve of the mean model with all the mean values of the aleatory uncertainties (i.e. the epistemic uncertainties); the red and the black lines are referred to the two considered load patterns, the mass proportional and the inverse triangular, respectively. The grey lines plot the remaining aleatory uncertainties involved in the analyses, i.e. other 14 PO analyses executed for each seismic pattern. The sense of the analysis is distinct by positive and negative contributions.

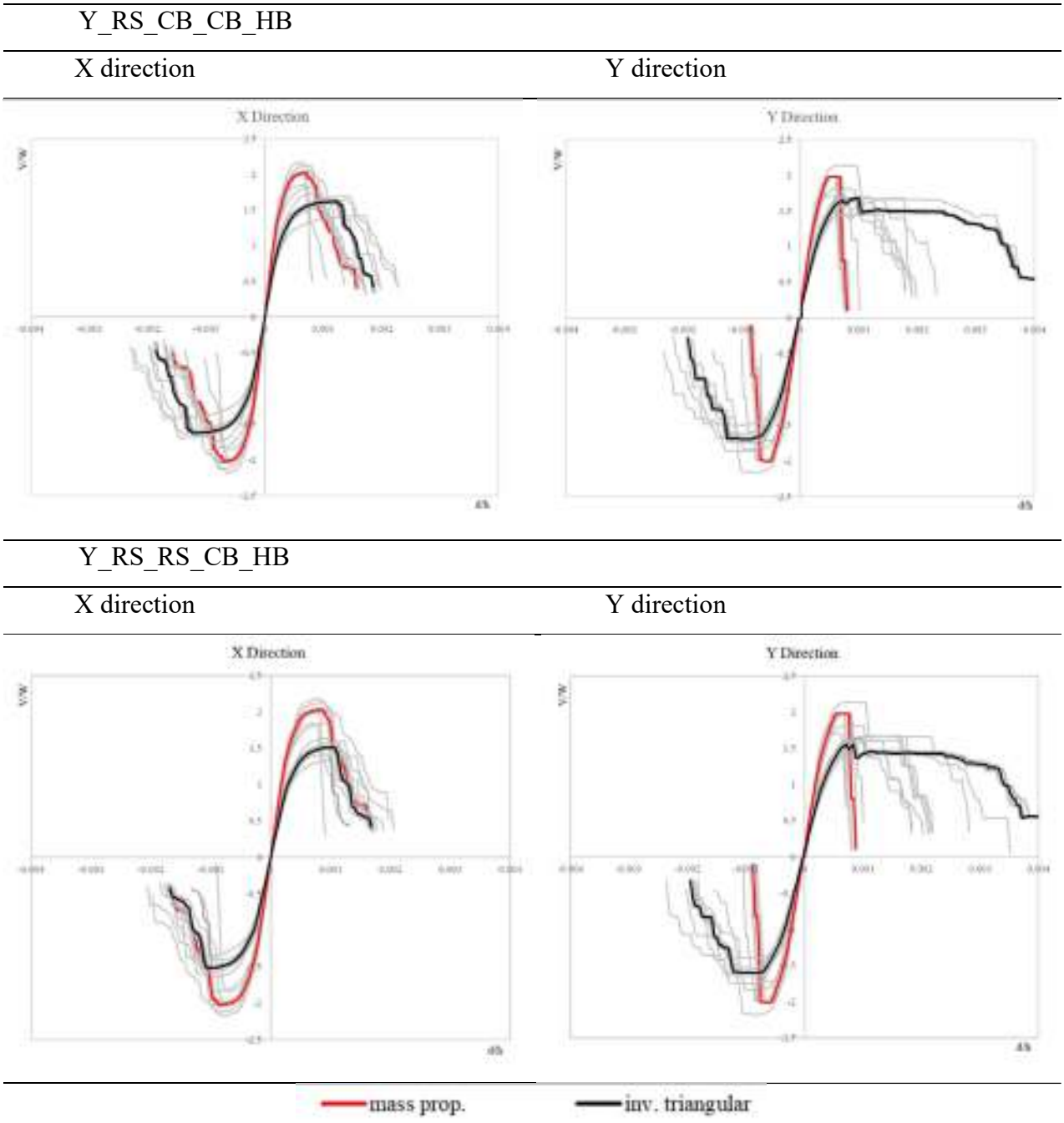

Figure 5.16. PO curves of the Yes-lintel models according to the two directions and the two load patterns.

Finally, in this work the comparison between the different models is obtained in terms of IM. For all the four logic tree branches, the PGA levels achieving the different DLs has been defined. The

sensitivity of each parameter was accounted in terms of comparisons between the PGA values needed for the attainment of a certain DL. According to the CNR-DT-212 recommendations and to Cattari et al. (2014), the sensitivity to variables X_k is assessed through the variable $\Delta_{PLi,Xk}$ computed by:

$$\Delta_{PLi,Xk} = 2\,\frac{IM_{PLi,k-max} - IM_{PLi,k-min}}{IM_{PLi,k-max} + IM_{PLi,k-min}} \tag{5.1}$$

The sensitivity of the different epistemic uncertainties can be assessed too. In this case, given M branches, the j-th epistemic uncertainty is expressed through the $\Delta_{PLi,Yk}$ parameter, as:

$$\Delta_{PLi,Yj} = 2\,\frac{max\left(u_{j,IM_{PLi},mean,q}\right) - min\left(_{j,IM_{PLi},mean,q}\right)}{max\left(u_{j,IM_{PLi},mean,q}\right) + min\left(_{j,IM_{PLi},mean,q}\right)} \tag{5.2}$$

Where $\mu_{j,IMPLi,mean,q}$ is the mean of the different IM_{Pli} values outcoming from the logic tree approach by assuming the mean value for all the random variables. The sensitivity of each parameter can be assessed by the definition of sensitivity classes (SC). Three SCs are here defined: high sensitivity (SCH), medium sensitivity (SCM) and low sensitivity (SCL) (Cattari et al. 2014). The three classes are defined as a function of the $\Delta_{PLi,Xk}$ (or $\Delta_{PLi,Yk}$):

- SCH: $\Delta_{PLi,Xk}$ *(or* $\Delta_{PLi,Yk}$*)* $>$ *2/3* $\Delta_{PLi,\,max}$
- SCM: *1/3* $\Delta_{PLi,\,max} \leq \Delta_{PLi,Xk}$ *(or* $\Delta_{PLi,Yk}$*)* $\leq$ *2/3* $\Delta_{PLi,\,max}$
- SCL: $\Delta_{PLi,Xk}$ *(or* $\Delta_{PLi,Yk}$*)* $\leq$ *1/3* $\Delta_{PLi,\,max}$

The results, in terms of PGA presents some deviation. Concerning the epistemic branches, the results of the sensitivity analysis showed a low sensitivity of the different models to the seismic response. On the other side, wider considerations may be done for the aleatory uncertainties. As example, the values for the attainment of the *DL3* for the N/RS/RS/CB/HB model are shown in Figure 5.17. A discrete variability between the directions and the different load patterns is pointed out. The outcomes in terms of SCs for the different aleatory variables are finally briefly shown in Figure 5.18.

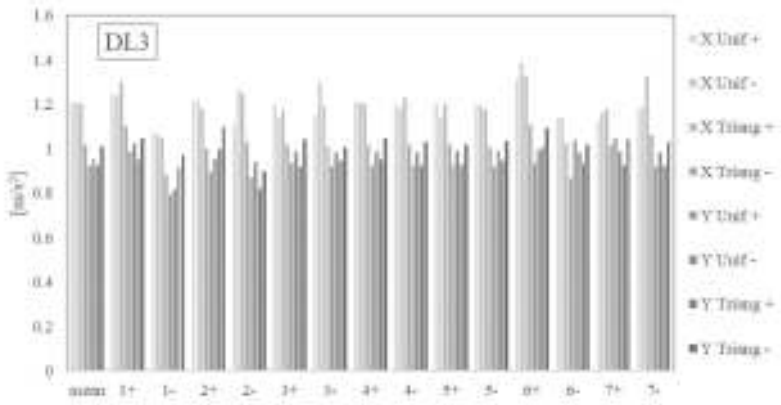

Figure 5.17. Variability of the capacity response due to the aleatory uncertainties.

Herein, the different SCs have been assessed for each seismic direction, for the two patterns according to the two positive and negative senses for the four DLs considered. For the different classes, the $\Delta_{PLi,\ max}$ has been found and the relative SC classes defined. In order to assess the sensitivity of each parameter not singularly referred to the DLs, the different LSs have been superimposed and their numerousness was weighed to the total of the SCs. In Figure 5.18 the superimposing procedure for each epistemic model is shown. In the Appendix, the SCs are presented one by one. The three colors identity the different SCs; orange for SCH, yellow for SCM and green for SCL. Basically, the definition of univocal judgments over the models, not related to the DLs is an important issue, nevertheless, it is important to collect separately the different contributions in order to define the sensitivity at the different PLs. Observing the Figure it is worth noting the aleatory variable X_1, X_2 and X_6 show the higher sensitivity. The first two parameters are referred to the mechanical properties of the RS and the CB masonry, respectively. Concerning X_1, the 65% of the variables are scheduled into the SCH class, approximately equally distributed along the different models and the different DLs, while 20% is given for SCM and the 15% for SCL. X_2 is divided as 56% for SCH, 23% for SCM and 21% for SCL. In this parameter, some difference is involved, especially for the higher DLs. In the case of no-lintel-models (N), the aleatory variable points out its sensitivity for the lower DLs, (*DL1* and *DL2*), while for the *DL3* and *DL4*, it is for the 53% of the times in SCL. On the other side, in case of yes-lintel-models (Y) the influence of the parameter is extremely sensitive especially for *DL4* (68.75% in SCH). The influence of the third mechanical typology investigated, X_3, which has been defined for the modeling of the bearing walls at the last level does not seem so relevant. This is ascribable to the failure collapses of the models, which mostly regard the lowest floors. Yet, the influence of the concrete variability ranges between the SCL and the SCM, with a prevalence of SCL (74% of the parameters are in SCL). A higher interest is pointed out by the variable X_5 especially in the definition of the DL1. This is highlighted in all the four models in a different way; nevertheless, the connection between the parameter definition and the first DLs is an intrinsic one. Concerning parameter X_6, it denounces a discrete sensitivity to the seismic response of the models. The 26.5% of the parameter enter in SCH class, with a 27.5% in SCM and the 46% in SCL, respectively. Despite the prevalence of the SCL class, this parameter mostly influences the performance of the models for the highest DLs. The sum of *DL3* and *DL4* it shows a SCH 26 out 32 times (81%). Finally, parameter X_7 shows a limited sensitivity. Looking at the SCs map patterns in the Appendix, it is worth noting that some load pattern is able to generate a higher variety in terms of seismic response. This is clear especially in the *Y* direction, where, depending on the models, the uniform and the inverse triangular pattern tends to enlarge the PGA variability. Between the models, it is possible to observe that the

lintels allow a more localized sensitivity, mostly referred to the three most sensitive parameters described.

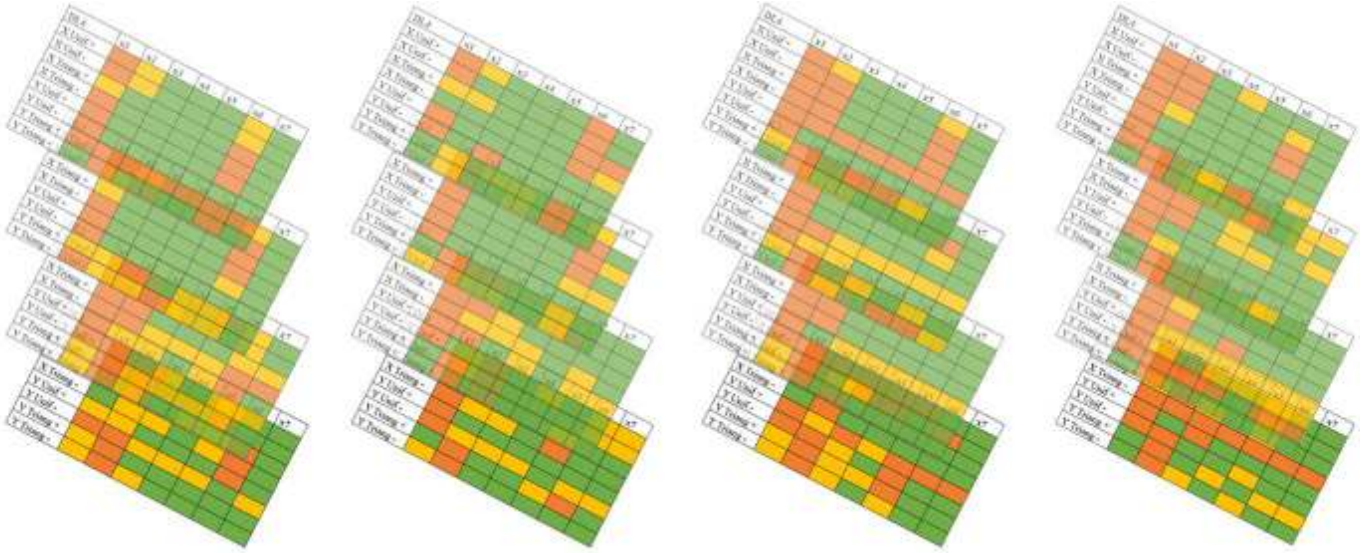

Figure 5.18. Superimposition assessment of the sensitivity of the different parameters investigated.

5.5 DERIVATION OF THE ANALYTICAL FRAGILITY CURVES

Assumed the PGA values for the different DLs and the aleatory and epistemic models, fragility curves can be finally derived. The analytical formulation has been applied separately to the four models, according to the assumption of statistical independence of the different logic tree branches. To derive the fragility curves, the total dispersion β_T of the models needs to be computed. According to the procedure described in 3.3.4, the dispersion herein utilized account for both contributions of the seismic demand and the building capacity. The final values are obtained by the geometrical mean of the two different parts. In Figure 5.19 the PGA values and the relative dispersions for the no-lintel and yes-lintel models, respectively, are shown.

The plotted PGA values are referred to the minimum value between the positive and the negative contributions according to each seismic load pattern and each direction. The four models show some difference between the seismic performances of the structures. Specifically, the ductility capacity expressed in the *X* direction and descripted in Section 5.2 is highlighted by the bigger differences involving the PGA values for the attainment of the different *LSs*. In the *Y* direction, the variations are minor, with closer PGA values, especially between *DL3* and *DL4*. The vicinity of the *PLs* in the nonlinear phase confirm the trends already pointed out with the *PO* curves. Concerning the dispersion values, β_T ranges between 0.1 and 0.22. It tends to increase along the development of the different *DLs*, especially in the *X* direction. The inverse triangular pattern is the one with the highest dispersions. Excluding those values, the dispersion rates are low, and they mostly range around 0.15.

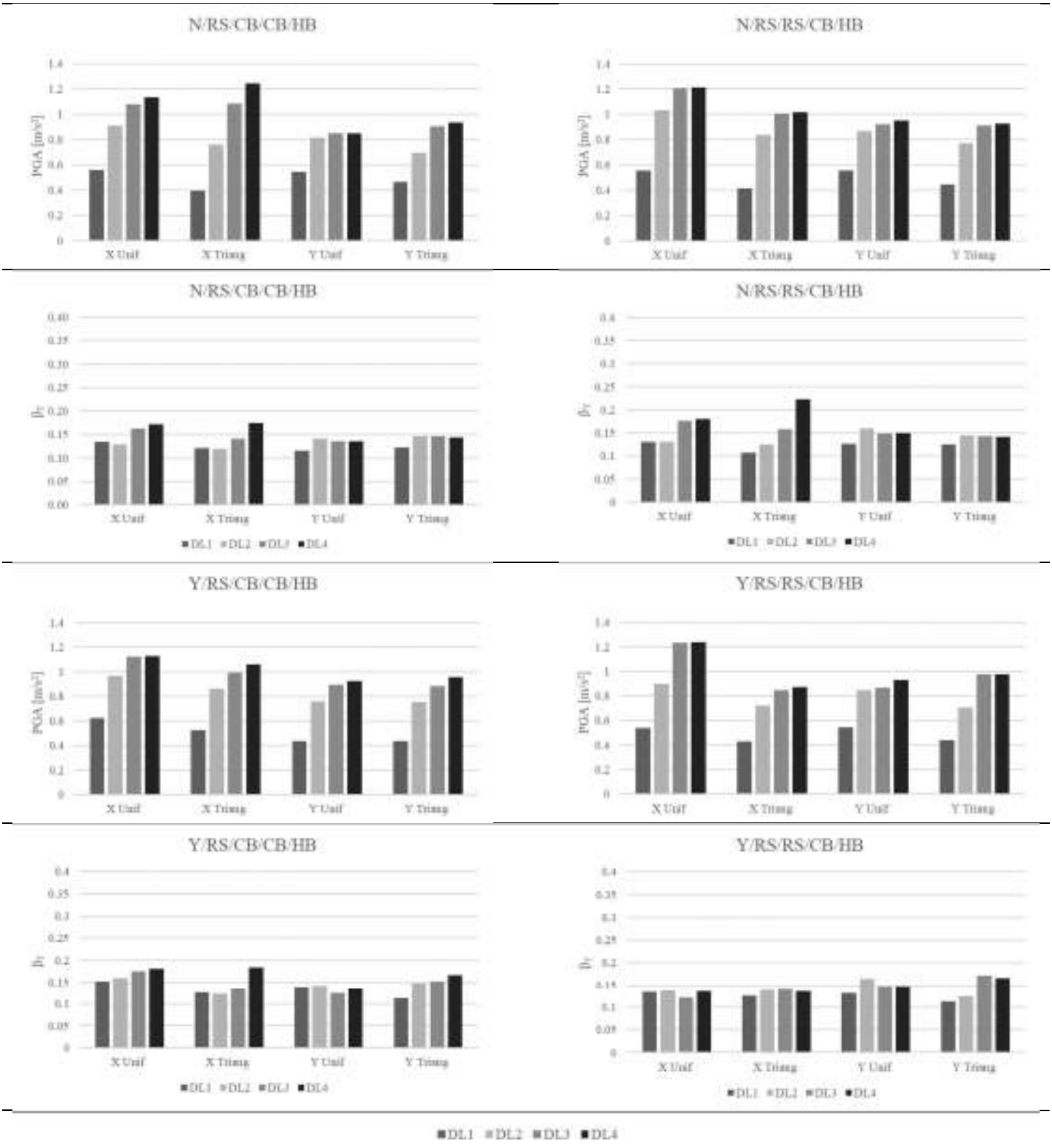

Figure 5.19. The PGA values and the relative dispersions for the four models.

Finally, the analytical curves can be derived for each direction and each seismic load pattern. In Figure 5.20 and Figure 5.21 the plots are shown. Each curve expresses the probability of exceedance of a certain *DL* for a given intensity measure. Namely, the PGA values for the different attainments set the central point of the curve, fixed at the 50% of the 0-1 distributions;

hence, the dispersion values rule the slope of the curve denouncing the variation of probability towards different seismic intensities. Looking at the figures, the performance of the models points out some differences. Concerning both load patterns, for the two directions, usually a higher offset distance insists between the *DL1* and *DL2*; then, the curves express a relative brittle behavior with a fast attainment of the further *LSs* and limited distances between *DL2*, *DL3* and *DL4*. This is pointed out by different models; in *X* direction, in models N/RS/RS/CB/HB Y/RS/CB/CB/HB, for the mass proportional pattern the fragility curves are plotted almost simultaneously. On the other side, the inverse triangular pattern generally exhibits a higher scatter between the two *LSs*, in all the models expect for Y/RS/RS/CB/HB. In the other cases, some superimposition between the two curves is pointed out, especially for low PGA intensities (models N/RS/RS/CB/HB and Y/RS/CB/CB/HB). This is justified by the different inclinations of the curves combined with the close distances of the PGA values for the attainment of the LSs and, because of the intrinsic definition of progressive *DLS*, it won't be considered in the definition of damage scenarios.

In the *Y* direction, the low ductility of these structures was already highlighted; the models show a relevant nearness between from *DL2* to *DL4*, which prove the rapid nonlinear degradation of the model. The mass proportional pattern leads to close fragility curves from *DL2* to *DL4*, especially for the two models without lintels. Furthermore, the inverse triangular pattern brings to overlaps for the last to curves. Despite the *PO* graphs showed a higher capacity in the plastic range, this is due to the achievement of the *LSs* along the nonlinear branch.

Comparing the fragility curves found through the four models, is not easy to define common trends. For this reason, the curves have been assessed together, considering the two load patterns for each direction. Between the four models, in the *X* direction a higher variability for the different *LSs* is shown, in particular for the inverse triangular pattern, where *c.o.v.* values range between the 8 and the 14%. In the *Y* direction, the mass proportional pattern shows the higher variability, especially for the lower *DLs*. Comparing the same *PLs* in terms of damage pattern it is worth noting a different behavior towards the two directions. In fact, the inverse triangular pattern achieves first its *DLs* in the *X* direction, for all the consider *PLs*. On the other side, for *Y* direction, a mixed result is expressed. The results are still coherent with the *PO* curves. Indeed, in *X* direction the inverse triangular pattern denounces lower base shear values and stiffness. Hence, despite longer plastic branches, with capacity curves almost horizontal, the capacity decreases rapidly, so it attains the *PLs* before than the mass proportional pattern. In the *Y* direction the stiffness and the maximum base shear of the inverse triangular pattern are lower than the other seismic one; in this case, both load patterns highlight a remarkable brittle behavior with an immediate decrease of strength and an immediate transfer from *DL3* to *DL4*.

N/RS/CB/CB/HB

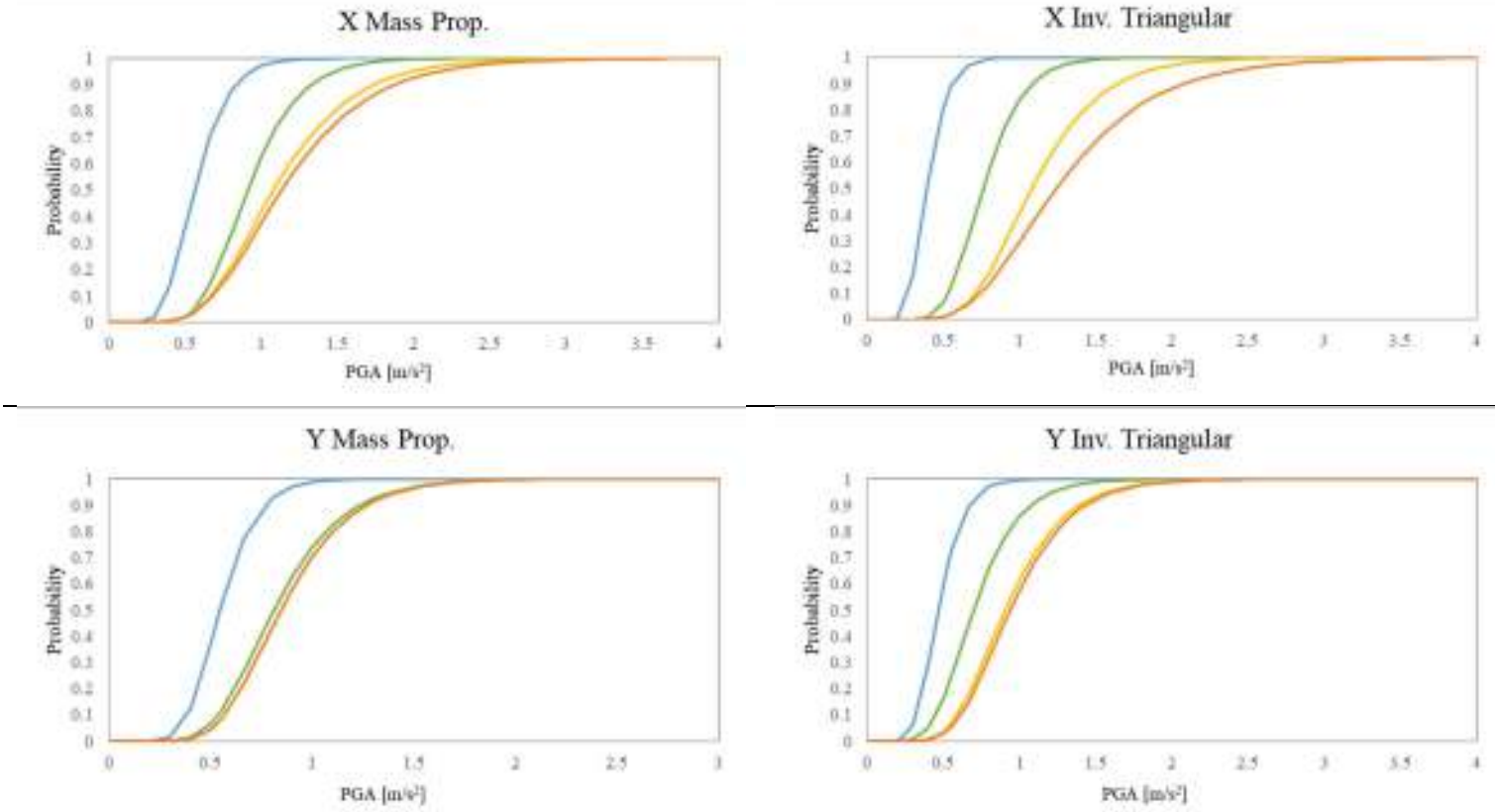

N/RS/RS/CB/HB

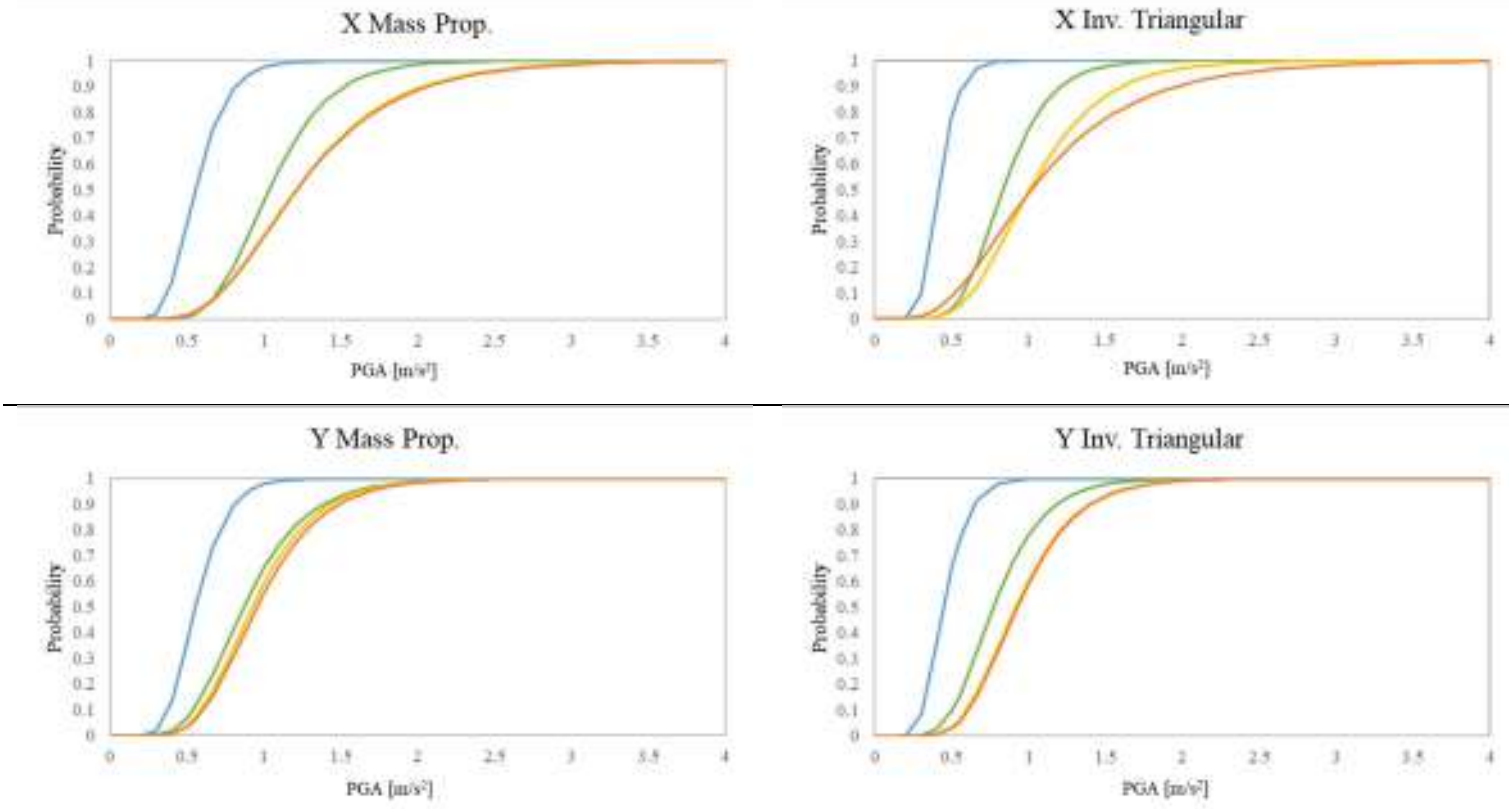

Figure 5.20. The fragility curves for the two no-lintel models.

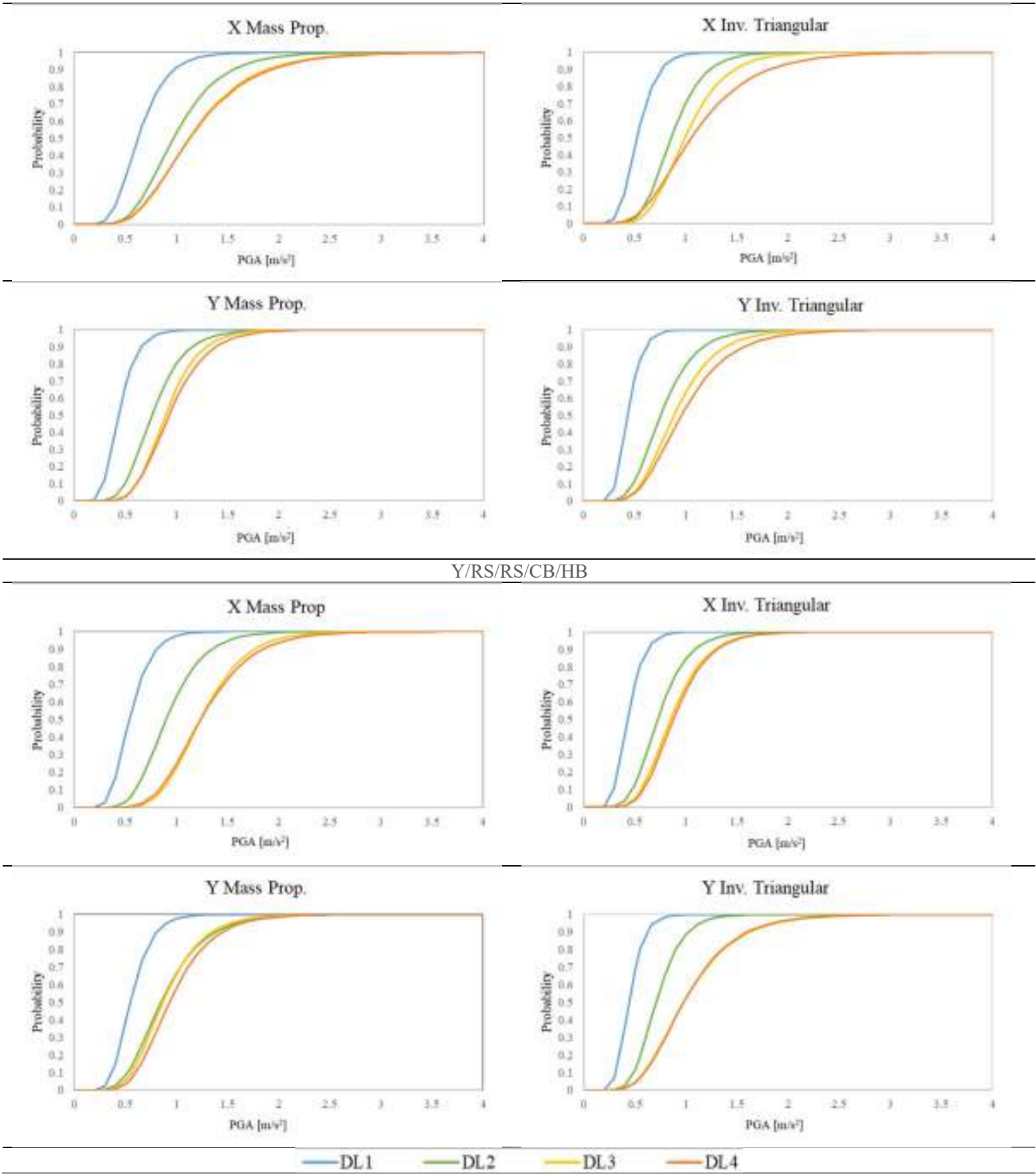

Figure 5.21. The fragility curves for the two yes-lintel models.

Finally, the damage scenarios have been forecasted adopting the *DS* probability distribution of the derived fragility curves. At this point of the work, the assumption of the most reliable load pattern would be necessary. Different approaches can be used. The execution of nonlinear dynamic analyses is probably the more adequate tool in order to define the reliability of the seismic load patterns. Otherwise, the choice of a specific load pattern can be justified by the assumption of the one that reaches before the attainment of the DLs. Moreover, a mean fragility curve, between the two different probabilities can be still defined (Milosevic *et al.* 2019). In this work, the criterium of the minimum *IM* value between the two different load patterns has been adopted. Observing the PGA values that attain the different *DLs*, considering the four models, the two directions and the two load patterns, 64 different *LS* has to be assessed; then, between them, 32 *LSs* need to the selected.

Complexly, the inverse triangular pattern is attained for lower levels of PGA 24 times out of the total 32, while the mass proportional pattern achieves his thresholds first only 8 times. Concerning the *X* direction, the inverse triangular pattern achieves the *DLs* first in the 87.5% of the cases. Referring only to the last two *LSs*, it represents the 75% of the total amount. For the *Y* direction, the inverse triangular pattern is again the one achieving first the performance points (62.5% of the cases). In this direction, despite the distribution of the first pattern achieving the *DLs* is unbalanced towards the lowest *DLs*, the inverse triangular pattern still was still assumed as the referred one. In fact, looking at the damage of the mass proportional pattern, is worth noting that the failure of the building is given by the shear collapse of the ventilation level (Figure 5.6). Nonetheless, this assumption is a tricky one. As described in Section 2.3 the highest percentage of the buildings presents a semi-underground level that leads the perimetral walls to behave as in the ventilation-floor model; perhaps, the internal bearing walls are characterized by a total height of the panels. Accounting for the case-study model, the collapse at the ventilation level depends on the resistant wall disposition at the considered floor and in the elevation. Even if it is representative for the mass proportional pattern for the assessed model, is not possible to deduce that this behavior is extendable to the other buildings of the class. Due to these reasons, in the presented thesis the inverse triangular has been assumed for both directions. Of course, further in-depth studies could confirm or deny these assumptions.

For the selected case study described in Section 5.1, four different statistically independent structural models have been studied, therefore, the probability of each logic tree branch is considered separately from the other, defining the probability distribution of the different fragility curves. Finally, each scenario represents the 25% of probability of occur given a seismic event.

In this work, considering the seismicity of Florence area, four different LSs associated with four Return Periods respectively have been assumed. The return period of 30, 50, 475 and 949 years have been associated to the different *DLs*.

Concerning the structure representative of the simple-block model, the results show a dual vulnerability. Specifically, the damage distributions describe inverse bell curves where the higher probabilities are expressed for the lowest and the highest *DL*s, avoiding the central *DSs*. This is due to the proximity of the fragility curves between the *PLs*, which also reflects the brittle behavior of the model. Once the elastic range of the structures is completed, the degradation of the buildings in the plastic range is immediate and it rapidly leads to the highest *DSs*. As long as the seismic excitations lead the buildings into their elastic branch, the models are able to respond; otherwise, they tend to slip towards the highest *DLs*. In Figure 5.22 the cumulative damage distributions of the models for the different return period are shown.

Despite the models point out different probability distributions, the results exhibit the same global trend. For the low return periods (30yrs ,50yrs) the behavior of the models is quite good, with an expected damage between *DL0* and *DL1*. Looking at the plots of the damage distribution, for a return period of 30 years, in the *X* direction the highest probability is given for *DL1*, when it ranges between the 78.77% and the 50.3% of the total amount. The same trend is found in the *Y* direction, with results slightly more conservative: the *DL1* ranges between 64.4% and 48.2%. In both directions the probability of not attaining any damage is the second most-likely one. Hence, the other probabilities decrease for the further *DLs*. The aforementioned damage distribution inverse-bell behavior is highlighted in Figure 5.22, where the probability to reach the *DL4* is higher than the one for the attainment of *DL3*. For a return period of 50 years the trend between the two distinct direction is more balanced. All the models set the most reliable probability in the attainment the *DL1* (max probability between 74.4% and 53.7% in *X* and 59.6% and 45.0% in *Y*) with an increase of the probability for *DL2*.

Considering the *SLV* and *SLC*, the probability of exceedance the threshold *LS* are quite pronounced towards the *DL4* and *5*. Specifically, for a seismic action of 475 years return period, in the *X* direction the four models show a probability concentrated between 44.5 and 47.7% to attain DL4. Lower values ranging around the 30% are given for *DL5* (except for model Y/RS/RS/CB/HB pointing out a 50.2% probability), which is the second probable LS. These percentages tend to increase for the *Y* direction, where the probability is mostly distributed between *DL4* and *DL5*. Specifically, *DL4* distributions obtain values between 48.0% and 50.3%, while *DL5* is distributed in the range 38.8-45.7%.

For the 949 years return period, the probabilities of *DL5* increase again, becoming the most probable damage class for earthquakes of such intensity. Specifically, in *X* direction the probability of attain *DL4* rounds around the 45% for both directions. Then, *DL5* exhibits a

probability between 41.2% and 56.7% in *X* (with a *mean* value of 47.5%), while in Y direction it denounces a less variations ranging between 50.5 and 55.3%.

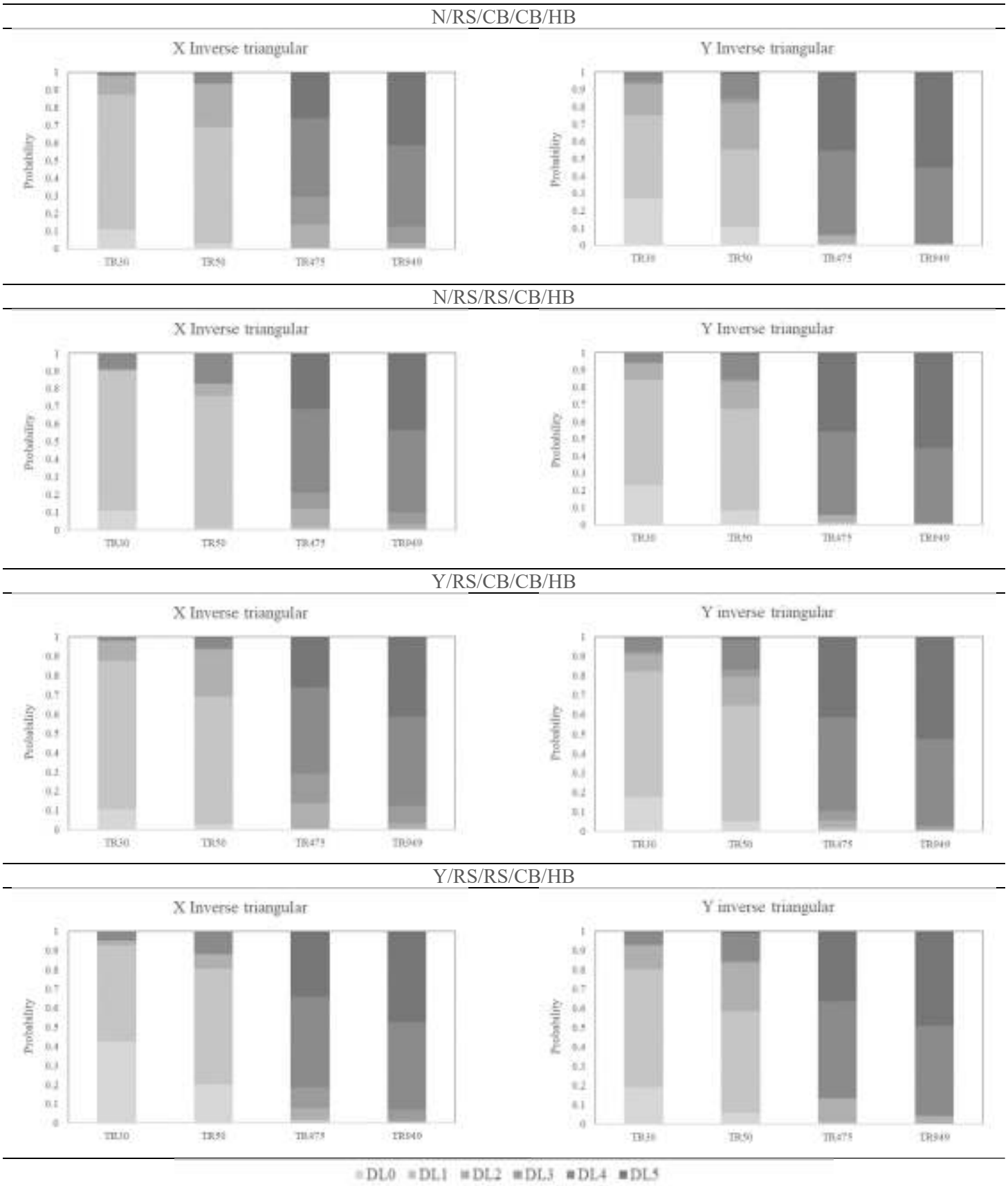

Figure 5.22. Damage scenarios for the four different models according the four considered return periods.

5.6 FINAL REMARKS OF THE ANALYTICAL PHASE

5.6.1 EVIDENCES FROM THE FRAGILITY CURVES

Dealing with the selected case study, the defined fragility curves show a brittle behavior that highlights a particular seismic vulnerability. The analysis of the global behavior of the structure has been widely done in all Chapter 5. The capacity of the building has been investigated by means of nonlinear static analysis, taking into account both epistemic and aleatory uncertainties in order to assess the range of variability insisting in the modeling. The results showed serious forecasts in case of severe seismic events. Specifically, for a seismic event with a return period of 475 years the building in the worst defined scenario has a probability of 50.2% that the collapse occurs, with a 46.3% of reaching the severe damage *DL4*. Comparing these distributions with the ones obtained from the GNDT second level approach presented in Section 4.1 it is clear the differences in terms of DLs and percentages. The analytical results obtained from the case study denounce a behavior influenced by the technical and mechanical characteristics of the models. It is worth noting that, despite the presence of ring beams and rigid diaphragms allows a box behavior, it also interrupts the vertical alignments of the piers, promoting a storey mechanism which reduces the nonlinear capacity of the model (Cattari and Lagomarsino, 2013b). This is an intrinsic characteristic for these buildings, which it has to be considered. Other outcomes have been pointed out from the presented research; if the epistemic uncertainties resulted not so relevant in terms of sensitivity, this is mostly due by the floor level where they have been considered. In fact, the *EF* models are mostly characterized by a shear failure of the lowest levels, while the epistemic uncertainties dealt with the masonry typology disposition at the upper floors. This represents a structural characteristic. On the other side, the mechanical properties of the materials have been collected in a high-sensitivity class, denouncing the importance of the mechanical values in the performance variability. As the empirical methodologies are not able to describe accurately the vulnerability of the investigated buildings, the analytical results suggest the implementation of the behavior pointed out in order to provide *1)* a seismic vulnerability assessment at urban scale (which is the target of the thesis); *2)* generic outcomes useful in the engineer practice. In the following Chapter of this work both points are fulfilled.

5.6.2 Q-FACTOR DEFINITION

In this section, the structural behavior factor q for the investigated building typology is provided. As known, it represents an approximation of the ratio of the seismic forces that would invest the structure if its response was completely elastic. An extensive discussion about the *q-factor* values can be found in Calvi (2006). The Italian standards provide values for q-factor in case of linear elastic analysis. Namely, q is given by:

$$q = q_0 \, k_r \tag{5.3}$$

where q_0 represents the ductility value and k_r depends by the vertical regularity of the construction (equal to 1 for regular structures, otherwise 0,8). The last Italian code for the existing buildings considers a q_0 value for URM equal to 1,75 OSR, increasing up to 2,5 OSR for masonry building with reinforced insertions (NTC2018). This last term, the overstrength ratio (OSR) expresses the ratio between the base shear at ultimate displacement and the one reaching the plasticity in the first wall. The q-factor has been assumed coming from the nonlinear analysis, assuming the ratio between the idealized maximum base shear $F_{el,max}$ and the one at the yielding point F_y (Figure 5.23):

$$q = \frac{F_{el,max}}{F_y} = q_0 \tag{5.4}$$

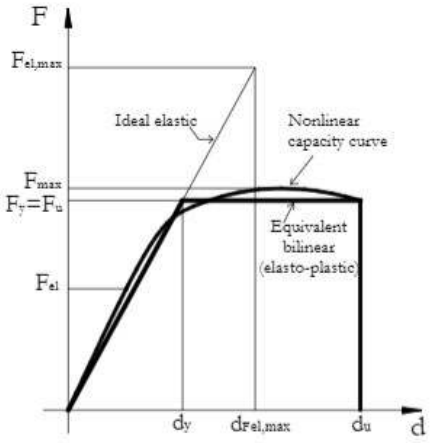

Figure 5.23. Definition of q-factor and the overstrength ratio (from Magenes, 2006).

As mentioned, the overstrength ratio (OSR), as for other structural typologies should be considered (Magenes and Morandi, 2008). In fact, given F_{el} as the force value for the attainment of the strength capacity of the first structural element in the model, the base shear capacity still permits the sustainment of some contribution until the achievement the maximum value given for the yielding point. The formulation is given by:

$$q = \frac{F_{el,max}}{F_{el}} = \frac{F_{el,max}}{F_y}\frac{F_y}{F_{el}} = q_0 \frac{F_y}{F_{el}} = q_0 \, OSR \tag{5.3}$$

In this work, the values for $q_0$and OSR have been directly computed from the PO analysis. In Figure 5.24 the results for the q_0 values for the four different models are shown. Differences are pointed out especially within the two seismic load patterns rather than according the two different directions. The Y direction denounces slight lower value. Moreover, the mass proportional pattern leads to lower values of q_0, ranging between 1.33. On the other side, a mean value of 1.69 is obtained for the inverse triangular pattern; so complexly, a mean value of equal to 1.51 is found.

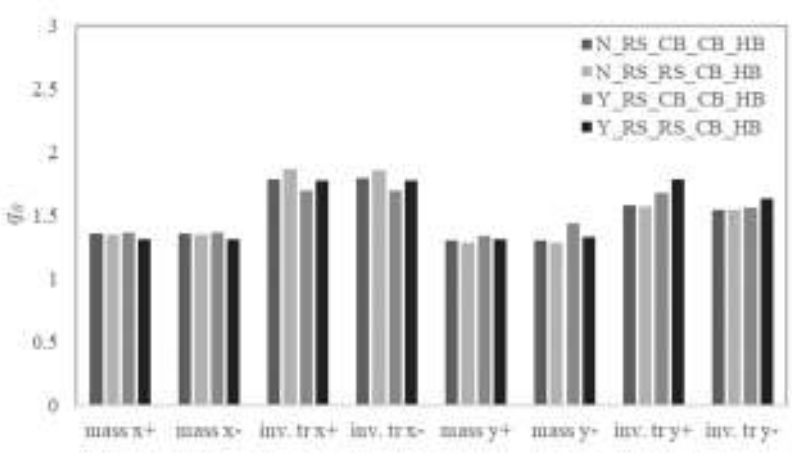

Figure 5.24. Computation of the q_0 values according to the different models.

Comparing the obtained values with the one proposed from the Italian codes, the computed ones are slightly conservative. This is due to the intrinsic vulnerability of the models towards the horizontal actions. As presented in Magenes (2006), the lower threshold equal to 1,5 was several times proposed, nonetheless, the models point out also minor computations. Complexly, they range from 1,28 to 1,86.

Concerning the definition of the OSR, the latter presents interesting outcomes. In fact, while the epistemic uncertainties showed a low sensitivity between the different logic tree models adopted in the research, *i.e.*, the *a-priori* assumption of only one model inside the four logic tree branches would not lead to improper results, the computation of the OSR targeted at the adoption of linear static analysis points out different characteristics. Looking at the results in Figure 5.25, a clear difference between the models with or without lintels over the openings is highlighted. The models without lintels exhibit low values of OSR; excluding the inverse triangular pattern in the *Y* direction, which it leads to OSR values between 1 and 1,07, the mean values of the two models without lintels for the other 6 combinations of seismic pattern and directions present a mean value equal to 2,35 and a standard deviation of 0,41. On the other side, the models with lintels, except for the mass proportional pattern in the *Y* direction, tend to exhibit OSR values smaller than 1,00. For the models without lintels the latter are coherent with other OSR values provided in literature (Magenes 2006), on the other side, further studies (experimental and analytical) are needed concerning the yes-lintels models. This outcome can be justified by the different hierarchical roles defined inside the masonry panels. The models without lintels in the first linear phase are characterized by a less relevant damage diffusion, pointing out in earlier phases the attainment of the plasticity. On the other side, the RC lintels over the opening allows a more diffuse localization of the damage along the masonry heights. Due to this, the shear or flexural strength of the panels is achieved only after that a higher number of panels already exploited their linear capacities. So, in terms of

idealized bilinear curve, this attainment is given after the yielding points, defining no longer OSR increment coefficient.

This result points out an important insight concerning the further studies concerning that should dissuade in the choice of linear elastic analysis for the seismic vulnerability assessment of these buildings: the lack of knowledges about building details such as the presence of RC lintels over the openings can significantly alter the linear elastic response of the considered buildings. Unless of an univocal achieved knowledge, this method become unreliable. On the contrary, the low sensitivity of the logic tree branches suggests the adoption of nonlinear analysis, where the modeling constitutive models denounced, a-posteriori, a similar performance.

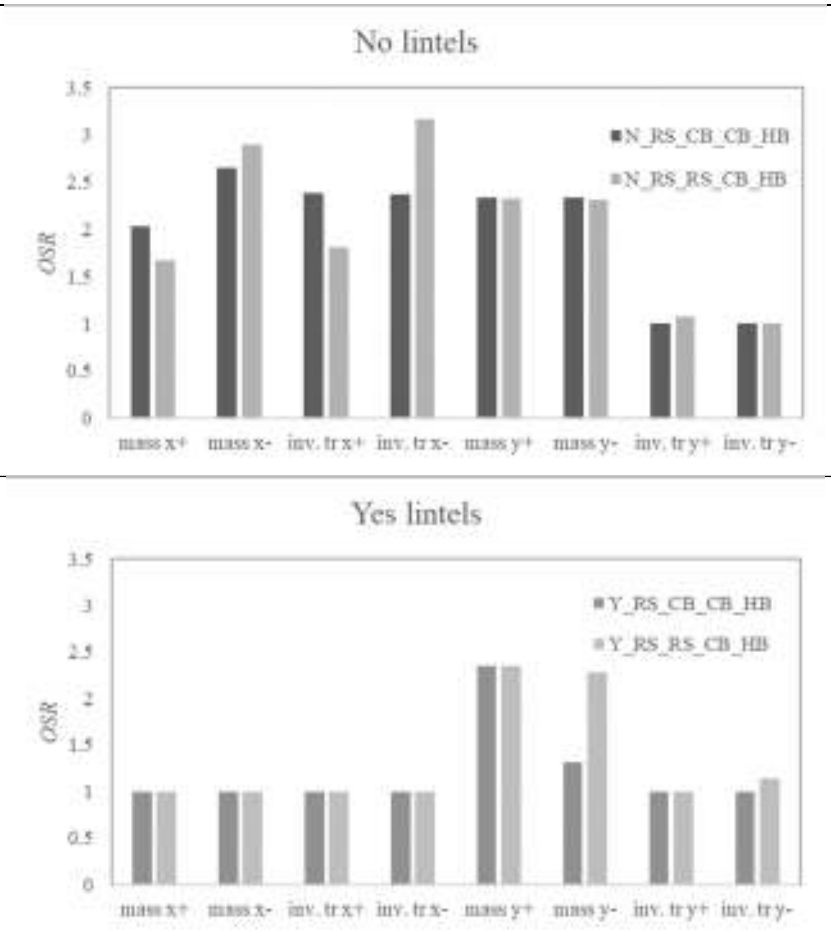

Figure 5.25. Computation of the *OSR* values according to the different models.

[this page intentionally left blank]

6. ADOPTION OF THE FRAGILITY CURVES AT URBAN SCALE

The urban scale overview of the presented thesis requires an implementation of the analytical results obtained from the case study to a higher number of buildings. To this aim, the definition of few parameters able to describe the seismic behavior of the model is needed. In this section, the implementation of the results coming from the analytical procedure performed on the single-block case study is presented. In a simplification perspective, the fragility curves coming from the four different models have been combined together in two unique plots, one for each direction. They have been realized considered the mean curves of the four fragility curves obtained for each DLs and each direction. The results, presented in Figure 6.1, show the reliability of the simplification conducted, both in terms of curves, as well as damage scenarios.

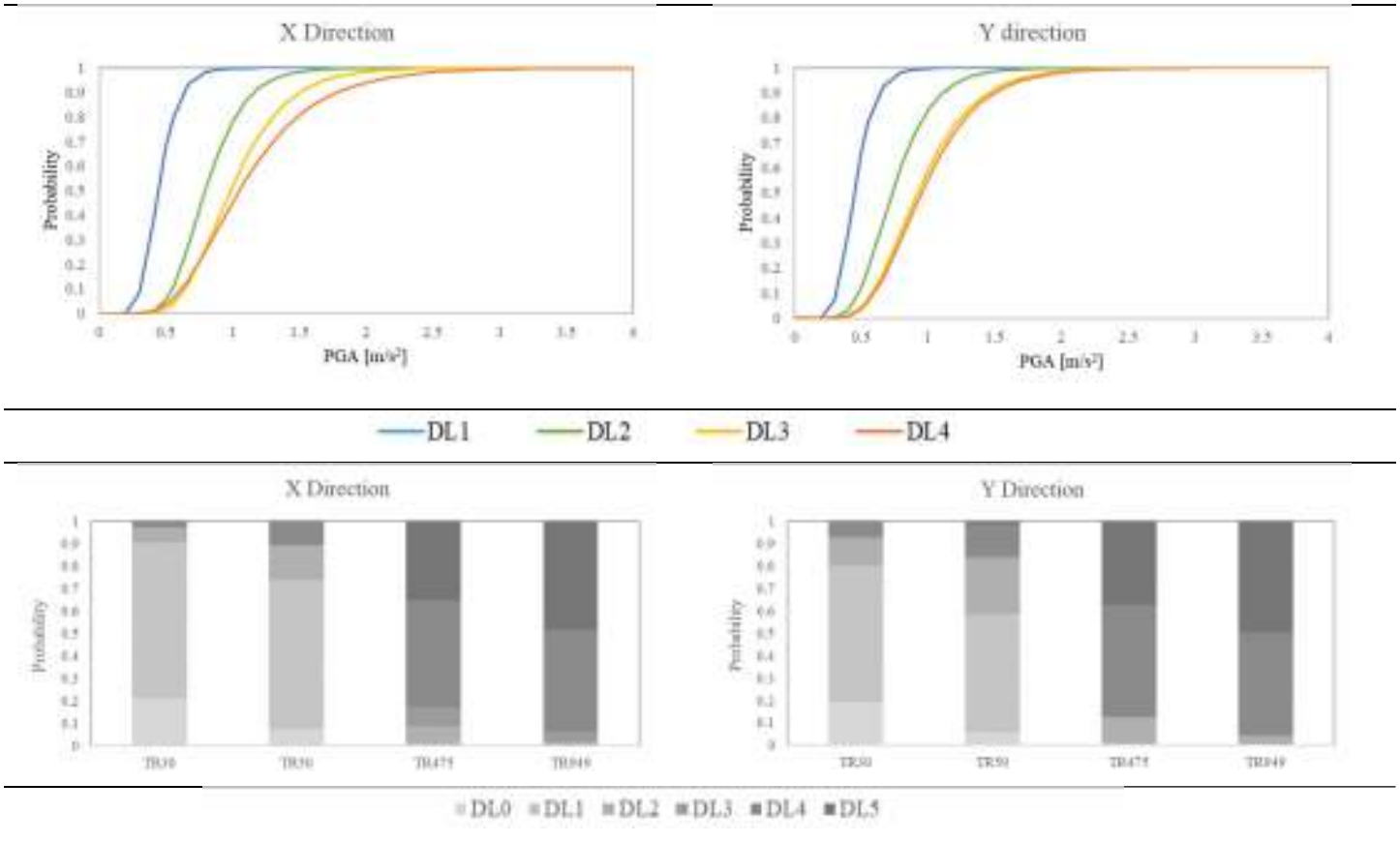

Figure 6.1. The fragility curves and relative damage scenarios considering the mean curves within the four logic tree branches.

The curves reflect the behavior already pointed out in previous section. Moreover, they facilitate the outcomes of the study due to obtainment of only two curves rather than four different scenarios with the 25% of probability for each. It is worth noting that the combination of statistical independent probabilities, based on the aforementioned assumptions, represents an improper operation. Therefore, in the analytical procedure they have been considered scrupulously separated. In this last part of the work, switching the scale of interest of the research the evidences

of the analytical phase highlighted a low sensitivity of the logic tree branches to the seismic response of the structure. Due to this, since the case study is a single building, this simplification has been considered a suitable one. The two sample of fragility functions express yet the capacity of the structure, which is higher in the *X* direction, with closer attainments within the DLs in *Y* direction. Concerning the damage distributions, for 475 years return period, in *X* direction a probability of 47.6% is expressed for *DL4*, with 35% for *DL5* and 8.8% of *DL3*. In *Y* direction, the probability tends to the highest DLs, with a 50.1% of probability for *DL4* and 38.6% for *DL5*.

In order to achieve the same structural behavior through a simplified approach, the first phase regarded the description of the capacity of the model through more streamlined procedures. To this aim, the Capacity curves coming from the nonlinear static analyses have been converted through a Bilinear relationship. This operation followed the path developed in Section 3.3; the equivalence of the area under the capacity curve has been conducted considering the curves until the attainment of *DL4*. In Figure 6.2, the plot of the bilinear curves along the two directions are presented. The grey lines indicate the 8 bilinear curves for each direction and two senses of the analysis obtained within the four models; the red line points out a mean capacity curve. Coherently with the previous analysis, the trends of the curves describe the behavior of the structures. In *X* direction a higher ductility is shown, despite slightly lower base shear values.

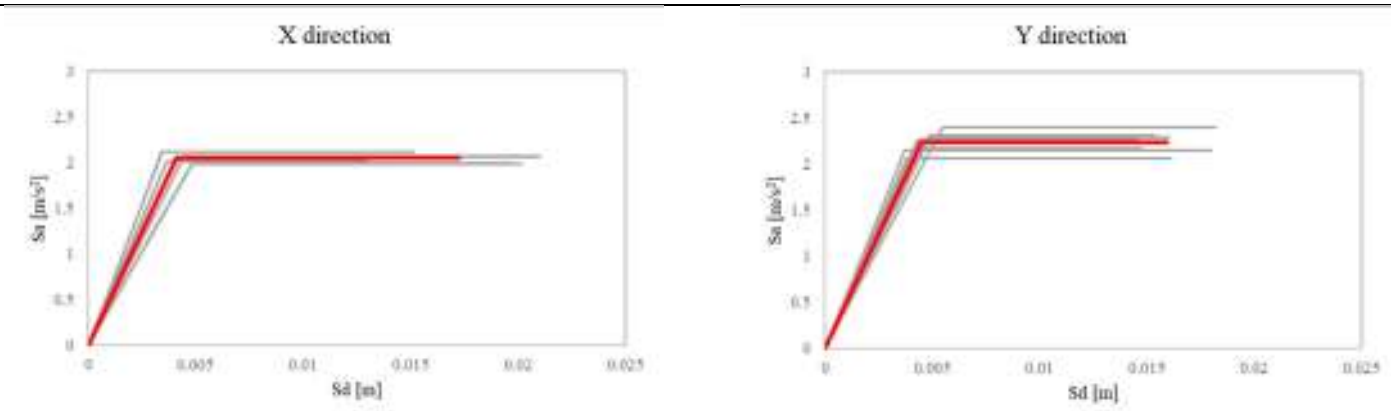

Figure 6.2. The bilinear simplification for the different PO curves. In red, the mean curve is plotted.

Observing the curves, in *Y* direction it is possible to observe a lower dispersion in terms of nonlinear branch, while, *X* direction shows a lower variability in the maximum spectral acceleration. Aiming to define the fragility curves, first of all the LSs need to be defined over the bilinear relationship. Hence, the PGA for the attainment of the DLs needs to be defined according to (3.16), (3.17) and (3.18).

Referring to the DLs, they have been scaled over the bilinear curve assuming proper linear correlations. In case of bilinear capacity curves, relationships in order to obtain the performance points, given the ultimate and the yield displacement are available in literature. In a bilinear

relationship, the thresholds are defined in terms of displacement as functions of the yield and the ultimate displacement (Calvi *et al.* 2006):

$$S_{d,1} = 0.7\ d_y \tag{6.1}$$

$$S_{d,2} = 1.5\ d_y \tag{6.2}$$

$$S_{d,3} = 0.5\ (d_y + d_u) \tag{6.3}$$

$$S_{d,4} = d_u \tag{6.4}$$

These values have been calibrated on the assessment of pushover analysis executed on several building prototypes. Finally, a comparison between the obtained performance points and the proposed literature values can be done. The case study exhibits different relationship along the two directions. Concerning the first two DLs, in *X* a relationship of $S_{d,1,X} = 0.76\ d_{y,X}$ is shown, with a $S_{d,1,Y} = 0.78\ d_{y,Y}$ for the *Y* direction. In the case of $S_{d,2}$ there is a more pronounced difference, specifically $S_{d,2,X} = 2.10\ d_{y,X}$ and $S_{d,2,Y} = 1.56\ d_{y,Y}$. For $S_{d,3}$ two considerations may be done. Observing the formulation proposed in (6.3), a mean variance equal to 17% and 14% for the two directions respectively is estimated. As well, (6.3) it centers the position of $S_{d,3}$ within the two different LSs, while for the case study its position is highly unbalanced towards the ultimate displacement. Due to this, a punctual correction could be done substituting the coefficient 0.5 with a 0.6 for *X* direction and 0.56 for *Y* direction. Otherwise, considering the attainment of DLs in the building, a different formulation can be defined expressing $S_{d,3}$ only as a function of the ultimate displacement. In this case, it results $S_{d,3,X} = 0.9\ d_{u,X}$ and $S_{d,3,Y} = 0.95\ d_{u,Y}$. This relationship reflects the brittle behavior of the model, especially towards the *Y* direction. This procedure allows the definition of specific DL relationships, calibrated for the representative case study of the thesis. The differences insisting between the two directions reflect the behavior of the case study towards the two directions. This can be related to the intrinsic characteristics of the masonry panels and their role in the definition of the residential box-structure.

Given the different bilinear curves, the spectral acceleration could be used in order to derive fragility curves. Nevertheless, aiming to compare the latter with the analytical results, the same *im* needs to be defined. The analytical outcomes of the in-depth studies developed on the simple-block buildings have been considered. Specifically, the period was computed through eq. (3.17) while the equivalent damping η has been assumed based on the results of the cyclic pushover analysis. Finally, the PGA values for the attainment of the different LSs can be obtained. The equivalent damping has been considered assuming the mean value for each LS for each direction of the analysis. For the seismic demand, in this final part of the work, two different strategies could be used. The first one would regard the adoption of the conditioned spectrum over a mean

fundamental period of the structure given by the four epistemic models considered in the analytical phase. The second approach considers instead the mean spectrum provided by the codes for the referred type of soil. This last assumption, despite its intrinsic simplification is specifically practice-oriented and addressed to the world of work. In this section, both assumptions have been assessed; in the first case, the spectra have been conditioned for the mean value obtained from Table 5.1. In the second, the mean soil spectrum of the city of Florence for a soil class B has been assumed. Observing equation (3.16) it is worth noting that the definition of the PGA values is function of the seismic demand (expressed by the specific spectrum) and the equivalent damping η of the model. Assuming the mean values of damping, is reasonable to consider that more the considered demand is close to the one used in the analytical model and less is the expected variation. In both models have been adopted the mean damping parameters, which are presented in Table 6.1. Hence, a first comparison of the two assumptions was conducted in terms of PGA differences.

Table 6.1. Equivalent damping values adopted in the simplified procedure.

	X	Y
DL1	89%	98%
DL2	72%	88%
DL3	67%	85%
DL4	64%	81%

The PGA variability for each LS has been considered through:

$$PGA_{\%} = 1 - \frac{PGA_s}{PGA_a} \tag{6.5}$$

Where the PGA_s is the intensity measure obtained from the two different in terms of spectrum, while PGA_a represents the analytical value obtained from the four different logic tree branches. In Figure 6.3 the variations in terms of DL attainment are presented for both models. Namely, the black point represents the variation of the analytical model, which is computed as zero, while *mcs* and *NTC* represent the mean-capacity-spectrum and the NTC code-spectrum respectively, considered as seismic demand for the two different proposed assumptions. Both models present suitable results, with the PGA differences within the 10% of variation.

In *X* direction there are more differences, according to both models. Looking to the highest DLs the *mcs* spectrum looks slightly more reliable; in *X* direction it presents differences around 7% for all the DLs except for the *DL2* (3%). In *Y* direction the same value is still obtained for *DL1*, then, the differences switch to negative values and with a peak of 9% for *DL3*. Considering the *NTC* model, the results looked less aligned towards the analytical ones; in *X* direction the

variations are respectively 6%, -6%, 8% and 9% for the different DLs. In *Y* directions, they tend to negative variations, such as especially for *DL2* and *DL3* while for *DL4* it is really close to the analytical solution. Both models lead to conservative results in *Y* direction, while they slightly increase the PGA values for the respective attainment in *X* direction.

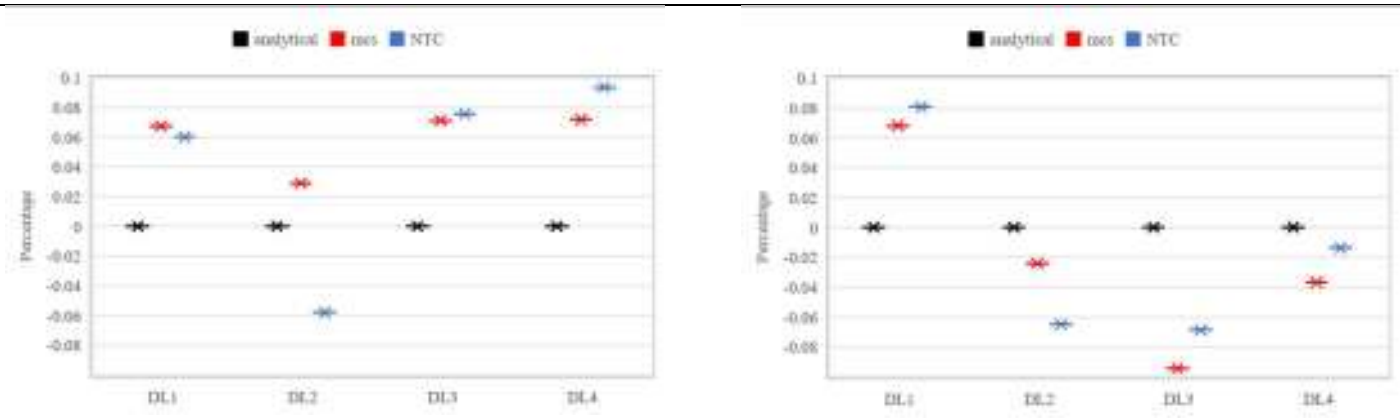

Figure 6.3. PGA differences for the attainment of the different LSs.

For the two strategies the fragility curves have been finally derived; the dispersion of each DL has been assumed from the analytical outcomes of the procedure. In Table 6.2 the dispersion values for the different LSs are presented. Finally, in Figure 6.4 the comparisons between the fragility curves obtained through the bilinear relationships and the ones obtained analytically are presented. It is worth noting that, despite some differences, the two assumptions result reliable. In *X* direction the main differences are shown for the highest DLs, where the two simplified results lead to an horizontal offset of the curves. On the other side, the results for *Y* directions looks more balanced over the analytical ones. In Table 6.3 a damage state (*DS*) comparison is proposed for the same return periods considered in the previous parts of this thesis. Concerning the *mcs* model, for 475 years return period, in *X* direction it forecasts a 47.3% of probability of *DL4* with a 30.4% for *DL5*; in *Y* direction the percentages are 46.8 and 47.7% respectively. Furthermore, for the same return period the *NTC* model forecasts in *X* direction a 46.5% and 29.4% for *DL4* and *DL5* respectively, while in *Y* direction it predicts a 48.8% and a 45.5%. Both previsions result similar to the values obtained and descripted in the first paragraph of this section, equal to 47.6% and 35% for *X* direction, with a 43.2 and 55.6% in *Y* direction.

Table 6.2. Values of the total dispersion β_T for the different LSs.

	X	Y
DL1	12.0%	11.8%
DL2	12.7%	14.1%
DL3	14.3%	15.3%
DL4	17.9%	15.4%

Table 6.3. DS percentage comparison for the two bilinear assumptions and the analytical solutions.

X direction						
475	DL0	DL1	DL2	DL3	DL4	DL5
analytical	0.00%	1.12%	7.39%	8.82%	47.63%	35.05%
mcs	0.00%	1.46%	11.09%	9.80%	47.27%	30.39%
NTC	0.00%	0.66%	12.19%	11.23%	46.51%	29.40%
975	DL0	DL1	DL2	DL3	DL4	DL5
analytical	0.00%	0.09%	1.66%	4.55%	45.49%	48.21%
mcs	0.00%	0.13%	2.85%	5.89%	46.32%	44.81%
NTC	0.00%	0.05%	3.03%	6.74%	46.32%	43.86%
Y direction						
475	DL0	DL1	DL2	DL3	DL4	DL5
analytical	0.00%	1.05%	6.02%	1.42%	48.71%	42.80%
mcs	0.00%	1.35%	1.50%	2.65%	46.80%	47.70%
NTC	0.00%	1.00%	2.37%	2.93%	46.95%	46.75%
975	DL0	DL1	DL2	DL3	DL4	DL5
analytical	0.00%	0.11%	1.44%	0.44%	44.43%	53.58%
mcs	0.00%	0.18%	0.21%	0.58%	43.09%	55.94%
NTC	0.00%	0.13%	0.36%	0.68%	43.22%	55.62%

Complexly, in *X* direction, both simplified results provide the same percentages of probability for *DL4* as for the analytical model, while they point out some conservative results towards the attainment of *DL5*. This is shown for the two highest considered return periods. On the other side, considering the *Y* direction, the two models tend to increase the probability for *DL5*, especially for 475 years return period. Nevertheless, in both directions, despite the slight differences presented in terms of fragility curves, the results of the damage distributions look reliable with the analytical forecasts. Considered the two different approaches in terms of seismic demand for the simplified procedure, in this final part of the work the *NTC* assumptions have been considered. In fact, although this final part of the section showed the reliability of the presuppositions, the *NTC* one, since it is spectrum-code based can be considered more oriented towards the engineer practice. Improvements of the simplified results could be done. Specifically, in order to set the PGA values closer to the attainment thresholds, the equivalent damping should be altered. For instance, this could be done setting, in *X* and *Y* direction the values of 95, 70, 70, 70 and 99, 82, 80 80 for the different LS, respectively. Nonetheless, this assumption would point out constant values of the equivalent damping for the higher DLs, which is not an outcome characteristic of this work. Due to this, the original equivalent damping values presented in Table 5.3 have been adopted.

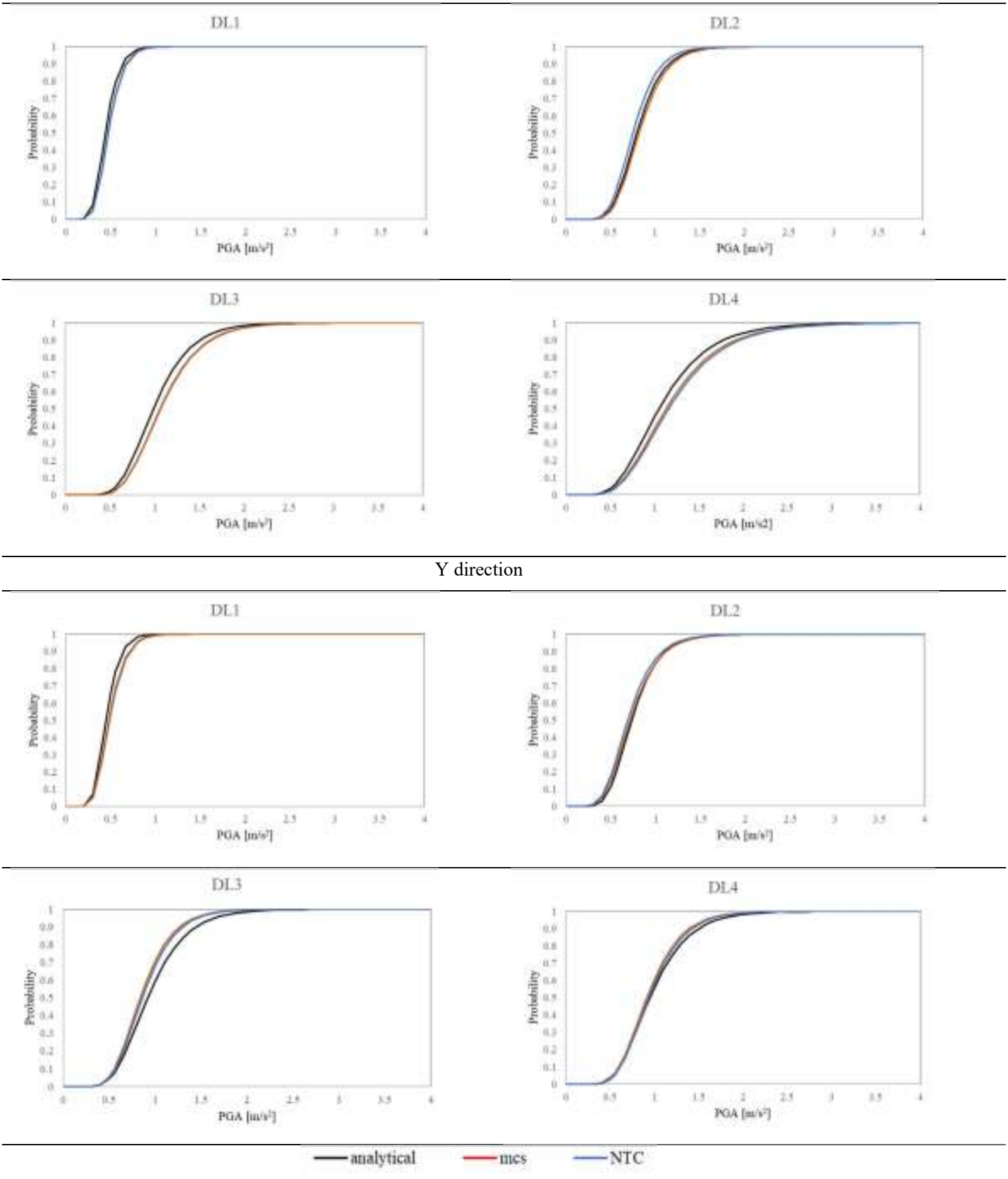

Figure 6.4. Fragility curve comparison between the analytical solutions and the two simplified ones.

6.1 THE MECHANICAL METHOD

In this section, the mechanical method described in Section 3.3 has been applied. The bilinear capacity curves presented in the previous section are targeted as the expected result of a simplified approach. Aiming to represent the mechanical features of the building through a limited number of parameters, some considerations need to be done. It is worth noting that, despite the availability of all the possible information regarding the selected case study, this part of the work is addressed to the extensions of the results over different buildings. Therefore, the punctual computations of the model characteristics need to the descripted by quantifiable formulations. Concerning the two bilinear curves assumed as representative of the buildings, as described in previous section, they have been selected assuming the inverse triangular pattern distribution.

Aiming to the describe the same behavior of the structure through a proper equivalent period, eq. (3.33) has been adopted. The masses of the different levels of the building have been considered, taking into account the dead loads and the 30% of the live loads. Assessing the disposition of the floors towards the two directions resulted that the 71% of the slab loads was insisting over the masonry walls in the *X* direction ($\zeta_{x,i}$ = 71%), while only the 29% of the slabs was disposed in the orthogonal sense. For the roof structure, the loads were considered coherently with the *Tremuri* modeling. Finally, the different specific weights of the masonry walls were assumed for the different levels of the structure; in details, 19 kN/m^3 was assumed for RC, 18 kN/m^3 for CB and 15 kN/m^3 for HB masonry typologies. Concerning the reduction in the thickness of the bearing walls along the height of the building, the specific quantities were computed. According to Section 3.3, this is described by parameter $\alpha_{X,Y,i}$; the distribution in the height of their different parameters is shown in Table 6.4; a different variation of the parameter is notable along the different levels.

Table 6.4. Distribution of the α coefficient towards the two directions along the different levels.

	α_1	α_2	α_3	α_4
X direction	0.144	0.0873	0.0737	0.0485
Y direction	0.0799	0.0674	0.0611	0.0495

Referring to formulation (3.12), the building has been assumed with a regular height; specifically, the latter leads to a unique value of Γ towards the two directions. From the seismic analysis obtained in Tremuri, two different Γ values were obtaining. Considering the mean values between the four different epistemic models, a Γ_x of 1.427 and Γ_y of 1.473 was found, with a mean value between the two directions of 1.45. It is worth noting that the Γ quantity is not so different from the analytical simplified formulation obtained assuming a constant distribution of the masses along the height, which is given by:

$$\Gamma = \left(\frac{2}{3} + \frac{1}{3N}\right)^{-1} \tag{6.6}$$

where, for a building of 4 storeys, it leads to a Γ equal to 1.33. Considering the simplified model, two different assumptions were assessed, assuming or not the presence or the ventilation floor under the superior regular levels. Hence, the mass distribution has been made according to the considered load. Considering both configurations, the premise of a ventilation floor leads to a Γ equal to 1.78; on the other side, the assumption of a regular structure without the presence of this offset from the ground brings to a Γ equal to 1.409, which is closer to the analytical mean value of 1.45. Therefore, the second case has been adopted. Considering the masses at the different levels assuming the ground floor as the one of reference, the upper levels present decrease in their masses equal to 10, 24 and 36% respectively. They are mostly given by the reduction in the thicknesses of the bearing walls combined with the specific weight of the masonry alteration. Then, a reduction of the load is considered for the roof.

Given these characteristics, also the average vertical compressive $\sigma_{x,y}$ can be obtained, and consequently, the shear strength of the wall through (3.32) and (3.31). From the analysis, the two different $\tau_{x,y}$ result equal to 98 and 86 kN/m^2 respectively, looking coherent with the values proposed in Cattari *et al.* (2004). Aiming to define the equivalent period of the structure along the two direction, the Elastic Shear Moduli G reduced of their 50% need to be considered. Coherently with the properties of the adopted masonry typologies (Table 2.5) the equivalent period has been defined. Here, the formulation introduces two correction factors k_5 and k_6 that need to be calibrated. In literature ranges for the two coefficients based on the structural behavior assumptions are proposed; k_5 was proposed in order to consider the flexural contribution in the piers, while k_6 considers the effects on the stiffness related to the spandrels influence on the boundary conditions on piers. Hence, for the WPSS models a range of 0.6-0.8 for k_5 is recommended, while for k_6 this is generally assumed equal to 1. In this work, for T^*_x a value of k_5 equal to 0.65 was considered, leading to an equivalent period equal to 0.281, which is equal to the one obtained by the analytical bilinear curve. For the Y direction, k_5 was assumed equal to 0.7, leading to a period of 0.283 comparable with the 0.281 of the analytical models. It is worth noting that the analytical bilinear result has the same period along the two different directions. Obviously, the floor disposition involves some uncertainty related to the masses along the two directions. Hence, the two values of $k_{5,x,y}$ could be assimilated by a single value.

Adopting eq. (3.12) a tricky question regards the total height H of the model, where, avoided the ventilation floor for the total height of the models would be 12.80 m against the 13.8m. In this work, despite the regular assumption the total height of the model was computed. This has been done in an urban scale view, aiming to extend the results to a larger number of buildings. In fact, the height of the different models is an information provided from the GIS database; on the other side, the participation factor Γ showed the reliability of a regular distribution. So, the two inputs have been combined together adopting the regular distribution and the real height of the buildings.

Further developments and studies concerning this point could improve the reliability of the simplified assumptions made at urban scale.

The base shear $f_{x,y}$ can now be found. Considering the four corrector coefficients provide in equation (3.30), as for the period of the model, some values was already proposed. Considering the model as a WPSS configuration, the coefficient k_1, since is the one that rules the failure behavior of the structure is the one that has been altered. Specifically, it has been adopted equal to 0.8 in *X* direction, where the flexural contributions are expected. In *Y* direction, since the prevalence of shear failure is expected, a value of the coefficient equal to 1.2 has been adopted. The bilinear capacity curves of the model can now be obtained. To this purpose, the last parameter that needs to be defined is Δ_{LS} , which it accounts the inter-story drift limit of the panel. In both directions, the drift value for the attainment of the *DL4* has been assumed equal to 0.004; coherently with the values found in Lagomarsino and Cattari (2014) for a *DL4* and a shear failure of the model. In Table 6.5 a resume of the different parameters adopted for the analysis is proposed. Finally, assuming the different parameters presented in this paragraph it is possible to obtain the PGA levels for the attainment of the different LS.

Table 6.5. Correction coefficients adopted for the calibration.

		X	Y
$f_{x,y}$	k_1	0.75	1.20
	k_2	1.00	1.00
	k_3	1.00	1.00
	k_4	1.00	1.00
$T_{x,y}$	k_5	0.65	0.70
	k_6	1.00	1.00
$D_{u,WSSP}$	Δ_{LS4}	0.004	0.004

Specifically, the equivalent damping has been accounted referring to the values presented in Table 5.3. In the adoption of the CSM, the simple code spectrum for the area of Florence account for a return period of 475 years and a soil class B has been adopted. For the two directions, the performance points have been computed on the capacity curves according to the relationship previously defined. In Figure 6.5 the final bilinear curves are presented, together with the variability of the DS attainment in the simplified model respect to the analytical one. The biggest difference is highlighted for *DL2* and *Y* direction. This can be explained by the assumption of the code spectrum that, compared with the sample of spectra scaled over the fundamental period of the models, being in the nearness of the referred point, leads to variations changing significantly point by point. In *Y* direction the results are more conservative, while the *X* direction tend to increase the values for the attainments of the DLs.

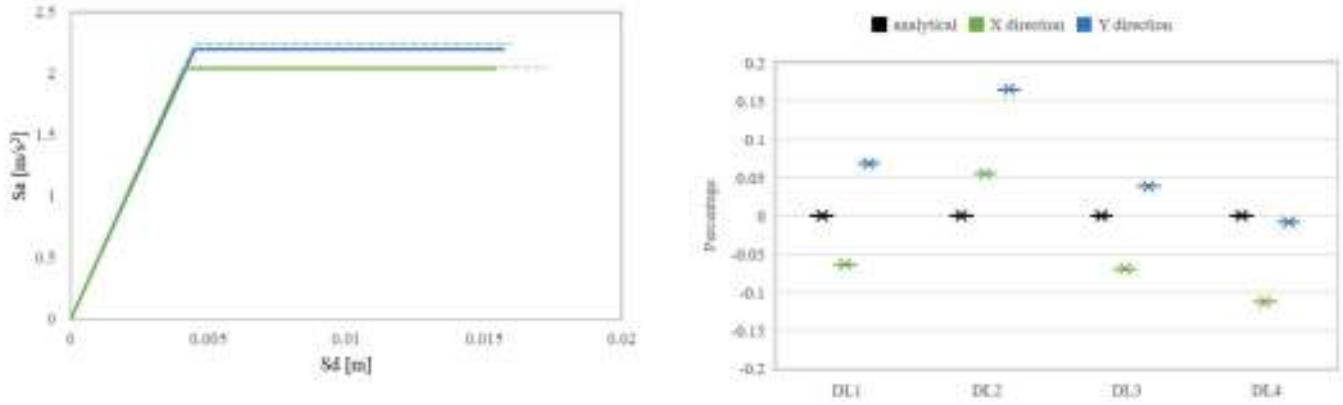

Figure 6.5. On the left, comparison between the analytical bilinear curves (dashed lines) and the simplified ones (continuous lines). On the right, percentage comparison in terms of PGA between the different attainment of the PLs for the analytical model and the mechanical method.

In Figure 6.6 a comparison between the analytical fragility curves and the simplified one is shown. The grey lines indicate the results coming from the PO curves, while the red lines describe the curves from the bilinear simplified curves. Finally, in Table 6.6 a comparison in DS terms is proposed.

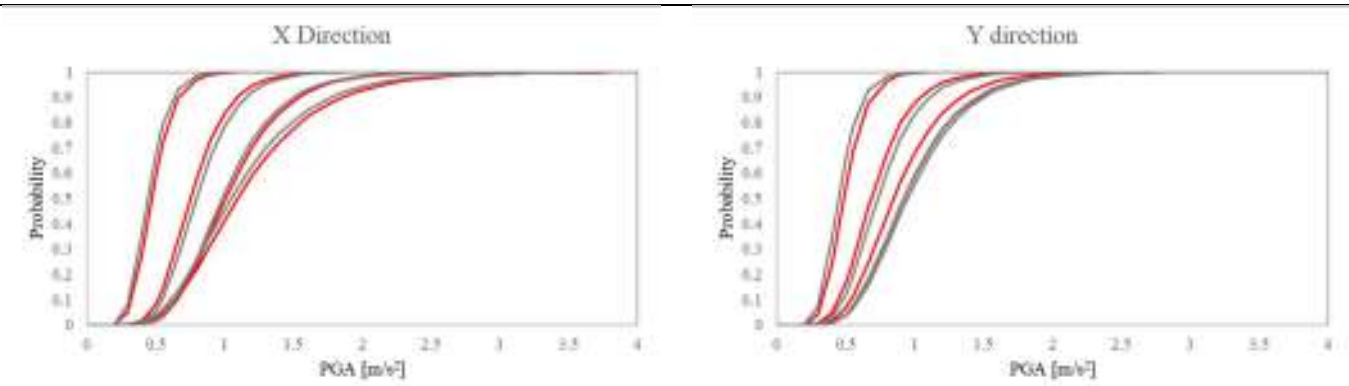

Figure 6.6. Comparison of the fragility curves. The red lines plot the simplified curves; the grey ones indicate the analytical results

Looking at both results, fragility curves and DS exhibit the same differences. In both directions, for *DL1* the simplified model reaches the threshold before the analytical results. On the other hand, the *DL2* is anticipated. Concerning the last two DLs, the two directions express a different trends; in *X* direction the mechanical model attains the LSs after the analytical results, while for *Y* direction it anticipates the values coming from the PO analysis. The distributions show similar trends, especially for the higher DLs. The more plausible LSs are characterized by the same percentages of probability, then, some difference occurs especially between the other DLs. For a return period of 475 years, in *X* direction both results provide a 47% for the attainment of *DL4*. The analytical result expresses a probability of 9% for *DL3* and 35% for *DL5*, while the simplified model leads to 10% for *DL3* and 33% for *DL5*. The results are strictly comparable especially for the highest return period seismic events. For 30 and 50 years Return Period, bigger differences

insist. While the analytical model exhibit major peaks around the *DL1*, the simplified models tend to decrease this probability increasing the ones in the margin (*DL1* and *DL3*). The differences between the probabilities vary between 4 and 16%.

Table 6.6. Damage scenarios for the different LSs for the analytical and simplified models.

X direction						
30	DL0	DL1	DL2	DL3	DL4	DL5
analytical	20.89%	69.30%	7.00%	0.00%	6.18%	0.65%
simplified	27.71%	57.97%	11.49%	0.00	4.96%	0.48%
50	DL0	DL1	DL2	DL3	DL4	DL5
analytical	7.19%	66.71%	15.51%	0.00%	12.77%	1.31%
simplified	10.51%	56.34%	23.50%	0.00%	10.61%	1.00%
475	DL0	DL1	DL2	DL3	DL4	DL5
analytical	0.00%	1.12%	7.39%	8.82%	47.63%	35.05%
simplified	0.00%	0.66%	9.07%	10.46%	47.03%	32.77%
975	DL0	DL1	DL2	DL3	DL4	DL5
analytical	0.00%	0.09%	1.66%	4.55%	45.49%	48.21%
simplified	0.00%	0.05%	2.06%	5.63%	45.79%	46.48%
Y direction						
30	DL0	DL1	DL2	DL3	DL4	DL5
analytical	21.67%	58.94%	11.94%	1.02%	6.12%	0.31%
simplified	30.20%	42.20%	16.18%	3.67%	7.35%	0.40%
50	DL0	DL1	DL2	DL3	DL4	DL5
analytical	7.29%	54.46%	20.47%	2.02%	14.37%	1.37%
simplified	11.71%	39.50%	24.15%	6.43%	16.37%	1.83%
475	DL0	DL1	DL2	DL3	DL4	DL5
analytical	0.00%	1.05%	6.02%	1.42%	48.71%	42.80%
simplified	0.00%	0.50%	3.88%	2.70%	47.23%	45.70%
975	DL0	DL1	DL2	DL3	DL4	DL5
analytical	0.00%	0.11%	1.44%	0.44%	44.43%	53.58%
simplified	0.00%	0.04%	0.79%	0.74%	43.63%	54.81%

6.2 EVIDENCES FROM THE ANALYSIS

Despite the differences shown in terms of fragility curves and damage scenarios, the simplified model is assumed reliable to describe the seismic performance of this building typology. The mechanical method previously described is targeted to characterize the performance of several buildings in the Florence area. Several information were assumed on the basis of the conducted analytical study. Of course, the gathered data need to be enough detailed to describe the building stock, but also generic, being not only referred to the single case study. The information has been compared with the general values provided in literature, defining new relationships based on the *site-specific* experience.

Mass distribution. The mass distribution along the elevation of the building was discussed. It depends on the thickness of the walls, the slab loads and the disposition of the floors towards the two directions. Observing Figure 6.7, a linear distribution of the weights is highlighted. Hence, this distribution has been compared with the simplified formulation presented in Cattari *et al.* (2004). Specifically, the m function was approximated through:

$$m = 0.75 + 0.25 \frac{1}{N_f^{0.75}} \tag{6.7}$$

Where N_f is the number of floors of the building. This difference mostly depends from the disposition of the thickness of the resistant walls along the height of the structure (Tab. 4.5). For the following models, the mass distribution depends from the disposition of the slabs along the two directions. Hence, for the specific weights and the loads at the different level, the outcomes of this research were used.

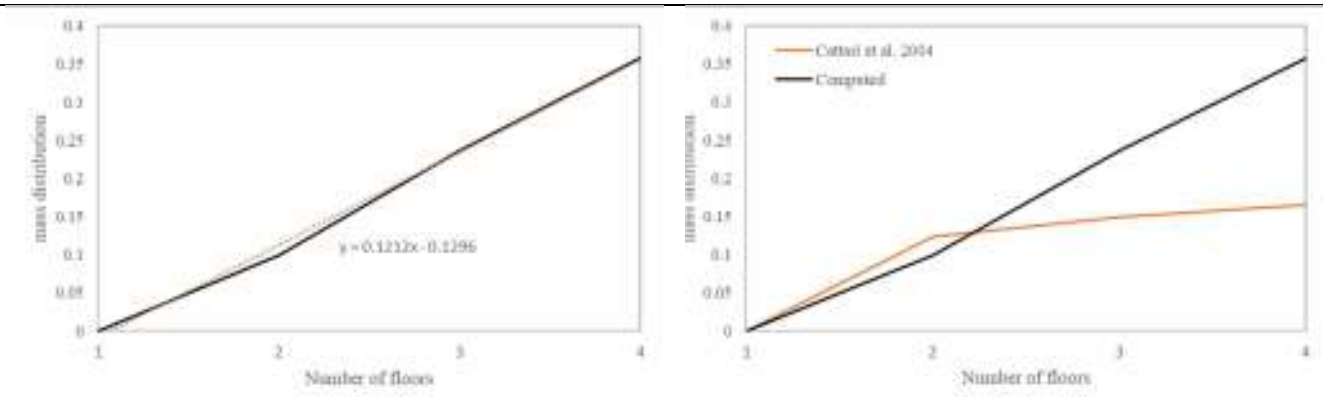

Figure 6.7. Mass distribution comparison along the height of the model.

Resistant walls ratio. The distribution of the resistant walls along the height has been compared with the analytical formulation provided by Cattari *et al.* (2004). The latter considers the α_{var} value as:

$$\alpha_{var} = (1 + 0.2\,(N - 1))^{-1} \tag{6.8}$$

Where *N* represents again the number of the floor. The assumptions made in this research, based on the different thicknesses of the walls along the height leads to a ladder distribution, presenting different values for the façades and the side walls. Considering the ground level as the referred one, the three superior floors are characterized by reductions of the bearing walls equal to 15%, 45% and 45% respectively, for the façades. The side walls have instead reductions of 10%, 25% and 25% for the three levels. In Figure 6.8 the distributions according to the different direction, a mean value and the formulation presented in literature are presented.

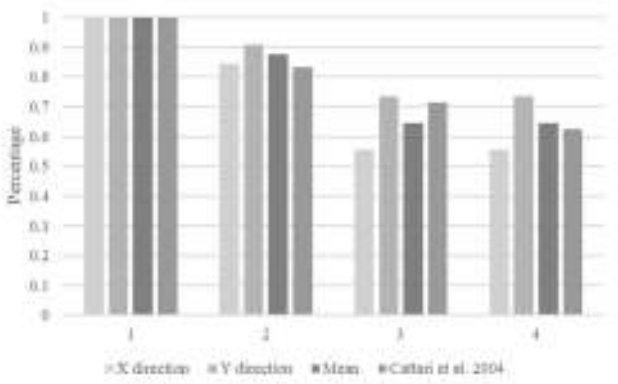

Figure 6.8. Comparison of the α distribution along the elevation of the building.

It is worth noting that the distribution of the thickness of the walls also depends by the total height of the building; *i.e.* the models with less number of floors tend to reduce the reductions of the bearing walls, developing constant thicknesses from the ground level to the roof. Assuming that the buildings of the database are constituted mainly by two, three and four levels (the buildings with more levels are residual, as well as the one-level buildings), different thickness-reduction laws can be deduced. The buildings realized by 4 levels usually follow the ladder distribution proposed in this work. On the other side, the buildings characterized by two floors have usually lower and constant bearing walls. Finally, the building with three levels can follow the two previous assumptions, depending from their dimensions and the empirical approaches adopted during the construction phases. Due to this, an intermediate value has been adopted.

Spandrels contributions factor. The spandrel contribution factor $k_{x,y,i}$ introduced in (3.29) shows constant values along the elevation of the structure. This denounce the vertical regularity of these buildings, where the openings are aligned between them. From a numeric point of view, between the side walls and the façades, different values are obtained. In *X* direction k_x has a value of 0.61, while in *Y* direction it has a value of 0.83. This can be related to the behavior of the masonry walls and the intrinsic issues of the resistant elements. Specifically, some rule can be empirically deduced, expressing a relationship between the discretization of the panels and their behavior under seismic actions. Considering (3.30), as presented in Table 6.5, different values of k_1 were used. They express the flexural and the shear tendencies of the masonry panels. Hence, looking at the side walls and the façades, some correlation can be done, expressing also intermediate

behaviors of the structures (Table 6.7). Clearly, different intermediate configurations can be obtained interpolating the listed coefficients. For k_1, in the Table, a value of 0.8 is proposed. The calibrated value found out for the building case-study was of 0.75, nevertheless, in this phase a slightly higher value was proposed. This was justified considering the strong shear behavior of the side walls of the investigated building, which they are characterized by no-openings at all.

Table 6.7. Proposed coefficient correlation between the spandrel contributions and the behaviour of the structures.

	Façades	Intermediate behavior	Side walls
$k_{x,y}$	1.60	1.40	1.20
k_1	0.8	1.0	1.2

Viscous damping. Hysteretic viscous damping exhibits an exponential behavior, increasing for *DL1* to *DL4* through a nonlinear curve. The two behaviors towards the different directions denounce the differences involved in the side walls and the façades of the buildings. For these reasons, the analytical values obtained for the case study have been extended to the other case studies. In Figure 6.9 the two trends are shown.

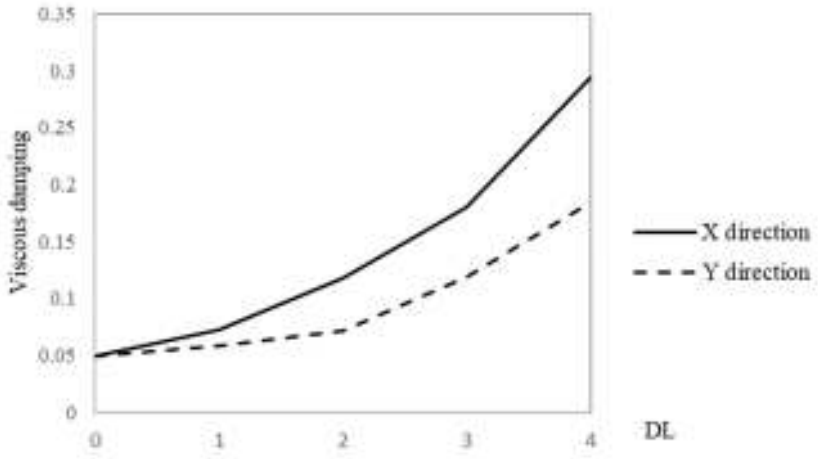

Figure 6.9. Equivalent damping distribution along the two directions.

Dispersion. The values of the dispersion have been assumed from the analytical phase. Considering the quantities presented in Section 5.5, in this part, some simplification has been adopted. Observing the values of dispersion towards the two directions, the dispersion tends to increase with the DLs, presenting slightly different specifications. In Table 6.4 the values from the different LS were shown. In this finale phase, a mean value of the dispersion equal to 0.154 was considered. It is worth noting that it has been assumed referring to the *DL4* for the *Y* direction. In fact, due to the slight differences of the LSs, this has been considered a reliable option, pointing out a conservative behavior only for the *DL4* in the *X* direction. Further studies will be able to improve these values to more proper specifications at the urban scale.

6.3 URBAN SCALE VULNERABILITY ASSESSMENT

The mechanical method has been finally applied to the simple-block model class. The buildings, presented in Section 4.2, despite the typological similitudes, present mutual differences. In this urban scale application, several parameters were assumed on the basis of the analytical phase, and they have been already listed in the previous section. The different mass distributions have been applied to the storeys of the structures, introducing the presented three masonry behaviors. Namely, façades, side walls and the bearing structure with an intermediate behavior. Given the mass distribution, the equivalent period of the building towards the two directions has been defined, as well as the stress in the bearing walls. The base shear *fx* can be defined, adopting the correction coefficient already presented. For k_1, three different coefficients were defined for the three discretization forms of the bearing walls. Looking at the cases, coefficient k_3 has been modified in order to account the plan irregularity of the structures decreasing the maximum shear values of the model. It ranged between 1,00 (no irregularity) to a minimum value of 0.8, which a conservative value coherent with the quantities proposed by Lagomarsino and Cattari (2014). A correlation between the spandrel contribution factor $k_{x,y}$ and the k_1 coefficient describing the masonry behavior ranging between flexural and shear propensity were pointed out (Table 6.7). Finally, bilinear capacity curves for the different models could be plotted. Complexly, 45 building plans for a total of 112 realized buildings in Florence were assessed. The results, calibrated on the representative case study previously analyzed, are shown in Figure 6.10. In this section, the plots account only the number of plans used for the intervention, without considering the numerousness of the realized structures; i.e., 45 capacity curves and their relative mean curve and standard deviations are shown.

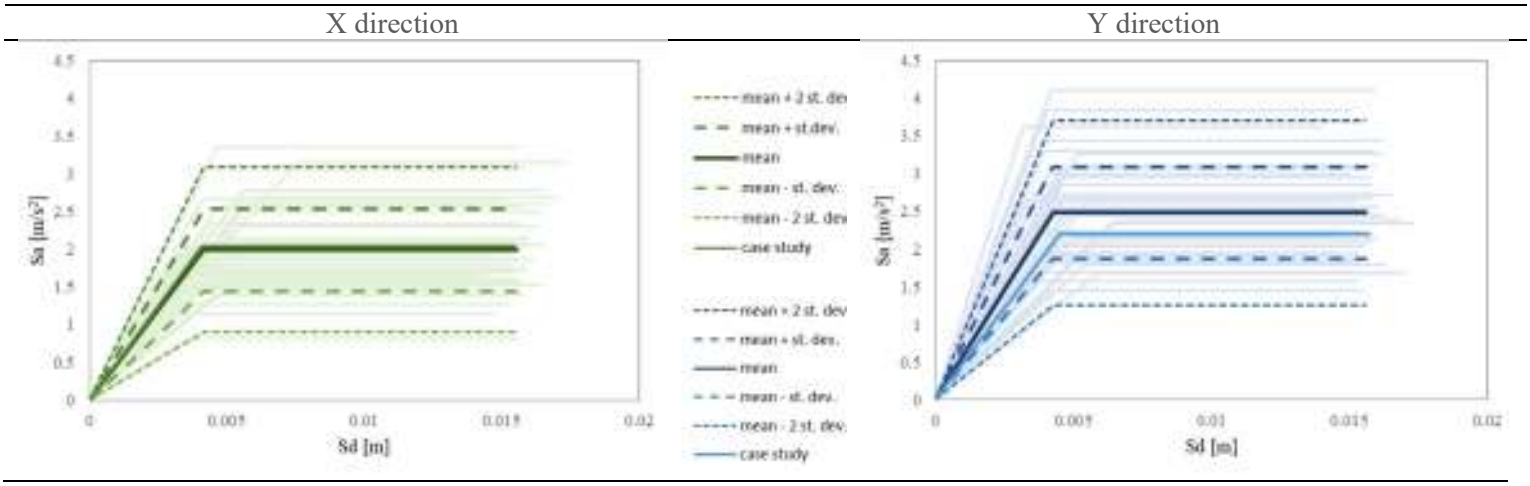

Figure 6.10. Bilinear capacity curves of the simple-block models along the two directions.

Looking at the curves, a bigger dispersion is pointed out in the *Y* direction, while in the *X* direction there is a relevant cluster of results around the *mean* value. This is due to the major variabilities offered by the side walls. As for the case-study, they can be characterized by massive side walls with few openings; however, elevations with openings or intermediate configurations can be

found. On the other side, the façades of the buildings, because of their intrinsic definition of front of buildings usually follow the same trends. In the *X* direction, the analytical model curve is almost superimposed to the mean one of the urban stock, while in the *Y* direction it presents a lower value. The results reflect the importance of the structural characteristics towards the two directions. Of course, some simplification needs to be justified by further analyses. For instance, in depth studies concerning the computation of the ultimate displacement of the different models are expected. Nevertheless, coherently with the analytical solutions forecasted for the representative case studies, the urban stock application points out: *1)* the good reliability of the case study compared to the database vulnerability; *2)* the variability of the seismic response of the different case studies due their structural configurations. Finally, fragility curves can be derived for the different case studies, presenting ranges of values for the different LS. Figure 6.10 points out as the mean curves accounting the double of the standard deviations are representative of the urban stock, with a few numbers of exceptions. Hence, their contributions have been finally considered.

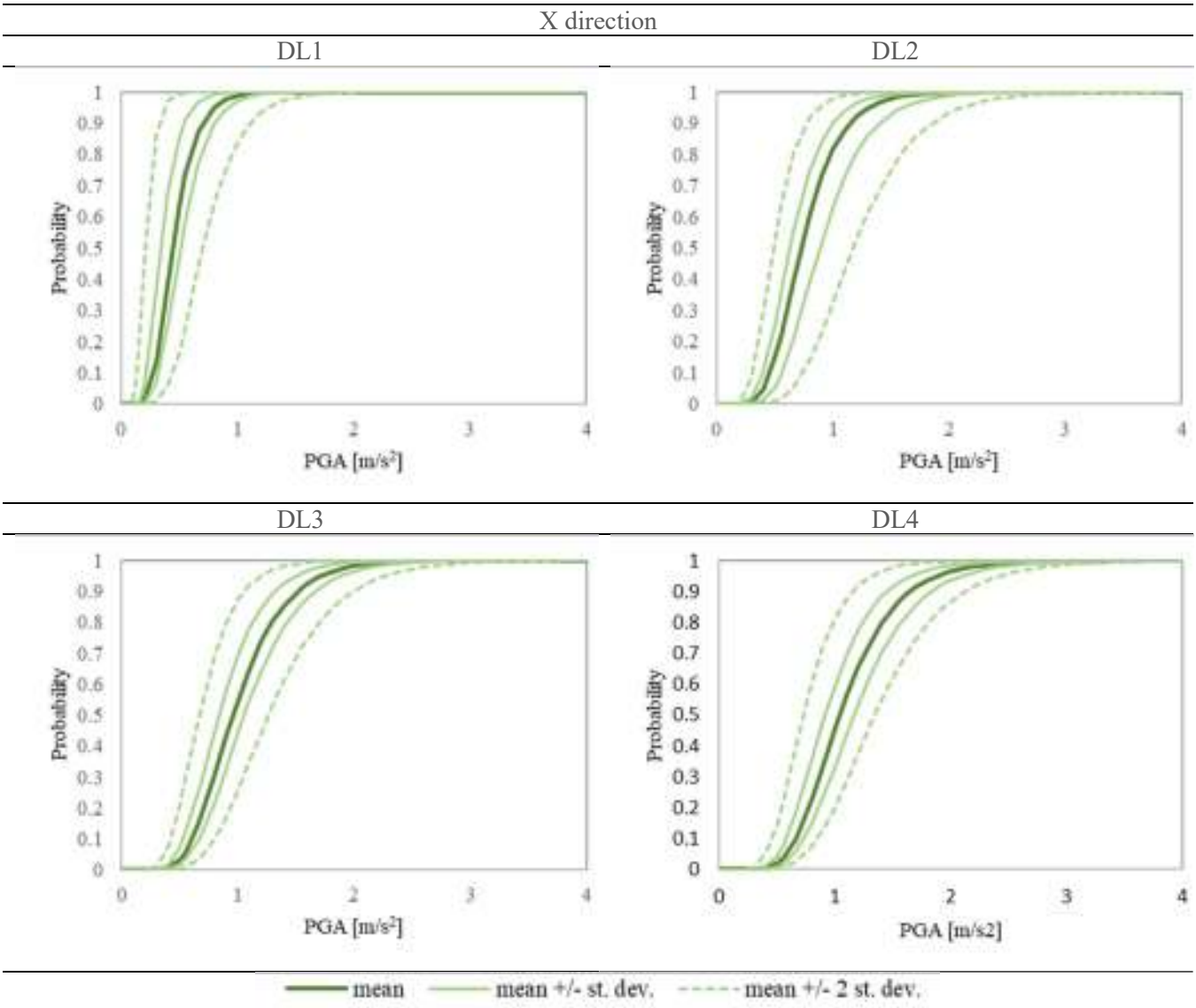

Figure 6.11. Fragility curves of the simple-block models along the X direction

In Figure 6.11 and 6.12 the fragility curves of the simple-block models along the two directions are shown. The equivalent damping and the dispersion values were accounted as described in the previous section.

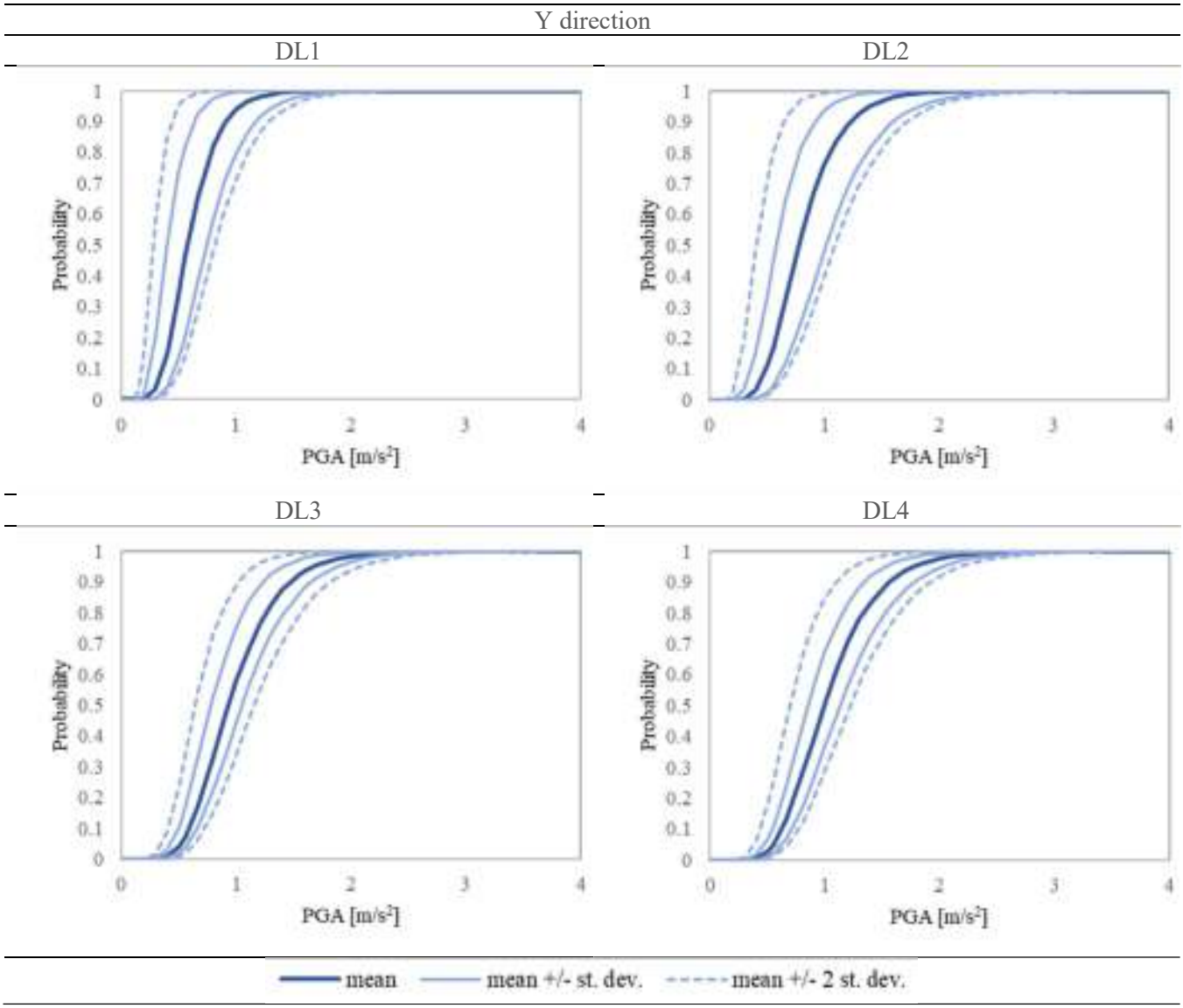

Figure 6.12. Fragility curves of the simple-block models along the Y direction.

Finally, the Damage scenarios for the different configurations can be examinated. In Figure 6.13, the *DS* for the *mean* model and the *mean* model accounting the double of the *standard deviation* of the database are presented. These forecasts are assumed as generally representative of the simple-block model for the Florentine area and they are extendable to other case studies of the same class. The *DSs* and the fragility curves points out a slight variability in terms of results; this was expectable from the analysis of the homogenous database descripted in Section 4.1. Observing the database, the *mean* curves show that for a seismic motion of 50 years return period, a model shows a 43% of probability attaining *DL1* and 32% for *DL2* in *X* direction; *Y* direction has more conservative results with a 33% of probability for *DL0*, 33% for *DL1* and only 17% for *DL2*. On the other side, for the bigger earthquakes, the *Y* direction is slightly more vulnerable. For a 475 yrs return period, in the *X* direction a 48.5% of attaining DL4 and 39% for *DL5* are

expected; in the *Y* direction, 49% and 40% for the two *DLs* are forecasted, respectively. Observing the model with the increasing of the double standard deviations, the values are more positive. For a 50 yrs return period there is the 56 and the 72% of probability of not having damage (*DL0*) along the *X* and *Y* directions, respectively. Moreover, for a 475 yrs return period, in the *X* direction 48% of probability of having *DL4*, 18% for *DL5* and 21% for *DL1* is obtained. As described in the analytical part, this behavior is ascribable to the brittle behavior of those kind of structures, who do not exhibit a particular plasticity and they quickly decrease to the highest *DLs*. In the *Y* direction, a 51% for *DL4* is expected, with a 23% of probability for collapse. Furthermore, as visible in the Figure, the results for the mean models less the double of the standard deviations tend to the highest *DLs*.

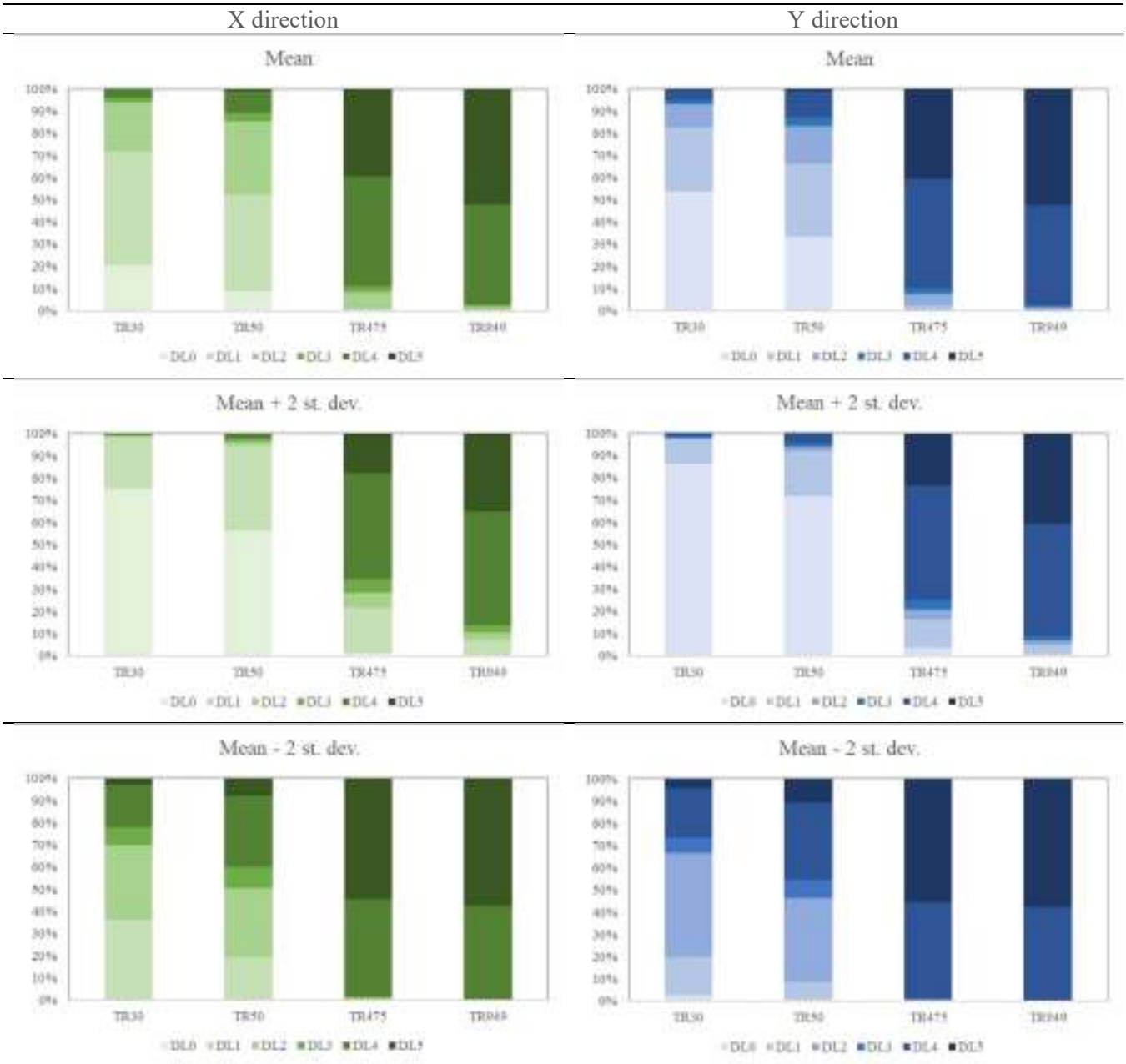

Figure 6.13. DS for the mean curve and the mean curve accounting for the double of the standard deviation.

In conclusion, in this chapter the DVM method was applied to the simple-block building class. The methodology was firstly calibrated setting the different parameters on the analytical results coming from the benchmark studied in Chapter 5. This phase was targeted to the definition of insights concerning the analytical results and simplified geometrical parameters. Specific relationship between the structural elements, the corrector coefficients and the spandrels contributions were found. Hence, the methodology has been applied to the different buildings of the same class; several characteristics collected in GIS and coming from the archive research have been used. A sample of bilinear capacity curves was obtained. The plots show the different structural responses, based on the specific distributions inside the buildings. Finally, the results have been expressed in terms of fragility curves and *DSs*, highlighting the variability of the response and quantifying the vulnerability of these structures in the city of Florence.

7. CONCLUSIVE REMARKS AND FURTHER FUTURE DEVELOPMENTS

7.1 FINAL REMARKS

In this thesis, the seismic vulnerability assessment of the residential URM buildings built during the XX century in Florence has been discussed. The research follows former studies conducted over the city of Florence for the seismic risk assessment and it deals with a hybrid approach aimed to an urban scale assessment. The residential URM structures of the XX century represent a relevant percentage of the Florentine stock. They have been realized through standardized design and urban planning, following architectonical concepts similar in all the Italian peninsula. Within this context, the public housing interventions, because of their amount in the city, have been targeted for this research and assumed as representative of the entire stock. The first part concerned a cognitive approach which obtained through an empirical methodology. This phase of the work dealt with the definition of the building classes. To this aim, an archive research was conducted, and a lot of information were collected into a GIS framework. Hence, the buildings have been divided considering typological and structural features, in order to determine the seismic behavior of the structures. A GIS environment was used, and the different collected buildings were geo-spatial referred. The buildings were divided into typological classes, based on their architectonical and structural forms. Hence, fast empirical methodologies were adopted, providing the first results in terms of vulnerability and damage scenarios. The GNDT second level approach was widely applied to the different buildings composing the database, pointing out a moderate vulnerability of the structure and a quite homogeneity of the investigated cases. This phase presents interesting outcomes concerning the homogeneity of the investigated constructions; furthermore, it pointed out a moderate vulnerability leading to non-severe damage scenarios. In order to in-depth investigate the risk of those buildings, an analytical procedure based on nonlinear static analysis was defined and applied to a selected case study. The simple-block buildings, accounted as the most numerous and the simplest ones in terms of morphology, were chosen as referred class for further investigations. Within the latter, a realized project was selected as benchmark for the analytical phase. This stage, which represents the core of the thesis, followed a probabilistic framework based on nonlinear static analysis. Theoretical assumptions presented in literature were assumed both for the modeling approaches, as for the uncertainty quantifications. The uncertainties were divided between epistemic and aleatory ones and treated separately. The epistemic uncertainties were modelled through a logic three approach, while the aleatory ones were computed through the central star approach. In the nonlinear static analysis, two different load patterns were considered towards the two different directions. The LSs were defined on the pushover curve adopting a

multi-scale approach involving three different levels of interest of the building. Hence, the capacity spectrum method was considered to define the PGA values for the attainment of the different *DLs*. The seismic demand was found through the definition of a sample of 30 accelerograms spectrum-compatible with the area of Florence, conditioned for the fundamental period of the structures. Finally, both dispersions, for capacity and demand were obtained. The first was defined through the use of the response surface method, while the second considered the percentiles of 16 and 84%. The derived analytical fragility curves pointed out aspects related to the structural configurations of the buildings and assimilable for the entire simple-block class.

The sensitivity analysis conducted over the building model pointed out relevant outcomes. Concerning the uncertainties, the epistemic modeling demonstrated a low sensitivity of the seismic response to the different logic tree branches. The latter points put how, in terms of vulnerability, despite the different behaviors expressed by the PO curves, the presence or not of the RC lintels over the openings does not significantly alter (or improve) the seismic vulnerability of those buildings. Namely, the lintels affect the seismic response and the damage evolution, but the PGA values for the attainment of the different LSs remain similar. Furthermore, the masonry disposition along the height of the models does not affect significantly the vulnerability of the case-study. This is related to the collapse modes of the building, which involve the lower levels of the structure. So, if the epistemic uncertainties proved how easier assumptions can be accepted in the engineer practice, limiting the number of epistemic models and reducing the time consuming of the procedure, the aleatory ones indicate in the mechanical properties of the materials the main issues that need to be investigated. The probabilistic Bayesian framework developed for the definition of the mechanical properties is coherent with the urban scale vocation of the project. Nonetheless, a series of mechanical investigation over several buildings belonging to the urban database is expected. The sensitivity model is targeted to the definition of the more relevant parameters that need to be in-depth studied, and the results of this research clearly indicate the objective to pursue. Concerning the mechanical properties adopted in this thesis, the prior values coming from MIT2019 were upgraded on the basis of experimental tests executed in Tuscany on buildings of the XX century. The exclusive upgrade of the materials through selected and geo-localized tests denounces the efforts made for a site-specific implementation of the material's properties. This has been possible thanks to the open source Tuscany Masonry Database, which led the obtainment of several destructive tests. Further studies could consider new updates of the initial mechanical values based on the acquisition of new experimental results, as well as the implementation of new tests coming from different Italian areas.

The results of the analytical procedure exhibited a relevant vulnerability of the buildings denouncing a brittle behavior in the nonlinear phase that, for the assumed hypothesis of homogeneity of the database, are expected for the other different structures. The analytical phase was at the basis of the final implementation procedure, aimed to: *1)* describe the expressed structural behavior by means of simplified procedures; *2)* extend the results to the other buildings of the same class. The results obtained for the benchmark model were assumed in order to extend the forecasts to a wider series of buildings. They were first converted in bilinear curves, then their reliability was discussed. The DVM was adopted in order to obtain the same curves through the definition of calibrated parameters valid for these structures. Specifically, the correlation between the different parameters of the DVM and the seismic performances of the building lead to assume specific relationships between those factors and the different parts of the structures. The three bearing wall typologies, *i.e.* façades, side walls and masonries with an intermediate behavior were listed, defining proper corrector coefficients based on the behavior of the different elements. The methodology was finally applied to the simple-block class. 112 different buildings realized following 45 architectonical and structural designs were studied. The results express the variability of the seismic response of the different buildings. In the *Y* direction, a higher dispersion is obtained, due to the possible major architectonical differences than the side walls may present. On the bilinear curves, the *LSs* and the ultimate displacement of the models were defined assuming the outcomes of the nonlinear static analysis of the benchmark model. Fragility curves were obtained assuming directly from the analytical phase the equivalent damping and the dispersions values. The results show the variability of the response, denouncing a medium/high vulnerability of the building class. For a seismic action with a return period of 475 years, the *DS* rounds around a 50% of probability receiving *DL4* and the 40% for the collapse of the structures. Coherently with the outcomes of the empirical methodology, the results are homogeneous in their extension, nonetheless, the final forecasts exhibit relevant damage scenarios. Despite the GNDT vulnerability indexes pointed out a low/moderate vulnerability for the benchmark building, the analytical results showed a high potential damage for the structure, given by a significant brittle behavior concerning the plastic phase. This first result demonstrates the inadequacy of the empirical methodology adopted for the vulnerability assessment of the XX century URM buildings. In fact, assuming the empirical rules of regularity, structural coherency and the presence of aseismic devices, these buildings perfectly respond to what is considered a non-vulnerable building and a *box-behavior* structure. Nonetheless, the presence of ring beam leads to WPSS models where the shear capacity of lowest storeys is demanded to the seismic resistance of structure.

The conclusions of this research show an important vulnerability for the investigated buildings that need to be considered. Further studies are expected, aiming to define additional case studies for analytical assessment in order to assess the reliability of the previous assumptions; the assessment of building with different height is still beneficial, both with considerations about the role of irregularity. These further analyses would also regard the extension of the procedure to different classes of buildings, excluded by the final simplified implementation because of the architectonical and intrinsic differences in their structural configurations. Last but not least, the research needs to continue in the evaluation of strengthening solutions for the improvements of safety of these structures and of the people who live in.

7.2 FURTHER DEVELOPMENTS OF THE RESEARCH

Further studies are certainly recommended and encouraged. They can be related both to the vulnerability/risk implementation, both to the computation of economic and human losses, as to the definition and cost/benefit analysis of strengthening solutions. Specifically:

- Starting from the mechanical properties of the materials adopted in this work, a specific campaign of experimental tests is recommended, in order to improve and better characterize the material properties adopted in the analysis.
- Performance of nonlinear dynamic analysis to check the reliability of the adopted nonlinear static procedure and the choice of considered load patterns are demanded.
- Analytical assessment of new case studies, coherently with the modeling assumptions made in this work, are expected. They can still deal with the simple-block model, in order to check the reliability of the DVM method or/and to implement it, or with different building typologies, in order to extend the applications to different classes.
- Extension of the results at the district scales, promoting geo-spatial damage scenarios able to rule the post-earthquake emergency planning can still be continuations of the work. To this aim, computation of the damages in terms of economic and human losses are natural extension of the research.
- Implementation at the urban scale of the ongoing micro-zonation studies concerning the city of Florence can be done. The latter would improve the seismic demand for the analysis, accounting for potential site-specific singularities not considered in this phase of the work.
- Definition of strengthening strategies able to reduce the seismic vulnerability of those buildings, proposing cost/benefit analysis indicating the best solutions for structural improvements.

8. REFERENCES

ASCE/SEI 41–13 (2014). Seismic evaluation and retrofit of existing buildings. American Society of Civil Engineers, Reston. ISBN 978-0-7844-7791-5

Aşıkoğlu, A., Vasconcelos, G., Lourenço, P. B., & Pantò, B. (2020). Pushover analysis of unreinforced irregular masonry buildings: Lessons from different modeling approaches. Engineering Structures, 218, 110830. doi:10.1016/j.engstruct.2020.110830

Astengo, G. (1951). Nuovi Quartieri in Italia, "Urbanistica", n.7, pp. 20-21 (in Italian)

Asteris, P.G., Moropoulou, A., Skentou, A.D., Apostolopoulou, M., Mohebkhah, A., Cavaleri, L., Rodrigues, H., Varum, H. (2019). Stochastic Vulnerability Assessment of Masonry Structures: Concepts, Modeling and Restoration Aspects. Applied Sciences, 9(2), 243–. doi:10.3390/app9020243

Aquilani, V., Di Sivo, M., Modica, V. (1979). La formazione dell'edilizia popolare e sovvenzionata a Firenze nell'analisi di alcuni programmi e interventi all'inizio del secolo, Firenze, Libreria editrice Fiorentina (in Italian)

Augenti, N., Parisi, F. (2010). Learning from construction failures due to the 2009 L'Aquila, Italy, earthquake, Journal of Performance of Constructed Facilities, 24(6), 536-555, 2010.

Bartoli, G., Betti, M., Marra, A. M., & Monchetti, S. (2019). A Bayesian model updating framework for robust seismic fragility analysis of non-isolated historic masonry towers. Philosophical Transactions of the Royal Society A: Mathematical, Physical and Engineering Sciences, 377(2155), 20190024. doi:10.1098/rsta.2019.0024

Bento, R., (2019). An Interdisciplinary Approach to the Seismic Assessment of Built Cultural Heritage: Case Studies in Lisbon and Outskirts, R. Aguilar et al. (Eds.): Structural Analysis of Historical Constructions, RILEM Bookseries 18, pp. 3–18, 2018. https://doi.org/10.1007/978-3-319-99441-3_1

Bertocci, S. (1998) I disegni dell'Archivio Storico Comunale di Firenze: territorio, città e architettura tra Ottocento e Novecento, Firenze, Polistampa, ISBN:978-8883040313 (in Italian)

Bettio, E., Romanelli, R. (2003). L'archivio storico Iacp/Ater di Firenze, in "Edilizia popolare", nn. gen.-giu., pp. 30-35 (in Italian)

Bettio, E., Romanelli, R. (2003). Inventario dell'Archivio delle Case Popolari di Firenze (1909-1986), Firenze (in Italian)

Beyer, K., and Dazio, A. (2012). Quasi-static cyclic tests on masonry spandrels. Earthquake Spectra, 28(3):907–929.;

Beyer, K., Petry, S., Tondelli, M., & Paparo, A. (2014). Towards Displacement-Based Seismic Design of Modern Unreinforced Masonry Structures. Geotechnical, Geological and Earthquake Engineering, 401–428. doi:10.1007/978-3-319-07118-3_12

Beyer K., Tondelli M., Vanin F., Petry S., Paparo A., (2015), Seismic behaviour of unreinforced masonry buildings with reinforced concrete slabs: Assessment of in-plane and out-of-plane response,

Blandon, C. A. and Priestley, M. (2005). Equivalent viscous damping equations for direct displacement based design. Journal of earthquake Engineering, 9(sup2):257–278.9

Boschi, S., Bernardini, C., Borghini, A., Ciavattone, A., Del Monte, E., Giordano, S., Ortolani, B., Signorini, N., Vignoli, A., (2015). Analisi dei risultati di prove sperimentali su murature toscane. Proceedings of XVI Convegno Nazionale ANIDIS, L'Aquila, Italia (in Italian)

Bracchi, S., Rota, M., Magenes, G. and Penna, A. (2016). Seismic assessment of masonry buildings accounting for limited knowledge on materials by Bayesian updating, Journal of Bulletin of Earthquake Engineering, Vol. 14, No. 8, pp.2273–2297, doi: 10.1007/s10518-016-9905-8

Braga, F., Dolce, M., Liberatore, D. (1982) A statistical study on damage buildings and an ensuing review ofthe M.S.K.—76 scale. In: Proceedings of the 7th European conference on earthquake engineering, Athens, Greece

Calderoni, B., Cordasco, E.A., Del Zoppo, M., Prata, A. (2020) Damage assessment of modern masonry buildings after the L'Aquila earthquake. Bull Earthquake Eng 18, 2275–2301 (2020). https://doi.org/10.1007/s10518-020-00784-5

Calvi, G.M. (1999). A displacement-based approach for vulnerability evaluation of classes of buildings. J Earthq Eng 3(3):411–438

Calvi, G.M., Pinho, R., Magenes, G., Bommer, J.J., Restrepo-Vélez, L.F., Crowley, H. (2006). Development of seismic vulnerability assessment methodologies over the past 30 years, ISET J. Earthq. Tech. 43 (2006) 75–104. Doi:10.1016/j.asej.2020.04.001

Cardinali, V., Tanganelli, M. (2018). Edilizia residenziale pubblica a Firenze: l'indagine storica archivistica per la valutazione del comportamento strutturale, VI Convegno Internazionale ReUSO Messina, 11-13 Ottobre 2018. (in Italian)

Cardinali, V., Viti, S., Tanganelli, M. (2019). Seismic vulnerability of the residential buildings of Florence, COMPDYN 2019 7th ECCOMAS Thematic Conference on

Computational Methods in Structural Dynamics and Earthquake Engineering M. Papadrakakis, M. Fragiadakis (eds.) Crete, Greece, 24–26 June 2019

Cardinali, V., Cristofaro, M. T., Ferrini, M., Nudo, R., Paoletti, B., & Tanganelli, M. (2020). An Interdisciplinary approach for the seismic vulnerability assessment of historical centres in masonry building aggregates: application to the city of Scarperia, Italy, ISPRS - International Archives of the Photogrammetry, Remote Sensing and Spatial Information Sciences, doi.org/10.5194/isprs-archives-xliv-m-1-2020-667-2020, 2020.

Cartis (2014). Sviluppo di una metodologia sistematica per la valutazione dell'esposizione a scala territoriale sulla base delle caratteristiche tipologico-strutturali degli edifici (in Italian)

Cattari, S., Curti, E., Giovinazzi, S., Lagomarsino, S., Parodi, S., Penna, A. (2005). Un modello meccanico per l'analisi di vulnerabilita` del costruito in muratura a scala urbana. In: Proceedings of 11th Italian conference on earthquake engineering, Genoa, Italy (in Italian)

Cattari, S., Lagomarsino, S. (2013a). Masonry structures, pp 151–200. In: Sullivan T, Calvi GM (eds) Developments in the field of displacement based seismic assessment. IUSS Press and EUCENTRE, Pavia, Italy, p 524, ISBN:978-88-6198-090-7

Cattari, S., and Lagomarsino, S. (2013b). Seismic assessment of mixed masonry-reinforced concrete buildings by non-linear static analyses. Earthq Struct, 4(3):241–264

Cattari, S., Lagomarsino, S., Bosiljkov, V., & D'Ayala, D. (2014). Sensitivity analysis for setting up the investigation protocol and defining proper confidence factors for masonry buildings. Bulletin of Earthquake Engineering, 13(1), 129–151. doi:10.1007/s10518-014-9648-3

Cattari, S., Camilletti, D., Magenes, G., Manzini, C.F., Morandi, P., Spacone, E., Camata, G., Marano, C., Caliò, I., Pantò, B., Cannizzaro, F., Occhipinti, G., Calderoni, B., De Luca, A., Cordasco, E.A., Brandonisio, G., Sandoli, A., Casapulla, C., Portioli, F., DeFelice, G. (2017). Comparative analysis of benchmark case studies for assessing the reliability of software packages targeted to the seismic assessment of URM buildings, XVII CONVEGNO ANIDIS "L'Ingegneria Sismica in Italia" Pistoia, 17-21 Settembre 2017 (in Italian)

Catulo, R., Falcão, A. P., Bento, R., & Ildefonso, S. (2018). Simplified evaluation of seismic vulnerability of Lisbon Heritage City Centre based on a 3DGIS-based methodology, Journal of Cultural Heritage, doi.org/10.1016/j.culher.2017.11.014, 2018.

Cavaleri, L., Di Trapani, F., & Ferrotto, M. F. (2017). A new hybrid procedure for the definition of seismic vulnerability in Mediterranean cross-border urban areas. Natural Hazards. https://doi.org/10.1007/s11069-016-2646-9, https://doi.org/10.1016/j.cageo.2012.08.016

Cescatti, E., Salzano, P., Casapulla, C., Ceroni, F., Da Porto, F., Prota, A. (2020). Damages to masonry churches after 2016–2017 Central Italy seismic sequence and definition of fragility curves. Bull Earthquake Eng 18, 297–329 (2020). https://doi.org/10.1007/s10518-019-00729-7

CNR-DT212, C. (2013). Guide for the Probabilistic Assessment of the Seismic Safety of Existing Buildings). Consiglio Nazionale delle Ricerche, Rome, Italy (in Italian)

Coli, M., & Rubellini P. (2013). Geological anamnesis of the Florence area, Italy. Z. Dt. Ges. Geowiss. (German J. Geosci.), 164 (4), p. 581–589.)

Coli, M., Guerri, L. & Rubellini, P., (2015). Geotechnical characterization of the Florence (Italy) soils. Proc. 5th Asian Regional Conference on Soil Mechanics and Geotechnical Engineering, Fukuoka November 9-13, Japan.,

Colombi, M., Borzi, B., Crowley, H., Onida, M., Meroni, F., Pinho, R. (2008). Deriving vulnerability curves using Italian earthquake damage data. Bull Earthq Eng 6(3):485–504

Como, M., (2013). Statics of Historic Masonry Constructions. Springer.

Correia Lopes, G., Vicente, R., Ferreira, T. M., Azenha, M. (2019). Intervened URM buildings with RC elements: typological characterization and associated challenges. Bull. Earthq. Eng. 2019, 17, 4987–5019, doi:10.1007/s10518-019-00651-y.

Cosenza, E., Del Vecchio, C., Di Ludovico, M., Dolce, M., Moroni, C., Prota, A., Renzi, E. (2018). The Italian guidelines for seismic risk classification of constructions: technical principles and validation. Bulletin of Earthquake Engineering, 16(12) (2018) 5905-5935.

Cristofaro, M.T., D'Ambrisi, A., De Stefano, M. (2009). Nuovi modelli previsionali per la stima della resistenza a compressione del calcestruzzo con il metodo Sonreb. In: ANIDIS, Bologna, 28 giugno- 2 luglio 2009, pp. 0-0, ISBN:9788890429200 (in Italian)

Croce, P., Landi, F., and Formichi, P. (2019). Probabilistic Seismic Assessment of Existing Masonry Buildings, Buildings, 9, 237, https://doi.org/10.3390/buildings9120237, 2019.

D'Altri, A. M., Sarhosis, V., Milani, G., Rots, J., Cattari, S., Lagomarsino, S., Sacco, E., Tralli, A., Castellazzi G., and de Miranda, S. (2019). A review of numerical models for masonry structures, Numerical Modeling of Masonry and Historical Structures, From Theory to Application, Woodhead Publishing Series in Civil and Structural Engineering, Pages 3-53

De Luca, F., Vamvatsikos, D., & Iervolino, I. (2012). Near-optimal piecewise linear fits of static pushover capacity curves for equivalent SDOF analysis. Earthquake Engineering & Structural Dynamics, 42(4),

Dolce, M., Prota, A., Borzi, B., da Porto, F., Lagomarsino, S., Magenes, Moroni C., Penna A, Polese M, Speranza E., Verderame G. M. Zuccaro, G. (2020). Seismic risk assessment of residential buildings in Italy. Bulletin of Earthquake Engineering. doi:10.1007/s10518-020-01009-5

Douglas, J., Seyedi, D.M., Ulrich, T., Modaressi, H., Foerster, E., Pitilakis, K., … Loli, M. (2014). Evaluation of seismic hazard for the assessment of historical elements at risk: description of input and selection of intensity measures. Bulletin of Earthquake Engineering, 13(1), 49–65. doi:10.1007/s10518-014-9606-0

EC 8-3 (2005). Design of structures for earthquake resistance, part 3: strengthening and repair of buildings. European standard EN 1998-3. European Committee for Standardization (CEN), Brussels

EN 1998-1 (2004). Eurocode 8: Design of structures for earthquake resistance - Part 1: General rules, seismic actions and rules for buildings, CEN (European Committee for Standardization), Brussels, Belgium.

Erberik, M.A. (2008). Generation fragility curves for Turkish masonry buildings considering in-plane failure modes, Earthq. Eng. Struct. D. 37, 387-405.

ESM working group, (2015). European Strong-Motion database, version 0.1, Network Activity 3: Networking acceleration networks and SM data users. Project NERA (www.nera-eu.org). URL http://esm.mi.ingv.it

Fajfar, P. (1999). Capacity spectrum method based on inelastic spectra. Earthq Eng Struct Dyn28(9):979–993

Fajfar, P. (2000). A nonlinear analysis method for performance-based seismic design. Earthq Spectra 16(3):573–591

Fantozzi Micali, O., Lolli, E. (2007). Novoli: alla periferia delle grandi trasformazioni: edilizia economica e popolare del secondo dopoguerra, Firenze, Alinea, 2007, ISBN: 978-88-6055- 197-9 (in Italian)

Faravelli, M., Borzi, B., Polli, D., & Pagano, M. (2019). Calibration of a mechanics-based method for large-scale vulnerability assessment. Bulletin of Earthquake Engineering. doi:10.1007/s10518-019-00560-0

Federal Emergency Management Agency, FEMA-356, (2000). Prestandard and Commentary for Seismic Rehabilitation of Buildings, Washington DC.;

FEMA, (2005). Improvement of nonlinear static seismic analysis procedures. FEMA-440 report Federal emergency management agency, Washington DC.

Federal Emergency Management Agency (FEMA) (2009). Quantification of building seismic performance factors. FEMA P695. FEMA, Washington, DC (2009)

Ferreira, T.M., Vicente, R., Varum, H., 2014: Seismic vulnerability assessment of masonry facade walls: development, application and validation of a new scoring method. Structural Engineering and Mechanics, 50: 541–561. doi: 10.12989/sem.2014.50.4.541.

Formisano, A., Florio, G., Landolfo, R., & Mazzolani, F. M., (2011). Un metodo per la valutazione su larga scala della vulnerabilità sismica degli aggregati storici. XV Convegno ANDIS - L'Ingegneria Sismica in Italia

Freeman, S.A. (1998). The capacity spectrum method as a tool for seismic design. In: Proceedings of 11th European conference of earthquake engineering. Paris, France

GL-INGV [Gruppo di Lavoro INGV sul terremoto di Amatrice] 2016. Secondo rapporto di sintesi sul Terremoto di Amatrice Ml 6.0 del 24 Agosto 2016 (Italia Centrale), doi:10.5281/zenodo.154400. (in Italian)

Gobbi Sica, G. (2006). Le origini della casa popolare a Firenze fra iniziativa pubblica e filantropia privata. Una rilettura, in "Firenze Architettura", anno X, n. 2, 2006, p. 96-105

Graziotti, F., Magenes, G., Penna, A., and Fontana, D. (2012). Experimental cyclic behaviour of stone masonry spandrels. Proc. of 15th 15th World Conference on Earthquake Engineering, Lisbon, Portugal

Grünthal, G. (1998). European Macroseismic Scale (EMS 1998). Council of Europe, Cahiers du Centre Européen de Géodynamique et de Sismologie, p 15

Gruppo Nazionale per la Difesa dai Terremoti - GNDT-SSN, (1994). Scheda di esposizione e vulnerabilità e di rilevamento danni di primo e secondo livello (muratura e c. a.). Gruppo Nazionale per la Difesa dai Terremoti, Rome (in Italian)

Haddad, J., Cattari, S., Lagomarsino, S. (2019). Use of the model parameter sensitivity analysis for the probabilistic- based seismic assessment of existing buildings. J Bull Earthq Eng 17:1983–2009. https ://doi.org/10.1007/s1051 8-018-0520-8

Hannewald, P., Michel, C., Lestuzzi, P., Crowley, H., Pinguet, J., & Fäh, D. (2020). Development and validation of simplified mechanics-based capacity curves for scenario-based risk assessment of school buildings in Basel. Engineering Structures, 209, 110290. doi:10.1016/j.engstruct.2020.110290

IACP Firenze, Istituto per le Case Popolari in Firenze. (1932). L'attività nel primo decennio dell'era fascista 1922-1932. X. Firenze, Tip. Giuntina.

Iervolino, I., Galasso, C., & Cosenza, E. (2009). REXEL: computer aided record selection for code-based seismic structural analysis. Bulletin of Earthquake Engineering, 8(2), 339–362. doi:10.1007/s10518-009-9146-1

Iervolino, I., Spillatura, A., & Bazzurro, P. (2018). Seismic Reliability of Code-Conforming Italian Buildings. Journal of Earthquake Engineering, 1–23. doi:10.1080/13632469.2018.1540372

ISI, (2015). Valutazione del grado di vulnerabilità sismica del patrimonio edilizio residenziale pubblico; Studio sullo stato conservativo di un campione del patrimonio gestito dagli Enti associati a Federcasa, 29-07-2015 (in Italian)

Jacobs, J. (1961). Death and life of great American cities. New York: Random House.

Jaiswal, K.S., Aspinal, W.P., Perkins, D., Wald, D. and Porter, K.A. (2012). Use of Expert Judgment Elicitation to Estimate Seismic Vulnerability of Selected Building Types. In Proceedings of the 15th World Conference on Earthquake Engineering (WCEE). Lisbon, Portugal

Kappos, A. J., Panagopoulos, G., Panagiotopoulos, C., & Penelis, G. (2006). A hybrid method for the vulnerability assessment of R/C and URM buildings. Bulletin of Earthquake Engineering, 4(4), 391–413. doi:10.1007/s10518-006-9023-0

Kappos, A. J. (2016). An overview of the development of the hybrid method for seismic vulnerability assessment of buildings. Structure and Infrastructure Engineering. https://doi.org/10.1080/15732479.2016.1151448

Kassem M.M., Nazri F.M., Farsangi E.N. (2020). The seismic vulnerability assessment methodologies: A state-of-the-art review. Ain Shams Engineering Journal, https://doi.org/10.1016/j.asej.2020.04.001

Kostinakis K., Fontara I.K., Athanatopoulou A.M. (2018). Scalar structurespecific ground motion intensity measures for assessing the seismic performance of structures: A review. Journal of Earthquake Engineering 22(4):630-665, DOI: 10.1080/13632469.2016.1264323

Lacanna, G., Deguy, P., Ripepe, M., Coli, M., Paoletti, B., Barducci, S., Tanganelli, M., Viti, S., De Stefano, M. (2016). Seismic hazard of urban areas: a case-study. In: ECCOMAS Congress 2016 - VII European Congress on Computational Methods in Applied Sciences and Engineering, Crete Island, Greece, 5–10 June 2016, M. Papadrakakis, V. Papadopoulos, G. Stefanou, V. Plevris (eds.), pp. 0-0.,

Lagomarsino, S. (2006). On the vulnerability assessment of monumental buildings. Bulletin of Earthquake Engineering, 4(4), 445–463. doi:10.1007/s10518-006-9025-y

Lagomarsino, S., Giovinazzi, S. (2006). Macroseismic and mechanical models for the vulnerability assessment of current buildings. Bull Earthq Eng 4(4):445–463 doi:10.1007/s10518-006-9024-z.

Lagomarsino, S., Penna, A., Galasco, A., Cattari, S. (2013). TREMURI program: An equivalent frame model for the nonlinear seismic analysis of masonry buildings, Engineering Structures, Vol. 56, 1787-1799

Lagomarsino, S. and Cattari, S. (2013). Seismic vulnerability of existing buildings: Observational and mechanical approaches for application in urban areas. Seismic vulnerability of structures, pages 1–62.

Lagomarsino, S. and Cattari, S. (2014). Fragility functions of masonry buildings. In SYNER-G: Typology definition and fragility functions for physical elements at seismic risk, pages 111–156. Springer.)

Lagomarsino, S., Cattari, S. (2015a). PERPETUATE guidelines for seismic performance-based assessment of cultural heritage masonry structures. Bull Earthq Eng 13(1):13–47

Lagomarsino, S., & Cattari, S. (2015b). Seismic Performance of Historical Masonry Structures Through Pushover and Nonlinear Dynamic Analyses. In A. Ansal (Ed.), Perspectives on European Earthquake Engineering and Seismology: Volume 2 (pp. 265–292). https://doi.org/10.1007/978-3-319-16964-4_11)

Lagomarsino S., Camilletti D., Cattari S., Marino S. (2018) Seismic Assessment of Existing Irregular Masonry Buildings by Nonlinear Static and Dynamic Analyses. In: Pitilakis K. (eds) Recent Advances in Earthquake Engineering in Europe. ECEE 2018. Geotechnical, Geological and Earthquake Engineering, vol 46. Springer, Cham

Lantada, N., Irizarry, J., Barbat, A. H., Goula, X., Roca, A., Susagna, T., Pujades, L. G., (2010). Seismic hazard and risk scenarios for Barcelona, Spain, using the Risk-UE vulnerability index method, Bullettin of Earthquake Engineering 8(2):201–229. doi: 10.1007/s10518-009-9148-z ;

Lopes Pegna, M. (1974). Firenze dalle origini al Medioevo, Firenze, Del Re Editore (in Italian)

Lourenço, P.B., Oliveira, D.V., Leite, J.C., Ingham, J.M., Modena, C., Da Porto, F. (2013). Simplified indexes for the seismic assessment of masonry buildings: International database and validation. Engineering Failure Analysis, 34(), 585–605. doi:10.1016/j.engfailanal.2013.02.014

Lourenço, P., Varum, H., Vasconcelos, G., & Rodrigues, H. (2015). Structural conservation and vernacular construction. Seismic Retrofitting: Learning from Vernacular Architecture, 37–42. doi:10.1201/b18856-8

Lourenço, P. (2015). Masonry Modeling, in: Michael Beer, Ioannis A. Kougioumtzoglou, Edoardo Patelli, Siu-Kui Au (Eds.), Encyclopedia of Earthquake Engineering, Springer Berlin Heidelberg, Berlin, Heidelberg, 2015, pp. 1419–1431, https://doi.org/10.1007/978-3-642-35344-4_153.)

Magenes G. (2006). Masonry building design in seismic areas: recent experiences and prospects from a European standpoint, Keynote 9, Proc. of 1st European Conf. on Earthquake Engineering and Seismology, Geneva, Switzerland

Magenes G., Morandi P. (2008). Some issues on seismic design and assessment of masonry buildings based on linear elastic analysis. Proc. of the Michael John Nigel Priestley Symposium, IUSS Press, Pavia, Italy, July 2008, 83-94.

Maio R. and Tsionis G. (2015). Seismic fragility curves for the European building stock: review and evaluation of analytical fragility curves. EUR 27635 EN. European Laboratory for Structural Assessment, Institute for the Protection and Security of the Citizen, Joint Research Centre of the European Commission, Ispra (Italy).)

Maio, R., Vicente, R., Formisano, A., & Varum, H., (2015). Seismic vulnerability of building aggregates through hybrid and indirect assessment techniques. Bulletin of Earthquake Engineering. https://doi.org/10.1007/s10518-015-9747-9

Mann, W., Müller, H. (1980). Failure of shear-stressed masonry – An enlarged theory, tests and application to shear-walls. In: Proceedings of the 7th international symposium on load-bearing brickwork, London;

Manzini, C. F., Magenes, G., Penna, A., da Porto, F., Camilletti, D., Cattari, S., & Lagomarsino, S. (2018). Masonry Italian Code-Conforming Buildings. Part 1: Case Studies and Design Methods. Journal of Earthquake Engineering, 22(sup2), 54–73. doi:10.1080/13632469.2018.1532358

Marcetti, C., Manetti, G., Aleardi, A., (2006). Firenze verso la città moderna : itinerari urbanistici nella citta estesa tra Ottocento e Novecento, Bagno a Ripoli : Il Bandino, stampa 2006 (in Italian)

Marino, S., Cattari, S., Lagomarsino, S. (2018). Use of nonlinear static procedures for irregular URM buildings in literature and codes. In: Proceedings of 16th European conference on earthquake engineering, Thessaloniki, 18–21 June 2018

Marino, S., Cattari, S., and Lagomarsino, S. (2019). Are the nonlinear static procedures feasible for the seismic assessment of irregular existing masonry buildings? Engineering Structures 200. doi:10.1016/j.engstruct.2019.109700

Marques R. and Lourenco, P. B. (2008). Benchmarking of commercial software for the seismic assessment of masonry buildings. Azores 1998 –International Seminar on Seismic Risk and Rehabilitation of Stone Masonry Housing, Horta, Faial Island, Portugal, 2008.9

Martínez-Cuevas, S., Benito, M. B., Cervera, J., Morillo, M. C., & Luna, M. (2017). Urban modifiers of seismic vulnerability aimed at Urban Zoning Regulations. Bulletin of Earthquake Engineering. https://doi.org/10.1007/s10518-017-0162-2

Matsumura, K. (1992). On the intensity measure of strong motion related to structural failures, Proc. of the 10th World Conference on Earthquake Engineering, Rotterdam, pp. 375–380.

Metelli, G. (2016). Prestazioni strutturali dell'edilizia residenziale Fiorentina in muratura del Novecento, tesi di laurea, Università degli Studi di Firenze, Scuola di Architettura, aa. 2015-2016, relatore prof. Tanganelli M. (in Italian)

Metelli, G., Rotunno, T., Tanganelli, M., and Viti, S. (2017). Florence: seismic assessment of not-historical masonry buildings population. COMPDYN 2017 6th ECCOMAS Thematic Conference on Computational Methods in Structural Dynamics and Earthquake Engineering M. Papadrakakis. M. Fragiadakis (eds.) Rhodes Island. Greece. 15–17 June 2017. Vol. 2. pp. 3189-3200.

Michel, C., Crowley, H., Hannewald, P., Lestuzzi, P., & Fäh, D. (2018). Deriving fragility functions from bilinearized capacity curves for earthquake scenario modelling using the conditional spectrum. Bulletin of Earthquake Engineering. doi:10.1007/s10518-018-0371-3

Michel, C., Karbassi, A., & Lestuzzi, P. (2018). Evaluation of the seismic retrofitting of an unreinforced masonry building using numerical modeling and ambient vibration measurements. Engineering Structures, 158, 124–135. doi:10.1016/j.engstruct.2017.12.016

Milosevic, J., Cattari, S., and Bento, R. (2018). Sensitivity analysis of the seismic performance of ancient mixed masonry-RC buildings in Lisbon. International Journal of Masonry Research and Innovation, 3(2):108–154

Milosevic, J. (2019). Seismic vulnerability assessment of mixed masonry-reinforced concrete buildings in Lisbon, PhD Dissertation

Milosevic, J., Bento, R., Cattari, S. (2019). Definition of fragility curves through nonlinear static analyses: procedure and application to a mixed masonry-RC building stock, Bull. Earthq. Eng. 18 (2019) 513–545,http://dx.doi.org/10.1007/s10518-019-00694-1.)

MIT (2009). Istruzioni per l'applicazione delle 'Norme tecniche per le costruzioni' di cui al Decreto Ministeriale 14/01/2008. Ministero delle Infrastrutture e dei Trasporti (MIT). Roma (In Italian)

MIT (2017). Decreto del Ministro delle Infrastrutture e dei Trasporti n°58 del 28/02/2017. Allegato A: Linee guida per la classificazione del rischio sismico delle costruzioni, Rome, Italy (in Italian)

MIT (2019), Circolare 21 gennaio 2019, n. 7 Istruzioni per l'applicazione dell'«Aggiornamento delle "Norme tecniche per le costruzioni"» di cui al decreto ministeriale 17 gennaio 2018. G.U. n. 47 del 26/02/2009, Supplemento Ordinario n. 27, Rome, (in Italian)

Molin, D. & Paciello, A. (1999). Seismic hazard assessment in Florence city Italy, Journal of Earthquake Engineering, 3(4), 475–494, doi:10.1080/13632469909350356

Morandi, P., Albanesi, L., Graziotti, F., Li Piani, T., Penna, A., Magenes, G. (2018). Development of a dataset on the in-plane experimental response of URM piers with bricks and blocks. Constr Build Mater. https ://doi.org/10.1016/j.conbu ildma t.2018.09.070 ;

NTC (2018). Min. LL. PP., "Aggiornamento delle «Norme tecniche per le costruzioni». G.U. No. 42 del 20 Febbraio D.M. Ministero Infrastrutture e Trasporti 17 gennaio 2018, Roma (in Italian). NTC (2008) Norme tecniche per le costruzioni. D.M. Ministero Infrastrutture e Trasporti 14 gennaio 2008, G.U.R.I. 4 febbraio 2008, Roma, 2018. (in Italian)

Oliveira, D.V., Araújo, A.S., Lourenço, P.B., Magenes, G., Penna, A. (2016). Modelling of the in-plane behavior of stone masonry panels. In: Van Balen K, Verstrynge E (eds) Structural analysis of historical constructions-anamnesis, diagnosis, therapy, controls. Taylor and Francis Group, London. ISBN 978-1-138-02951-4

Palermo, O., Cardinali, V., Azzara, M.R., Tanganelli, M. (2019). Valutazione delle prestazioni strutturali di edifici residenziali pubblici: due insediamenti INA CASA a Firenze, VII Convegno Internazionale ReUSO Matera, 23-26 Ottobre 2019 (in Italian)

Parisi, F., De Luca, F., Petruzzelli, F., De Risi, R., Chioccarelli, E., Iervolino, I. (2012). Field inspection after the May 20thand 29th2012 Emilia-Romagna earthquakes, available on http://www.reluis.it.

Peduto, D., Ferlisi, S., Nicodemo, G., Reale, D., Pisciotta, G., & Gullà, G. (2017). Empirical fragility and vulnerability curves for buildings exposed to slow-moving landslides at medium and large scales. Landslides, 14(6), 1993–2007. doi:10.1007/s10346-017-0826-7

Penna, A., Lagomarsino, S., Galasco, A. (2014). A nonlinear macroelement model for the seismic analysis of masonry buildings, Earthquake Engineering and Structural Dynamics, Vol. 43(2), 159-179

Petry, S., Beyer, K. (2014). Cyclic test data of six unreinforced masonry walls with different boundary conditions. Earthq Spectra. https ://doi.org/10.1193/10151 3eqs2 69

Piano incremento occupazione operaia. (1949). Case per lavoratori, 1, Suggerimenti, norme e schemi per la elaborazione e presentazione dei progetti, Roma

Pierin,i R. (2001). La citta distante: piani e progetti di edilizia residenziale pubblica. Pisa, ETS, 2001. ISBN: 88-467-0497-5 (in Italian)

Pinto, P.E., Giannini, R., Franchin, P. (2004). Seismic reliability analysis of structures. IUSS Press, Pavia. ISBN 88-7358-017-3

Pitilakis, K. et al. (2014) (eds.), SYNER-G: Typology Definition and Fragility Functions for Physical Elements at Seismic Risk, Geotechnical, Geological and Earthquake Engineering 27, DOI 10.1007/978-94-007-7872-6_5, © Springer Science+Business Media Dordrecht 2014

Polese, M,. Di Ludovico, M., Gaetani d'Aragona, M., Prota, A., Manfredi, G. (2020). Regional vulnerability and risk assessment accounting for local building typologies. Int J Disaster Risk Red 43:141400

Ratti, A. (2001). Il fondo INA-Casa nell'archivio storico dell'INA, in La grande ricostruzione, a cura di Di Biagi, Roma, Donzelli, 2001, pp. 129-132, ISBN: 978-88-6036-534-7

Ripepe, M., Lacanna, G., Deguy, P., Cristofaro, M.T., De Stefano, M., Tanganelli, M., Paoletti, B., Cardinali, V., Viti, S. Bertaccini, B., Rocco, E., Giommi A. (2018). RISCHIO SISMICO DI AREE URBANE COMPLESSE: PROGETTO SISMED. In: ReUSO 2018: VI Convegno Internazionale sulla documentazione, conservazione e recupero del patrimonio architettonico e sulla tutela paesaggistica, Messina, 11 - 13 ottobre 2018, Gangemi Editore spa, pp. 903-910, ISBN:9788849236590

Remki, M., Kehila, F. (2018). Analytically Derived Fragility Curves and Damage Assessment of Masonrybuildings. In: Rodrigues H., Elnashai A., Calvi G. (eds) Facing the Challenges in Structural Engineering. GeoMEast 2017. Sustainable Civil Infrastructures. Springer, Cham. https://doi.org/10.1007/978-3-319-61914-9_4

RINTC Workgroup (2018). Results of the 2015-2017 Implicit seismic risk of codeconforming structures in Italy (RINTC) project. ReLUIS report, Rete dei Laboratori Universitari di Ingegneria Sismica (ReLUIS), Naples, Italy, available at http://www.reluis.it/

Roca, P., Lourenço, P.B., Gaetani, A. (2019). Historic Construction and Conservation: Materials, Systems and Damage, Routledge; 2019

Rossetto, T., Elnashai, A. (2003) Derivation of vulnerability functions for European-type RC structures based on observational data. Eng Struct 2003;25:1241–63.

Rosti, A., Rota, M. & Penna, A. (2020). Empirical fragility curves for Italian URM buildings. Bull Earthquake Eng (2020). https://doi.org/10.1007/s10518-020-00845-9

Rota, M., A. Penna, and G. Magenes. (2010). A methodology for deriving analytical fragility curves for masonry buildings based on stochastic nonlinear analyses. Engineering Structures. Elsevier Ltd 32 (5):1312–23. doi:10.1016/j.engstruct.2010.01.009.

Rovida, A., Locati, M., Camassi, R., Lolli, B., Gasperini, P. (2016). Catalogo Parametrico dei Terremoti Italiani, release 2015, INGV., https://emidius.mi.ingv.it/CPTI15-DBMI15/description_CPTI15.htm, 2016.

Sandoli, A., Calderoni, B. (2018). Assessment of the seismic vulnerability at territorial scale: a new structural classification of existing buildings and definition of fragility curves. In: Proceedings of 10th international masonry conference (IMC), Milano

Siano, R., Roca, P., Camata, G., Pelà, L., Sepe, V., Spacone, E., & Petracca, M. (2018). Numerical investigation of non-linear equivalent-frame models for regular masonry walls. Engineering Structures, 173, 512–529. doi:10.1016/j.engstruct.2018.07.006

Simoes, A. (2019). Evaluation of the seismic vulnerability of the unreinforced masonry buildings constructed in the transition between the 19th and 20th centuries in Lisbon, Portugal, PhD Dissertation

Sivori, D., Lepidi, M., Cattari, S. (2020). Ambient vibration tools to validate the rigid diaphragm assumption in the seismic assessment of buildings. Earthq. Eng. Struct. Dyn.2020,49, 194–211

STA Data (2015). 3Muri program: Seismic analyser of 3D masonry buildings. Release 12.6.0.2

Sullivan T., Calvi G.M. (2013). Development in the field of displacement based seismic assessment, Ed. IUSS Press (PAVIA) and EUCENTRE, p 524, ISBN:978-88-6198-090-7

Tanganelli, M., Rotunno, T., Cardinali, V., & Viti, S. (2018). Public Housing in Florence: Seismic Assessment of Masonry Buildings. Procedia Structural Integrity, 11, 266–273. doi:10.1016/j.prostr.2018.11.035

Turnšek, V. and Cacovic, F. (1970). Some experimental results on the strength of brick masonry walls. In Proc. of the 2nd International Brick Masonry Conference, pages 149–156;

Turnšek, V. and Sheppard, P. (1980). The shear and flexural resistance of masonry walls. In International Research Conference on Earthquake Engineering, Skopje, Macedonia, pages 517–573.)

Vamvatsikos, D., Cornell, C.A. (2006). Direct estimation of the seismic demand and capacity of oscillators with multi-linear static pushovers through Incremental Dynamic Analysis. Earthquake Engineering and Structural Dynamics 2006; 35(9):1097–1117

Varum, H., Rodrigues, H., Lourenço, P.B., Vasconcelos, G. (2015). Seismic behaviour of vernacular architecture, in Seismic Retrofitting: Learning from Vernacular Architecture, 151. Available at: https://repositorium.sdum.uminho.pt/handle/1822/38134

Verderame, G.M., Stella, A., Cosenza, E. (2001). Le proprietà meccaniche degli acciai impiegati nelle strutture in cemento armato realizzate negli anni ’60, X Convegno Nazionale "L'Ingegneria Sismica in Italia", Potenza e Matera 9-13 Settembre 2001 (in Italian)

Vicente, R., Parodi, S., Lagomarsino, S., Varum, H., Mendes Silva J.A.R. (2011). Seismic vulnerability and risk assessment: case study of the historic city centre of Coimbra, Portugal, Bull Earthquake Eng (2011) 9:1067–1096 DOI 10.1007/s10518-010-9233-3.)

Yakut, A. and Yilmaz, H. (2008). Correlation of deformation demands with ground motion intensity, Journal of Structural Engineering 134(12), 1818–1828.

Whitman, R. V., Reed, J. W., and Hong, S. T. (1973). Earthquake damage probability matrices, in Proceedings of the Fifth World Conference on Earthquake Engineering (Rome), 2531–2540.;)

Zuccaro, G., Dolce, M., De Gregorio, D., Speranza, E., Moroni, C. (2015) La scheda CARTIS per la caratterizzazione tipologico- strutturale dei comparti urbani costituiti da edifici ordinari. Valutazione dell’esposizione in analisi di rischio sismico, 2015. In: Proceedings of GNGTS 2015 (in Italian)

9. APPENDIX

In this section additional material obtained during the research is presented. The presented outcomes have been necessary to achieve the final outcomes of the thesis and, even though their presentation is not essential for the fulfillment of the work, they still can provide useful information.

In *Appendix 1* the building plans of the other defined building classes are presented. The drawings show the variability of shapes and architectures found by the archive research. It is worth noting as the pigeonhole of several structures is not easy, especially for the more irregular configurations. Also for this reason, the simple-block class has been selected for the in-depth studies.

Appendix 2 shows the Bayesian update of the material's properties of the different masonry typologies adopted in this research are presented.

In *Appendix 3* the different branches of the logic tree approaches are presented and discussed in terms of pushover comparison. The latter has been done considering the maximum base shear and the ultimate displacement values of the different models.

Appendix 4 presents the cyclic pushover analysis for all the four epistemic models. The plots are done for the different DLs and the two senses of the analyses. In the analyses converge problems happened sometimes, especially during the opposite sense of load, in the negative loading phase. This is mostly remarkable in the Y direction with the mass proportional pattern.

Finally, in *Appendix 5* the sensitivity classes (*SCs*) of the different aleatory variables are presented.

[this page intentionally left blank]

APPENDIX 1

Building plans of the studied buildings divided according to the classification presented in Section 4.1

IIBT plans

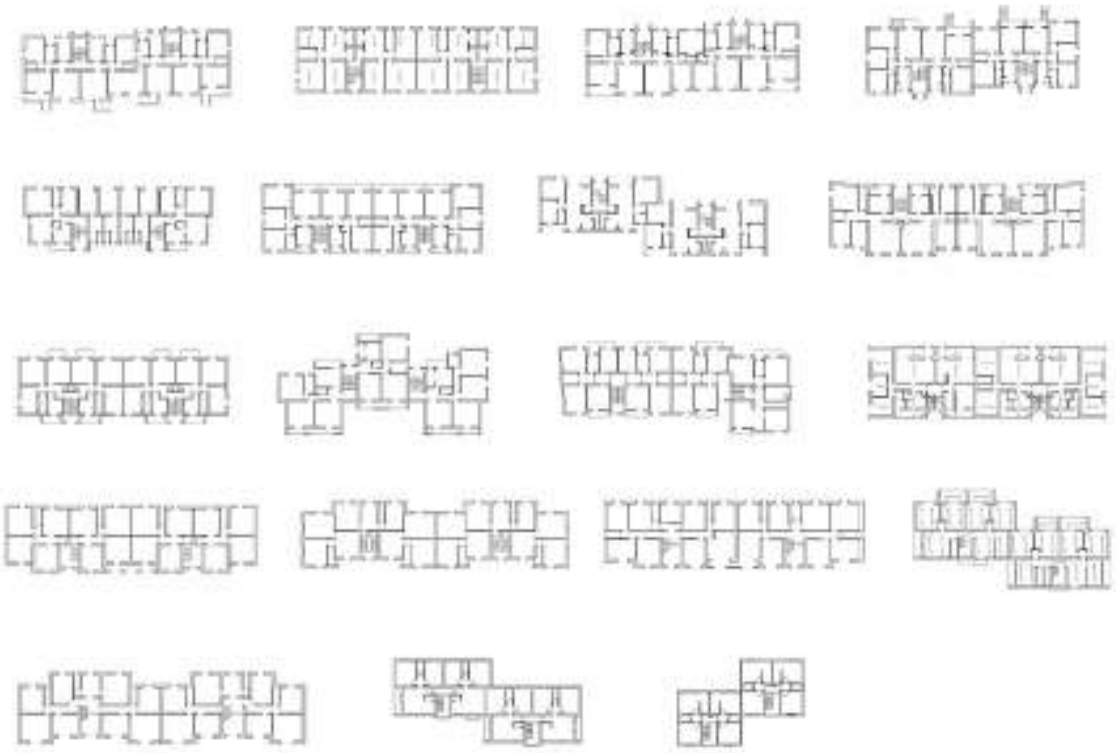

IIIBT plans

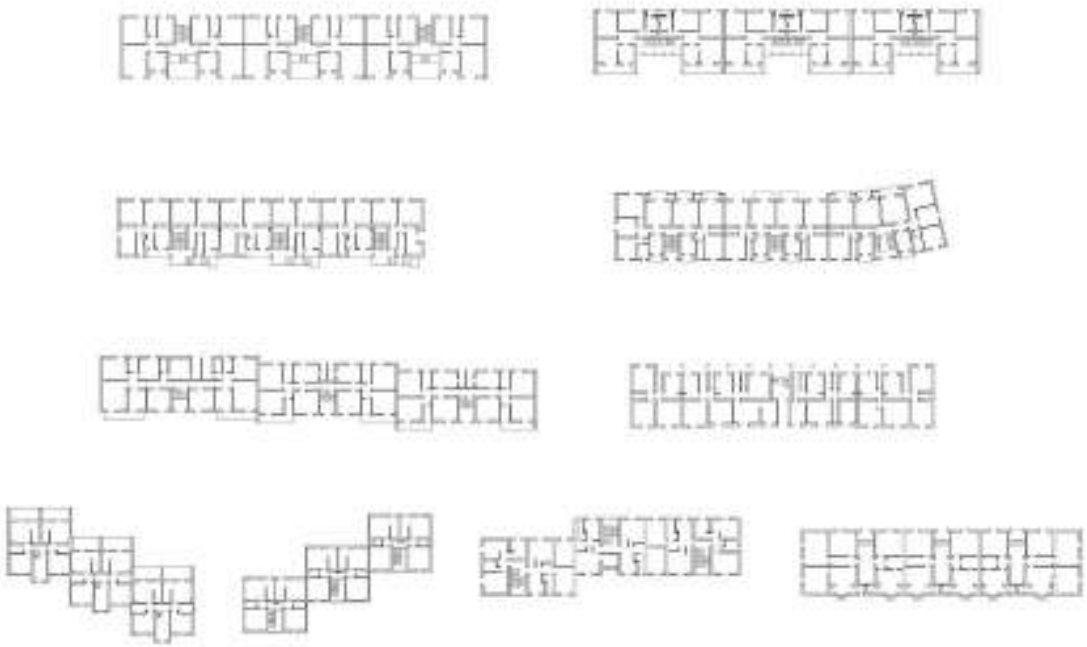

IVBT plans

L plans

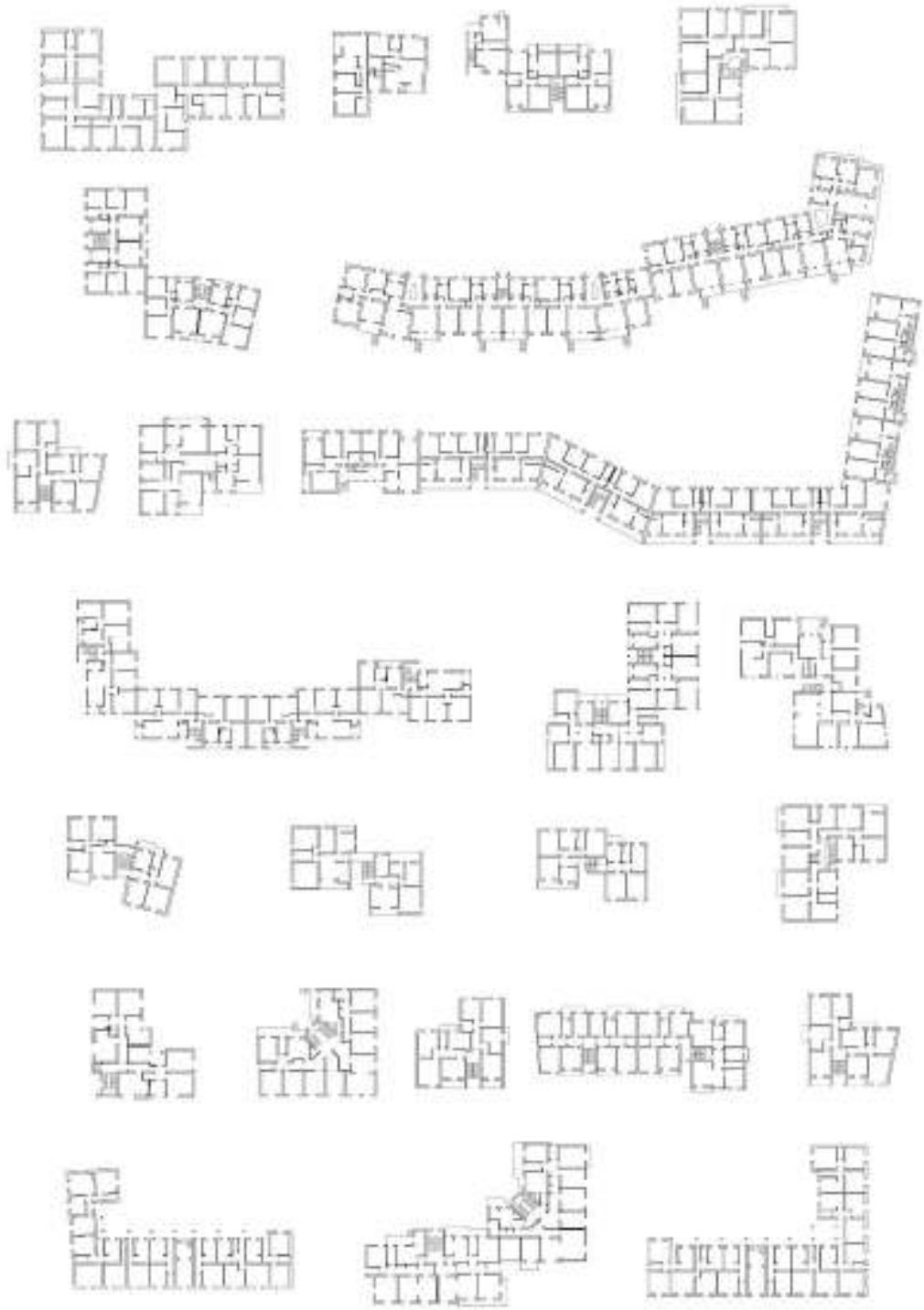

TBT plans

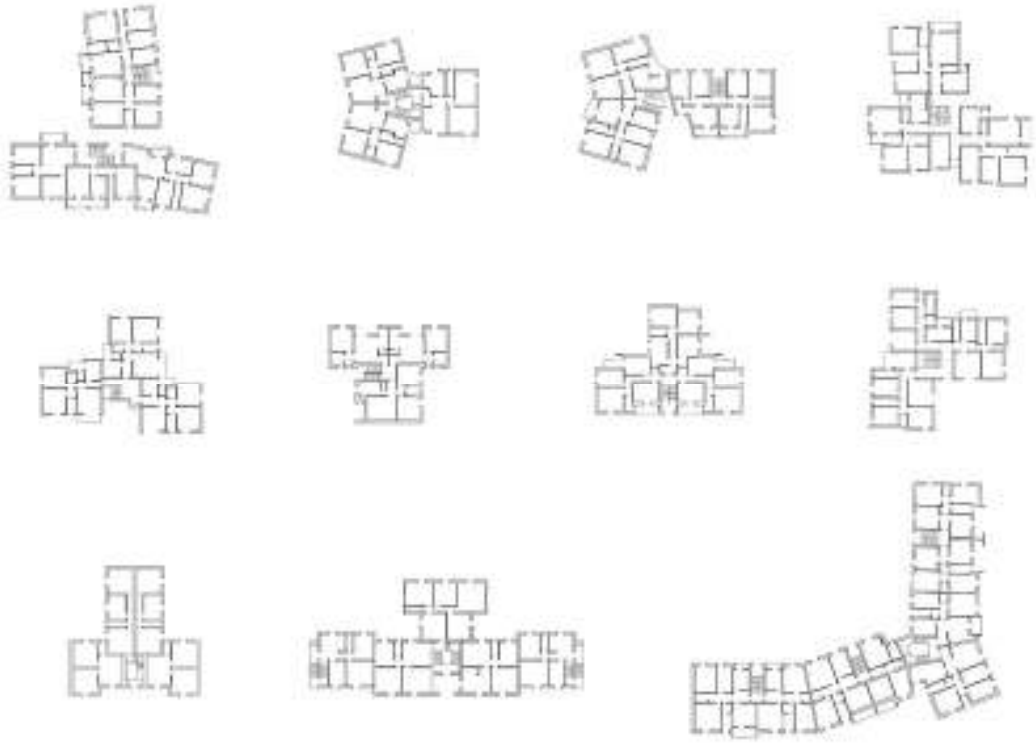

CBT plans

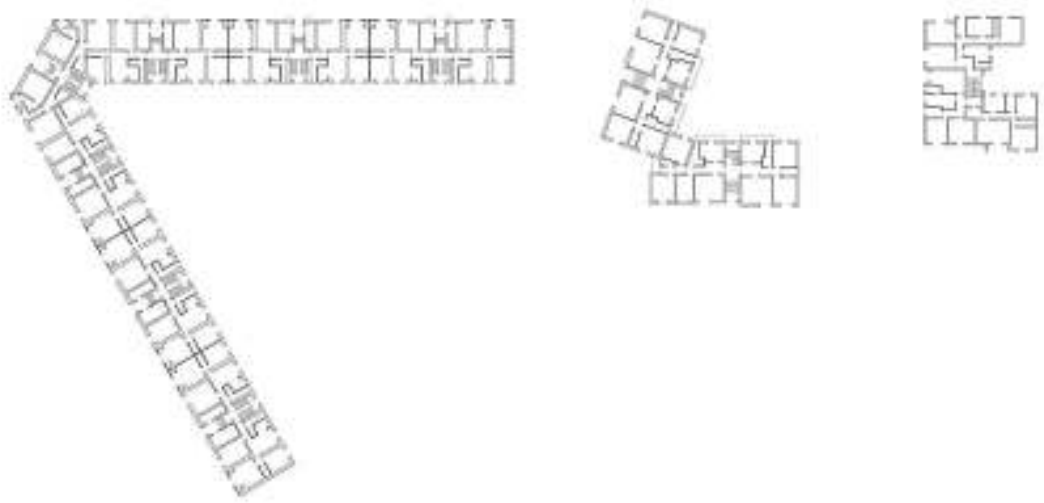

XBT plans

THT plans

APPENDIX 2

Bayesian update of the material properties.

			f_m (MPa)	cov	τ_0 (MPa)	cov	E (MPa)	cov	G (MPa)	cov
clay bricks and lime mortar	*prior*	MIT2019	3.45	0.25	0.09	0.44	1500	0.2	500	0.2
	DJF	MP059					3521			
		MP060					3093			
		MP054					2601			
		MP055					4372			
		MP056					2868			
		MP057					2687			
		MP088					1832			
		MP089					2778			
		MP105	1.098				1562			
	CD	CD032			0.091		322		1124	
		CD040			0.065		456		1853	
	mean		1.098		0.078		2812.67		1488.5	
	updated		**2.666**	**0.260**	**0.082**	**0.398**	**2625.14**	**0.130**	**1064.86**	**0.087**
			2.666	**0.260**	**0.082**	**0.398**	**2625.14**	**0.130**	**875.048**	**0.130**

			f_m (MPa)	cov	τ_0 (MPa)	cov	E (MPa)	cov	G (MPa)	cov
quasi-full bricks with cement mortar	*prior*	MIT2019	6.5	0.23	0.125	0.36	4550	0.23	1137.5	0.23
	DJF	MP093	2.621				2500			
		MP094	3.326							
	CD	CD035			0.224				2676	
		CD036			0.2				2783	
		CD045			0.32					
		CD046			0.181					
	mean		2.9735		0.23125		2500		2729.5	
	updated		**4.73675**	**0.317**	**0.21**	**0.192**	**3730**	**0.218**	**2047.21**	**0.119**
			4.73675	**0.317**	**0.21**	**0.192**	**3730**	**0.218**	**1243.33**	**0.218**

			f_m (MPa)	cov	τ_0 (MPa)	cov	E (MPa)	cov	G (MPa)	cov
semi-hollow concrete blocks	*prior*	MIT2019	3.7	0.189	0.21	0.143	2825	0.150	740	0.189
	CD	CD012			0.205				1298	
		CD027			0.275				1897	
	mean				0.24				1597.5	
	updated		**3.7**	**0.189**	**0.23**	**0.106**	**2825**	**0.150**	**1230**	**0.105**
			3.7	**0.18919**	**0.23**	**0.1065**	**3690**	**0.10538**	**1230**	**0.10538**

[this page intentionally left blank]

APPENDIX 3

Pushover comparison between the different models of the logic tree

In the Figure below, the initial logic tree branches studied in the work are presented. The results are then discussed in terms of ultimate displacement and maximum base shear values. The comparisons are proposed distinguishing between the models without or with RC lintels over the openings. Hence, the disposition of the masonry types at the different levels has been considered accounting the specificity of the first floor. The models are compared three by three, in terms of mean values and relative *c.o.v.*; the low differences between the triplets of RS/CB/--/-- and RS/RS/--/-- models show the reliability of the assumptions made in thesis. The bigger c.ov values between the comparison within the six models prove the reason that led to the final logic tree adopted in the thesis and explained in Section 5.2.

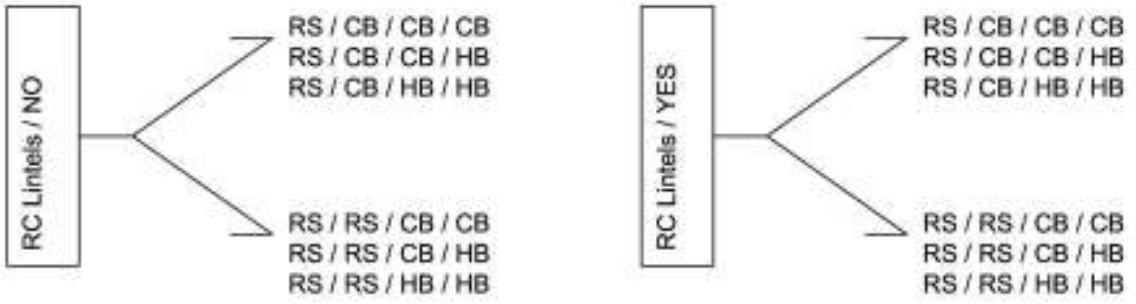

NO-LINTELS MODELS

	X Mass Prop.		X Inv. Triang.		Y Mass Prop.		Y Inv. Triang.	
	Displ. [cm]	Max Base shear [kN]	Displ. [cm]	Max Base shear [kN]	Displ. [cm]	Max Base shear [kN]	Displ. [cm]	Max Base shear [kN]
RS / CB / CB / CB	2.14	2672.76	4.56	1962.82	1.46	2701.68	2.32	2285.84
RS / CB / CB / HB	2.01	2659.00	4.46	1961.42	1.46	2661.54	2.37	2231.49
RS / CB / HB / HB	2.05	2632.10	4.32	1945.51	1.52	2620.74	2.46	2187.00
Mean	2.07	2654.62	4.45	1956.58	1.48	2661.32	2.38	2234.77
C.o.v.	0.031	0.008	0.028	0.005	0.024	0.015	0.029	0.022
RS / RS / CB / CB	2.96	2610.64	4.16	1875.79	1.60	2711.64	2.74	2211.47
RS / RS / CB / HB	2.71	2619.41	4.12	1865.68	1.59	2671.42	2.75	2179.75
RS / RS / HB / HB	2.87	2590.23	4.09	1836.68	1.65	2630.50	2.93	2129.46
Mean	2.85	2606.76	4.12	1859.38	1.61	2671.19	2.81	2173.56
C.o.v.	0.045	0.006	0.009	0.011	0.019	0.015	0.036	0.019
Mean of the six	2.46	2630.69	4.28	1907.98	1.55	2666.25	2.59	2204.17
C.o.v. of the six	0.411	0.378	0.380	0.379	0.381	0.378	0.388	0.379

BUILDINGS WITH RC LINTELS

	X Mass Prop.		X Inv. Triang.		Y Mass Prop.		Y Inv. Triang.	
	Displ. [cm]	Max Base shear [kN]	Displ. [cm]	Max Base shear [kN]	Displ. [cm]	Max Base shear [kN]	Displ. [cm]	Max Base shear [kN]
RS / CB / CB / CB	1.48	2757.89	2.13	2239.83	1.33	2713.06	2.20	2306.25
RS / CB / CB / HB	1.43	2732.21	2.05	2200.33	1.29	2674.46	2.23	2266.80
RS / CB / HB / HB	1.49	2706.18	2.01	2172.89	1.35	2633.40	2.38	2226.60
Mean	1.47	2732.09	2.06	2204.35	1.33	2673.64	2.27	2266.55
C.o.v.	0.021	0.009	0.029	0.015	0.021	0.015	0.043	0.018
RS / RS / CB / CB	1.66	2770.18	1.76	2074.65	1.41	2721.92	2.39	2210.40
RS / RS / CB / HB	1.61	2744.05	1.74	2046.34	1.36	2682.02	2.51	2187.36
RS / RS / HB / HB	1.70	2713.26	1.84	2012.18	1.41	2640.60	2.90	2152.14
Mean	1.66	2742.49	1.78	2044.39	1.39	2681.51	2.60	2183.30
C.o.v.	0.027	0.010	0.029	0.015	0.021	0.015	0.102	0.013
Mean of the six	1.56	2737.29	1.92	2124.37	1.36	2677.58	2.43	2224.92
C.o.v. of the six	0.383	0.378	0.386	0.380	0.379	0.378	0.390	0.379

APPENDIX 4

Cyclic pushover curves for the different models, according the two directions and the two load patterns.

MODEL N/RS/CB/CB/HB

X DIRECTION – MASS PROP

DL1

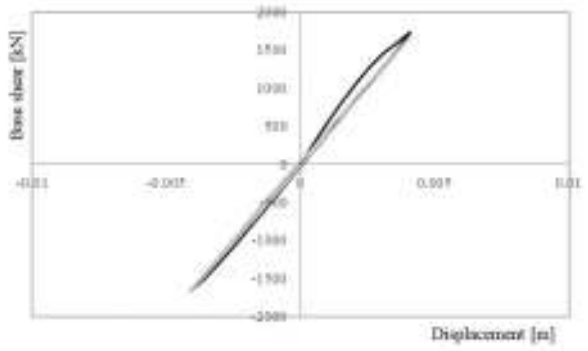

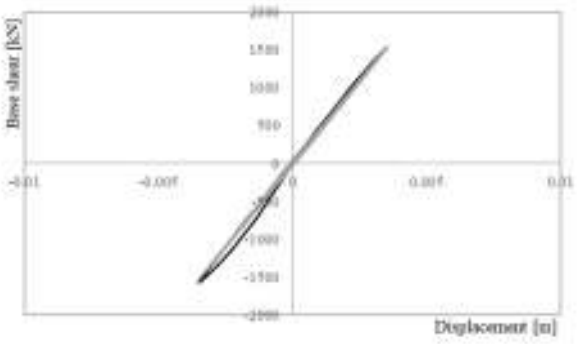

DL2

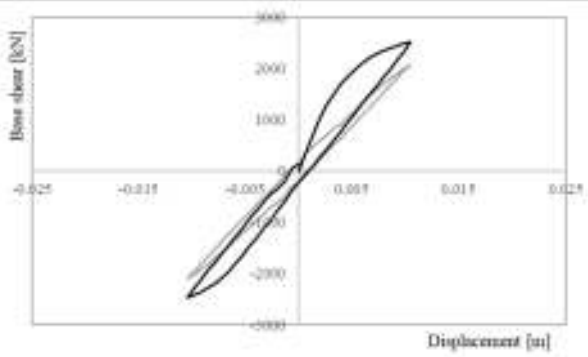

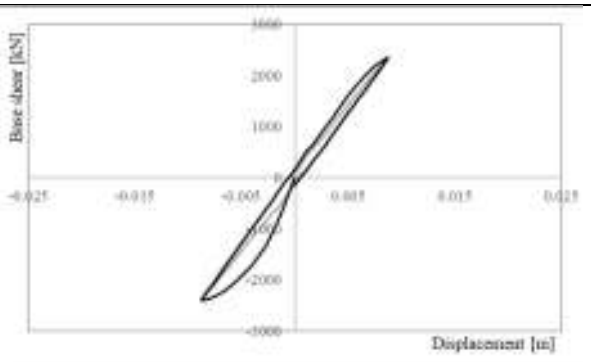

DL3

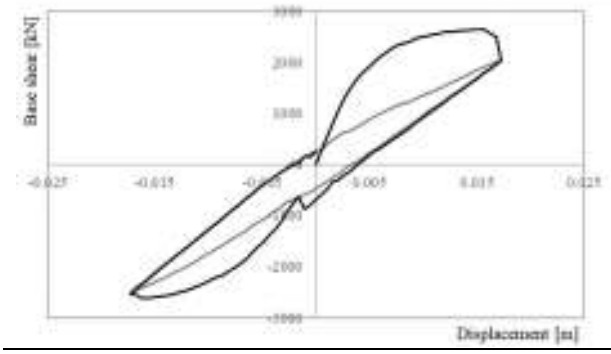

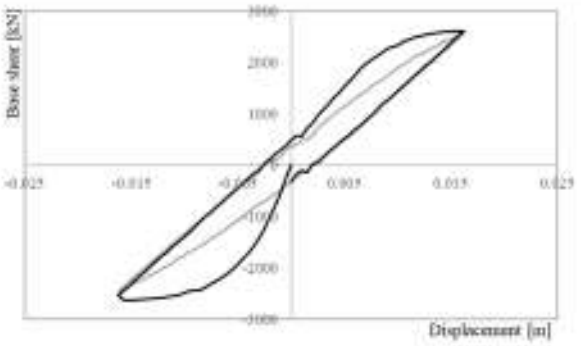

DL4

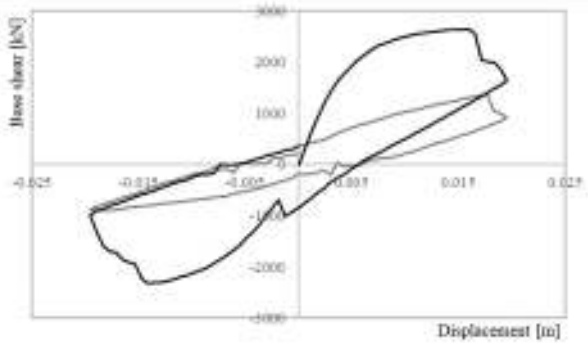

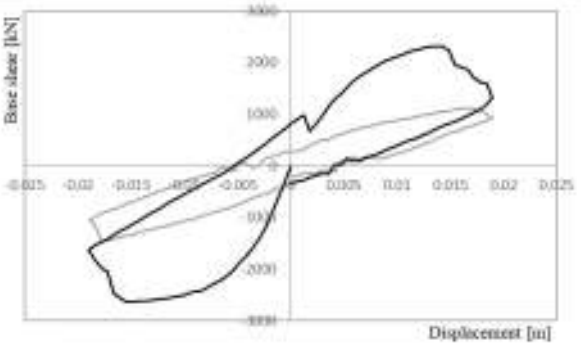

X DIRECTION – INVERS TRIANG	
DL1	
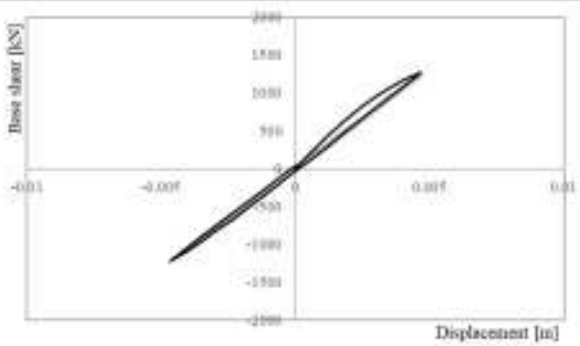	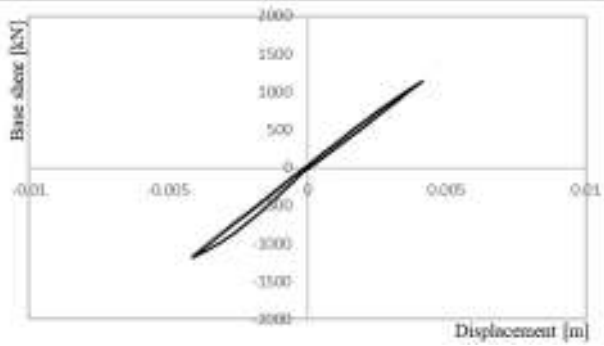
DL2	
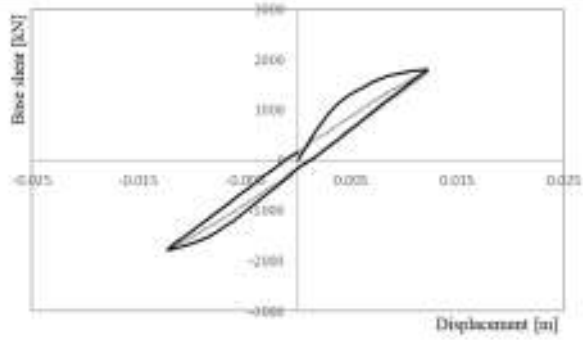	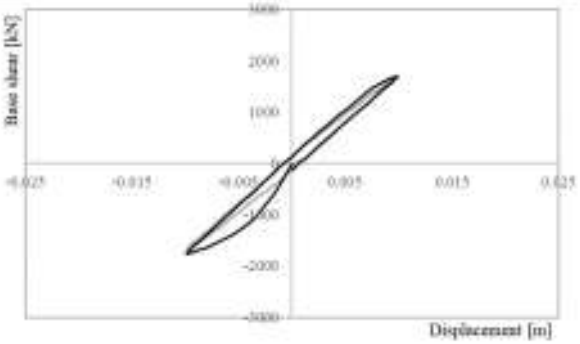
DL3	
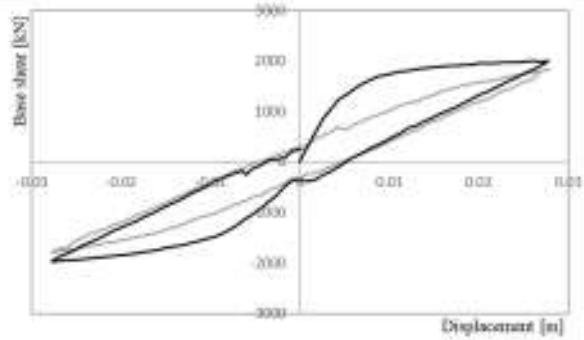	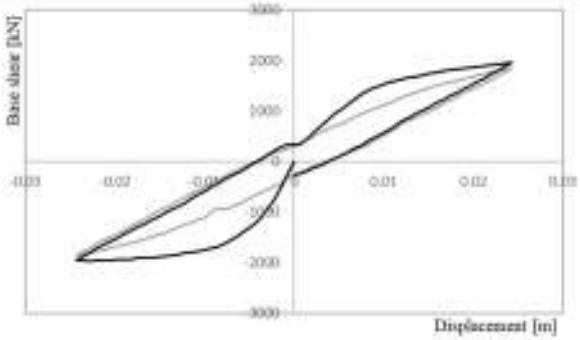
DL4	
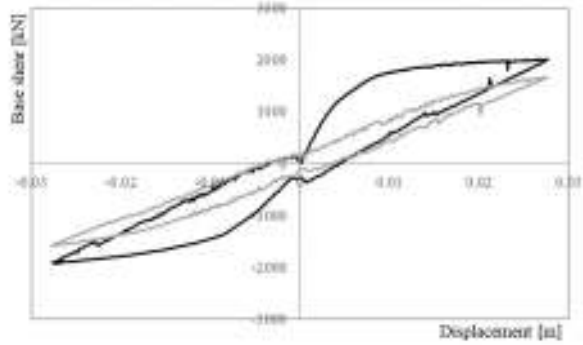	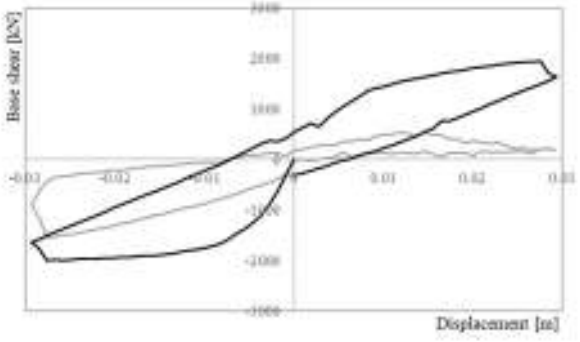

Y DIRECTION – Mass Prop.	
DL1	
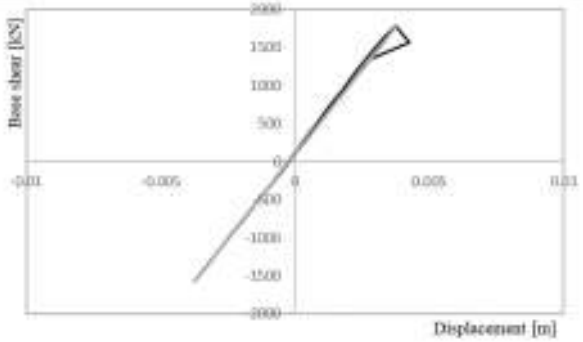	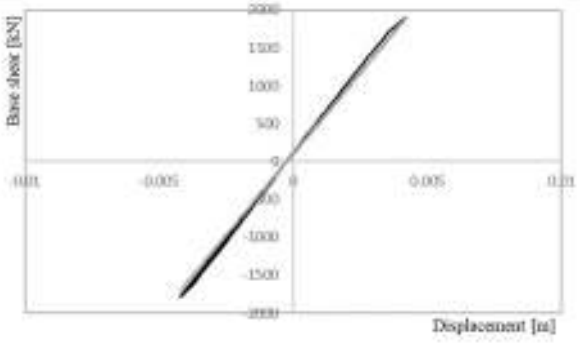
DL2	
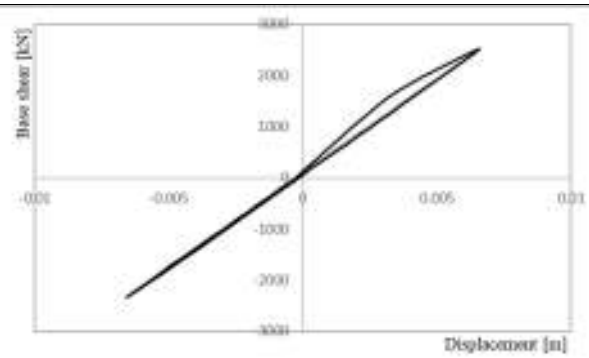	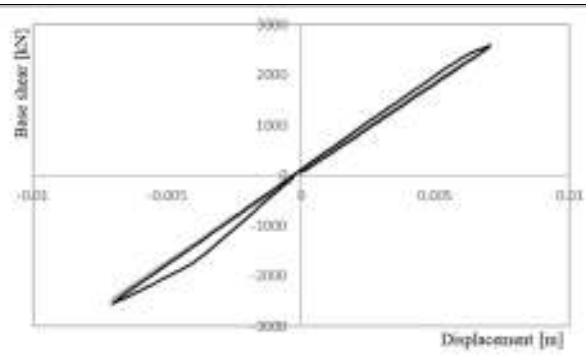
DL3	
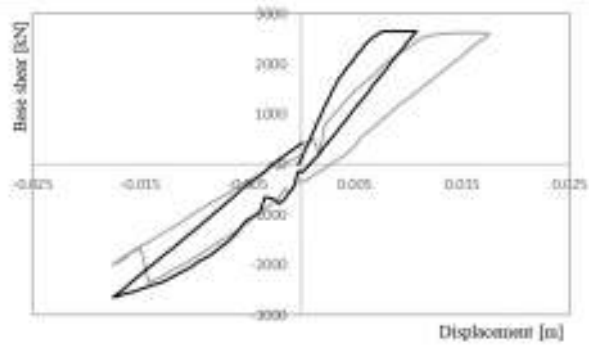	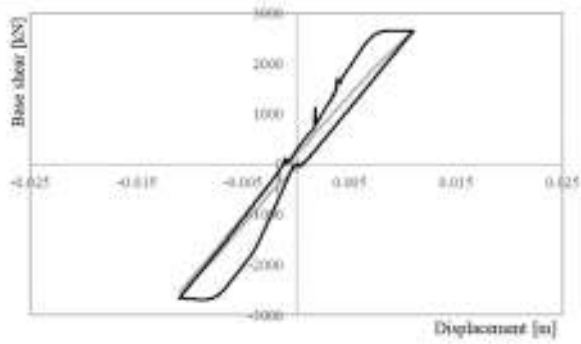
DL4	
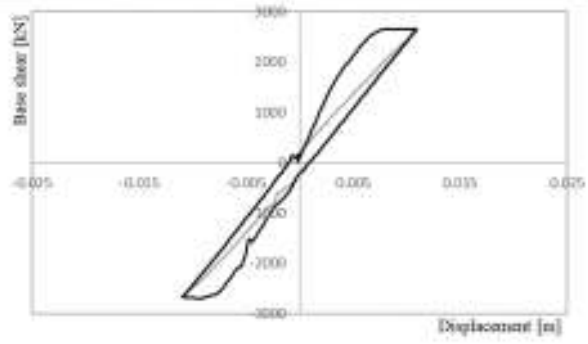	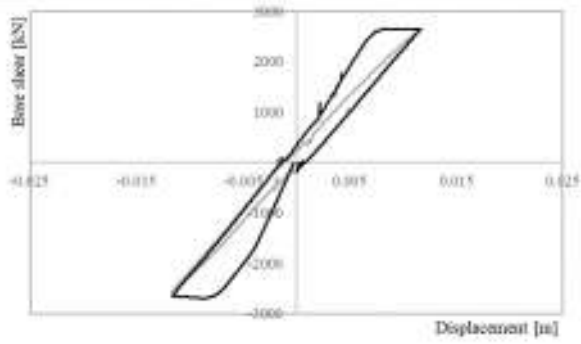

MODEL N/RS/RS/CB/HB

X DIRECTION – Mass prop.

DL1

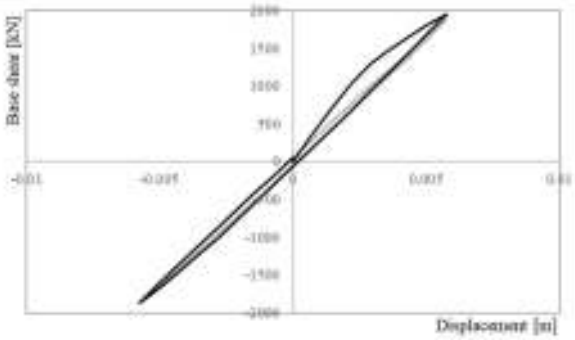

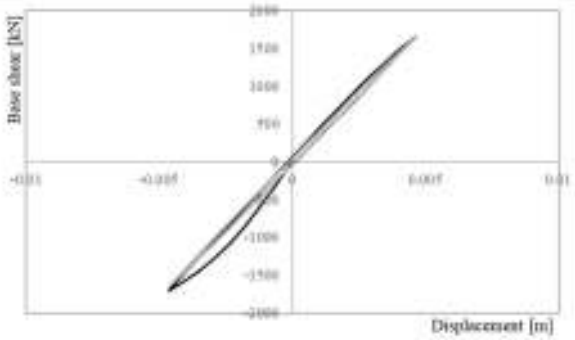

DL2

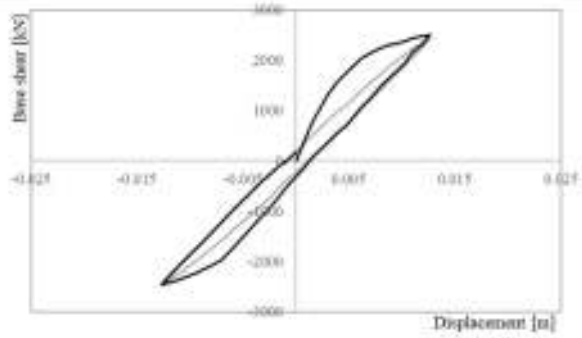

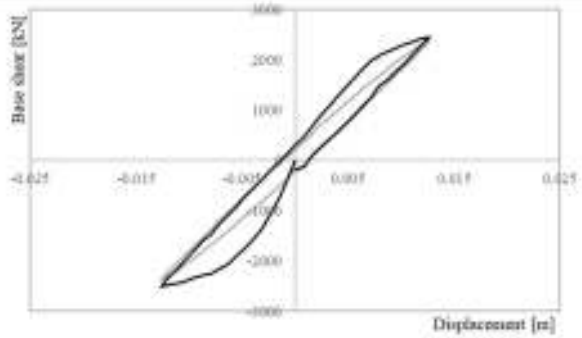

DL3

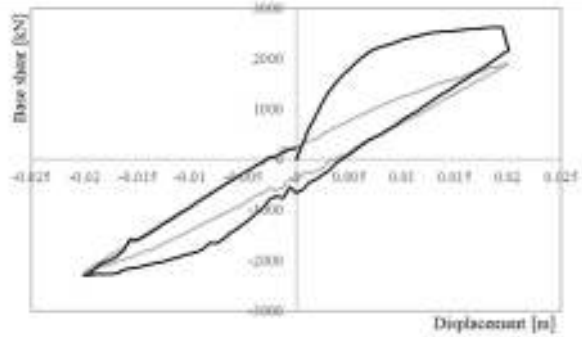

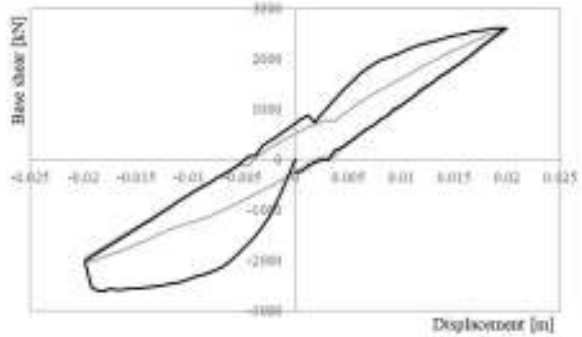

DL4

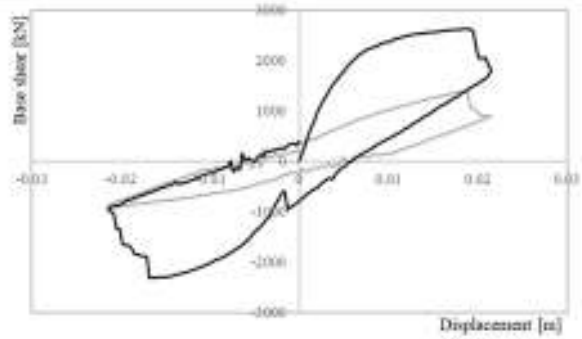

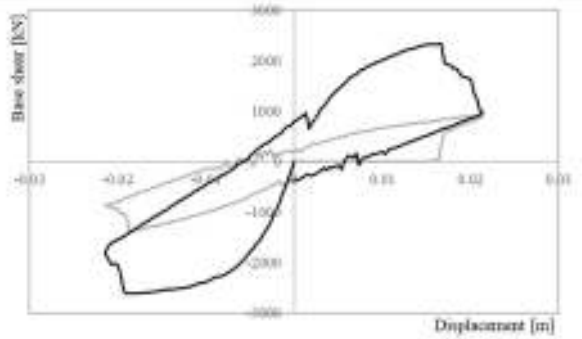

X DIRECTION – Inv Triang.	
DL1	
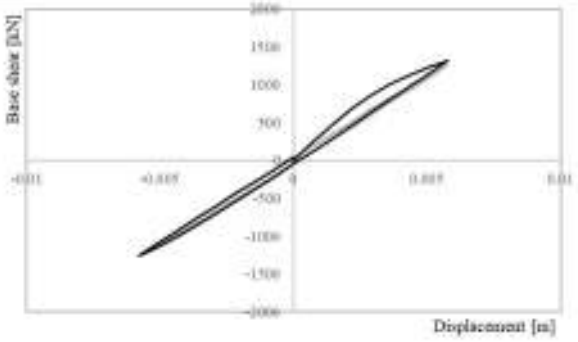	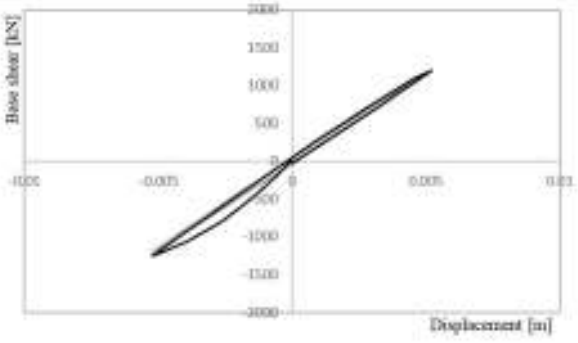
DL2	
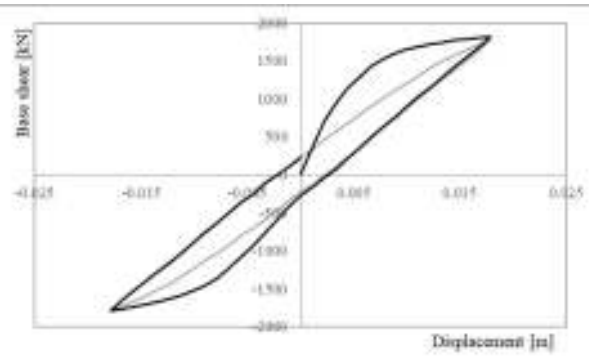	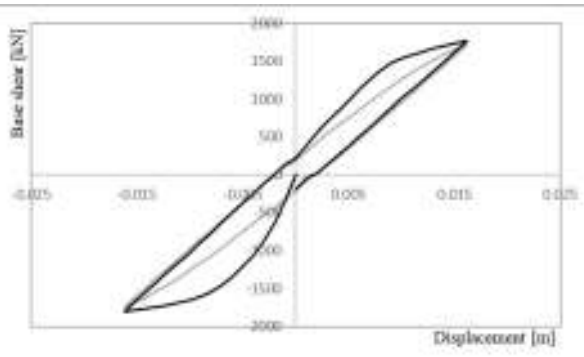
DL3	
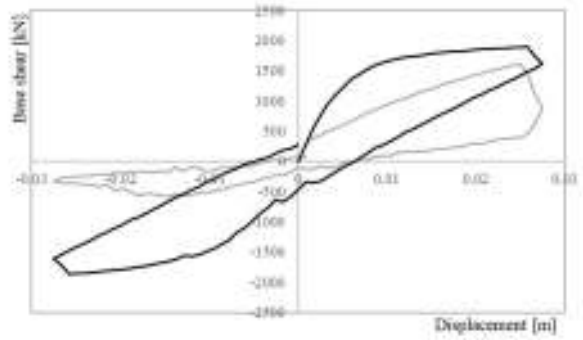	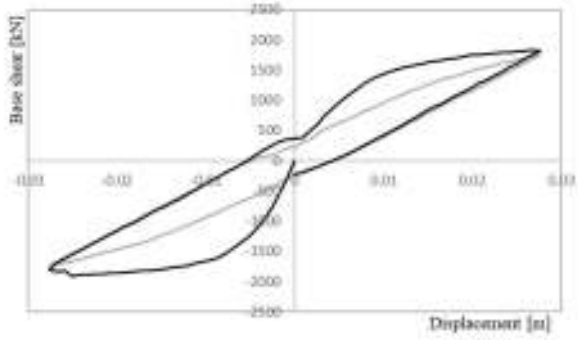
DL4	
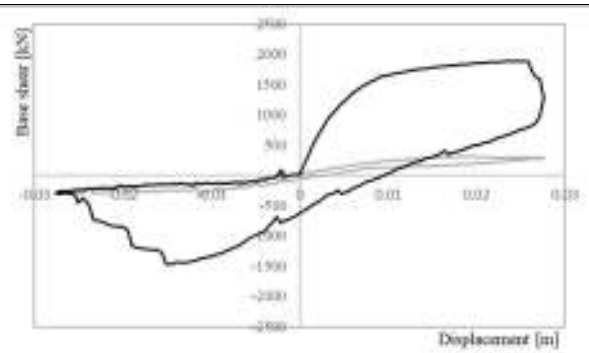	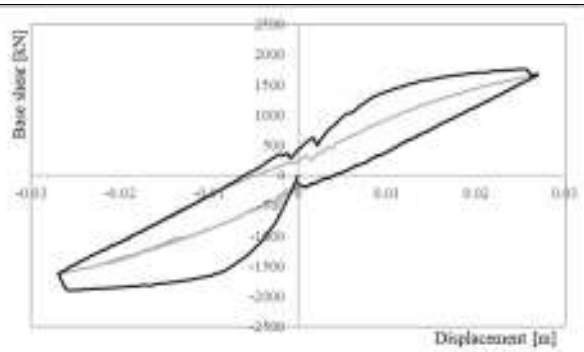

Y DIRECTION – Mass prop.	
DL1	
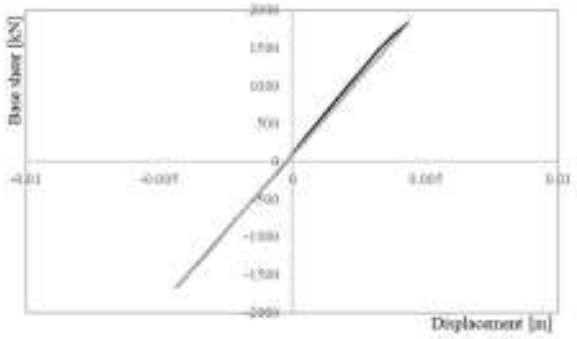	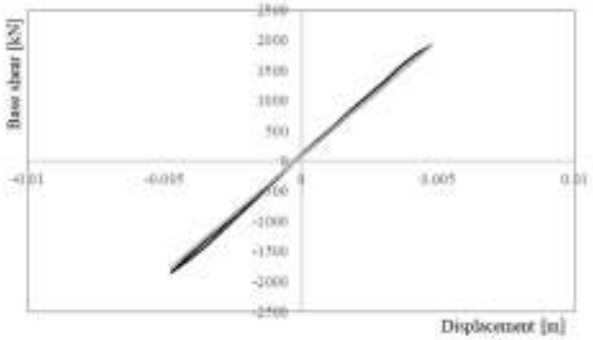
DL2	
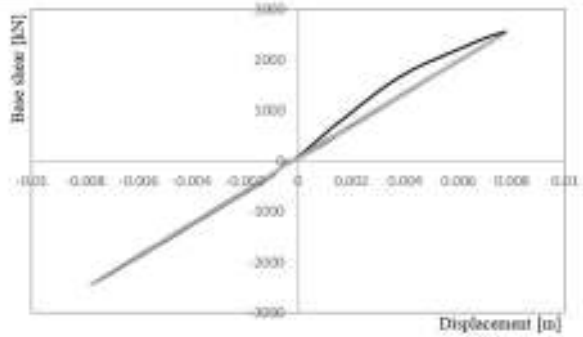	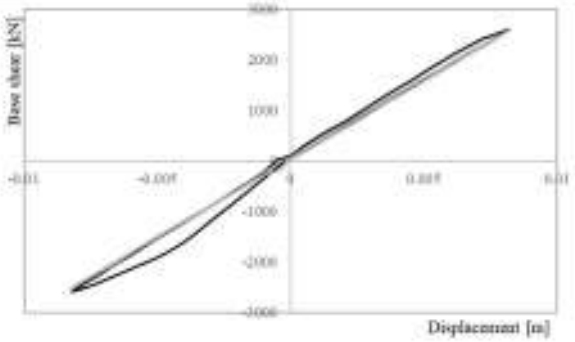
DL3	
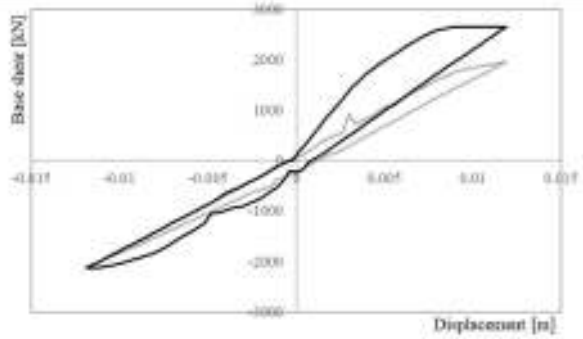	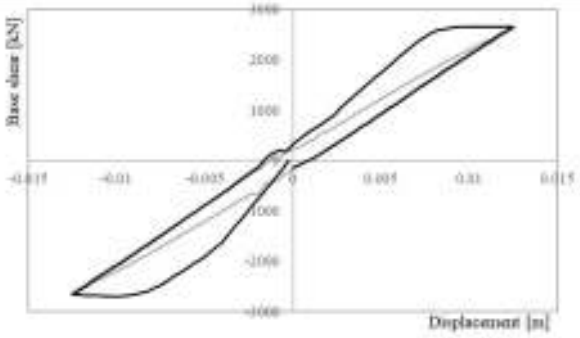
DL4	
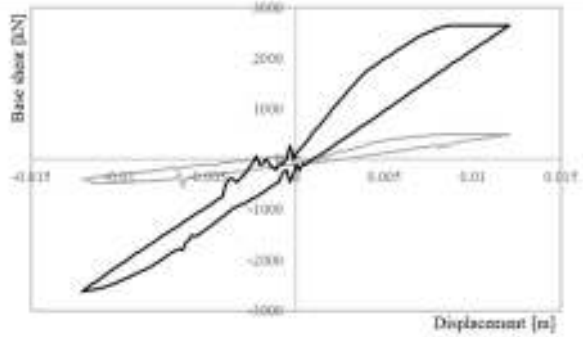	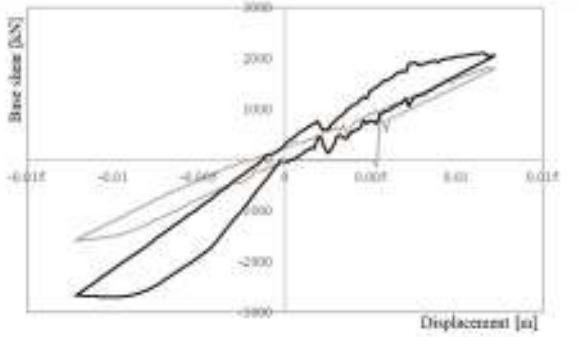

Y DIRECTION – Inv. Triang.

DL1

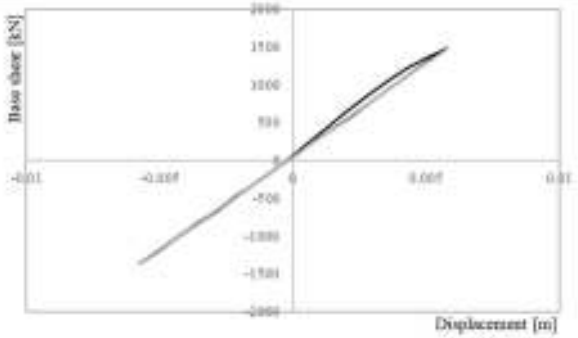

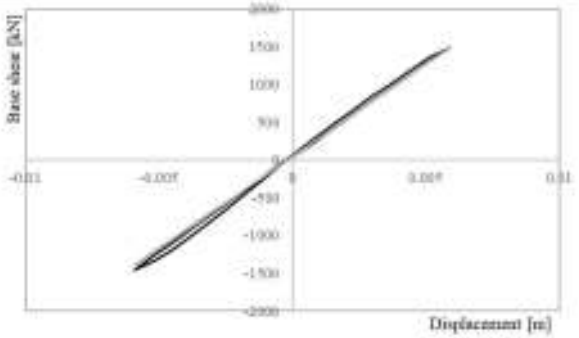

DL2

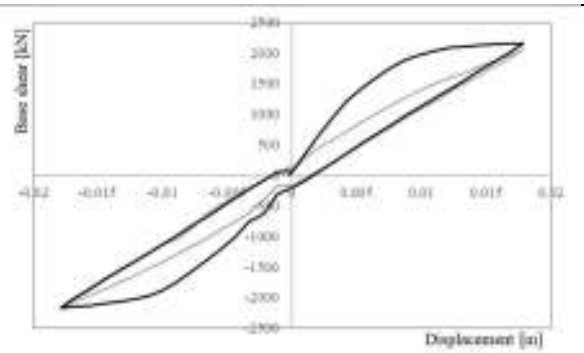

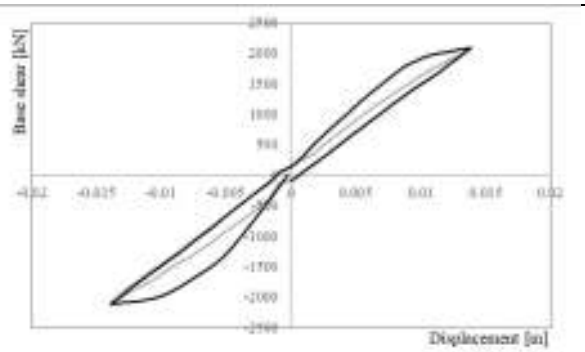

DL3

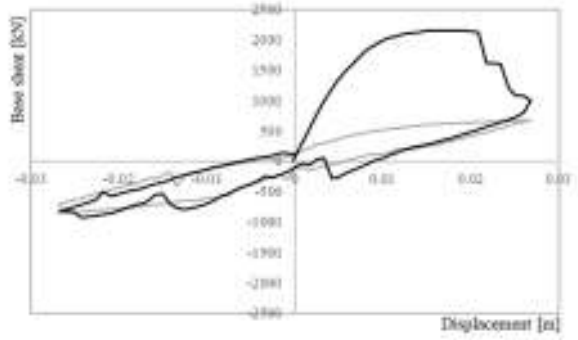

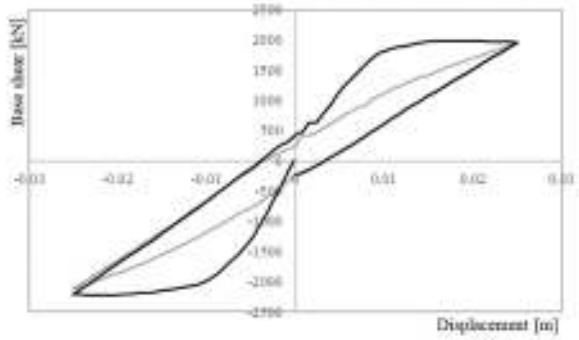

DL4

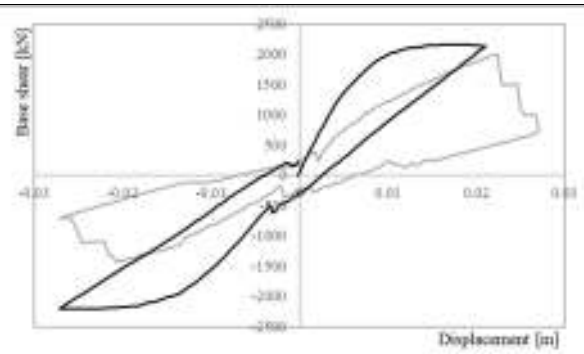

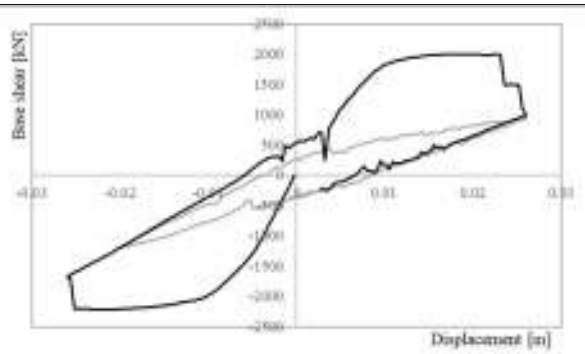

MODEL Y/RS/CB/CB/HB

X DIRECTION – Mass prop.

DL1

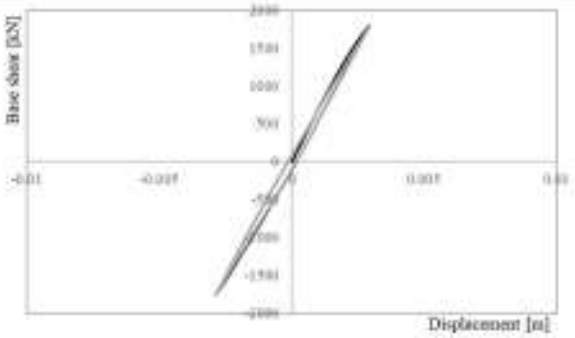

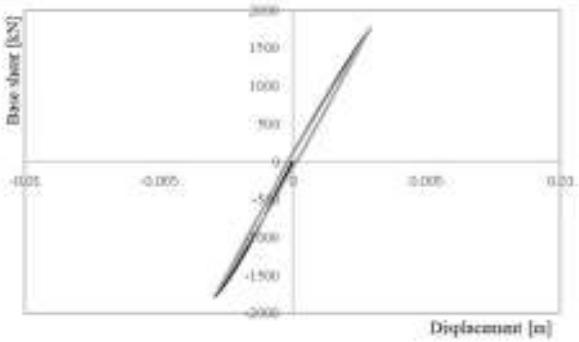

DL2

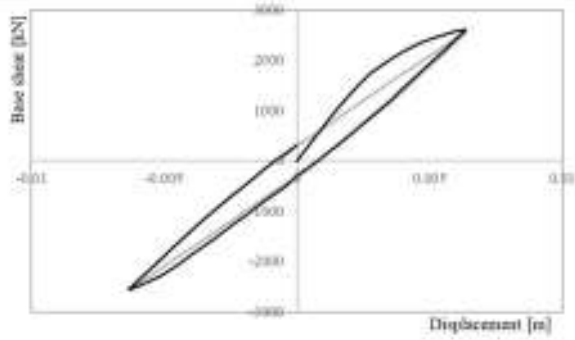

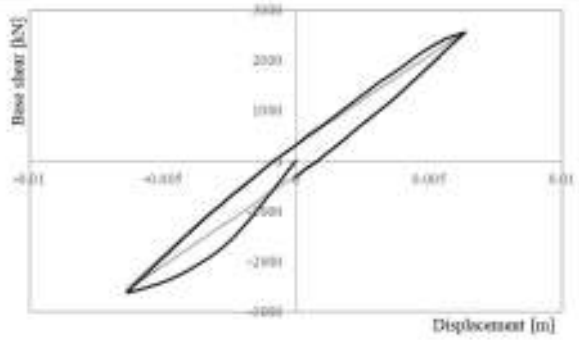

DL3

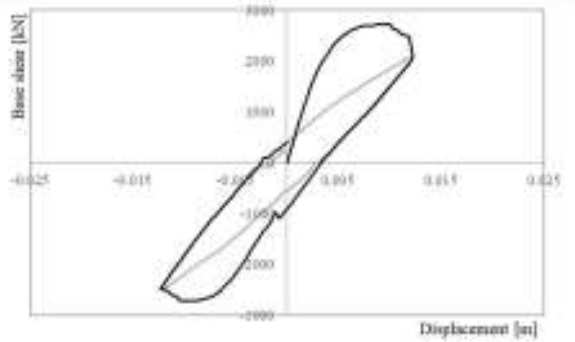

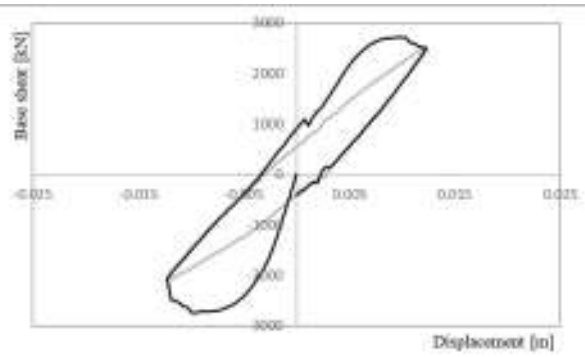

DL4

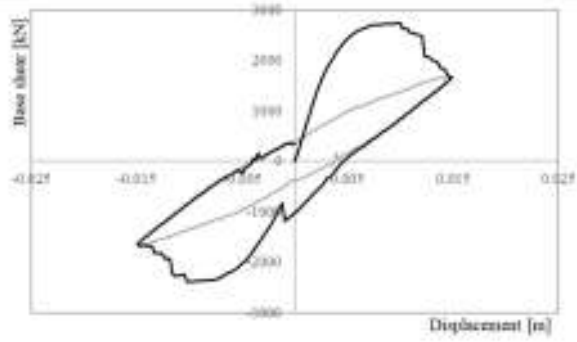

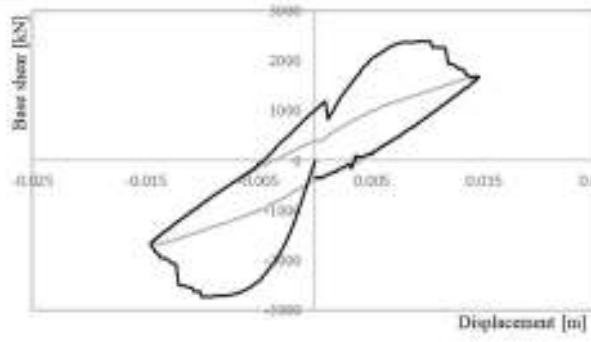

X DIRECTION – Inv. Triang.

DL1

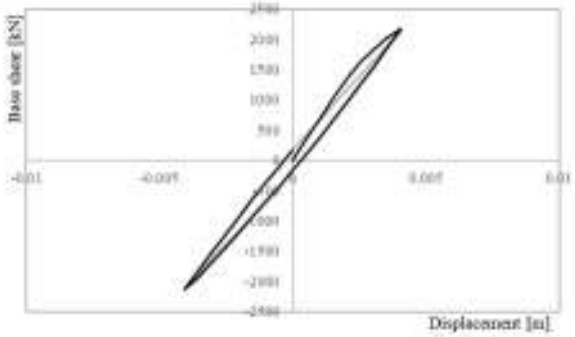

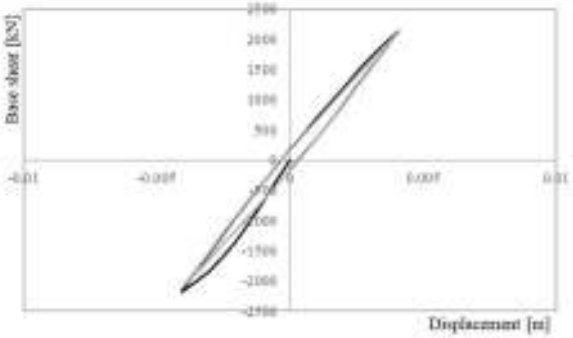

DL2

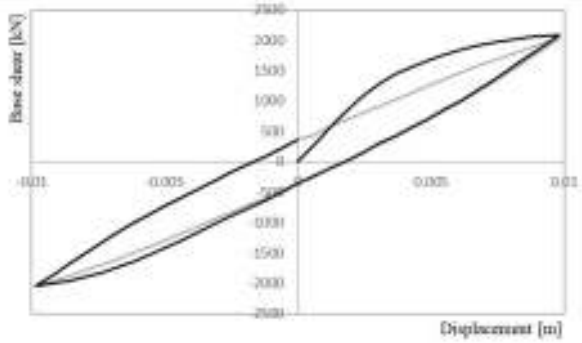

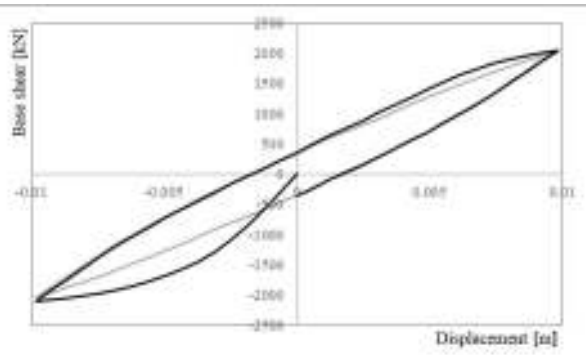

DL3

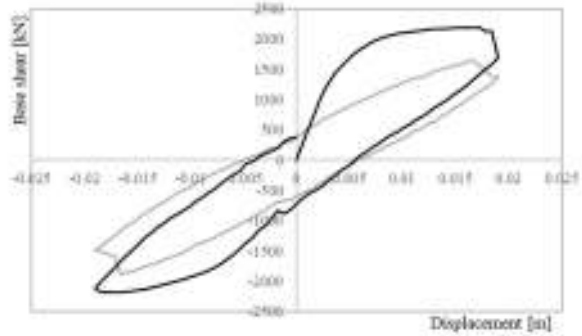

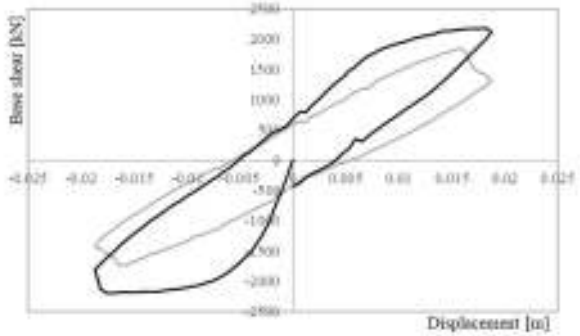

DL4

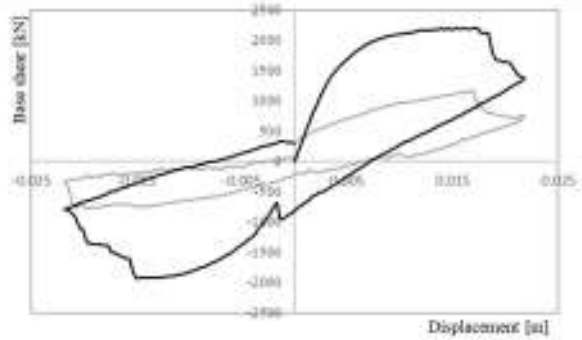

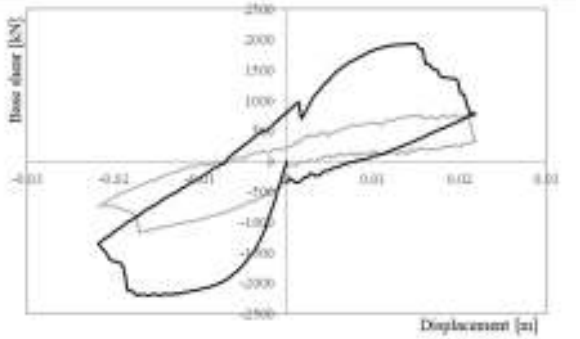

Y DIRECTION – Mass prop.	
DL1	
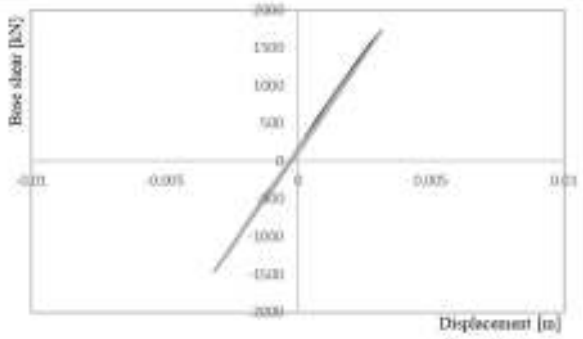	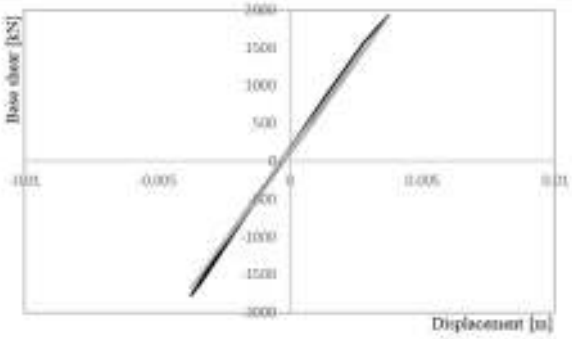
DL2	
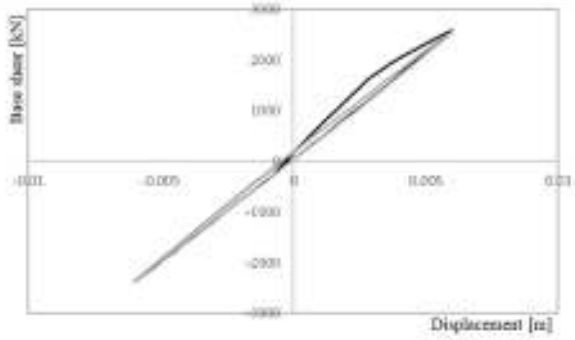	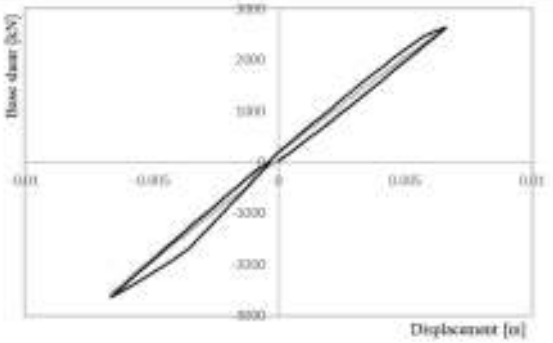
DL3	
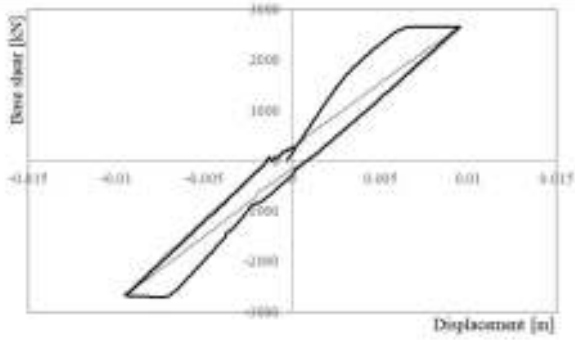	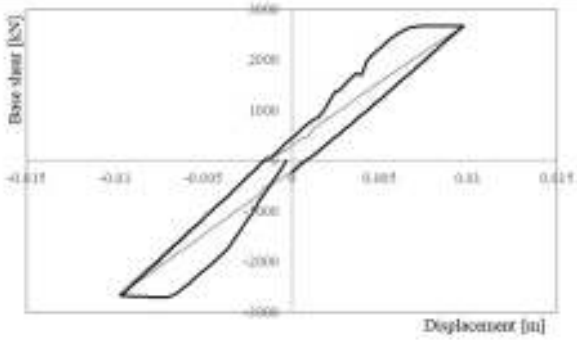
DL4	
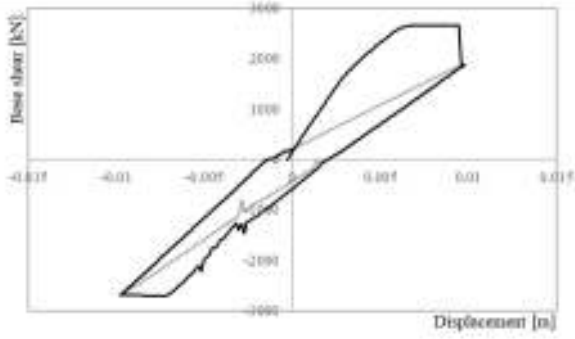	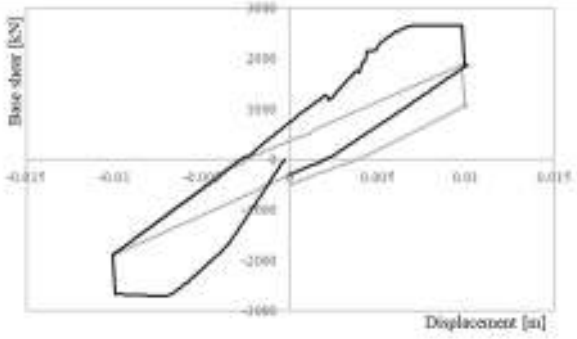

Y DIRECTION – Inv. Triang.

DL1

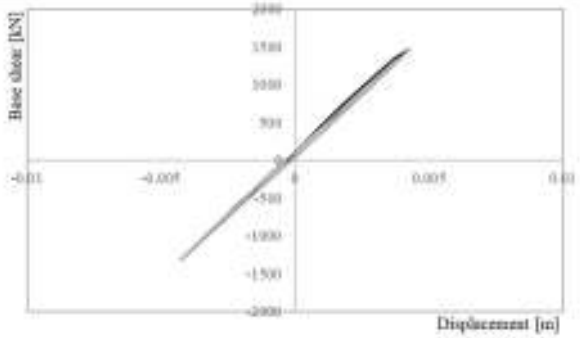

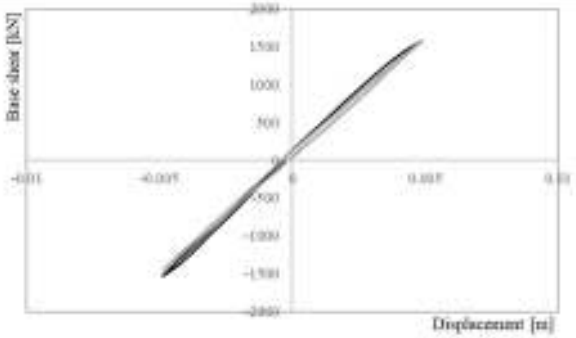

DL2

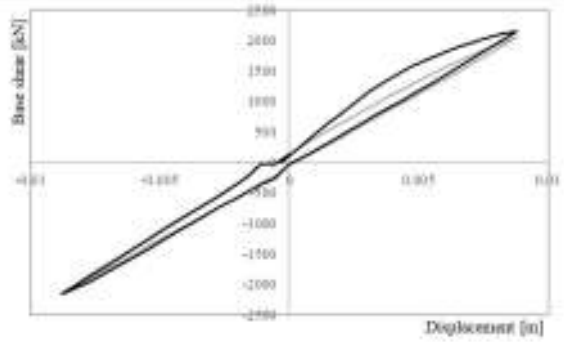

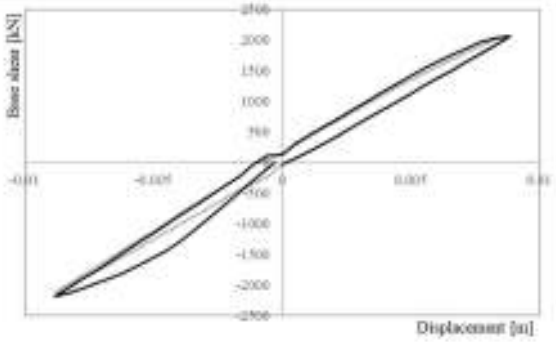

DL3

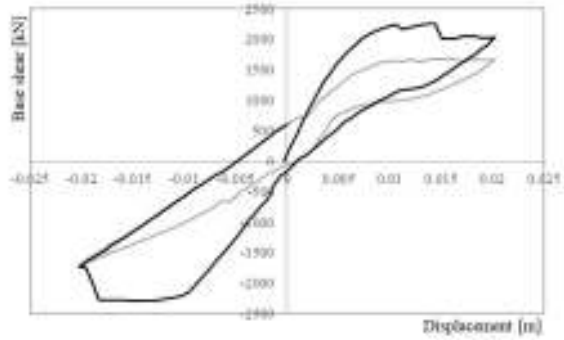

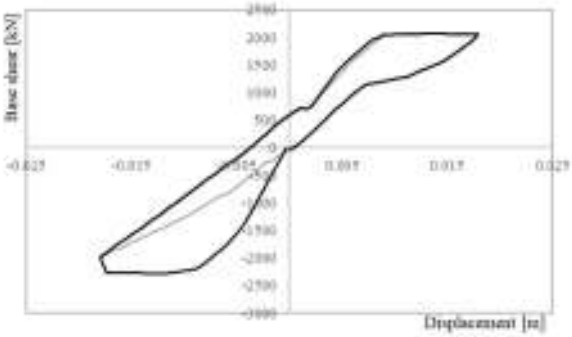

DL4

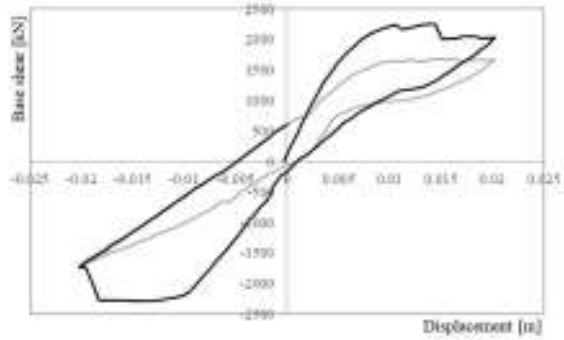

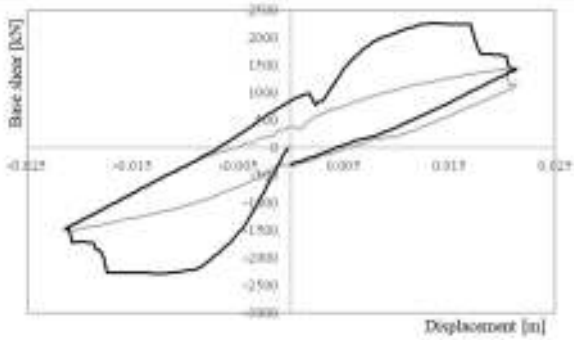

MODEL Y/RS/RS/CB/HB

X DIRECTION – Mass prop.

DL1

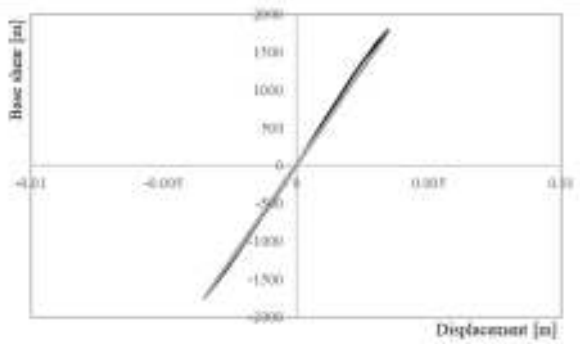

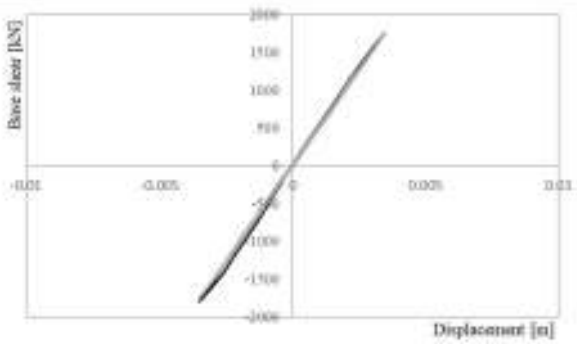

DL2

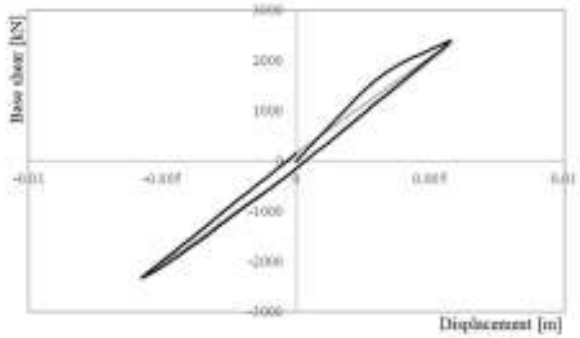

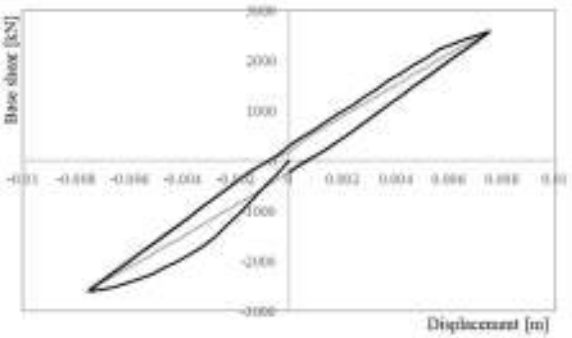

DL3

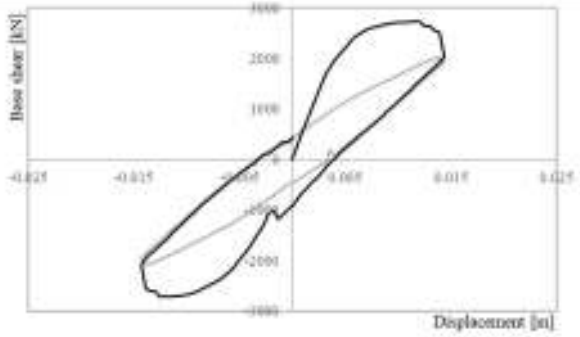

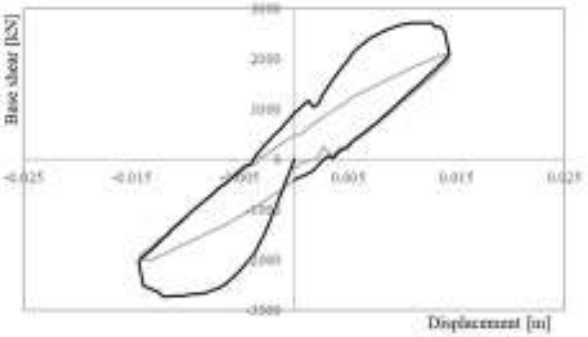

DL4

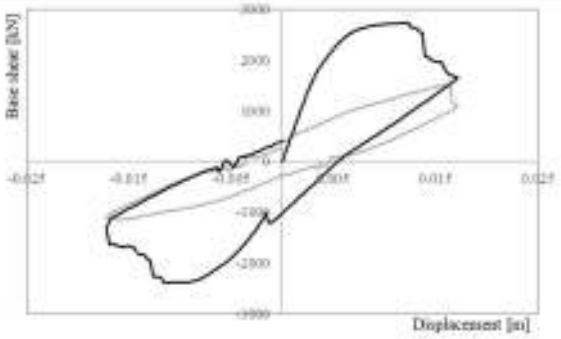

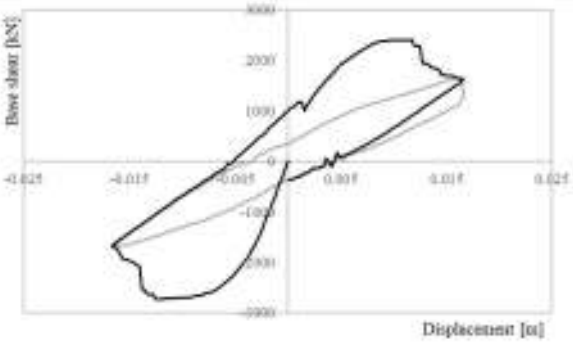

X DIRECTION – Inv. Triang.	
DL1	
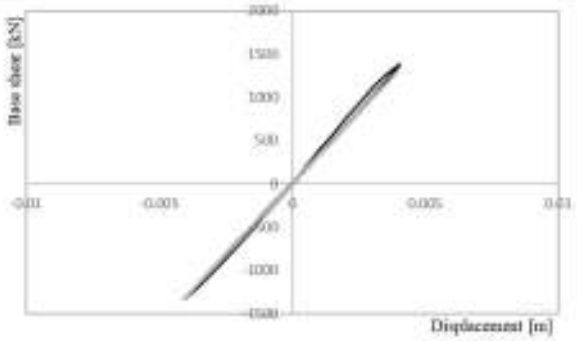	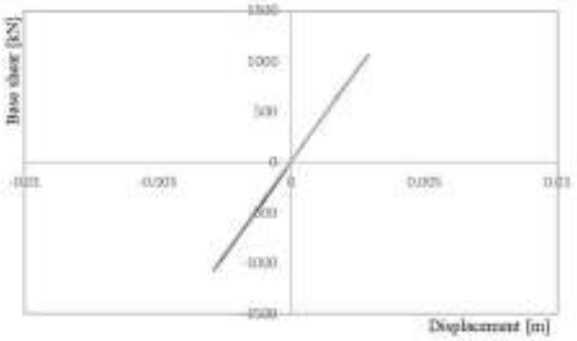
DL2	
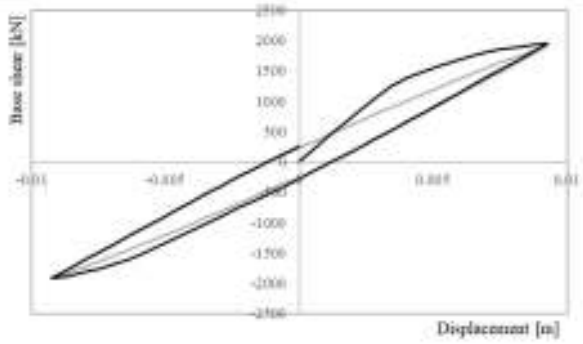	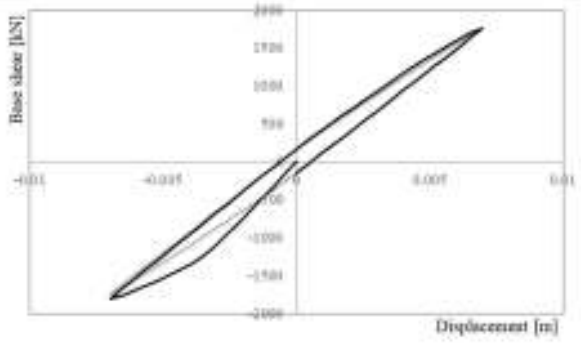
DL3	
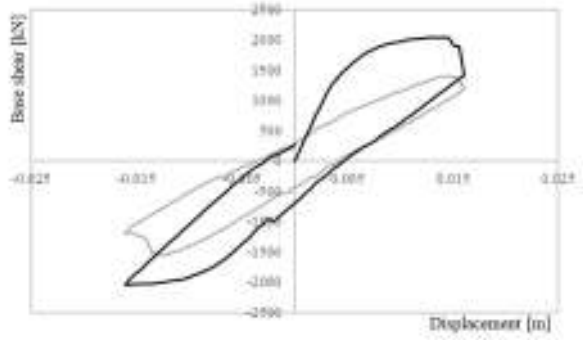	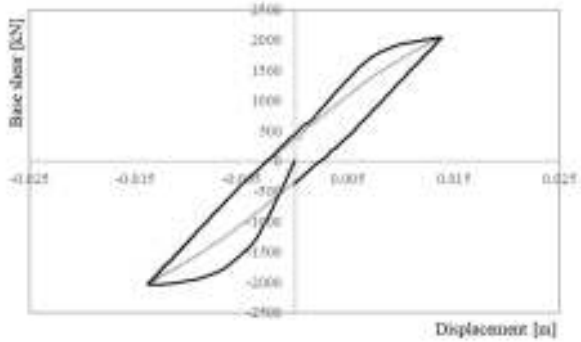
DL4	
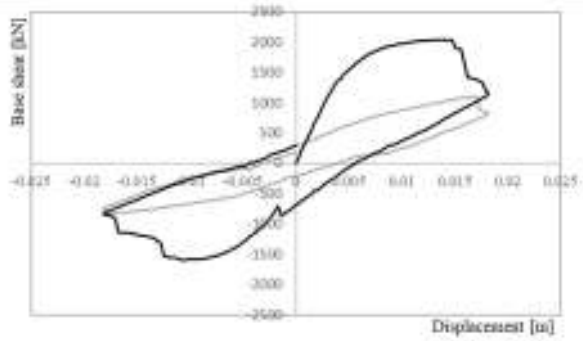	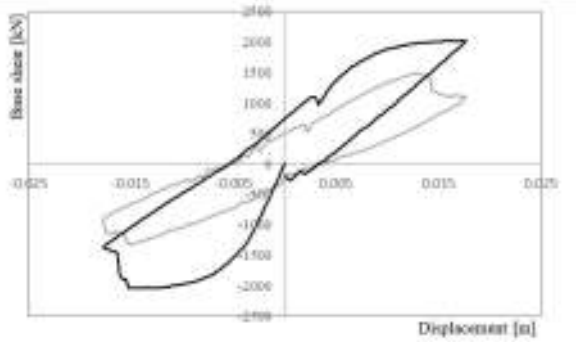

Y DIRECTION – Mass prop.	
DL1	
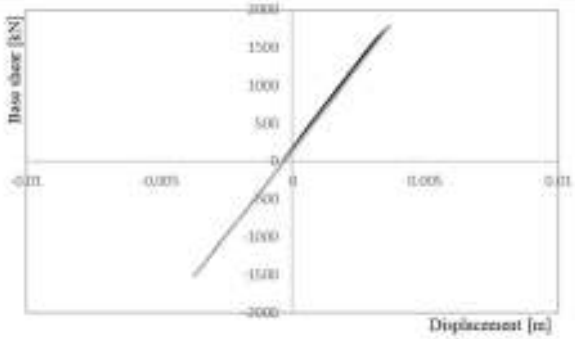	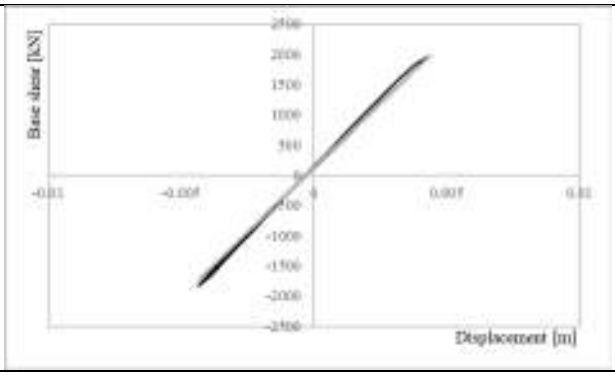
DL2	
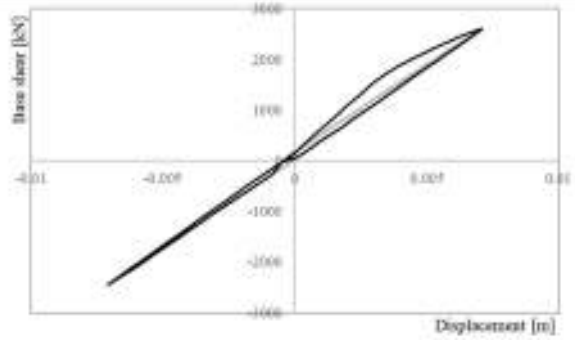	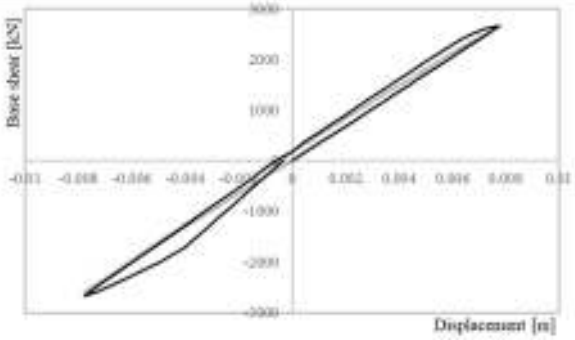
DL3	
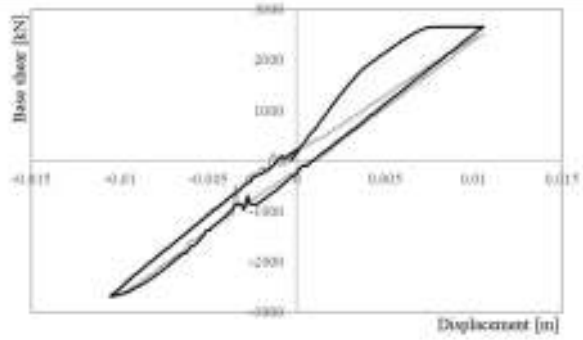	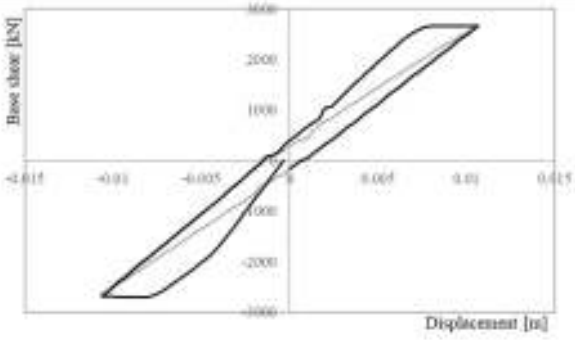
DL4	
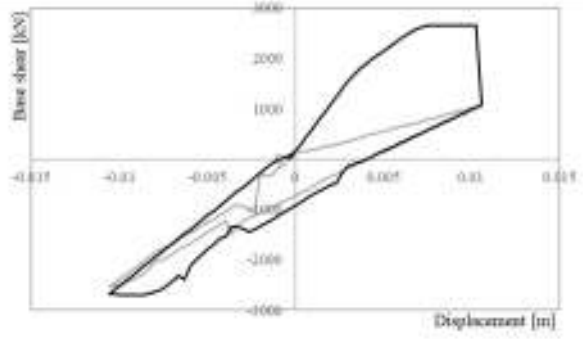	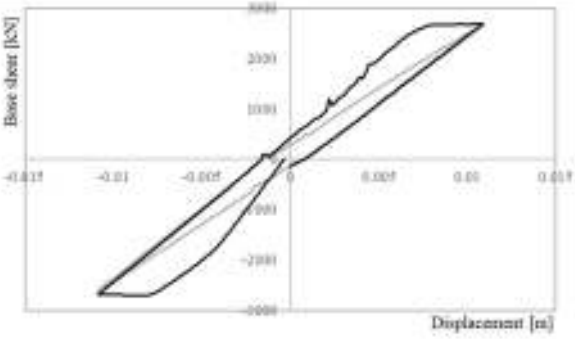

Y DIRECTION – Inv. Triang.	
DL1	
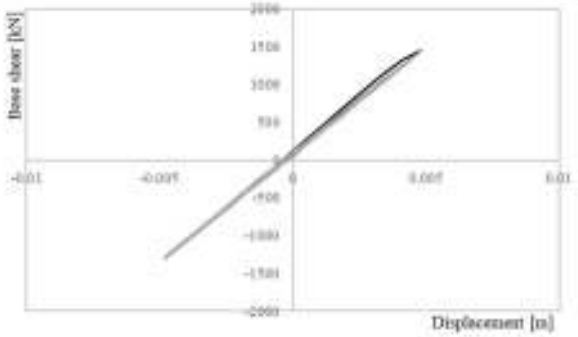	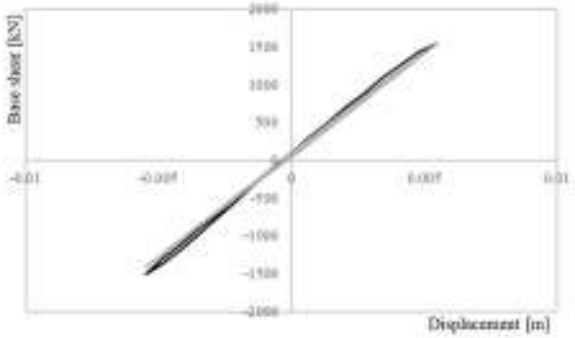
DL2	
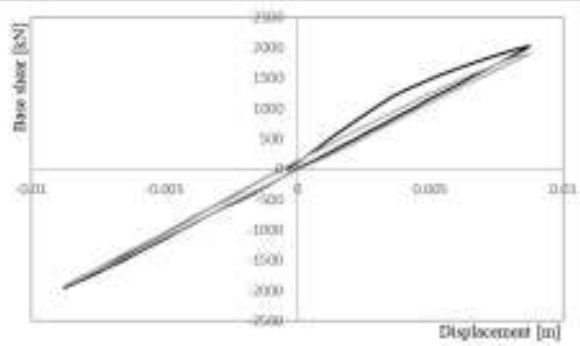	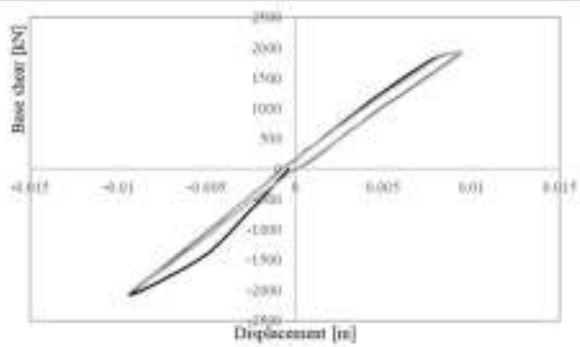
DL3	
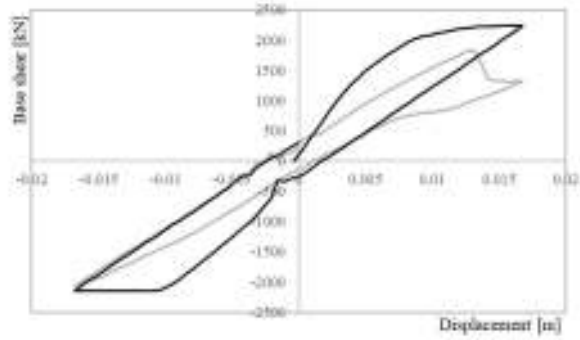	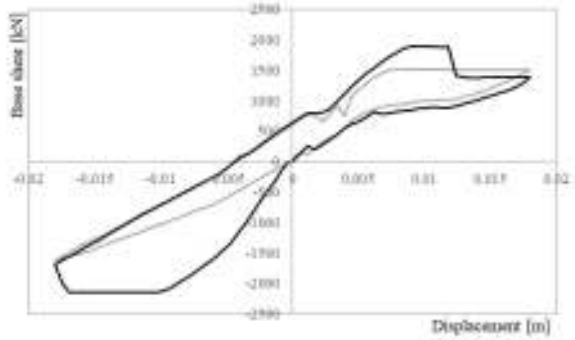
DL4	
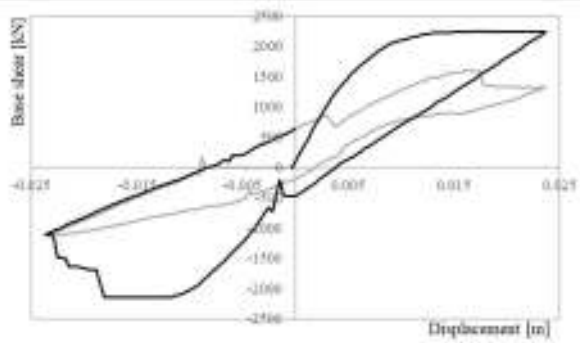	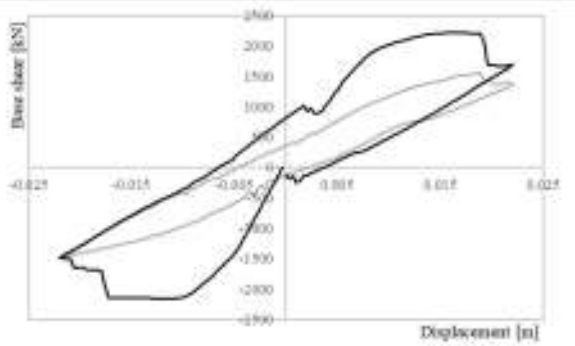

[this page intentionally left blank]

APPENDIX 5

The sensitivity classes (SCs) for all the models for the different LSs. The orange represents the SCH, yellow for SCM and green for SCL

N_RS_CB_CB_HB

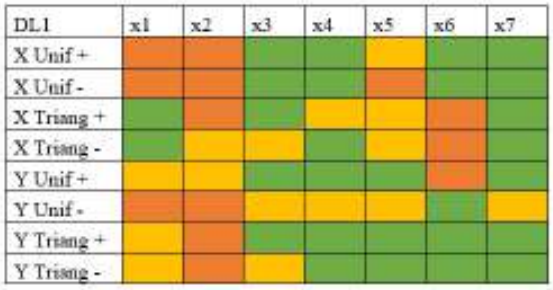

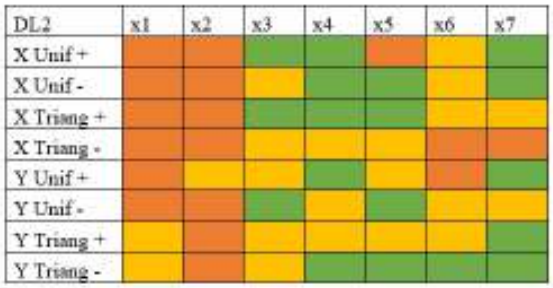

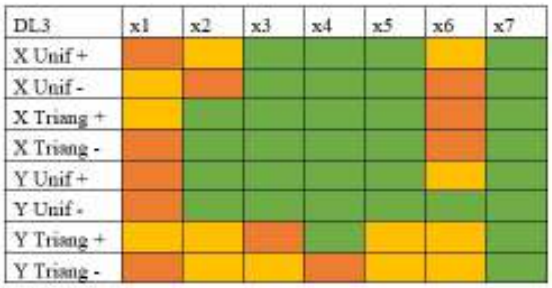

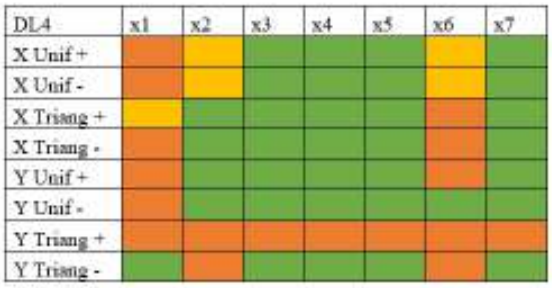

N_RS_RS_CB_HB

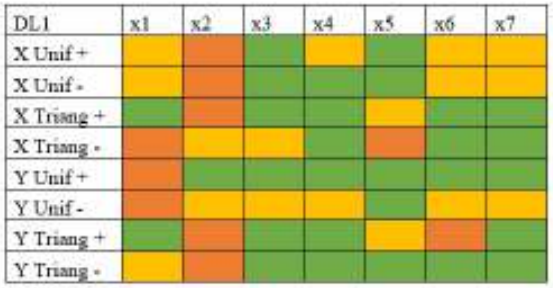

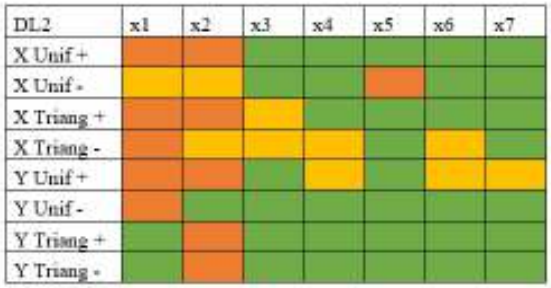

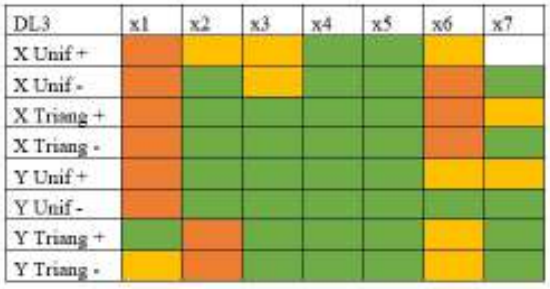

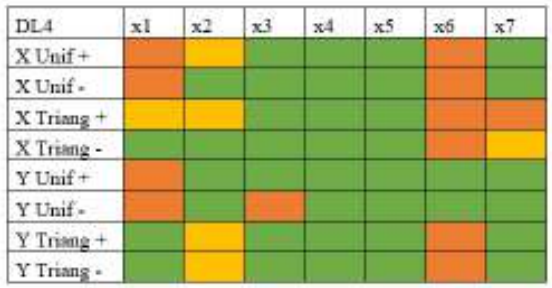

Y_RS_CB_CB_HB

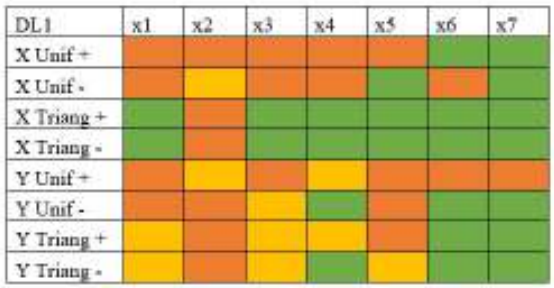

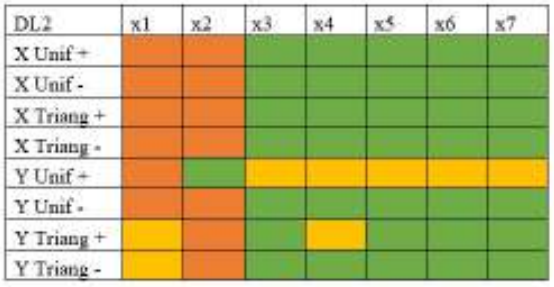

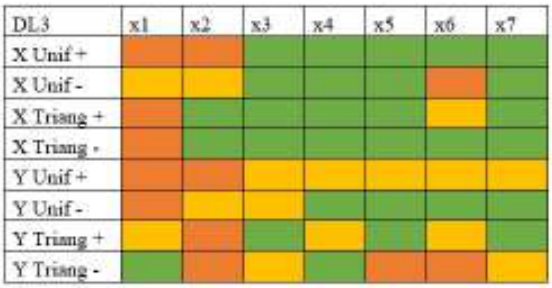

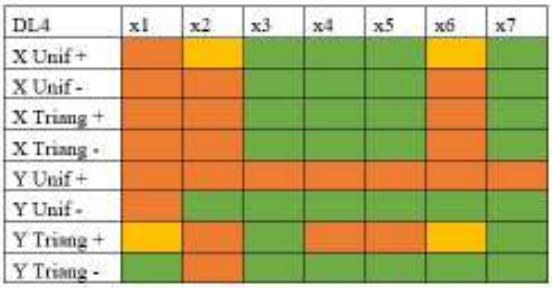

Y_RS_RS_CB_HB